

IL NUOVO CIMENTO

ORGANO DELLA SOCIETÀ ITALIANA DI FISICA

SOTTO GLI AUSPICI DEL CONSIGLIO NAZIONALE DELLE RICERCHE

VOL. XVIII, N. 1

Serie decima

1° Ottobre 1960

On the Interpretation of Cosmic Ray μ -Meson Data.

D. STERN

University of Maryland - College Park, Md.

(ricevuto il 15 Febbraio 1960)

Summary. — An analysis is carried out of the extent to which primary interactions can be investigated using data obtained from cosmic-ray μ -mesons. The analytic dependence of the μ -meson flux at various depths and energies is developed and computations about the energy distribution of pions in primary interactions are carried out. The results agree with a power law lab-system energy distribution.

1. — Introduction.

Of all cosmic ray particles reaching sea level, muons (μ mesons) are by far the most numerous. As a consequence, a large amount of experimental data about them has accumulated. It is the aim of this article to investigate what information can be derived from these data about the interactions of the nucleonic component at high altitudes, in which the muonic component originates.

The problem can be formulated as follows: Let $N(E_\pi, E') dE_\pi$ stand for the average number of pions in the energy interval E_π, dE_π created in the atmosphere by an interaction of a nucleon with energy E' , and let similarly $M(E, E') dE$ be the average number of muons in the interval E, dE resulting from such an interaction. The problem then is, whether the functions $N(E_\pi, E')$ and $M(E, E')$ can be derived from experimental results on muons. If it is possible, the next step would obviously be to carry out such a reconstruction, using available data. If not, it would be useful to find out what constitutes

the maximum information on these two functions contained in the muon component.

The transformation from $N(E_\pi, E')$ to $M(E, E')$ was investigated by ASCOLI⁽¹⁾. He showed that if $N(E_\pi, E')$ is a smooth function, the transformation is closely approximated by

$$(1) \quad N\left(\frac{E_\pi}{0.789}, E'\right) \frac{dE_\pi}{0.789} = M(E, E') dE$$

provided all pions decay. At higher energies there is an appreciable probability that the pion, instead of decaying, undergoes nuclear interaction. At 20 GeV this probability is about 25 %; at very high energies only a small fraction of the pions manage to decay⁽²⁾. Strictly speaking, therefore, the function $N(E_\pi, E')$ in equation (1) should be multiplied by the « average pion decay probability » $g_\pi(E_\pi)$. It may be shown that for low energies (< 30 GeV)

$$(2) \quad g_\pi(E_\pi) = \left(1 - \frac{\lambda_p}{\lambda_\pi} \frac{E_\pi}{158}\right),$$

where λ_π is the interaction mean free path of pions, λ_p is the nucleonic attenuation m.f.p. and $E_\pi \simeq E/0.789$ is the pion's energy in GeV.

In what follows, only the structure of $M(E, E')$ will be investigated. The energy range considered reaches from about 0.5 GeV (arrival energy) up to about 30 GeV.

2. - The mean survival probability.

Because of the large number of factors involved, rather extensive approximations are necessary. Muons are assumed to retain the direction of their generating nucleons (see⁽³⁾ for a detailed investigation) and a constant, energy independent attenuation mean free path $\lambda = 130$ g/cm² is assumed. Furthermore, all primary particles are treated as nucleons. On the other hand, energy losses due to ionization are taken into account. The distance traversed by pions before decaying is disregarded.

Under the above simplifications, the muon flux I reaching sea level (or any other altitude) can be regarded as made up from contributions of various generating nucleon energies, E' , various muon energies at production, E , and

⁽¹⁾ G. ASCOLI: *Phys. Rev.*, **79**, 812 (1950).

⁽²⁾ G. YEKUTIELI and U. HABER-SHAIM: *Nuovo Cimento*, **11**, 172, 683 (1954).

⁽³⁾ E. BRUNBERG: *Ark. for Fys.*, **14**, 195 (1958).

various atmospheric depths l g/cm². Denoting the (differential) primary energy spectrum by $p(E')$ and the probability that a muon produced at depth l with energy E will reach sea level without decaying by $f(l, E)$, we obtain

$$(3) \quad I = \iiint p(E') M(E, E') \exp \left[-\frac{l}{\lambda} \right] f(l, E) dl dE dE'.$$

The integration on l involves only known functions and can therefore be performed. Let us define the «mean survival probability»

$$g(E) = \int_0^{1033 \text{ g/cm}^2} f(l, E) \exp \left[-\frac{l}{\lambda} \right] dl,$$

The function $f(l, E)$ for the case of a constant rate of energy loss ε GeV g⁻¹ cm² has been calculated by JÁNOSSY⁽⁴⁾. Expressing eq. (18), p. 179 of ref. (4) in terms of initial energy (instead of arrival momentum) we obtain, in the extreme relativistic approximation

$$(4) \quad g(E) = \int_0^{1033 \text{ g/cm}^2} \exp \left[-\frac{l}{\lambda} \right] \left[\frac{l}{1033} \left(1 - \frac{\Delta - l\varepsilon}{E} \right) \right]^{1.3/(E + l\varepsilon)} dl,$$

where $\Delta = 1033 \varepsilon$ is the energy loss of a muon traversing the whole atmosphere vertically.

If $l\varepsilon$ is neglected, the result is an incomplete Γ function multiplied by the probability of a muon originating at depth λ to escape decay in flight. For sea level observations, the Γ function is very nearly complete (for observations at high altitudes it is not) and as its value is close to unity the error introduced by eliminating it altogether is not large. Thus the «production layer approximation» in which all muons are assumed to originate at atmospheric depth λ is justified. A better approximation is obtained if 1) the Γ function is not disregarded or approximated 2) $l\varepsilon$, instead of being neglected, is replaced by $\lambda\varepsilon$ (this also leads to a Γ function); or better still, if the atmosphere is divided into sections and in each section $l\varepsilon$ is replaced by $\bar{l}\varepsilon$, where \bar{l} is the section's average depth.

The values of $g(E)$ obtained (for sea level) by replacing $l\varepsilon$ by $\lambda\varepsilon$ are reproduced in Table I. For comparison, the values obtained when the atmosphere is divided into 3 sections (designated by $g_3(E)$) are also given for some energies.

(4) L. JÁNOSSY: *Cosmic Rays* (Oxford, 1950), 2nd edition.

TABLE I.

E_{GeV}	$g(E)$	$g_3(E)$	E_{GeV}	$g(E)$
1.5	0	0.020 1	7	0.602 0
2	0.064 4	0.091 7	10	0.703 9
2.5	0.178 5		15	0.793 6
3	0.265 2	0.281 9	20	0.840 6
4	0.393 0	0.407 0	30	0.889 3
5	0.484 3			

3. - The interpretation of experiments.

After integrating over l the muon flux remains expressed by an integral over the variables E and E' ,

$$(5) \quad I = \iint g(E) p(E') M(E, E') dE dE'.$$

This integral cannot be evaluated or simplified, as it involves the unknown function $M(E, E')$. However, if the relative contributions to it from various values of E and E' are known, (5) may be regarded as a differential equation and solved. Experimental evidence can therefore be classified as follows:

1) Measurements giving the dependence of I on E . These include energy spectrum, height and depth measurements, and they enable one to derive the « production spectrum » ⁽⁵⁾

$$(6) \quad G(E) = \int_{\substack{\text{geomag.} \\ \text{cut off}}}^{\infty} p(E') M(E, E') dE'.$$

2) Measurements giving the dependence of I on E' . These include measurements of the geomagnetic latitude and east-west effects and result in the « yield function » ⁽⁶⁾

$$(7) \quad Y(E') = \int_0^{E'} g(E) M(E, E') dE.$$

⁽⁵⁾ M. SANDS: *Phys. Rev.*, **77**, 180 (1950).

⁽⁶⁾ J. J. QUENBY and W. R. WEBBER: *Phil. Mag.*, **4**, 654 (1959). The same function, under the name of « total multiplicity », was used by NEHER ⁽¹⁰⁾.

A combination of both kinds of measurement—for instance, a measurement of the latitude effect at various altitudes—ought to make it possible to derive $M(E, E')$ empirically. Since the only way to vary E' is by employing the geomagnetic field, it seems that the complete reconstruction of $M(E, E')$ is possible only for relatively low energies, such as are obtainable—or will be in the near future—by artificial means. At higher energies, experiments can give only one «point of information»—by means of the total rate—namely, the average multiplicity for any value of E

$$(8) \quad \bar{M}(E) = \frac{\int M(E, E') p(E') dE'}{\int p(E') dE'}.$$

This can be used to check various production models ^(7,8).

Before concluding this classification a remark should be made concerning angular distribution measurements. Such measurements are difficult to interpret, because the dependence of the mean survival probability $g(E)$ on the zenith angle θ is not a simple one. In principle, however, experimental measurements of energy distributions in various inclinations to the east and to the west ⁽⁹⁾ may also be used to derive $M(E, E')$ —and even for higher values of E' than is possible by other means.

4. — Analysis of data.

An attempt was made to reconstruct $M(E, E')$ using data about the latitude effect—expressed by the yield function $Y(E')$ —at various altitudes. Two sets of data were available: Those of NEHER ⁽¹⁰⁾ giving $Y(E')$ at five altitudes, and those of QUENBY and WEBBER ⁽⁶⁾ giving it at only two. Neher's results were based on an inaccurate primary energy spectrum $p(E')$ and had to be revised to conform with more recent measurements. In order to use these data for solving eq. (7), the continuous function $M(E, E')$ was replaced by an approximation $M'(E, E')$, containing contributions from only a finite number k of values of E

$$M'(E, E') = \sum_{i=1}^k a_i(E') \delta(E - E_i)$$

(δ is the Dirac delta-function).

(7) G. ISHIKAWA and K. MAEDA: *Nuovo Cimento*, **7**, 53 (1958).

(8) S. OLBERT: *Phys. Rev.*, **96**, 1400 (1954).

(9) J. R. MORONEY and J. K. PARRY: *Austral. Journ. Phys.*, **7**, 423 (1954).

(10) H. V. NEHER: *Phys. Rev.*, **76**, 914 (1950); *Progress in Cosmic Ray Physics*, **1**, 243 (1952).

Substituting this approximation into (7) results in a set of linear equations, whose number equals the number of altitudes at which $Y(E')$ was measured. Solving this set, one obtains the coefficients $a_i(E')$, which represent the meson production probabilities in various (meson) energy ranges. If $Y(E')$ is known for five altitudes, it would seem that five unknown coefficients a_i may be obtained; that is, we may choose $k = 5$. Actually, experimental inaccuracies prevent such a full solution, so it was preferred to use a smaller number of coefficients, and adjust them to give best fit to the data (this would generally be done by the method of least-squares; however, since here an additional limitation is imposed that the a_i are non negative, other methods have to be employed).

Using Neher's data for the primary energy $E' = 10$ GeV the following values were obtained:

E_i (GeV)	0.5	1	1.5	2
a_i	5	2.3	1	0.2

As may be seen, the resulting multiplicity is higher, and the energy spectrum steeper than has been found by other methods.

QUENBY and WEBBER give only two values of $Y(E')$, namely for sea level and for $l = 312$ g/cm². Hence only two equations involving $M(E, E')$ are available, and these may be used to determine two parameters in any given model. Here a model $M(E, E') = a(E')E^{-n(E')}$ was chosen (this obviously cannot hold down to the lowest meson energies but only for the high-energy «tail»). The value of $a(E')$ was here found from the value of $Y(E')$ at sea level and that of the exponent n from the ratio $Y_{312}/Y_{\text{sea level}}$.

The computation was carried out for a primary energy $E' = 10$ GeV and a mean free path $\lambda = 75$ g/cm² was assumed (since at such low energies only the first collision contributes significantly to meson production, λ should be set about equal to the interaction—and not the attenuation—mean free path).

The results are in fair agreement with Heisenberg's model

$$M(E, 10 \text{ GeV}) = 0.67 E^{-2} \text{ GeV}^{-1}.$$

According to Heisenberg's theory, $M(E, E')$ should increase with E' like E'^γ where γ descends from a high value to an asymptotic value of unity. According to the results of (6), this asymptotic value is near 1.25, but this may be due to secondary interactions, which increase the number of mesons produced by higher energies.

In addition, various production models were tested by comparing the energy spectra obtained from them to the measured results of OWEN and WILSON (11).

(11) B. G. OWEN and J. G. WILSON: *Proc. Phys. Soc.*, **68 A**, 409 (1955).

It was found that the simple model in which all mesons are assumed to be produced in the C system isotropically and with equal energies leads to a spectrum markedly steeper than the observed one. A relation $M(E, E') = \text{const.} \cdot E' \cdot E^{-2}$ results in a spectrum slightly less steep than observed, while

$$M(E, E') = \text{const.} \cdot E' \cdot E^{-2.5}$$

gives a fairly good fit.

5. - Conclusions.

It has been shown that the energy spectrum of pions produced in primary interactions of cosmic radiation can be investigated by means of the muon component at various altitudes and geomagnetic latitudes. Actual measurements indicate that at its high energy end this spectrum behaves like E^{-2} or $E^{-2.5}$. The information lacks in detail, however, because of the scarcity of available data; anyway, the possibility of obtaining full information by this method is inherently limited to low energies.

* * *

The author wishes to thank Professor K. SITE for his advice and interest and Professor G. YEKUTIELI for several illuminating discussions.

APPENDIX

Proof of equation (2).

With the notation of eq. (2), the relative probability of a pion being produced at atmospheric depth l to $l+dl$ (g/cm^2) is

$$\exp \left[-\frac{l}{\lambda_p} \right] \frac{dl}{\lambda_p}.$$

Since pions generally do not proceed very far from the point where they are created, we may assume uniform atmospheric density $\varrho = \varrho_0(l/l_0)$ along their entire path. The probability of a pion interacting after traversing a

depth L —and not decaying before—is then

$$\exp \left[-\frac{L}{c\tau_0} \right] \cdot \frac{dL}{\lambda_\pi},$$

hence the probability of interacting anywhere is

$$\int_0^\infty \exp \left[-\frac{L}{c\tau_0} \right] \frac{dL}{\lambda_\pi} = \frac{c\tau_0}{\lambda_\pi} = \frac{c\tau_0}{\lambda_\pi} \cdot \frac{E_\pi}{mc^2} \cdot \frac{\rho_0}{l_0} l.$$

Weighing the probability of interacting by the probability of being created at various values of l , we obtain for the total interaction probability

$$\frac{c\tau_0\rho_0}{mc^2 l_0} \frac{E_\pi}{\lambda_\pi} \int_0^\infty l \exp \left[-\frac{l}{\lambda_p} \right] \frac{dl}{\lambda_p} = \frac{c\tau_0\rho_0}{mc^2 l_0} \frac{\lambda_p}{\lambda_\pi} E_\pi,$$

hence the probability of escaping interactions is

$$g_\pi(\varepsilon) = \left(1 - \frac{c\tau_0\rho_0}{mc^2 l_0} \frac{\lambda_p}{\lambda_\pi} E_\pi \right).$$

RIASSUNTO (*)

Si esamina fino a qual punto le interazioni primarie possono essere studiate usando i dati ottenuti dai mesoni μ dei raggi cosmici. Si sviluppa la dipendenza analitica del flusso dei mesoni μ a varie profondità ed energie e si eseguono calcoli sulla distribuzione dell'energia dei pioni nelle interazioni primarie. I risultati si accordano con una distribuzione dell'energia nel sistema del laboratorio secondo una legge esponenziale.

(*) Traduzione a cura della Redazione.

On the Steady-State Theory of Cosmology.

P. ROMAN

Dept. of Theoretical Physics, The University - Manchester ()*

(ricevuto l'8 Marzo 1960)

Summary. — It is shown that there is no contradiction between « energy conservation » and the continuous creation of matter in an expanding universe. By applying Noether's theorem to the substratum, a modified conservation law is obtained which accounts automatically for the creation of matter. The substratum is treated as a relativistic fluid and the solution of the equations of motion determines the characteristics of the substratum and gives a picturesque interpretation to the process of creation of matter. An equivalent model within the framework of general relativity is set up.

1. — Introduction and basic concepts.

The steady-state theory of the universe was first introduced by BONDI and GOLD ⁽¹⁾ in 1948, and was based on the powerful perfect cosmological principle. Later HOYLE ⁽²⁾ showed that the theory can be gotten from a modification of Einstein's field equations. A more attractive deduction of the theory from general relativity was given by MCCREA ⁽³⁾, based on a re-definition of the zero-level of pressure.

An arresting feature of the steady-state theory is the continuous creation of matter. It has usually been argued that energy conservation is only an empirical law and must be given up if facts compel us to do so. In spite of this argument, at first sight it seems as if continuous creation would contradict the basic steadiness-assumption of the theory. For, in fact, energy conser-

(*) Present adress: Physics Dept., Boston University, Boston 15, Mass.

(¹) H. BONDI and T. GOLD: *Month. Not. Roy. Astron. Soc.*, **108**, 252 (1948).

(²) F. HOYLE: *Month. Not. Roy. Astron. Soc.*, **108**, 372 (1948).

(³) W. H. MCCREA: *Proc. Roy. Soc.*, A **206**, 562 (1951).

vation, as well as any other conservation law, may be expressed as an invariance property of a system. In particular, energy conservation is equivalent to invariance under a time-displacement transformation $t \rightarrow t + \delta t$. Hence, if energy conservation does not hold, this seems to indicate that the universe is not homogeneous in time. We shall show, however, that this is by no means the case: by applying the perfect cosmological principle consistently, we not only can achieve invariance under time-displacement but obtain also a modified form of the usual energy conservation law, which automatically gives account of the continuous creation of matter. By combining this law with the equations of motion, we can find also the characteristics of the basic substratum.

The *substratum* will be considered as the basic physical background against which all quantities must be measured, rather than an approximation of the overall motion of matter. Briefly speaking, the substratum will be looked upon as a geometry endowed with physical properties: co-ordinates x_μ , density ρ , pressure p , and velocity \mathbf{v} . By the perfect cosmological principle ρ and p are independent of x_μ , and the flow is stationary, $\partial \mathbf{v} / \partial t = 0$. We exclude the oversimplification of the static case with $\mathbf{v} = 0$; thermodynamical non-equilibrium shows that this cannot hold. Then, the velocity of a point of the substratum at a distance \mathbf{r} from any fundamental observer may be inferred from the cosmological principle, isotropy, and self-consistency. As is well known, one finds

$$(1) \quad \mathbf{v} = \frac{1}{T'} \mathbf{r},$$

where, by the steadiness-assumption, T' is a *constant* of the dimensions [s].

Since the velocities of distant parts of the substratum are large we must use the (special) theory of relativity if we wish to discuss its motion. First of all, we need the components of the relativistic four-velocity

$$(2) \quad u_\mu = v_\mu \frac{dt}{d\tau}, \quad (v_4 = ic).$$

But here

$$(3) \quad \frac{dt}{d\tau} = 1,$$

because

$$ds^2 = -c^2 d\tau^2 = dr^2 - c^2 dt^2,$$

hence

$$1 = -\frac{1}{c^2} \left(\frac{dr}{d\tau} \right)^2 + \left(\frac{dt}{d\tau} \right)^2,$$

where

$$\frac{d\mathbf{r}}{d\tau} = 0$$

at any point and at any time, since any point is stationary along its own world-line. Hence (2), (3) and (1) give (*)

$$(4) \quad u_i = v_i = \frac{1}{T} x_i, \quad u_4 = ic.$$

It is now evident that the equation of continuity does not hold for the substratum; instead we have

$$(5) \quad \partial_\mu (\varrho u_\mu) = \varrho \partial_i v_i = \frac{3\varrho}{T}.$$

That is, mass will be created at a local rate of

$$(6) \quad m = \frac{3\varrho}{T}$$

per cm^3 and s. This is of course a purely kinematical consequence of the assumption $\varrho = \text{const}$ and the expansion law.

In order to discuss dynamical properties of the substratum, we need to know its *energy-momentum tensor*, which will be that of a relativistic fluid. In the earlier literature there was a considerable amount of confusion regarding the form, derivation, and application of this tensor, but now the problem is settled. A completely satisfactory derivation of the tensor was recently given and discussed by MARX (4). This tensor is of the form

$$(7a) \quad T_{\mu\nu} = -\varrho u_\mu u_\nu - g_{\mu\nu} p.$$

For a flat metric, which we shall use throughout, except in Section 4, this reduces to

$$(7b) \quad T_{\mu\nu} = -\varrho u_\mu u_\nu - \delta_{\mu\nu} p.$$

It should be emphasized that here ϱ is the proper rest-mass density and p the proper pressure as measured by a co-moving local geodetic observer.

(*) Greek indices run from 1 to 4, while latin indices from 1 to 3. Summation over repeated indices is understood.

(4) G. MARX: *Bull. Acad. Pol. Sci.*, Cl. III, 4, 29 (1956).

2. — The modified conservation law.

We now proceed to derive the conservation law arising from invariance under time-displacement, this invariance being essential for the steady-state hypothesis. To see clearly the meaning of the following procedure, we recall that in Section 1. We have «equated» the substratum with the «geometrical background», and thus it is the latter which is expanding and thereby sweeping away with itself the matter present. The geometrical co-ordinates of matter are thus related to the velocity of the substratum and hence, by the fluid equations of motion to be derived, to q and p . In this fact we may see an expression of Mach's principle.

We assume that the substratum is described by some Lagrangian L which depends on some field variables ψ . The concrete form of the Lagrangian and the specification of the variables ψ are not relevant.

It has been shown long since (see, for example, HILL⁽⁵⁾) that according to Noether's theorem, the general form of the conservation law arising from invariance under the transformation $x_\mu \rightarrow x_\mu + \delta x_\mu$ is

$$(8) \quad \partial_\mu \left[\left(L \delta_{\mu\nu} - \frac{\partial L}{\partial \hat{\partial}_\mu \psi} \partial_\nu \psi \right) \delta x_\nu \right] = 0.$$

We consider now a time-displacement

$$(9a) \quad x_4 \rightarrow x_4 + ic \delta t.$$

Due to the expansion of the geometry, this transformation will be necessarily accompanied by a transformation of the space-co-ordinates x_i . We have

$$(9b) \quad x_i \rightarrow x_i + v_i \delta t = x_i + \frac{1}{T} x_i \delta t.$$

(Another interpretation of these simultaneous transformations will be given at the end of the paper.) (9a) and (9b) may be jointly written

$$(10) \quad \delta x_\nu = \left(\frac{1}{T} x_i \delta_{i\nu} + ic \delta_{4\nu} \right) \delta t.$$

⁽⁵⁾ E. L. HILL: *Rev. Mod. Phys.*, **23**, 253 (1951).

Hence, (8) gives, since δt is arbitrary,

$$(11) \quad \frac{\partial}{\partial t} \left(L - ic \frac{\partial L}{\partial \partial_4 \psi} \partial_4 \psi - \frac{1}{ic} \frac{\partial L}{\partial \partial_k \psi} \partial_k \psi \frac{1}{T} x_i \right) + \\ + \partial_k \left[\left(L \delta_{ki} - \frac{\partial L}{\partial \partial_k \psi} \partial_i \psi \right) \frac{1}{T} x_i - ic \frac{\partial L}{\partial \partial_k \psi} \partial_4 \psi \right] = 0.$$

We now make use of the following conventional definitions (see, for example, ref. ⁽⁵⁾ or WENTZEL ⁽⁶⁾) of the energy density W , momentum density G_i , stress T_{ki} , and energy flow density S_k :

$$(12) \quad \left\{ \begin{array}{l} -L + \frac{\partial L}{\partial \partial_4 \psi} \partial_4 \psi \equiv W, \\ -\frac{1}{ic} \frac{\partial L}{\partial \partial_k \psi} \partial_k \psi \equiv G_i, \\ L \delta_{ki} - \frac{\partial L}{\partial \partial_k \psi} \partial_i \psi \equiv T_{ki}, \\ ic \frac{\partial L}{\partial \partial_k \psi} \partial_4 \psi \equiv S_k. \end{array} \right.$$

Using (12), eq. (11) can be rewritten as

$$(13) \quad \frac{\partial}{\partial t} \left(W - \frac{1}{T} x_i G_i \right) + \partial_k \left(S_k - \frac{1}{T} x_i T_{ki} \right) = 0.$$

This is the conservation law, replacing the usual one,

$$\frac{\partial W}{\partial t} + \partial_k S_k = 0.$$

We thus may say that energy conservation holds, but if an observer looks into a region at a distance he will find an energy density

$$(14a) \quad W' = W - \frac{1}{T} x_i G_i,$$

and an energy flow density

$$(14b) \quad S'_k = S_k - \frac{1}{T} x_i T_{ki}.$$

⁽⁵⁾ G. WENTZEL: *Einführung in die Quantentheorie der Wellenfelder* (Wien, 1943), p. 9.

A more fruitful interpretation is, however, obtained if we rewrite (13) as follows:

$$(15) \quad \frac{\partial W}{\partial t} + \partial_k S_k = \frac{1}{T^2} x_i G_i + \frac{1}{T} \delta_{ki} T_{ki} + \frac{1}{T} x_i \left(\frac{\partial G_i}{\partial t} + \partial_k T_{ki} \right) \equiv \alpha.$$

As compared with the conventional conservation law, the right hand side, α , gives clearly the apparent «creation of energy». Using now $T_{\mu\nu}$ as given by (7b), noticing that $G_i = (1/c) T_{4i} = \rho v_i = (\rho/T) x_i$, and that, due to the stationarity of flow, $\partial G_i / \partial t = 0$, we obtain after a slight calculation for the r.h.s. of eq. (15)

$$(16) \quad \alpha = -\frac{3\rho}{T} - \frac{4\rho}{T^3} r^2.$$

Since for any fundamental observer $\mathbf{r} = 0$, the first term of (16) gives the *local* rate of apparent energy creation. Thus, the local rate of matter creation is

$$m = -\frac{3\rho}{Tc^2},$$

and comparing this with the kinematical result (6), we find that

$$(17) \quad p = -\rho c^2.$$

That is, the substratum possesses a negative (outward) pressure. It is notable that the relation (17) between pressure and density was also obtained in McCrea's theory ⁽³⁾.

Using (17), eq. (16) may be rewritten in the form

$$(18) \quad \alpha = \frac{3\rho c^2}{T} \left(1 - \frac{4}{3} \frac{r^2}{R^2} \right),$$

where $R = cT$ is the radius of the observable universe. The factor in brackets is obviously a transformation factor with which the local rate of energy creation must be multiplied if the observer looks into a region at a distance r away, and it is due to the expansion of the geometry, which immediately sweeps away a fraction of the locally created matter.

We notice that the local production of energy may be thought of originating from the work done by the pressure during the expansion. Indeed, the work of pressure is

$$(19) \quad A = -\int p \, dV,$$

and, since a simple calculation shows that as a consequence of (1)

$$\frac{dV}{dt} = \frac{3V}{T},$$

(19) gives

$$(20) \quad \frac{d^2 A}{dV dt} = -\frac{3p}{T} = \frac{3\rho c^2}{T},$$

in accord with (18).

3. — The equations of motion.

In order to obtain a numerical value for ρ , we must solve the equations of motion of the substratum. They are

$$(21) \quad \partial_\mu T_{\mu\nu} = F_\nu,$$

where F_ν is the force per unit volume. This we identify with the gravitational force, since the substratum is subject to this body force. When we want to write down this force, we must carefully distinguish between the inertial mass density ρ and the gravitational mass density σ . The gravitational mass is defined through the acceleration it causes on an inertial mass in its field. Since the substratum is under pressure, the gravitational mass will differ from the inertial mass, because the mass equivalent of the pressure-energy will also contribute to gravitation. Consequently, the spatial components of the force-density are

$$(22) \quad F_i = -\frac{4\pi}{3} \gamma \rho \sigma x_i,$$

where γ is the gravitational constant. Thus, using (7b), and (22), the first three components of (21) give

$$\frac{4\rho}{T^2} x_i = -\frac{4\pi}{3} \gamma \rho \sigma x_i,$$

hence

$$(23) \quad \sigma = -\frac{3}{\pi} \frac{1}{\gamma T^2}.$$

The next step is to find the relation between this gravitational density and the inertial mass density ρ . WHITTAKER⁽⁷⁾ has shown that under very general

(7) E. T. WHITTAKER: *Proc. Roy. Soc.*, A **149**, 384 (1935).

conditions, which apply in our case,

$$\sigma = \frac{1}{c^2} (T_{44} - T_{11} - T_{22} - T_{33}) .$$

Using (7b), this relationship gives in the present case

$$(24) \quad \sigma = -\varrho .$$

Hence, with (23),

$$(25) \quad \varrho = \frac{3}{\pi} \frac{1}{\gamma T^2} .$$

HOYLE⁽²⁾ and MCCREA⁽³⁾ obtained in their theories a value 8 times less than we have here. The difference in Hoyle's case arises essentially from the fact that he did not allow for a pressure, and in McCre'a's case it stems from identifying the energy density with the rest mass density.

Using Sandage's⁽⁸⁾ recent value

$$\frac{1}{T} \approx 2.5 \cdot 10^{-18} \text{ s}^{-1}$$

for Hubble's constant, (25) gives numerically

$$(26) \quad \varrho \approx 9.6 \cdot 10^{-29} \text{ g/cm}^3 ,$$

a very reasonable value.

According to (6), the local rate of matter creation is then

$$(27) \quad m \approx 7.2 \cdot 10^{-46} \text{ g/cm}^3 \text{ s} .$$

Our picture is completed if we work out the fourth component of the equations of motion (21). We then get

$$\frac{3\varrho}{T} ic = F_4 ;$$

but, since $(c/i)F_4$ is, from the customary point of view, the density a of work done per second by the force-density F_i , we may write

$$(28) \quad \frac{da}{dt} = \frac{3\varrho c^2}{T} .$$

⁽⁸⁾ A. SANDAGE: *Astrophys. Journ.*, **127**, 513 (1958).

Hence the work done by the gravitational force per cm^3 and s is just $3\rho c^2/T$, i.e., according to (16), the locally created energy. On the other hand, gravitation is necessary to keep the universe in a steady state: since p is constant, the hydrodynamical equations of motion do not permit a steady flow *unless* there is a body force. In a sense, we may say that gravitation works against a change in rate of expansion and keeps balance, thereby creating mass. However, the expansion is not brought about by the pressure directly, because p is constant and its gradient does not appear in the equation of motion. Nevertheless, the pressure, through its negative contribution to the gravitational mass and hence to the gravitational force, determines the constant rate of expansion. Otherwise the gravitational force would tend to bring the system to an accelerated flow. So that, as an alternative to our above point of view, we may also say that the pressure constantly changes the inertial mass to its gravitational value in order to keep up a steady rate of expansion. While doing this work, it alters the energy of the system and produces energy. We have indeed seen in (20) that the work of pressure is also $3\rho c^2/T$, so that the two viewpoints yield an identical result.

Incidentally, it is interesting to note that since in this picture the work of the gravitational force is positive and ρ must be necessarily positive, (28) shows that T must be positive too. That is, we must have expansion and not contraction.

We may also visualize the situation from another point of view. In recent works on relativistic dynamics (see, for example, SZAMOSI⁽⁹⁾) it has been pointed out that if the four-force is not perpendicular to the four-velocity, the rest mass will not be constant. The expression $-F_\mu u_\mu$ may be taken as a measure of the change of rest-energy density per second; in our problem this expression gives exactly the quantity (16).

4. - The equivalent relativistic model.

We now show that an interesting equivalent model may be constructed in the framework of general relativity.

As was shown by ROBERTSON⁽¹⁰⁾ and discussed by BONDI⁽¹¹⁾, it follows from purely kinematical considerations that the line-element of any cosmology has the form

$$ds^2 = -c^2 dt^2 + f^2(t)(1 + \frac{1}{4}kr^2)^{-2} dr^2,$$

(9) G. SZAMOSI: *Acta Phys. Hung.*, **6**, 207 (1957).

(10) H. P. ROBERTSON: *Astrophys. Journ.*, **82**, 284 (1935).

(11) H. BONDI: *Month. Not. Roy. Astron. Soc.*, **108**, 104 (1948).

where f is a real and positive function and k is a constant, characterizing the three-dimensional curvature. Einstein's field equations read

$$G_{\mu\nu} - \frac{1}{2} g_{\mu\nu} G + \lambda g_{\mu\nu} = -8\pi\gamma T_{\mu\nu}.$$

BONDI⁽¹¹⁾ then showed that if *for any local observer at his own position at rest and at any epoch t the T_4^i elements of the energy-momentum tensor vanish and $T_1^1 = T_2^2 = T_3^3 = T_4^4$* , then f satisfies the equations

$$(30a) \quad \frac{8\pi\gamma}{c^2} T_4^4 = \frac{3f'^2}{f^2} + \frac{3ke^2}{f^2} - \lambda,$$

$$(30b) \quad \frac{8\pi\gamma}{c^2} T_i^i = 2 \frac{f''}{f} + \frac{f'^2}{f^2} + \frac{ke^2}{f^2} - \lambda.$$

Now, in accord with the perfect cosmological principle we must take T_4^4 and T_i^i to be constants. Then it is easy to show that (30a) and (30b) are compatible if and only if

$$(31) \quad T_i^i = T_4^4.$$

In that case

$$(32) \quad f(t) = A \exp [Nt] + B \exp [-Nt],$$

where

$$(33) \quad N = \left(\frac{8\pi\gamma}{3} \frac{T_4^4}{c^2} + \frac{\lambda}{3} \right)^{\frac{1}{2}}.$$

For an infinitely old universe, as is the case in the steady-state theory, the second term in (32) will have died out, and we have

$$(34) \quad f(t) = A \exp [Nt].$$

It then follows further that

$$(35) \quad k = 0.$$

Hence we obtained a de Sitter metric

$$(36) \quad ds^2 = -c^2 dt^2 + \exp [2Nt] dr^2.$$

The interesting point now is that in our hydrodynamical model, developed in the previous sections, we have, by (7a) (*) for the locally observed com-

(*) Note that for the metric (29) $g_1^1 = g_2^2 = g_3^3 = g_4^4 = 1$.

ponents

$$(37) \quad T_4^4 = \rho c^2 - p, \quad T_i^i = -p.$$

Comparison with (31) shows that in the equivalent relativistic model $\underline{g} = 0$, *i.e.* the *restmass* density vanishes. Hence, *in this sense* the resulting de Sitter universe is empty. The total *energy* density, however, is of course not zero, $T_4^4 = T_i^i = -p$. We may say that all of the energy is present in the form of *elastic energy* (pressure energy). This statement seems at first sight surprising, because an incompressible fluid cannot have elastic energy. But we must keep in mind that the substratum is not an ordinary fluid and its intrinsic expansion makes some conventional concepts void.

The rate of expansion in the relativistic model is

$$(38) \quad \frac{f'}{f} = N.$$

Since this must be equated with the rate $1/T$ in the hydrodynamical model, we obtain, using (34), (33), (37) and (38),

$$(39) \quad \lambda = \frac{3}{T^2} + \frac{8\pi\gamma}{c^2} p.$$

If we equate the pressure with its value

$$p = -\frac{3}{\pi} \frac{c^2}{\gamma T^2}$$

obtained in the equivalent non-relativistic model, (39) gives for the cosmological constant

$$(40) \quad \lambda = -\frac{21}{T^2} \approx -1.3 \cdot 10^{-36} \text{ s}^{-2},$$

a very reasonable value.

In conclusion we mention that the co-ordinate displacement transformation (9b) which accompanies the time displacement (9a), may be obtained also from the metric (36). The perfect cosmological principle demands that this metric must reproduce itself at any epoch t . This criterion is obviously satisfied if at a time $t + \delta t$ the unit of length is changed by a factor $\exp[-N \delta t]$. Therefore at this moment a fundamental observer will measure for a fixed

point the co-ordinates of which were x_i at the time t , the value $\exp[N\delta t]x_i \approx x_i + N\delta t x_i$. Since $N = 1/T$, this means that while $t \rightarrow t + \delta t$, $x_i \rightarrow x_i + (1/T)x_i \delta t$. This, however, is the content of the simultaneous transformations (9a) and (9b).

* * *

The author is obliged to Professor H. BONDI at London University for arising his interest in the topic and for a most delightful discussion with him and his staff.

RIASSUNTO (*)

Si dimostra che non c'è contraddizione fra « conservazione dell'energia » e la creazione continua di materia in un universo in espansione. Applicando al substrato il teorema di Noether, si ottiene una legge di conservazione modificata che rende automaticamente conto della creazione della materia. Il substrato è trattato come un fluido relativistico e la soluzione delle equazioni del moto determina le caratteristiche del substrato e dà una pittoresca interpretazione del processo di creazione della materia. Si stabilisce un modello equivalente nello schema della relatività generale.

(*) Traduzione a cura della Redazione.

Effect of the Dipolar Rotation of Liquids - III.

E. GROSSETTI

Istituto di Fisica Sperimentale dell'Università - Napoli

(ricevuto il 14 Marzo 1960)

Summary. — In previous papers the values of rotational momenta for certain polar liquids in rotating electric fields having frequencies ranging between 0.125 and 8.5 MHz and between 8.5 and 23.0 MHz, were determined. In this paper however, are reported the rotational momentum values for some polar liquids (toluene, nitrobenzene, ethyl alcohol, amyl alcohol, distilled water, acetic acid) in a rotating electric field at much higher frequencies, that is 100.0; 120.0; 150.0 MHz, in order to determine in a different way the viscosity coefficient values. The values of the viscosity coefficient η , obtained by comparing the experimental rotational momentum with that given by the Born formula—in which M is substituted by the values of the electric momentum measured in the Debye polarization processes—are relatively in agreement with those obtained by classical methods.

In previous papers ^(1,2) the values of rotations momenta for certain polar liquids in rotating electric fields, having frequencies ranging between 0.325 and 8.5 MHz and between 8.5 and 23.0 MHz, were determined.

In the first paper the difference noted between experimental and theoretical values may be attributed to the conductivity of the liquid examined.

In the second paper, however, because of the use of rotating electric fields having higher frequencies, the effect of conductivity may be considered as

⁽¹⁾ E. GROSSETTI: *Nuovo Cimento*, **10**, 193 (1958).

⁽²⁾ E. GROSSETTI: *Nuovo Cimento*, **13**, 350 (1959).

negligible and therefore the differences noted between experimental and theoretical values may be attributed to a variation of the viscosity coefficient of the liquids examined with the frequency of rotation.

This gives the possibility to determine the latter coefficient by means of a method which is totally different from the classical one, *i.e.* by means of the effect of the rotation of the molecules in connection with the center of gravity axis, instead of being determined by the effect of the displacement of the particles in relation to each other.

In view of the differences encountered, it was decided to raise also the frequency of the variable field in order to discover what effect such increase might have on the value of η . The increase was such that it was possible to reach frequencies ranging from 100 to 150 MHz. The theoretical rotation momentum L is given by the Born formula

$$(1) \quad L = \frac{4}{3} \pi a^3 \eta \omega (ME/kT)^2,$$

in which M is the value of the electrical momentum obtained from the Debye formula for the polarization processes and η the viscosity. Evidently under the assumption that M is independent of the frequency, the experimental measurement of L gives the possibility of obtaining η in these special conditions.

The generator for the production of the rotating field ((100–150) MHz) is built differently from the one employed for the lower frequencies which had been used previously. The electrical rotating field results from the composition of two alternating fields dephased by 90° and produced by two couples of plates opposite each other and disposed according to the lateral faces of a parallelepiped having a square base and in the center of which a teflon container is set, holding the liquid under study. The container is suspended from a torsional wire (of tungsten) 95 cm long and whose radius is 2.10^{-3} cm. The rotation momenta were determined by means of the mirror and scale method, with a scale placed at approximately 6.80 m from the mirror. It was possible to detect momenta of approximately $2.44 \cdot 10^{-4}$ dine cm.

A transmitter is used to triplicate the frequency from a signal generator ((33.33–50.0) MHz, Fig. 1) in such a way that it is possible to obtain, at the output, amplified signals ranging from 100.0 to 150.0 MHz. On the plates of the generator it is possible to obtain radiofrequency voltages ranging between 100 and 1000 V.

The voltages producing the alternating fields are obtained from the transmitter, and the phase shift among them is obtained by drawing them at the input and at the output of a π cell in which, as it is known, such voltages are dephased by 90° when the reactances of the elements have equal absolute values (Fig. 2).

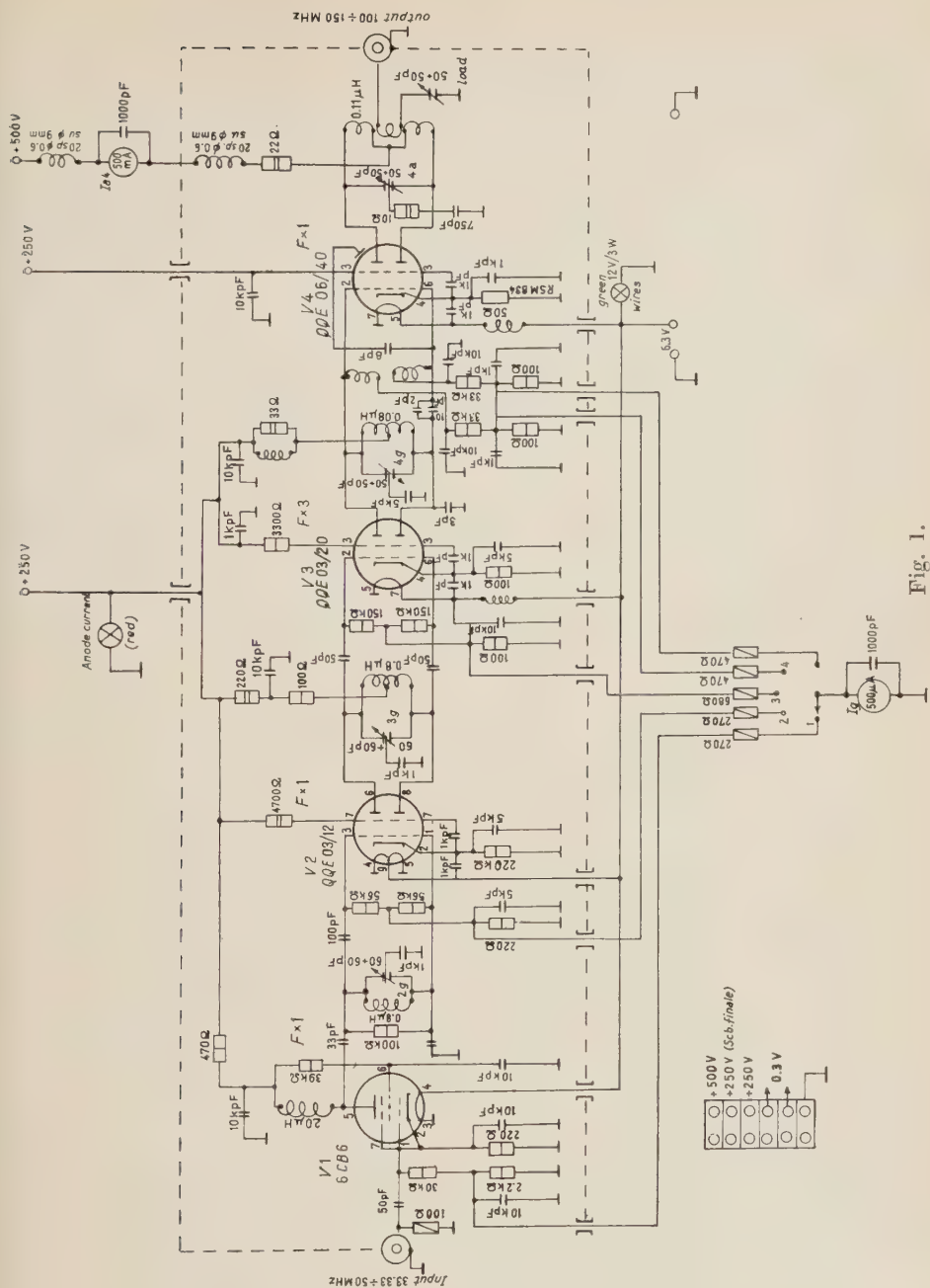


Fig. 1.

The reactances X_{LD} , X_{LA} , (parallel) are included in the tuning circuits at the input and output of the mentioned cell, while the capacity reactance X_c (series) acts as a coupling.

Each one of the two wattless voltages feeds, through a symmetrizer (S_D , S_A) formed by lengths of coaxial cable) supplying the two voltages opposed and balanced in regards to the earth, one of the couples of plates.

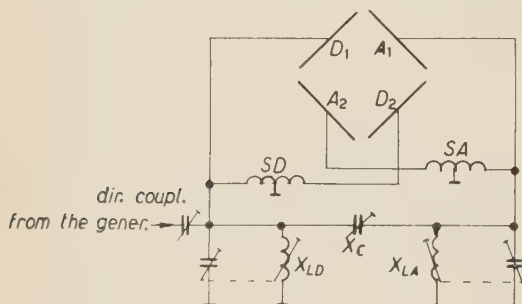


Fig. 2.

regulating it, the input impedance of the device may be varied until it reaches 60Ω , which is the characteristic impedance of the input coaxial cable. Such a condition of equality is revealed by a minimum in the intensity of the

The coupling capacity and the two variable tuning circuits, consisting of coaxial lines, as the symmetrizers, cover the range 100 to 150 MHz (Fig. 3). The movable short-circuiting jumpers can be operated from the exterior.

The input of the π , from which the plates are fed, is coupled to the generator by means of a variable condenser called « direct coupling » and, by regul-

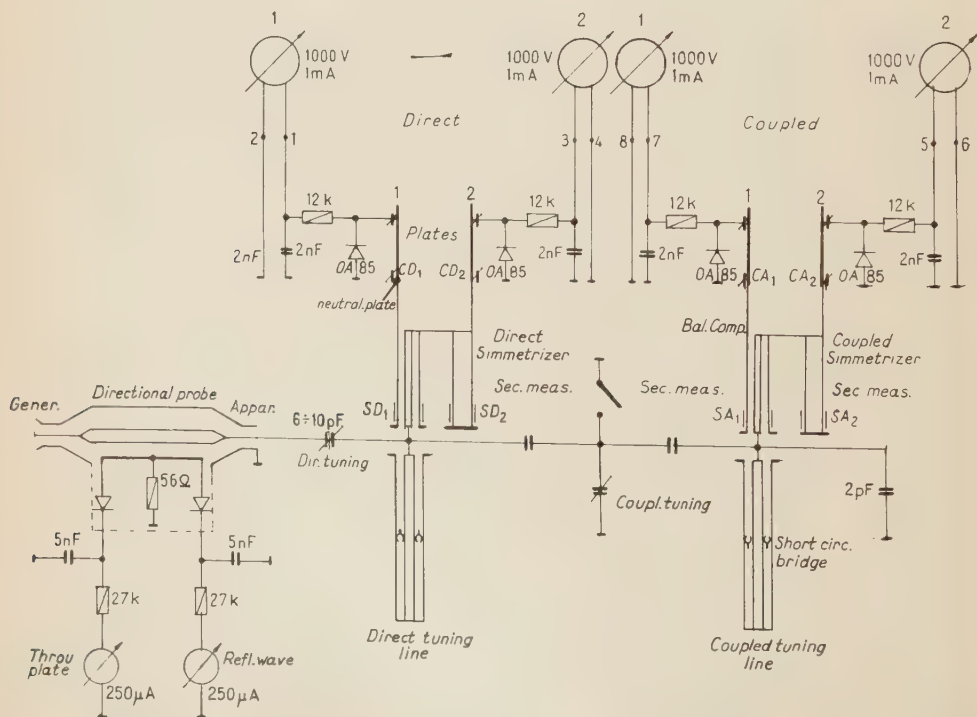


Fig. 3.

reflected waves, which minimum is reported by the corresponding instrument in the directional probe placed at the input of the rotating field generator. Directional probes operate on the principle of the summing and subtracting of two induced voltages, respectively from the electric field, on a length of wire running parallel to the cable along which alternating current runs. The voltages are either in phase or in opposition according to whether the wire runs in the generator-to-load way or in the opposite direction. By operating in such a way that the two component tensions, the capacitive and the inductive, have equal absolute values, and by rectifying separately the two resultants obtained on two lengths of wire of the same length but having opposite sense, from one an indication will be obtained which is in proportion to the progressive current or tension, and from the other the indication will be zero in the only case when there is no reflected power. Therefore any indication of this latter instrument is a reflection index, which means that it indicates a non-accommodation of the load with respect to the $60\ \Omega$ of the present case, through which impedance the generator feeding the instrument can convey the maximum power.

The voltage on the individual plates is revealed by four instruments (Direct 1, Direct 2, Coupled 1, Coupled 2) fed by capacitive probes set up against the plates themselves. Mechanical dissymmetries that result in an unbalancing of these tensions may be counterbalanced by means of compensators connected to the plates and operated from the exterior (balanced compensators CD_1 , CD_2 , CA_1 , CA_2).

The same dissymmetries are the origin of undesirable couplings between the two couples of plates and the respective symmetrizers. Such couplings may be neutralized by means of special, orientable, neutralizing small plates.

To reveal the phase shift of the voltages a phase bridge operates see (Fig. 4a). The measuring secondaries SD_1 , SD_2 , SA_1 , SA_2 consist in lengths of tubes placed outside the symmetrizer lines from which they are insulated (Fig. 3).

The warm ends are connected to each other by means of diodes as in Fig. 4a; loads are connected to the cold ends. Observing Fig. 4b, it is evident that being the two voltages SA_2 and SA_1 equal, the points α and β , which result from the coupled composition of the voltages, will be equipotential only if SD_2 is dephased by 90° with respect to SA_1 and SA_2 . Should this condition not be fulfilled (Fig. 4c), between α and β there shall be a voltage difference equal to the difference between the two resultants, that shall be revealed by

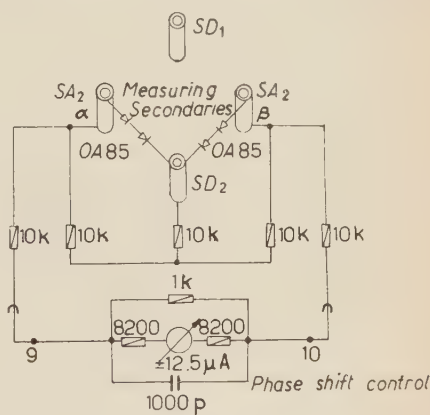


Fig. 4a).

the resulting indication on the central zero instrument (control-wattless). The tuning of the two lines in terms of the frequency was obtained by changing the position of the short-circuiting bridges.

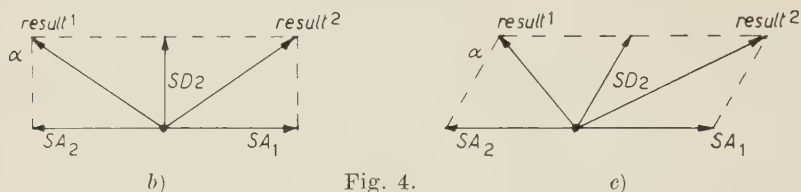


Fig. 4.

Fig. 5 represents the diagrams of the coupled line (A) and of the direct line (D) which give us the position of the bridges in connection with the frequency.

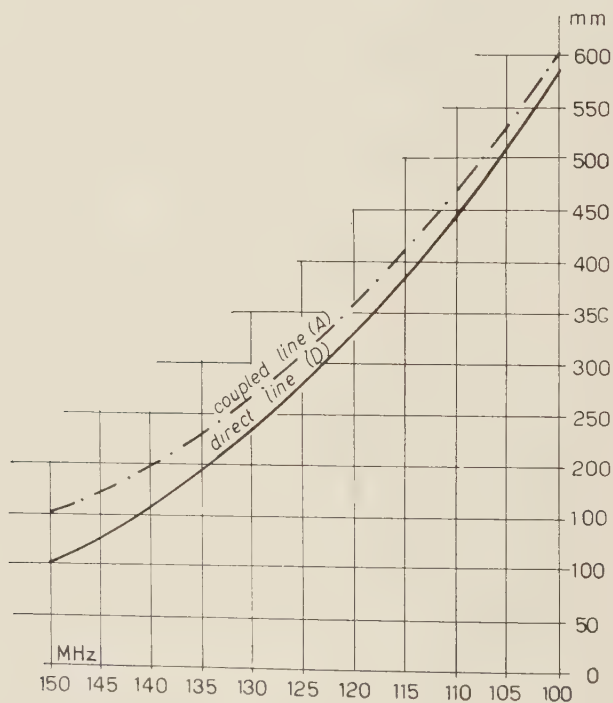


Fig. 5.

In order to determine the phase between the component fields that are formed between opposite plates A_1A_2 and D_1D_2 of the generator (Fig. 6) a small rotating spiral probe was inserted in the center of the four plates of the generator of the electrical rotating field (Fig. 7). The voltages applied between A_1 and A_2 and between D_1 and D_2 give rise to two solenoidal fields (Fig. 6).

The vector of the field (electric, magnetic) resulting in the space contained by $A_1A_2D_1D_2$ is a function of the phase between the vectors of the component fields. On a plane at right angles with the plates, in a general direction forming an angle α with the centerline of the fields D_1D_2 , taken as reference, the intensity X of the field (say electric) is given by the equation

$$(2) \quad X = I\sqrt{1 + 2 \sin \alpha \cos \alpha \cos \varphi},$$

where $(0 \leq \alpha \leq \pm 90^\circ)$ and φ is the angle of the phase $(0 \leq \varphi \leq \pm 90^\circ)$ of the field A_1A_2 referred to the zero phase of the field D_1D_2 and I is the intensity of the individual component fields which is thought to be equal for the two. Relation (2) is represented in Fig. 8 as function of α for the different values of parameter φ . It is therefore evident that the circular rotating field is obtained when $\varphi = 90^\circ$; and as a consequence, relation (2) becomes $X_{\varphi=90^\circ} = I$ (for each value of α).

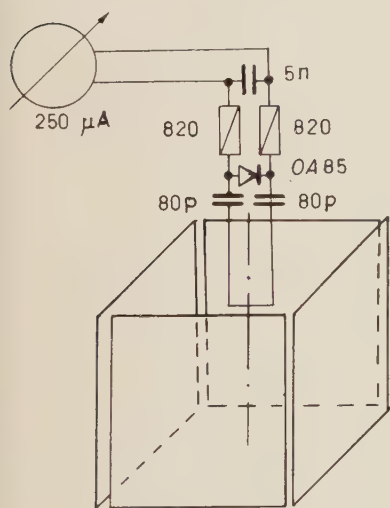


Fig. 7.

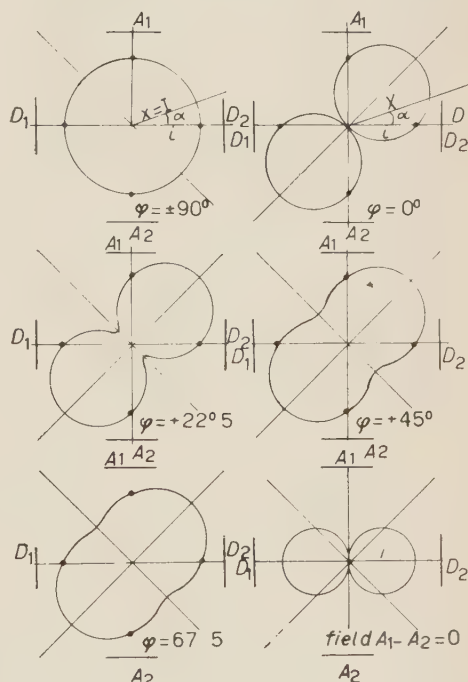


Fig. 8.

When $\varphi \neq 90^\circ$ the field presents maximums and minimums in correspondence with the diagonals ($\alpha = \pm 45^\circ$) in which the relation (2) stands for

$$(4') \quad X_{\max} = X_{\alpha=+45^\circ} = I\sqrt{1 + \cos \varphi}; \quad X_{\min} = X_{\alpha=-45^\circ} = I\sqrt{1 - \cos \varphi}.$$

The ratio K between a maximum and the corresponding minimum for a given φ is

$$(5) \quad K = \sqrt{\frac{1 + \cos \varphi}{1 - \cos \varphi}}$$

From eq. (5), and knowing the maximum and minimum values of the field, (on which the two diagonals exist) it is possible to come back to the phase displacement between the components of the field itself or of the voltages producing it.

Equation (5) is represented in Fig. 9 when φ has a value between 45° and 90° .

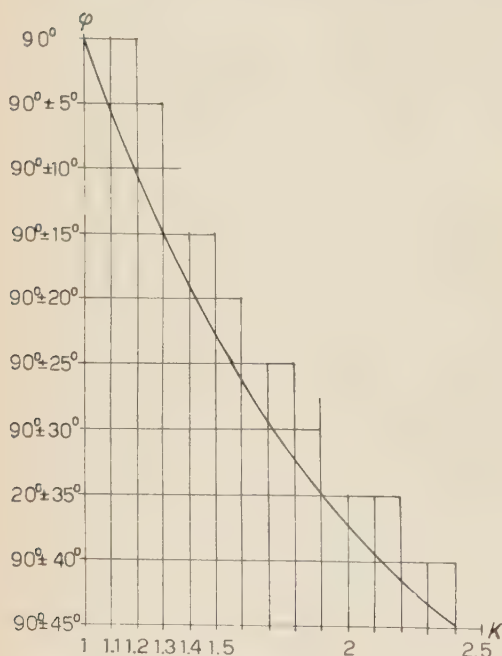


Fig. 9.

For φ an indication has been used that immediately gives to difference of the two wattless voltages.

The knowledge of the maximum and minimum values is obtained by means of the small flat spiral probe having its center of rotation in correspondence with the symmetry center of the plates.

The spiral is situated within an electrostatically shielded cage and therefore responds only to the magnetic field that surrounds it more or less according to the orientation of the spiral itself. The voltage, which is induced in it, rectified and filtered, is conveyed to an instrument which, using the same indication, gives a relative measurement of the field in the various directions.

In order to determine the phase between the fields it is therefore necessary: to determine the values of the two maximums and of the two minimums within a 360° angle of the probe; to calculate the average of the maximums and that of the minimums (in order to compensate as much as possible for errors in symmetry); to calculate the ratio $K = \text{average of maximums} / \text{average of minimums}$ and from Fig. 9 it is possible to note the corresponding phase displacement angle between the two voltages « direct and coupled ».

The value of the voltage difference of radiofrequency applied to the opposite plates, at the distance of 9.0 cm from each other, for the generation

of the rotating electric field, was of approximately 240 V. It was necessary to apply a low voltage difference because with higher voltage differences it was discovered that during the time necessary to carry out the measurements of the rotation momentum (about six minutes) there was an increase of about 1 °C in the temperature, due to dielectric hysteresis, that resulted in an instability of the deviation.

The liquids examined are the following: amyl alcohol, distilled water, toluol, nitro-benzol, isopropyl alcohol and acet acid. The values of the viscosity coefficient η , obtained by comparing the experimental rotational momentum with that given by the Born formula—in which M is substituted by the values of the electric momentum measured in the Debye polarization processes—are comparatively in agreement with those obtained through classical methods.

The relation between the values of η , measured with the two different methods does not exceed, for most of the liquids examined, the value of 2. Only in the case of nitrobenzol a remarkably higher ratio was found. This might point out an effective difference at frequency of η (supposing M is constant).

TABLE I. — *Values of the ratios L_s/L_t .*

Liquids	100.0 MHz	120.0 MHz	150.0 MHz
	L_s/L_t	L_s/L_t	L_s/L_t
Amyl alcohol	$7.0 \cdot 10^{-1}$	$7.6 \cdot 10^{-1}$	$7.8 \cdot 10^{-1}$
Ethyl alcohol	$5.7 \cdot 10^{-1}$	$5.2 \cdot 10^{-1}$	$4.6 \cdot 10^{-1}$
Metyl alcohol	$10.1 \cdot 10^{-1}$	$11.1 \cdot 10^{-1}$	$10.0 \cdot 10^{-1}$
Isopropil alcohol	$10.4 \cdot 10^{-1}$	$10.4 \cdot 10^{-1}$	$12.5 \cdot 10^{-1}$
Acetic acid	$12.4 \cdot 10^{-1}$	$12.5 \cdot 10^{-1}$	$12.3 \cdot 10^{-1}$
Nitrobenzene	$3.6 \cdot 10^{-2}$	$3.4 \cdot 10^{-2}$	$3.2 \cdot 10^{-2}$
Toluol	$25.8 \cdot 10^{-1}$	$29.5 \cdot 10^{-1}$	$32.6 \cdot 10^{-1}$
Distilled water	$3.7 \cdot 10^{-1}$	$4.6 \cdot 10^{-1}$	$4.2 \cdot 10^{-1}$

In Table I are reported the values of the ratios between the rotational momenta (L_s) obtained experimentally for the various liquids used, at frequencies of 100.0; 120.0 and 150.0 MHz, and the calculated rotational momenta (L_t).

In Figs. 10 and 11 are noted the logarithm curves of the momenta L_s and L_t in relation to the frequencies logarithms, while in Fig. 12 are reported the

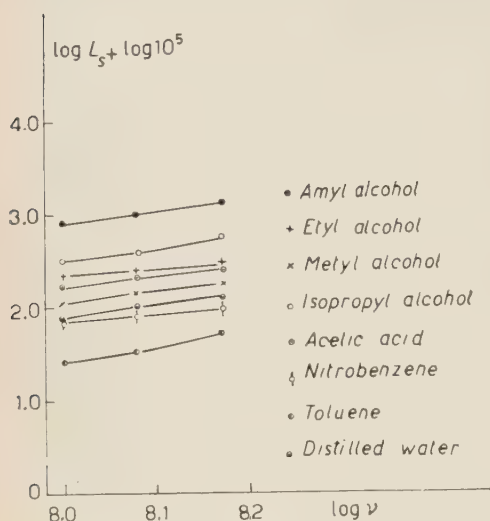


Fig. 10.

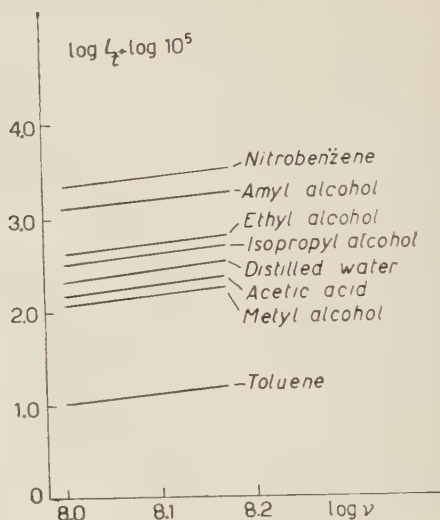


Fig. 11.

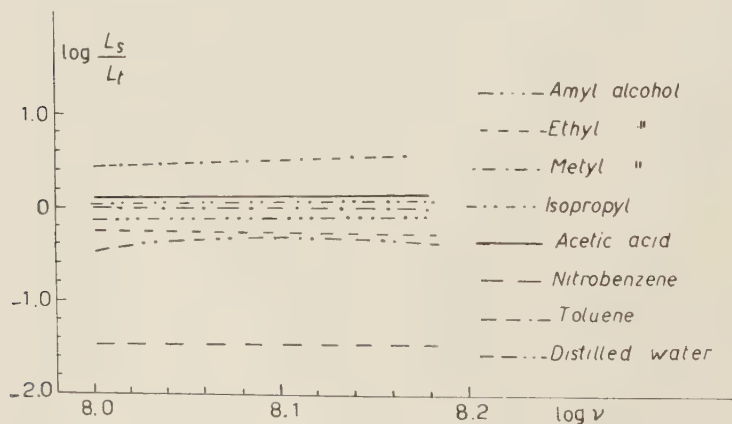


Fig. 12.

logarithms of the ratios between L_s and L_t of the various liquids as the frequency varies.

* * *

We owe thanks to Prof. A. CARRELLI, Director of the Institute, for the advice he gave and for the interest he took in the work. We are also indebted to the Directors of the Technical Office of the Italian Radio and Television who designed and built the electric rotating field generator.

RIASSUNTO

In lavori precedenti sono stati determinati i valori dei momenti di rotazione per alcuni liquidi polari in campi elettrici rotanti per frequenze da 0.325 a 8.5 MHz e da 8.5 a 23.0 MHz. In questo lavoro si riportano i valori dei momenti di rotazione per alcuni liquidi polari (toluene, nitrobenzene, alcool etilico, alcool amilico, alcool metilico, acqua distillata, acido acetico) posti in campi elettrici rotanti a frequenze molto più elevate, e cioè di 100.0; 120.0; 150.0 MHz allo scopo di poter determinare, in modo completamente diverso, il coefficiente di viscosità. I valori ottenuti per il coefficiente di viscosità η , confrontando il momento di rotazione sperimentale con quello dato dalla formula di Born, quando in essa si sostituiscono ad M i valori del momento elettrico misurati nei processi di polarizzazione di Debye, sono relativamente in accordo con quelli che si deducono con i metodi classici.

Invariants of General Relativity (*).

I. — Canonical Formalism.

A. PERES

Department of Physics, Israel Institute of Technology - Haifa

(ricevuto il 24 Marzo 1960)

Summary. — It is shown that, if the Einstein equations are satisfied, the gravitational field invariants must be functions of the Dirac canonical variables only. It is further shown that the non-canonical variables $g_{0\mu}$ can be *explicitly* expressed as functions of the canonical ones (and their first time derivatives) and therefore can be eliminated from the Einstein equations.

The Quantum Theory of Gravitation has hitherto been pioneered along two main lines of approach: the canonical formalism of Dirac ^(1,2) and the method of field invariants of Bergmann and his co-workers ⁽³⁻⁷⁾. The purpose of this paper is to show that both methods are intimately connected because, if the Einstein gravitational equations are satisfied, the field invariants must

(*) Partly supported by the U. S. Air Force, through the European Office of the Air Research and Development Command.

(1) P. A. M. DIRAC: *Proc. Roy. Soc., A* **246**, 333 (1958).

(2) P. A. M. DIRAC: *Phys. Rev.*, **114**, 924 (1959).

(3) P. G. BERGMANN: *Nuovo Cimento*, **3**, 1177 (1956).

(4) P. G. BERGMANN: *Helv. Phys. Acta Suppl.*, **4**, 79 (1956).

(5) E. NEWMAN and P. G. BERGMANN: *Rev. Mod. Phys.*, **29**, 443 (1957).

(6) A. KOMAR: *Phys. Rev.*, **111**, 1182 (1958).

(7) P. G. BERGMANN and A. B. KOMAR: *Status report on the quantization of the gravitational field* (preprint, 1960).

be functions of the canonical variables ⁽⁸⁾ only ⁽⁹⁾. As a consequence we shall be able to eliminate the non-canonical variables $g_{0\mu}$ from the Einstein equations, and thereby to write these equations in terms of the CV and their first time derivatives only.

The bridge between both methods is the Cauchy problem for General Relativity: it is well known ⁽¹⁰⁾ that a convenient set of Cauchy's data on a hypersurface $x^0 = \text{const.}$ consists ⁽¹¹⁾ in the six g_{mn} and six $g_{mn,0}$. From them, it is possible to *compute* the four $g_{0\mu}$ on this hypersurface, while the time derivatives of $g_{0\mu}$ remain completely undetermined, corresponding to the possibility of arbitrary co-ordinate transformations outside this hypersurface.

As these Cauchy data completely determine the *physical* situation, they must be sufficient to compute all the field invariants on the hypersurface. These invariants can therefore be functions ⁽⁹⁾ of the g_{mn} , their canonical momenta ⁽¹⁾ p^{mn} and (until proof of the contrary) of the $g_{0\mu}$, but *not* of the $g_{0\mu,0}$. Let I be such an invariant and let us consider

$$J = g^{\mu\nu} I_{,\mu} I_{,\nu}.$$

Obviously, J is also an invariant.

Following DIRAC ⁽¹⁾ let us define

$$e^{mn} = g^{mn} - (g^{0m} g^{0n} / g^{00}),$$

so that $e^{mn} g_{ns} = \delta_s^m$: Thus e^{mn} is a function of the CV only, and one can write J as

$$(1) \quad J = e^{mn} I_{,n} I_{,n} + g^{00} (I_{,0} - e^{mn} g_{0m} I_{,n})^2.$$

Now J , being an invariant, must be independent of $g_{0\mu,0}$. This implies that I must be independent of $g_{0\mu}$. We have thus proved that, if the Einstein gravitational equations are satisfied, *all the field invariants must be functions of the CV only* ⁽⁹⁾.

⁽⁸⁾ Hereafter referred to as CV.

⁽⁹⁾ Throughout this paper, it will be understood that the phrase « A is a function of B » means that A depends on B and its *spatial* derivatives, but not on the *time* derivatives of B .

⁽¹⁰⁾ A. PERES and N. ROSEN: *Nuovo Cimento*, **13**, 430 (1959).

⁽¹¹⁾ Latin indices run from 1 to 3, Greek indices from 0 to 3.

In particular J , being an invariant, must be independent of the $g_{0\mu}$, so that for any invariant I one must have, from eq. (1),

$$(2) \quad I_{,0} = e^{mn} g_{0m} I_{,n} + A(g^{00})^{-\frac{1}{2}},$$

where A depends on the CV only ⁽⁹⁾.

The two theorems that have just been proved are extremely useful for the practical computation of the invariants and their corresponding A 's, as functions of the CV. As the final result is independent of the $g_{0\mu}$, one may arbitrarily take, from the beginning, $g_{00} = 1$ and $g_{0k} = 0$, thus saving an enormous amount of computational labour.

Let us now consider eq. (2) and take in turn four independent ⁽¹²⁾ invariants, $I^{(\lambda)}$ say ⁽¹⁵⁾. One can then solve (2) for $(g^{00})^{-\frac{1}{2}}$ and g_{0m} as functions ⁽⁹⁾ of the CV and the first derivatives of the $I^{(\lambda)}$. The $I^{(\lambda)}$, however, are functions ⁽⁹⁾ of the CV, so that one may obtain $(g^{00})^{-\frac{1}{2}}$ and the g_{0k} as linear homogeneous functions of the first time derivatives of the CV, the coefficients being known functions ⁽⁹⁾ of the CV themselves.

Substituting these results into the Hamiltonian form ⁽²⁾ of the Einstein equations, one obtains them in terms of the g_{mn} , $g_{mn,0}$, p^{mn} , $p^{mn}_{,0}$ and their spatial derivatives only. As the Hamiltonian ⁽²⁾ is linear in $(g^{00})^{-\frac{1}{2}}$ and g_{0k} , the resulting equations are linear in $g_{mn,0}$ and $p^{mn}_{,0}$, and by a proper choice ⁽¹²⁾ of the invariants $I^{(\lambda)}$, may contain no higher than third derivatives of $p^{mn}_{,0}$ and fourth derivatives of $g_{mn,0}$.

These twelve equations form a highly redundant set, as they are subject to eight identities: these are the four Bianchi identities, which express the fact that $T^0_{\mu,0} = 0$ if $T^{\nu}_{\mu} = 0$ on the initial hypersurface, and four other (still unknown) identities which are necessary in order to maintain general covariance (*i.e.* the possibility of arbitrary co-ordinate transformations outside the initial hypersurface, in spite of the elimination of the four arbitrary functions $g_{0\mu}$).

Thus, there remain only four independent CV, corresponding to the two

⁽¹²⁾ For a given metric, it is not always possible to find four invariants which are functionally independent, *e.g.* when there exists a group of motions ⁽¹³⁾. However, we here consider the invariants not as functions of the coordinates, but as functions of the CV, so that it is always possible to find four functionally independent invariants, *e.g.* the Witten curvature invariants ⁽¹⁴⁾, which include no higher than first derivatives of p^{mn} and second derivatives of g_{mn} .

⁽¹³⁾ A. KOMAR: *Proc. Nat. Acad. Sci.*, **41**, 758 (1955).

⁽¹⁴⁾ L. WITTEN: *Phys. Rev.*, **113**, 357 (1959).

⁽¹⁵⁾ Bracketed indices are enumerators.

degrees of freedom of the field ⁽¹⁶⁾. How to find these independent CV without impairing the general covariance by co-ordinate conditions ⁽¹⁷⁾ is a hitherto unsolved problem ⁽¹⁸⁾.

⁽¹⁶⁾ J. L. ANDERSON: *Phys. Rev.*, **110**, 1197 (1958).

⁽¹⁷⁾ R. ARNOWITT, S. DESER and C. W. MISNER: *Phys. Rev.*, **117**, 1595 (1960) and **118**, 1100 (1960).

⁽¹⁸⁾ Since this paper was submitted for publication, some similar results were obtained by P. G. BERGMANN and A. KOMAR: *Phys. Rev. Lett.*, **4**, 432 (1960).

RIASSUNTO (*)

Si mostra che, se le equazioni di Einstein sono soddisfatte, gli invarianti del campo gravitazionale devono essere funzioni delle sole variabili canoniche di Dirac. Si mostra inoltre che le variabili non canoniche $g_{0\mu}$ possono essere espresse esplicitamente come funzioni di quelle canoniche (e delle loro prime derivate temporali) e quindi possono essere eliminate dalle equazioni di Einstein.

(*) Traduzione a cura della Redazione.

In the case of general relativity, the simplest canonical transformation consists in choosing as new co-ordinates any four invariants of the metric ⁽²⁾, the Jacobian of which with the old co-ordinates does not vanish. If no such four invariants exist, (i.e. if any four invariants are functionally dependent) the metric admits a group of motions ⁽³⁾ and there must exist one or more Killing vector fields. The problem of deciding whether two such metrics are equivalent is much more complicated. However, its theoretical importance is generally minimized, as such metrics represent a set of zero measure ⁽⁴⁾ among all possible gravitational fields.

In the present paper, we shall restrict ourselves to the construction of those invariants that can be derived from the Riemann curvature tensor by algebraic and/or differential operations. Following the method of Pirani ⁽⁴⁾ we shall use the algebraic properties of the Riemann tensor in order to define, at each point of space-time, in an invariant fashion, a tetrad of orthonormal vectors. The *physical components* ^(4,5) of the Riemann tensor and of its covariant derivatives of all orders, with respect to this invariantly defined tetrad, obviously are invariants of the gravitational field.

2. - Mathematical preliminaries.

The task that has just been proposed is greatly simplified by means of an isomorphism existing between the Lorentz group for *real* antisymmetric tensors, and the three-dimensional rotation group for *complex* vectors.

Let A_{mn} be a real covariant four-dimensional antisymmetric tensor. Its dual B_{mn} is defined by

$$B_{mn} = \frac{1}{2} g^{\frac{1}{2}} \eta_{mnsr} A^{sr},$$

where g is the determinant of the g_{mn} , and $\eta_{mnsr} = -1$ if $mnsr$ is an even permutation of 0123, $\eta_{mnsr} = +1$ if $mnsr$ is an odd permutation of 0123, and $\eta_{mnsr} = 0$ if any two indices are equal.

It may easily be checked that the dual of B_{mn} is A_{mn} , so that duality is a symmetric property. The tensor

$$C_{mn} = A_{mn} - \frac{1}{2} g^{\frac{1}{2}} \eta_{mnsr} A^{sr}$$

(2) A. KOMAR: *Phys. Rev.*, **111**, 1182 (1958).

(3) A. KOMAR: *Proc. Nat. Acad. Sci.*, **41**, 758 (1955).

(4) F. A. E. PIRANI: *Phys. Rev.*, **105**, 1089 (1957).

(5) F. A. E. PIRANI: *Acta Phys. Pol.*, **15**, 389 (1956).

(6) F. A. E. PIRANI: *Bull. Acad. Pol. Sci.*, **5**, 143 (1957).

is called self-dual. Note that as A_{mn} is real, and $g^{\frac{1}{2}}$ purely imaginary, one can easily obtain A_{mn} if C_{mn} is known.

We suppose henceforth that the metric is locally Minkowskian, at the point under consideration. This may be obtained by the use either of a locally geodetic system of co-ordinates, or of the physical components^(5,6) of the tensor under consideration. We choose the signature of the metric as $(+---)$ and take $g^{\frac{1}{2}} = i$.

Let now A_{mn} and B_{mn} be self-dual tensors, and let us define

$$A_I = A_{23} = A^{23} = iA^{01} = -iA_{01},$$

with similar definitions for A_{II} and A_{III} , as well as for B_{μ} . (Greek indices will take the values I, II and III). It may easily be checked that

$$(1) \quad A_{\mu} B_{\mu} = \frac{1}{4} A_{mn} B^{mn}.$$

This expression is a *scalar*. The lengths and angles of the «vectors» A_{μ} and B_{μ} are therefore invariant under Lorentz transformations of A_{mn} and B_{mn} . It thus follows that to each Lorentz transformation of A_{mn} , there corresponds an ordinary rotation (three dimensional orthogonal transformation) of A_{μ} .

Indeed, it is easily found that if

$$A_{m'n'} = a_{m'}^m a_{n'}^n A_{mn},$$

it follows

$$A_{\mu'} = a_{\mu'}^{\mu} A_{\mu},$$

where, *e.g.*,

$$(2) \quad a_I^I = a_2^2 a_3^3 - a_2^3 a_3^2 + i a_2^0 a_3^1 - i a_2^1 a_3^0.$$

One notes that the a_m^m have six arbitrary real components, while the $a_{\mu'}^{\mu}$ have three arbitrary *complex* components, as one should expect. It is easily found, with the help of (2) that a *real* rotation in the II-III plane corresponds to the same real rotation in the 23 plane, while a purely imaginary rotation in the II-III plane corresponds to a Minkowski «rotation» in the 01 plane. Obviously, both operations commute.

We shall later need the four dimensional analogs of the invariant tensors $\delta_{\mu\nu}$ and $\eta_{\mu\nu\sigma}$ of the auxiliary three-dimensional space. The unit tensor $\delta_{\mu\nu}$ is defined, as usual, by $A_{\mu} \delta_{\mu\nu} = A_{\nu}$. There corresponds to it, in Minkowski space, a tensor δ_{mnst} , self-dual in mn and in st , and symmetric in $(mn) \leftrightarrow (st)$. In order to keep the analogy with equation (1), one wishes to have

$$A_{mn} = \frac{1}{4} \delta_{mnst} A^{st},$$

whence it follows that

$$(3) \quad \delta_{mnst} = g_{ms}g_{nt} - g_{mt}g_{ns} + g^{\frac{1}{2}}\eta_{mnst}.$$

We now turn to $\eta_{\mu\nu\rho}$. The vector product of A_ν and B_ρ is

$$C_\mu = \eta_{\mu\nu\rho} A_\nu B_\rho,$$

e.g.,

$$C_I = A_{II}B_{III} - A_{III}B_{II}.$$

It may easily be checked that this corresponds, in Minkowski space, to

$$(4) \quad C_{mn} = \frac{1}{2}(A_m^s B_{sn} - A_n^s B_{sm}).$$

Obviously, C_{mn} is also self-dual.

3. - Algebraic invariants of the Weyl tensor.

Following GÉHÉNIAU and DEBEVER⁽⁷⁾, we split the Riemann tensor R_{mnst} into two algebraically independent parts, which are the Ricci tensor

$$R_{mn} = R^s_{mns},$$

and the Weyl tensor

$$(5) \quad S_{mnst} = R_{mnst} + \frac{1}{2}(g_{ms}R_{nt} + g_{nt}R_{ms} - g_{mt}R_{ns} - g_{ns}R_{mt}) - \frac{1}{6}R(g_{ms}g_{nt} - g_{mt}g_{ns}).$$

The Weyl tensor has all the well known symmetries of the Riemann tensor, and further satisfies the ten identities $S^k_{mnk} \equiv 0$. It follows that R_{mn} and S_{mnst} each have ten independent components.

From S_{mnst} one can construct the twice self-dual tensor

$$(6) \quad Q_{mnst} = \frac{1}{2} [S_{mnst} + \frac{1}{2}g^{\frac{1}{2}}(\eta_{mnab}S^{ab}_{st} + S^{ab}_{mn}\eta_{abst}) + \frac{1}{4}g\eta_{mncb}S^{abcd}\eta_{cdst}],$$

to which there corresponds, in the three-dimensional auxiliary space, a *symmetric tensor* $Q_{\mu\nu}$, which satisfies

$$(7) \quad Q_{\mu\mu} = 0.$$

$Q_{\mu\nu}$ thus has five independent complex components, corresponding to the ten independent real components of S_{mnst} .

(7) J. GÉHÉNIAU and R. DEBEVER: *Helv. Phys. Acta Suppl.*, **4**, 101 (1956).

The problem now consists in finding a local Lorentz transformation (or, if one prefers, a suitable rotation of the local tetrad) such that $Q_{\mu\nu}$ will take some canonical form. Such a problem is rather unfamiliar to the theoretical physicist, who is accustomed to deal with the diagonalization of *hermitian* matrices, while here $Q_{\mu\nu}$ is a *complex-symmetric* matrix, and the allowed transformations are now *complex-orthogonal*, rather than *unitary*.

The various cases which may occur have been classified by PETROV ^(8,9), according to the reducibility properties of $Q_{\mu\nu}$.

Class I. The matrix $Q_{\mu\nu}$ is completely diagonalizable. This is always the case if the three roots of the characteristic equation

$$(8) \quad |Q_{\mu\nu} - \lambda \delta_{\mu\nu}| = 0,$$

are different.

With the help of (7), this may be written

$$(9) \quad \lambda^3 + \lambda Z_{\mu\mu} - Q = 0,$$

where

$$Z_{\mu\nu} = \frac{1}{2} \eta_{\mu\pi_2} \eta_{\nu\sigma\tau} Q_{\pi\sigma} Q_{\sigma\tau},$$

is the cofactor of $Q_{\mu\nu}$, and

$$Q = \frac{1}{3} Q_{\mu\nu} Z_{\mu\nu},$$

is the determinant of the $Q_{\mu\nu}$.

With the help of (1) and (4), and of the symmetries of Q_{mnst} , one gets

$$Z_{\mu\nu} \rightarrow Z_{mnst} = \frac{1}{4} (Q_{masb} Q_n^a{}_{t^b} - Q_{nasb} Q_m^a{}_{t^b}),$$

whence

$$(10) \quad Z = Z_{\mu\mu} = \frac{1}{4} Z_{mn}{}^{mn} = -\frac{1}{16} Q_{manb} Q^{namb},$$

and

$$(11) \quad Q = \frac{1}{48} Q^{mnst} Z_{mnst} = \frac{1}{96} Q^{mnst} Q_{masb} Q_n^a{}_{t^b}.$$

The Petrov invariants are the real and imaginary parts of the roots of equation (9). Note that Z and Q are now written in an *invariant* fashion, and thus can be computed without the need of quasi-Galilean co-ordinates, as in Petrov's original work ^(8,9), or tetrads ⁽⁴⁾, or spinors ⁽¹⁰⁾.

⁽⁸⁾ A. Z. PETROV: *Ush. Zap. Kazan Gos. Univ.*, **114**, 55 (1954).

⁽⁹⁾ A. Z. PETROV: *Izv. Vus. Ush. Zav., Math.*, **6**, 226 (1958).

⁽¹⁰⁾ L. WITTEN: *Phys. Rev.*, **113**, 357 (1959).

It thus follows from equation (9) that a given metric always belongs to the first class of Petrov's classification if

$$(12) \quad (Q/2)^2 + (Z/3)^3 \neq 0.$$

We now turn to investigate the case where equation (12) is not fulfilled. Equation (9) then has two identical roots, which will be denoted by C :

$$C = (Q/2)^{\frac{1}{3}} = (-Z/3)^{\frac{1}{3}}.$$

By equation (7), the third root must be $-2C$. We first suppose that $C \neq 0$, and consider

$$(13) \quad P_{\mu\nu} = (C\delta_{\mu\nu} - Q_{\mu\nu})/3C.$$

The eigenvalues of $P_{\mu\nu}$ are 1, 0 and 0, and it is always possible to reduce $P_{\mu\nu}$ to the form

$$P_{\mu\nu} = \begin{pmatrix} 1 & 0 \\ 0 & K \end{pmatrix},$$

where K is a 2×2 matrix, both invariants of which vanish. Such a matrix must have the form

$$K = \begin{pmatrix} u & \pm iu \\ \pm iu & -u \end{pmatrix},$$

where u is any complex number. Note that

$$K^2 = 0.$$

We must now distinguish between two cases. It may occur that $u = 0$. It then follows from (13) that $Q_{\mu\nu}$ can be diagonalized, and thus belongs to the first class of Petrov's classification^(8,9). A necessary and sufficient condition for this case to occur is that

$$P_{\mu\nu}P_{\nu\varrho} = P_{\mu\varrho},$$

which is equivalent to

$$(14) \quad \frac{1}{4}Q_{mnab}Q^{ab}{}_{st} + CQ_{mnst} - 2C^2\delta_{mnst} = 0.$$

Class II. If the latter criterion is not satisfied, the matrix K is irreducible and u may be given any arbitrary (non null) value by a suitable complex rotation in the II-III plane (*i.e.* by rotating the tetrad in the 01 and 23 planes). If the rotation angle is θ , u is multiplied by $\exp[\pm 2i\theta]$. The Weyl tensor then belongs to the second class of Petrov's classification ^(8,9).

We have hitherto supposed that $C \neq 0$. If $C = 0$, $Q_{\mu\nu}$ still belongs to the second class of Petrov's classification if, and only if, it is possible to bring $Q_{\mu\nu}$ to the form

$$Q = \begin{pmatrix} 0 & 0 \\ 0 & K \end{pmatrix}.$$

A necessary and sufficient condition for this case to occur is that

$$Q_{\mu\nu} Q_{\nu\varrho} = 0,$$

or

$$(15) \quad Q_{mnab} Q^{ab}_{st} = 0.$$

Class III. If $C = 0$ but the latter criterion is not satisfied, the matrix $Q_{\mu\nu}$ is completely irreducible, and can always be brought to the following canonical form ⁽¹¹⁾:

$$Q_{\mu\nu} = \begin{pmatrix} 0 & u & 0 \\ u & 0 & \pm iu \\ 0 & \pm iu & 0 \end{pmatrix},$$

whence it follows that

$$Q_{\mu\nu} Q_{\nu\varrho} Q_{\varrho\sigma} = 0,$$

or

$$(16) \quad Q_{mnab} Q^{abcd} Q_{cdst} = 0.$$

The Weyl tensor then belongs to the third class of Petrov's classification ^(8,9). As in the second class, u may be given any arbitrary (non null) value by a suitable rotation in the I-III plane. However, if the angle of rotation is θ , u is now multiplied by $\exp[\pm i\theta]$, rather than $\exp[\pm 2i\theta]$, as previously.

Class IV. For the sake of completeness, we may add a fourth class, defined by $Q_{mnst} = 0$. (If, moreover, $R_{mn} = 0$, space-time is euclidean). However, this fourth class may also be considered as a further degeneracy of the degenerate case of class I, defined by equation (14).

⁽¹¹⁾ F. R. GANTMACHER: *Applications to the Theory of Matrices* (New York, 1959), p. 13.

4. - Extension to the Ricci tensor.

If $R_{mn} \neq 0$, further invariants may be obtained by taking the physical components of this tensor. Several cases must be distinguished, according to the class of Q_{mnst} .

Class I (non-degenerate case). The tetrad which diagonalizes $Q_{\mu\nu}$ (hereafter referred to as the *canonical tetrad*) is uniquely and invariantly defined by the Weyl tensor. The physical components ^(5,6) of R_{mn} , with respect to the canonical tetrad, are therefore ten new invariants. One thus gets a total of fourteen algebraic invariants, as expected ⁽⁷⁾.

Further invariants may be obtained by computing the physical components, with respect to the canonical tetrad, of the covariant derivatives of R_{mnst} .

Class I (degenerate case). The canonical tetrad is only partially defined: it still may be arbitrarily rotated in the 01 and 23 planes. This degeneracy may be removed, *e.g.*, by requiring that the submatrices

$$A = \begin{pmatrix} R_{00} & R_{01} \\ R_{10} & R_{11} \end{pmatrix} \quad \text{and} \quad B = \begin{pmatrix} R_{22} & R_{23} \\ R_{32} & R_{33} \end{pmatrix}$$

be diagonalized. Note that A and B are real symmetric matrices, but there is an important difference between them: while B has to be diagonalized by a rotation through a real angle (an operation which is always possible), A has to be diagonalized by a Lorentz transformation, which is equivalent to require

$$A' = \begin{pmatrix} R_{00} & -i R_{01} \\ -i R_{10} & -R_{11} \end{pmatrix}$$

to be diagonalized by a rotation through a pure imaginary angle. This is possible, however, if and only if

$$\pm R_{01} \neq \frac{1}{2}(R_{00} + R_{11}).$$

It follows that one must distinguish, within the degenerate case of Petrov's class I, several subclasses according to whether A can be diagonalized or not, and to whether A' and/or B eventually may already be multiples of the unit matrix, or even vanish. In such cases, one may further try to reduce the freedom of rotation of the canonical tetrad by imposing some condition on

the submatrix

$$C = \begin{pmatrix} R_{02} & R_{03} \\ R_{12} & R_{13} \end{pmatrix}.$$

If this gives no result, one may try to impose some restrictions on the physical components of the covariant derivatives of R_{mnst} , etc. Obviously, there is no limit to the further refining of Petrov's classification into narrower and narrower subclasses.

Class II. As in the degenerate case of class I, the canonical tetrad still may be arbitrarily rotated in the 01 and 23 planes, so that similar considerations apply also here. There is, however, an important difference. Let us suppose that

$$\pm R_{01} = \frac{1}{2}(R_{00} + R_{11}) = v \neq 0,$$

so that it is impossible to diagonalize the submatrix

$$L = A' - \frac{1}{2}(R_{00} - R_{11}) \begin{pmatrix} 1 & 0 \\ 0 & 1 \end{pmatrix} = \begin{pmatrix} v & \pm iv \\ \pm iv & -v \end{pmatrix}.$$

One sees, however, that L is proportional to the matrix K , defined in the previous section. Furthermore, L and K have the same transformation properties under rotations in the 01 plane. It follows that $|v/u|$ is an invariant. (Only the absolute value of this ratio is invariant, because a rotation in the 23 plane multiplies u by $\exp[\pm 2i\theta]$, but does not affect v .)

This interesting situation will now be illustrated by an example, based on a recent work of the author^(12,13). Let us consider the metric

$$(17) \quad ds^2 = dt^2 - dx^2 - dy^2 - dz^2 - 2f(x, y, z + t) dz dt.$$

The physical components of the Weyl and Ricci tensors are found to be^(12,13)

$$Q_{\mu\nu} = \begin{pmatrix} u & -iu & 0 \\ -iu & -u & 0 \\ 0 & 0 & 0 \end{pmatrix},$$

⁽¹²⁾ A. PERES: *Phys. Rev. Lett.*, **3**, 571 (1959).

⁽¹³⁾ A. PERES: *Phys. Rev.* **118**, 1105 (1960).

and

$$R'_{mn} = \begin{pmatrix} v & 0 & 0 & -iv \\ 0 & 0 & 0 & 0 \\ 0 & 0 & 0 & 0 \\ -iv & 0 & 0 & -v \end{pmatrix},$$

with

$$v = f_{xx} + f_{yy},$$

and

$$u = -(\tfrac{1}{4}v^2 + f_{xy}f_{yx} - f_{xx}f_{yy})^{\frac{1}{2}}.$$

It follows from the above considerations that v/u is an invariant. This fact is here particularly interesting, because all fourteen G  h  niau-Debever invariants vanish for the metric (17).

The existence of the invariant v/u could also have been directly seen from the equation

$$(18) \quad R_{mn}R_{st} = \tfrac{1}{4}(v/u)^2 R^a_{mn}R^b_{sta},$$

which can easily be checked with the help of the formulae given in reference (13). The form of equation (18) shows that v/u is an algebraic function of the components of the Riemann tensor, but not an algebraic *entire* function, as the invariants of G  h  niau and Debever.

Obviously, the occurrence of invariants such as $|v/u|$ is rather exceptional, and it seems to be limited to pure radiation fields (14). Usually, it will then be possible to find additional similar invariants with the help of the covariant derivatives of the Riemann tensor.

Class III. Considerations similar to the above also apply here. The only difference is that a rotation through an angle θ now multiplies u by $\exp[\pm i\theta]$, rather than by $\exp[\pm 2i\theta]$, so that now the new invariant, if it exists, is $v/|u|^2$.

Class IV. As Weyl's tensor vanishes, the canonical tetrad must be de-

(14) L. BEL: *Compt. Rend.*, **246**, 3015 (1958).

terminated by the properties of the Ricci tensor only. We write it as

$$R'_{mn} = \begin{pmatrix} R_{00} & -iR_{01} & -iR_{02} & -iR_{03} \\ -iR_{10} & -R_{11} & -R_{12} & -R_{13} \\ -iR_{20} & -R_{21} & -R_{22} & -R_{23} \\ -iR_{30} & -R_{31} & -R_{32} & -R_{33} \end{pmatrix}$$

and make an attempt to diagonalize it by an *orthogonal-complex* transformation. Four cases have to be distinguished, which we briefly consider:

Subclass IVa. R'_{mn} is completely diagonalizable. If it is non-degenerate, the canonical tetrad is thereby fixed. Otherwise, there remains some freedom which may perhaps be removed by considering the covariant derivatives of R_{mn} .

Subclasses IVb and IVc. R'_{mn} is partially diagonalizable, and can be brought to the form ⁽¹¹⁾

$$R'_{mn} = \begin{pmatrix} A+u & \pm iu & 0 & 0 \\ \pm iu & A-u & 0 & 0 \\ 0 & 0 & B & 0 \\ 0 & 0 & 0 & C \end{pmatrix}$$

or

$$R'_{mn} = \begin{pmatrix} A & \pm iu & 0 & 0 \\ \pm iu & A & u & 0 \\ 0 & u & A & 0 \\ 0 & 0 & 0 & B \end{pmatrix}.$$

A , B and C are invariants, while u can be given any arbitrary real value. These subclasses are similar to Petrov's classes II and III respectively.

Subclass IVd. R_{mn} is completely irreducible. Its canonical form is ⁽¹¹⁾

$$R'_{mn} = \begin{pmatrix} A & u & iu & 0 \\ u & A+iu & u & -iu \\ iu & u & A-iu & u \\ 0 & -iu & u & A \end{pmatrix}.$$

This is, however, impossible, if R_{mn} is real. This last subclass is therefore empty.

APPENDIX

In view of the results of Sect. 4, the question may be raised whether any non-flat metric has at least one invariant that can be constructed from the Riemann tensor. The answer is negative, as may be seen from the following example. Let us consider the metric (17) with $f = \frac{1}{2}(x^2 - y^2)$. It follows that $u = -1$ and $v = 0$. The invariant $v\mu = 0$ is therefore valueless.

We now turn to investigate the covariant derivatives of R_{mnst} , or, what amounts to the same, those of Q_{mnst} . This task may be considerably simplified by noting that in this case one can write $Q_{uv} = Q_\mu Q_\nu$ with $Q_\mu = (i, 1, 0)$. Thus

$$Q_{mnst} = Q_{mn} Q_{st},$$

with

$$Q_{mn} = \begin{pmatrix} 0 & 1 & -i & 0 \\ -1 & 0 & 0 & -1 \\ i & 0 & 0 & i \\ 0 & 1 & -i & 0 \end{pmatrix}.$$

It is now sufficient to consider the covariant derivatives of Q_{mn} . However, a straightforward computation gives $Q_{mn;s} = 0$. Therefore, no invariant can be constructed from the Riemann tensor and its derivatives alone. The question of the existence of other kinds of invariants is still open.

RIASSUNTO (*)

Si generalizza la classificazione di Petrov dei puri campi gravitazionali al caso in cui si ha presenza di materia. Si mostra come gli invarianti di Petrov si possano calcolare direttamente, cioè senza lo stadio intermedio delle coordinate (o tetradi, o spinori) quasi-Galileane, che era richiesto nel lavoro precedente. Si mostra inoltre che se alcuni degli invarianti di G  h  niau e Debever si annullano,   possibile talvolta trovare nuovi invarianti algebrici del tensore di Riemann, che sono indipendenti dagli invarianti di G  h  niau e Debever. Questo fatto   molto interessante nel caso in cui tutti gli invarianti di G  h  niau e Debever si annullano, come si mostra con un esempio.

(*) Traduzione a cura della Redazione.

Imperfections, Lattice Constants and Densities of Cold-Drawn and of Recrystallized Aluminium Wires (*).

M. E. STRAUMANIS and T. EJIMA

*Department of Metallurgy, University of Missouri
School of Mines and Metallurgy, Rolla, Mo.*

(ricevuto il 5 Aprile 1960)

Summary. — Aluminum contains in lesser or larger amounts excess atoms, depending on the kind of mechanical or thermal treatment and on the concentration of trace impurities. The number of excess atoms in a 99.9 % pure recrystallized Al wire is 18 per 10 000 unit cells, and they may be a constituent of the denser segregations. The lattice constant of a cold drawn Al wire in the direction of its axis was slightly smaller ($a_{25}=4.049\,44$) than that of the recrystallized wire ($a_{25}=4.049\,47\text{ \AA}$), but was larger in the transverse direction ($a_{25}=4.049\,63\text{ \AA}$). The thermal expansion coefficient of the recrystallized wire ($\alpha=22.9\cdot 10^{-6}$) between 10 and 60 °C did not differ (significantly) from that of the hard drawn wires. The density of the whole hard wire was $d_{25}=2.700\,4\text{ g/cm}^3$ (core — 2.6989), that of the recrystallized wire was smaller (2.6993 g/cm³). The concentration of interstitials was largest in the outside layers of the wire (at least 4 atoms per 1 000 unit cells or $1.5\cdot 10^{13}$ atoms per cm²). Previous measurements, giving lower densities for cold worked metals, may be explained by the fact that crack and capillary formation during cold work frequently outbalance the effect of density increase due to increase of interstitial atom (blocking dislocation) concentration, created by the process of slipping and deformation. Strain hardening appears then as a consequence of the increasing number of interstitial atoms. The latter processes are in agreement with the theories as discussed by SCHMID and BOAS. From the density decrease of the hard wire (after heating) the volume of submicroscopic fissures per cm³ was estimated: 10^{-4} cm^3 . They may be created by moving dislocations and vacancies (formation of dislocation cracks), during the deformation process. Only both, lattice constant and density measurements of the same material give a correct picture of conditions inside (in terms of n') of a deformed as well as of a recrystallized metal or another crystalline material.

(*) Presented in part by M. E. STRAUMANIS at the University of Rome on April 14 1958, under the title: *Imperfezioni nell'alluminio ricristallizzato e lavorato a freddo e incrudimento.*

1. - Introduction.

Although there is some experimental evidence that the density of cold worked metals is smaller than that of recrystallized ones (^{1,2}), the question is still open because of the following reasons: 1) already TAMMANN (¹) stated that there are metals (Sn, Cu, Cd, Ag, Au) which show little or no decrease of density with cold work, and 2) it appears that the effect of density decrease depends upon the concentration of impurities in the respective metal, *e.g.*, oxygen containing Cu exhibits a much larger decrease in density than the pure metal (³). This may be explained by the frequent increase of the brittleness of metals (because of presence of impurities), which under cold work may develop microscopic cracks (⁴), decreasing the density (⁵). It is probable that heat treatment closes the fissures (^{6,7}) and increases the density (⁸), as *e.g.* observed with nickel (^{9,5}). However, reports on precise density measurements are very rare in the literature.

Aluminium showed one of the largest density decreases with cold work (up to 0.13%) (¹); however at that time (1905, measurements by KAHLBAUM and assoc.) aluminium was not available in a degree of high purity. Therefore, the density measurements were repeated once more (with cold drawn and recrystallized wires), but simultaneously precise lattice parameter determinations were also made. These data give the advantage of estimating the perfection of the Al lattice, in a deformed as well as in a recrystallized state, in terms of the *actual* number of atoms n' per unit cell. n' then can be used to decide upon the processes occurring in the aluminium lattice during cold work.

2. - Materials and methods.

The wires were drawn from aluminium strips (1×1) mm² in cross-section, cut from a sheet (about 1 mm thick) received from the Aluminum Company

(¹) See *e.g.* in G. TAMMANN: *Metallkunde*, 4-th Ed. (Leipzig, 1932), p. 169-172.

(²) W. C. BURGERS, in G. MASING: *Handbuch der Metallphysik* (Leipzig, 1940), vol. 3, 2, p. 101.

(³) J. S. SMART, A. A. SMITH and J. A. PHILIPS: *Am. Inst. M. M. Eng.*, **143**, 272 (1941).

(⁴) N. F. MOTT: *Proc. Roy. Soc.*, A **220**, 1 (1953).

(⁵) A. N. STROH: *Phil. Mag.*, **2**, 1 (1957).

(⁶) M. E. STRAUMANIS and Y. N. WANG: *Corrosion*, **12**, 177, 181 (1956).

(⁷) W. BOAS: in *Dislocations and Mechanical Properties of Crystals*, J. C. FISHER and Assoc. (New York, 1957), p. 342, 346.

(⁸) J. L. SNOEK: *Phil. Mag.*, **41**, 1188 (1950).

(⁹) L. M. CLAREBROUGH, M. E. HARGREAVES and G. W. WEST: *Phil. Mag.*, **1**, 528 (1956), also *Proc. Roy. Soc.*, A **232**, 252 (1955).

of America. According to the analysis supplied with the material, the metal (99.99% pure) contained (in % b.w.): Si-0.0015, Fe-0.0007, Cu-0.0004 and Mg-0.0007.

By drawing the strips through successive holes of a drawing plate (*), which was cooled with ice to avoid heating and recrystallization effects, wires of 0.3 mm in diameter (cold reduction over 90%) were finally obtained. They were stored under dry argon in a refrigerator below 0 °C. For density and always for lattice parameter determinations the wires were etched down with $\frac{1}{2}$ N hydrofluoric acid to a diameter of 0.10 to 0.15 mm in about 2 hours. Then the samples were treated with dilute hydrochloric acid, washed with water, dried in vacuum and inspected under a microscope for cleanliness of the surface.

Some of the wires were recrystallized by heating them at 250, 300 and 350 °C for 15 min to 1 h in vacuum. Then their diameter was reduced by etching.

To determine the soundness of the lattice of the cold drawn and of the recrystallized aluminium, the number of atoms per unit cell, n' , rather than the atomic weight of the aluminium ⁽¹⁰⁾, was calculated. The knowledge of n' as compared with n of the ideal lattice, reveals at once the kind of imperfection present (if $n' > n$ -interstitials, excess atoms, are predominant, if $n' = n$ the lattice may be sound or ideal, and if $n' < n$ -vacancies are predominant). Besides, $n' - n$ gives the concentration of excess imperfections, in atoms or molecules, per unit cell. n' for aluminium was computed from lattice parameter ($v = a^3$ in Å³) and density (d in g/cm³) measurements from

$$(1) \quad n' = v d N_0 / A,$$

where N_0 is the absolute Avogadro's number $[(6.024 03 \pm 0.000 25) \cdot 10^{23} \text{ g mole}^{-1} \text{ chemical scale}]$ ^(11,12) and A the chemical or mass-spectroscopy weight of aluminium.

The lattice constants were determined by the powder method with films in the asymmetric position ⁽¹²⁻¹⁵⁾, gluing the thin wires mentioned above to

(*) Plate F; Joubert, France.

⁽¹⁰⁾ M. E. STRAUMANIS: *Acta Cryst.*, **2**, 83 (1949); *Chimia*, **12**, 136 (1958).

⁽¹¹⁾ M. E. STRAUMANIS: *Phys. Rev.*, **92**, 1155 (1953); **95**, 566 (1954).

⁽¹²⁾ H. P. KLUG and L. E. ALEXANDER: *X-ray Diffraction Procedures* (New York, 1954), p. 454.

⁽¹³⁾ M. STRAUMANIS and A. IEVINŠ: *Die Präzisionsbestimmung von Gitterkonstanten nach der asymmetrischen Methode* (Berlin, 1940). Partial translation by K. E. BEU: Dept. of Commerce, Washington 25, D.C. (1959).

⁽¹⁴⁾ M. E. STRAUMANIS: *Journ. Appl. Phys.*, **20**, 726 (1949).

⁽¹⁵⁾ M. E. STRAUMANIS: *Analyt. Chemistry*, **25**, 700 (1952).

the tip of the sample holder of the powder camera 64 mm in diameter. To secure smooth diffraction lines especially of the recrystallized samples, they were not only rotated but also scanned⁽¹⁶⁾ in the camera. Furthermore, to check the uniformity of the temperature expansion of the distorted aluminium lattice, and to observe whether it changes its dimensions as a result of recovery from the strained condition, powder patterns were made at constant temperatures of the sample in the range between 10.0 to 60.0 °C in increments of 10.0 °C⁽¹²⁻¹⁴⁾, starting with the lowest temperature of (10 ± 0.02) °C.

Two kinds of powder patterns with the hard wire were made: with the fiber axis (drawing direction) parallel and perpendicular to the axis of rotation of the sample. The latter kind pattern was obtained with samples prepared as follows: hard aluminium wires (0.3 mm in diameter) were drawn into slightly smaller holes drilled vertically in a thin cellophane sheet. The emerging ends of the wires on both sides of the sheet were cut-off with a sharp blade and then the sheet was slowly ground down on both sides with 3/0 emery paper, which was copiously impregnated with oil. With the sheet reduced to about 0.2 mm, the whole was etched with a $\frac{1}{2}$ N HF solution for 15 minutes. The acid attacked the exposed ends of the wire etching down the ~ 0.3 mm discs to a thickness of less than 0.12 mm. After dissolution of the cellophane in acetone, the tiny aluminum discs remained, one of which was glued to a glass hair mounted to the tip of a small goniometer head⁽¹⁷⁾. In all cases Cu-radiation ($\lambda K\alpha_1 = 1.537395 \times 1.00202$ Å) was used, and the lattice constant was calculated from the last line 27 ($333\alpha_1$)⁽¹⁸⁾. This line is here insofar significant as slip during cold work occurs along the (111)-planes and thus the spacings between them (in terms of a -constants) parallel and perpendicular to the drawing direction could be directly measured.

Only the refraction correction was applied⁽¹⁹⁾. Corrections for absorption, e.g. using the Nelson and Riley function^(20,21), are unnecessary in case of thin samples and they were disregarded⁽²²⁾. Besides, all the samples had nearly the same diameters.

For density determinations the very surface layer of the recrystallized and of the hard drawn wires was removed by slight etching in HF. Densities of the cores were found by etching the surface layer down up to a core of about 0.10 mm in diameter. The determinations were made by a modified suspension

(16) M. E. STRAUMANIS: *Rev. Scient. Instr.*, **22**, 843 (1951).

(17) M. E. STRAUMANIS and C. H. CHENG: *Inst. Metals*, **88**, 287 (1959-60).

(18) M. E. STRAUMANIS: *Zeits. f. Kristallogr.*, **104**, 167, 173 (1942).

(19) M. STRAUMANIS: *Acta Cryst.*, **8**, 654 (1955).

(20) J. B. NELSON and D. F. RILEY: *Proc. Phys. Soc.*, **57**, 160 (1945).

(21) L. V. AZÁROFF and M. J. BUEGER: *The Powder Method* (New York, 1958).

p. 231, 238.

(22) M. E. STRAUMANIS: *Journ. Appl. Phys.*, **30**, 1965 (1959).

method⁽²³⁾, using for that mixtures of heavy liquids, *e.g.* tetrabromoethane or bromoform with carbon tetrachloride or benzene. The density of such a liquid was determined (by weighing the pycnometer) in which the aluminium wire stood suspended for 10 minutes, as observed through an optical device. The temperature of the bath was controlled with a precision of $\pm 0.01^\circ\text{C}$; the temperature readings and the weighings were made with thermometers and weights calibrated by the U.S. Bureau of Standards. All the weighings were carried out in the same manner and were reduced to vacuum.

The densities of the various samples differed only slightly, as did the lattice parameters measured. Therefore, to attain reliable results, a series of measurements for each determination was necessary. The final value was calculated by the method of least squares. In order to find whether a small difference is still significant, the standard deviation of the respective measurements was computed⁽²⁴⁾. In case of n' calculation (eq. (1)) the accidental error due to error propagation was found from the equation^(23,25)

$$(2) \quad \Delta n'/n' = \pm [(\partial N_0/N_0)^2 + 3(\partial a/a)^2 + (\partial d/d)^2 + (\partial A/A)]^{\frac{1}{2}}.$$

$\partial N_0/N_0$, $\partial a/a$ etc., are the relative errors determined from the measurements of the respective quantities.

3. - Results.

3.1. Lattice parameter and soundness of recrystallized Al wires. -

Lattice parameters. The recrystallization temperature of aluminium depends upon its purity⁽²⁶⁾. On our X-ray patterns the first signs of crystallization were observed with wires annealed above 175° . However, only wires annealed at 300°C for 15 minutes showed the most distinctive X-ray lines and a complete recrystallization (longer annealing gave spotty patterns).

In Table I, the lattice parameters obtained at 6 different temperatures are given. They were reduced to a temperature of 25°C , using an expansion coefficient calculated from the average values of lattice parameters at various temperatures between 10 and 60°C . The refraction correction⁽¹⁹⁾ was added to the final 25° -value of the constant.

⁽²³⁾ M. E. STRAUMANIS: *Amer. Mineralog.*, **38**, 662 (1953).

⁽²⁴⁾ Y. BEERS: *Theory of Error* (Cambridge, Mass., 1953).

⁽²⁵⁾ M. E. STRAUMANIS: *Chimia*, **12**, 136, 140 (1958).

⁽²⁶⁾ J. C. BLADE, J. W. H. CLARE and H. J. LAMB: *Acta Met.*, **7**, 136 (1959); see also J. CALVET, J. J. TRILLAT and M. PAID: *Compt. Rend.* (1935), p. 426.

TABLE I. — Lattice parameter of a recrystallized Al wire; each measurement is an average of 2 or 3 films; Cu-radiation; 333 α_1 line.

Temp. in °C	a_t in kX	a_{25} in kX
10.0	4.039 93	4.041 32
20.0	4.040 73	19
30.0	4.041 78	32
40.0	4.042 67	28
50.0	4.043 54	22
60.0	4.044 55	31
		Ave. 4.041 27 kX
		Refr. corr. 4
		4.041 27 kX \pm 0.000 04 (*)
		or 4.049 47 Å

(*) Standard deviation $s=0.675 \sqrt{\Sigma \Delta^2/(n-1)}$.

The expansion coefficient ($\alpha = 22.93 \cdot 10^{-6}$) was calculated from

$$(3) \quad \alpha = \Delta a / a \Delta t,$$

where Δa is the change of the parameter due to the temperature change Δt . The lattice constant increases linearly in the temperature interval between 10 and 60 °C without any detectable bend. The constant is smaller than that obtained with a still purer aluminium (99.998%, $a = 4.049 61$ Å at 25°) ⁽²⁷⁻³⁰⁾ but agrees well with the constants of other investigators ⁽³¹⁻³³⁾.

Densities. Lattice constants can be measured easier and with much higher precision than densities. Therefore, in determining the latter greatest care was observed. At first it was found out qualitatively which of the wire, the recrystallized one or the cold drawn, is heavier. For this purpose short pieces (5-8 mm in length) of each kind of the wires were dropped in pairs into a test tube, located in a water thermostat supplied with an exact temperature controller (± 0.01 °C). The tube contained the heavy liquid of a density

⁽²⁷⁾ A. IEVINŠ and M. STRAUMANIS: *Zeits. Physik. Chem.*, B **34**, 402 (1936).

⁽²⁸⁾ M. E. STRAUMANIS and T. EJIMA: *Journ. Chem. Phys.*, **32**, 629 (1960).

⁽²⁹⁾ M. E. STRAUMANIS and T. EJIMA: *Zeits. Physik. Chemie*, **23**, 440 (1960).

⁽³⁰⁾ B. F. FIGGINS, G. O. JONES and D. P. RILEY: *Phil. Mag.*, **1**, 747, 754 Tab. III (1956).

⁽³¹⁾ E. R. JETTE and F. FOOTE: *Journ. Chem. Phys.*, **3**, 605 (1935).

⁽³²⁾ A. J. C. WILSON: *Proc. Phys. Soc.*, **53**, 235 (1941).

⁽³³⁾ H. J. AXON and W. HUME-ROTHERY: *Proc. Roy. Soc.*, A **193**, 1 (1948).

nearly in between that of the two kinds of Al wires. By changing slightly the temperature, the density of the liquid was adjusted so exactly (it took several hours) that the wire pair became completely gravity separated or it was suspended in the liquid. The heavier, lighter and wires of equal weight were then registered (Table II).

TABLE II. — Comparison of densities of the cold drawn ($d_{c,d}$) and of recrystallized parts (d_r) of the same wire.

No. of wire pairs	Cold drawn wire	Wire recrystallized at	$d_{c,d} > d_r$ in %	$d_{c,d} = d_r$ in %	$d_r > d_{c,d}$ in %
10	Fresh (*)	350 °C 1 hour	30	30	50
20	Old, 12 months on air (**)	350 °C 1 hour	25	45	30
10	Fresh, in air	350 °C 1 hour	40	40	20
37	Fresh, kept in dry Ar	350 °C 1 hour	43	41	16
20	Fresh, kept in dry Ar	250 °C 15 min	70	30	—

(*) Drawplate cooled with dry ice.
 (**) Drawplate ice cooled or at room temperature.

The last column of Table II shows clearly that recrystallized wires were heavier than cold drawn only then, if the drawing operation occurred at low (dry ice) temperature, or when the cold drawn wires were stored on air for a long time. In all other cases the probability that a cold drawn wire piece were denser than a recrystallized one was larger. Having this unexpected qualitative result it was now essential to make the quantitative measurements.

For this purpose wires were used which were annealed at 350 °C for one hour under vacuum. Densities of the whole (slightly etched) wire and of its core were determined. The same was done with cold drawn wires. The results of all density determinations are summarized in Table III.

However, for the X-ray pictures the samples were annealed 15 min at 300 °C. In order to find whether the densities of such wires will agree with those of Table III, density determinations with wires heated 15 min at 250 °C in vacuum were made and it was obtained $\bar{d}_{25} = 2.6989 \pm 0.0005$ as an average from 8 samples. This value agrees within the limits of error with that one found for a wire heated at 350 °C for one hour (Table III).

The densities of the recrystallized material closely agree with those obtained by SNOEK⁽⁸⁾, if reduced to 25 °C. For instance his sample B, heated 2 h at 600 °C, had a density of 2.6993 g/cm³ which is the same value as obtained by us for the whole recrystallized wire, or for its inside (Table III).

Higher densities obtained in the last decades for cold worked metals were

TABLE III. — *Densities of recrystallized and of cold drawn Al wires reduced to 25 °C in g/cm³. Densities of the whole wire and of the core of the samples.*

Sample	Recrystallized wire		Cold drawn wire	
	whole	core	whole	core
1	2.698 0	2.698 7	2.700 7	2.699 6
2	8 1	8 8	5	700 3
3	7 4	8 6	4	697 3
4	9 9	9 2	5	697 1
5	.700 2	8 6	3	700 9
6	7	9 7	.699 8	699 7
7	5	.700 3		700 5
8		4		695 6
Aver.	2.699 2	2.699 3	2.700 4	2.698 9 (*)
± (**)	0.000 9	0.000 5	0.000 2	0.001 5

(*) A later series of measurements gave for density of the core the same value.

(**) Most probable errors s.

also reported *e.g.* by MAIER ⁽³⁴⁾ and by LOWRY and PARKER ⁽³⁵⁾. The latter found an expansion of cold worked metals if annealed at low temperatures. This agrees well with our own observations: going through a minimum (at 250 °C) the densest Al was obtained heating it at 350 °C and it remained the same even when heated at 500 °C.

Perfection of the 99.99 % Al lattice. Now the soundness of the lattice of recrystallized aluminium can be determined, using eq. (1), *i.e.*, by calculation of n' . It was found previously that aluminium contains interstitial atoms ^(14,36) but then older data for atomic weights and densities had been used. In Table IV some data obtained for n' from various combinations of newest Avogadro numbers, atomic weights for aluminium, lattice parameters and of densities are summarized.

Table IV shows clearly that the lattice of recrystallized 99.99% aluminium wire contains excess atoms averaging $n' - n = 0.0018/\text{at unit cell}$, or about 18 atoms per 10 000 unit cells. Whether this result is real can be checked by estimating the error of the determination using for this purpose eq. (2), in which the relative errors were substituted by the values as follows: $\partial N_0/N_0 = 4.96 \cdot 10^{-5}$; $\partial a/a = 2.97 \cdot 10^{-5}$, $\partial d/d = 18.5 \cdot 10^{-5}$ and $\partial A/A = 7.14 \cdot 10^{-5}$.

⁽³⁴⁾ C. G. MAIER: *Trans. AIME*, **122**, 121 (1936).

⁽³⁵⁾ T. M. LOWRY and R. G. PARKER: *Journ. Chem. Soc. Tr.*, **107**, 1005, 1013, 1018 (1915).

⁽³⁶⁾ M. STRAUMANIS: *Zeits. f. Phys.*, **49**, 55 (1949).

TABLE IV. - Number of atoms n' per unit cell of recrystallized 99.99% Al, computed from eq. (1). d and v at 25 °C.

	n' calculated from		
	vd	$v'd$	$v''d'$
N_0/A_{ch}	4.002 10	4.001 80	4.000 63
N_0/A_{sp}	4.001 73	4.001 42	4.000 24
N'_0/A_{ch}	4.001 87	4.001 57	4.000 40
N'_0/A_{sp}	4.001 49	4.001 19	4.000 02
Aver.	4.001 80		

$N_0 = 6.02403 \cdot 10^{23}$ ⁽¹¹⁾
 $N'_0 = 6.02368 \cdot 10^{23}$ ⁽²⁷⁾
 $A_{ch} = 26.98$ (*)
 $A_{sp} = 26.98256$ ⁽²⁷⁾
 (*) The change of this weight due to presence of impurities is insignificant.
 $r = (4.04947)^3 \text{ \AA}^3$ (Table I)
 $r' = (4.04936)^3 \text{ \AA}^3$ (HILL and AXON) ⁽²⁹⁾
 $r'' = (4.04961)^3 \text{ \AA}^3$ ⁽²⁷⁾
 $d = 2.6993 \text{ g/cm}^3$ (Table III)
 $d' = 2.69801 \text{ g/cm}^3$ ⁽²⁷⁾

Then for $\Delta n' = \pm 0.00083$ is obtained, showing that the number of excess atoms calculated is well outside the limits of error. Thus, the lowest concentration of excess atoms detectable by the method is about 8 Al atoms per 10000 unit cells.

However, there are lattice constant measurements of purest aluminium by others, for instance, by HILL and AXON ⁽²⁷⁾, who obtained a much lower parameter $a_{25} = 4.04936 \text{ \AA}$, as compared with that of Table I. In Table IV, n' under $r'd$ is computed for that case, but as a result there are still interstitials in the aluminium, exceeding well the error limit. SMAKULA, KALNAJS and SILS measured with greatest care the density of single but *purcr* aluminium crystals and obtained a very low value ⁽²⁷⁾. n' (Table IV, under $r''d'$) still exceeded $n - 4.0000$, though the deviation was already within the limits of error. Only if it was assumed in the latter case that the lattice constant of the single crystal was lower or equal to that of Table I, n' closely approached n .

All this leads to the statement that recrystallized aluminium contains *excess atoms* in various concentrations, depending on the history of the treatment of the metal and on its impurities. The perfection of the lattice of a very pure slowly cooled metal should approach the ideal state ⁽²⁹⁾. Other metals should

⁽²⁷⁾ A. SMAKULA, J. KALNAJS and V. SILS: *Phys. Rev.*, **99**, 1747 (1955).

⁽²⁸⁾ R. B. HILL and H. J. AXON: *Research Corr.*, **6**, 235 (1953).

behave similarly. The question next is the perfection of the lattice of cold worked aluminium.

3.2. *Lattice parameter and soundness of cold drawn Al wires.* — Surprisingly the last doublet $333\alpha_1$ and α_2 of the fibre diagram, obtained from the core of the cold drawn wire, rotated around its axis, was sharp and uniform enough to make precision measurements of the lattice constant. This fact was already known previously and it was concluded that only a very little lattice distortion was produced by the deformation (³⁹). To reduce the rate of recovery of the hard wire, the lattice parameter determinations were started at 10 °C. The results of the measurements are given in Table V.

TABLE V. — *Lattice parameter of the core of a cold drawn 99.99% aluminium wire, rotated around its axis. Averages of 2 films; Cu-radiation; $333\alpha_1$ line.*

Temperature in °C	Sample I a_1 in kX	Sample II a_t in kX	a_{35} in kX
10.0	4.040 03		
20.0	4.040 98	4.040 94	4.041 41
30.0	4.041 93		40
40.0	4.042 72	4.042 73	47
50.0	4.043 81		34
60.0	4.044 63	4.044 60	51
			41
			Aver. 4.041 43 kX
			Refr. corr. 4
			4.041 47 kX
			$\pm 0.000 04$
			or 4.049 63 Å

The expansion coefficient $\alpha = 22.86 \cdot 10^{-6}$ was calculated from eq. (3) and was practically the same as obtained for the recrystallized wire. There was no bend in the straight lattice constant-temperature line, and no change in the constant with time due to a possible recovery or recrystallization of the wire. A second sample showed exactly the same behavior (Table V). This is in a certain contradiction with the results of OWEN *et al.*, who also found a considerable increase of the lattice parameter of compressed aluminum, but which, at room temperature, gradually returned nearly to the value of the fully annealed material (⁴⁰). The increase of the constant perpendicular to the wire

(³⁹) U. DEHLINGER: *Zeits. Krist.*, **75**, 241 (1930).

(⁴⁰) E. A. OWEN, Y. H. LIU and D. P. MORRIS: *Phil. Mag.*, (7) **39**, 831 (1948).

fibre due to cold work is in agreement with the results of other authors (WOOD^(41,42), CRUSSARD⁽⁴³⁾, GREENOUGH⁽⁴⁴⁾).

The lattice parameter in the direction of the cold drawn aluminum wire was calculated from the X-ray pictures of the small discs rotating in the transverse direction. They exhibited only a very slight fibre structure⁽¹⁷⁾. The parameter measurements are listed in Table VI.

TABLE VI. — *Lattice parameter of a cold drawn aluminum wire (disc) rotated perpendicular to axis of the wire. Averages of two films, Cu-radiation; 333 α_1 line.*

Temperature in °C	a_t in kX	a_{25} a in kX
10.0	4.038 83	4.041 21
20.0	4.040 75	4.041 21
30.0	4.041 74	4.041 28
40.0	4.042 64	4.041 26
50.0	4.043 58	4.041 17
60.0	4.044 39	4.041 17
		Aver 4.041 24
		Refr. corr. 4
		4.041 28
		$\pm 0.000\,03$ kX
		or 4.049 44 Å

The thermal expansion coefficient of the plastically deformed metal in the direction of the wire axis was $\alpha = 22.77 \cdot 10^{-6}$, which agrees with that of the recrystallized material ($22.9 \cdot 10^{-6}$) between 10 and 60 °C⁽⁴⁵⁾. The lattice constant in the same direction was slightly lower than that of the recrystallized material.

The Tables V and VI show clearly that the unit cell of the distorted aluminum is less symmetric: it seems to be hexagonal (or tetragonal) with a larger d -value perpendicular to the surface of the wire ($a_1 = 4.049\,63$ Å) and a smaller one in the direction of the wire ($a_2 = 4.049\,44$ Å). Slip during wire drawing occurs along the (111)-planes and they are nearly parallel to the axis of the wire. These planes, however, are equivalent to the (0001)-planes of the close packed hexagonal lattice. Thus, having in mind that the volume of such

⁽⁴¹⁾ S. L. SMITH and W. A. WOOD: *Proc. Roy. Soc. (Lond.)*, **182**, 404 (1944).

⁽⁴²⁾ See also C. S. BARRETT: *Structure of Metals* (New York, 1952), p. 431, 443.

⁽⁴³⁾ C. CRUSSARD and F. AUBERTIN: *Rev. Metall.*, **46**, 354 (1949).

⁽⁴⁴⁾ G. B. GREENOUGH: *Progr. Metal Phys.*, **3**, 176 (1952); *Nature*, **160**, 258 (1947).

⁽⁴⁵⁾ A. R. ROSENFELD and B. L. AVERBACH: *Journ. Appl. Phys.*, **47**, 154 (1956).

a hexagonal unit cell is only half of the cubic cell, n' for a hexagonally distorted cubic cell can be calculated from $a_{\text{hex}} = 2.86340 \text{ \AA}$ (obtained from a_2) and $c_{\text{hex}} = 4.67611 \text{ \AA}$ (found from a_1). The results are listed in Table VII (*). A slightly lower number n' was calculated for the core of the cold drawn wire than for the recrystallized aluminium (Table IV, second column). But the difference was within the limits of error (± 0.0008 at/unit cell).

TABLE VII. - *Number of atoms n' per unit cell of a cold drawn Al wire.*
 $N_0 = 6.02403 \cdot 10^{23} \text{ g mole}^{-1}$ and $A_{\text{ch}} = 26.98$.

	Diam. in mm	Vol. in \AA^3	d in g/cm^3	n' in at/unit cell
Core of wire	0.1	33.203 ₁	2.6989	4.00167
The whole wire	0.28	33.203 ₃	2.7004	4.00390

However, the cold drawn wire as a whole is denser than the core, meaning that the outside layer of the wire is heavier than $2.700 \pm \text{g/cm}^3$. Accordingly, fragments of the outside layers of the wire perpendicular to the surface showed an inclination for a larger lattice constant ($a_{25} = 4.04964 \text{ \AA}$) than given in Table V. Under such conditions the number of interstitial atoms in the outside layer of the hard wire exceed 0.004 atoms per unit cell or 4 Al atoms per 1000 cells (Table VII). This result, which is the first of its kind (⁴⁶), shows that for the description of the state of a deformed lattice, single high precision density or lattice constant measurements are insufficient, but that *both of them are necessary*.

4. - Discussion.

The results of the present investigation allow one to make the following conclusions concerning the processes of wire drawing, slipping and strain hardening.

It is well known that the slip plane of aluminium, as a face centered metal, is the (111)-plane. Consequently, if a wire is drawn from a piece of this metal, the [111] direction will run parallel to the wire axis (³⁹). Lamellae of the metal while the wire is drawn, rotate and slip along the (111)-planes so that finally these planes stretch themselves nearly parallel (cone fibre structure) to the

(*) Dr. A. NIGGLI (Zürich, E.T.H.) suggested a rhombohedral deformation of the cubic cell. However, the calculated number of atoms per unit cell was the same within the limits of error.

(⁴⁶) A. L. TITCHENER and M. B. BEVER: *Progr. Metal Phys.*, **7**, 247, 322 (1958).

surface of the wire. The other (111)-planes of the same lamellae locate themselves nearly perpendicular, but not oriented to each other, to the axis of the wire. Slip between the lamellae continues only over a certain distance and then strain hardening begins. Slip within the lamellae themselves may occur only to a limited extent⁽⁴⁷⁾. The location of the lamellae in a 90% cold drawn wire is sketched in Fig. 1, and a work hardened crystal in Fig. 2.

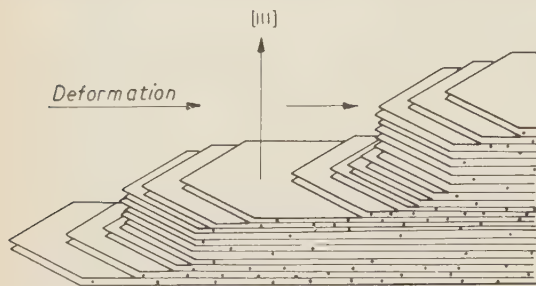


Fig. 1. - Arrangement of the slip lamellae or bands in the outside layer of a cold drawn Al wire. Blocking dislocations causing strain hardening are created in and between the bands (slip lines are shown).

concentration of interstitial atoms accompanied by the increase of the spacing between the (111)-planes (the increased a constant was calculated from the 333-interference). These phenomena are explained by the slip along the (111)-planes and by the partial disintegration of single lattice planes causing strain hardening. According to SCHMIDT and BOAS⁽⁴⁸⁾, and especially as pointed out by BOAS⁽⁴⁹⁾, hardening occurs due to the appearance of *arresting* or *blocking* dislocations, being created by the deformation and slipping processes themselves. Evidently these dis-

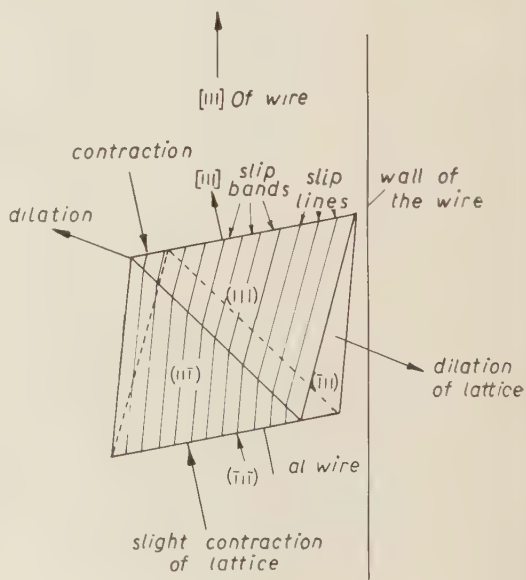


Fig. 2. - Section through a work hardened Al crystal. Deformation by slip. Interstitial atoms between the atomic planes.

⁽⁴⁷⁾ M. E. STRAUMANIS: *Zeits. Kristallogr.*, (A) **83**, 29 (1932).

⁽⁴⁸⁾ E. SCHMID and W. BOAS: *Kristallplastizität* (Berlin, 1935); English ed. (London, 1950).

⁽⁴⁹⁾ W. BOAS: *Physics of Metals and Alloys* (New York, 1949), p. 131, 132.

locations appear between the gliding planes in form of interstitial atoms, as found by the X-ray and density method. The interstitials widen the distance between (111)-planes, but not that in the direction of slip, although thin lamellae having an appreciably larger c -constant may also appear in the direction of the wire. As the blocking dislocations oppose the stress applied, the stress has to be increased to produce further slip. The increased stress in turn produces more blocking interstitial atoms, finally leading to stress hardening. It is assumed that the stress applied increases exponentially with the increase of concentration of interstitial atoms (blocking dislocations).

The amount of such dislocations in a hard Al wire is not at all small (4 atoms per 1000 unit cells). Assuming a uniform distribution of dislocated atoms, their density δ per cm^2 can be calculated:

$$\delta = [(n' - n)N_0 d / nA]^{\frac{1}{3}}.$$

Substituting 0.004 for $n' - n$ (Table VII), $\delta = 1.53 \cdot 10^{13}$ atoms cm^{-2} is obtained. The estimated concentration of edge dislocations in deformed metals is about 10^{11} cm^{-2} ⁽⁵⁰⁾ (according to TAYLOR ⁽⁵¹⁾ 10^{12} cm^{-2}), a figure which is not very far from $1.53 \cdot 10^{13}$, the density of blocking dislocations. However it is assumed that the former is produced by introducing *edge* dislocations which cause a *decrease* in density of the cold worked metal ^(52,53), while the dislocated atoms here are interstitials the concentration of which was computed from the *increase* of experimental density and of lattice constant due to cold work.

However, it is frequently found that the density of cold worked metals is lower than that of recrystallized material ⁽¹⁾ (see also Table II). This overall decrease in density can be explained by some secondary phenomena which undoubtedly occur during cold work, *e.g.* crack, capillary or fissure formation of even atomic dimensions, which *overbalance* the effect of density increase due to strain hardening (see Fig. 3). The evidence for crack formation in the present work is as follows: 1) wires produced with drawplates cooled with dry ice were less dense (crack formation because of increased brittleness of the Al); 2) cold drawn wires stored in a refrigerator became gradually less dense but not those kept under dry argon (widening of fissures due to corrosion attack—although not visible—by oxygen and moisture ⁽⁵⁴⁾); 3) the density of the

⁽⁵⁰⁾ P. B. HIRSCH: *Progr. Metal Phys.*, **6**, 236, 252, 292 (1956). See also various places in J. C. FISHER and Assoc.: *Dislocations and Mechanical Properties of Crystals* (New York, 1956).

⁽⁵¹⁾ G. I. TAYLOR: *Proc. Roy. Soc., A* **145**, 362, 388 (1934).

⁽⁵²⁾ A. SEEGER and P. HAASEN: *Phil. Mag.*, (8), **3**, 470 (1958).

⁽⁵³⁾ W. M. LOMER: *Phil. Mag.*, (8), **2**, 1053 (1957).

⁽⁵⁴⁾ See *e.g.* J. HARWOOD in W. D. ROBERTSON: *Stress Corrosion Cracking* (New York, 1956), p. 9.

cold worked Al decreased from 2.7004 to 2.6989 g cm⁻³ (at 25 °C) when heated at 250 °C for 15 min (recovery of the strained metal, the dislocated atoms leave their interstitial positions, dilation), and increased up to 2.6992 when

heated at 350 or 500 °C (closure of fissures). From these figures the decrease in fissure volume per cm³ can be calculated: $(2.6992 - 2.6989)/2.7 = 1.1 \cdot 10^{-4}$ cm³; here the interstitials outbalance the density decrease due to cracks. Crack formation is also the reason why the core of an aluminium wire of the present investigation was less dense (see Table III). TAMMANN has shown that fissures are present in recrystallized as well as in cold worked

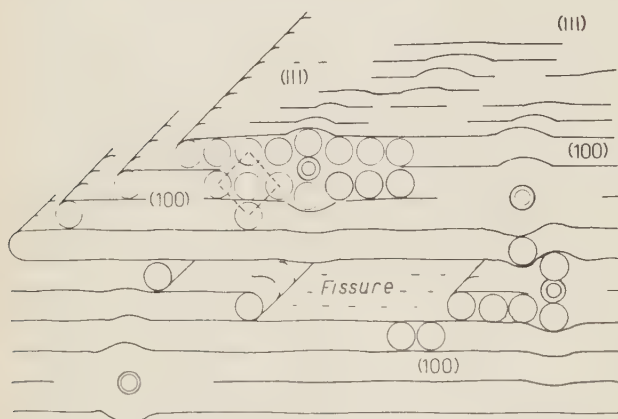


Fig. 3. - Scheme of a work hardened Al crystal (see Fig. 2). Interstitial atoms (double rings). Fissure. Increase of average d -value in the direction [111].

metals, the latter usually having a larger fissure volume⁽⁵⁵⁾. WOOD described fatigue cracks⁽⁵⁶⁾ and theoretical considerations concerning crack formation were advanced by MOTT⁽¹⁾ and STROH⁽⁵⁾. Cracks may be formed by vacancies which in turn may be created according to SEITZ⁽⁵⁷⁾ together with interstitial atoms by moving dislocations (dislocation cracks)^(58,59). The latter are introduced by mechanical deformation and the interstitial atoms produced block the slipping process.

Whatever the reasons, cold worked aluminium consists of fibres of higher density due to presence of interstitial atoms (corresponding to the ω -phase of MAIER⁽³⁴⁾) and of cracks or fissures, which may or may not, depending on various obstacles, outbalance the density increase because of cold work. A picture of such a work hardened fragment of an Al crystal is shown in Fig. 3.

In Fig. 3 the interstitial Al atoms forced into the lattice are drawn in a smaller size, because these atoms might be partially or completely stripped of the valence electrons. Thus, being appreciably reduced in size they will

⁽⁵⁵⁾ G. TAMMANN and H. BREDEMEIER: *Zeits. anorg. allgem. Chem.*, **142**, 54 (1925).

⁽⁵⁶⁾ W. A. WOOD: *Phil. Mag.*, (8), **3**, 692 (1958).

⁽⁵⁷⁾ F. SEITZ: *Advanc. Physics*, **1**, 43 (1952).

⁽⁵⁸⁾ J. W. ALLEN: *Phil. Mag.*, **4**, 1406 (1959).

⁽⁵⁹⁾ A. S. KEH, J. C. N. LI and T. T. CHOU: *Acta Met.*, **7**, 694 (1959).

cause a lesser distortion of the (111)-planes. The presence of such interstitial atoms, more resembling ions, should cause a slight change in the properties of cold worked metals. Indeed, it was especially emphasized by TAMMANN that cold worked metals have a greater hardness, a slightly different color, they exhibit a slight change in their electrochemical behavior, and show mostly an increased electrical resistance etc.⁽⁶⁰⁾. The possibility of appearance of interstitial atoms is also considered by other investigators, *e.g.* COTTRELL⁽⁶¹⁾.

As the wire drawing process involves some pressure which causes a number of atoms to go into interstitial positions, the electrical resistance of a wire should be less than of recrystallized material. This is because pressure usually decreases the resistance of metals⁽⁶²⁾. On the other hand elongation of the Al, which is also involved in wire drawing, increases its resistivity⁽⁶³⁾. Thus, the relationships are complicated. However, the recovery of a hard wire mostly accompanied by a decrease in electrical resistivity⁽⁶⁴⁾ occurs already at low temperatures (for an Al wire it is complete in 15 minutes at 175 °C and even at lower temperatures). Therefore, the process of recovery should be simple: it merely consists in the return of dislocated interstitial atoms to their normal lattice positions. This events is facilitated by the increase of temperature and evidently occurs under release of energy. At still higher temperatures the microcracks start to close and recrystallization of Al begins⁽²⁵⁾.

The presence of excess atoms in recrystallized 99.99% Al can be explained by formation of segregations⁽²⁹⁾, detectable according to CUFF and GRANT by electron microscopic observation⁽⁶⁵⁾.

* * *

The present investigation was sponsored by National Science Foundation under the contract 2099-g-2585. We are grateful to Dr. W. J. JAMES of the Department of Chemical Engineering of the School for his interest in the work and for assisting with the manuscript, and to Dr. C. H. CHENG for the lattice parameter measurements.

⁽⁶⁰⁾ See *e.g.* G. TAMMANN and C. L. WILSON: *Zeits. anorg. allgem. Chem.*, **173**, 156 (1928).

⁽⁶¹⁾ See *e.g.* W. M. LOMER: *Progr. Metal Phys.*, **8**, 255, 289 (1959).

⁽⁶²⁾ A. W. LAWSON: *Progr. Metal Phys.*, **6**, 1 (1956).

⁽⁶³⁾ H. R. PFEIFFER: *Journ. Appl. Phys.*, **29**, 1581 (1958).

⁽⁶⁴⁾ G. TAMMANN and M. STRAUMANIS: *Zeits. anorg. allgem. Chem.*, **169**, 365 (1928).

⁽⁶⁵⁾ F. B. CUFF and N. J. GRANT: *Journ. Inst. Metals*, **87**, 248 (1958-59).

RIASSUNTO (*)

L'alluminio contiene atomi in eccesso in maggiore o minore quantità, in dipendenza del genere di trattamento termico o meccanico e della concentrazione delle tracce di impurità. Il numero di atomi in eccesso in un filo di alluminio ricristallizzato puro al 99.9% è 18 su 10 000 celle unitarie, e questi atomi possono essere un costituente delle aggregazioni più dense. La costante reticolare di un filo di alluminio tirato a freddo era in direzione del suo asse leggermente minore ($\alpha_{25} = 4.0494 \text{ \AA}$) di quella di un filo ricristallizzato ($\alpha_{25} = 4.04947 \text{ \AA}$), ma in direzione trasversale era maggiore ($\alpha_{25} = 4.04963 \text{ \AA}$). Il coefficiente di dilatazione termica del filo ricristallizzato ($\alpha = 22.9 \cdot 10^{-6}$) fra 10 e 16 °C non differiva (in maniera significativa) da quello dei fili trafilati temperati. La densità complessiva del filo temperato era $d_{25} = 2.7004 \text{ g/cm}^3$ (strato centrale 2.6989), quella del filo ricristallizzato era minore (2.6993 g/cm³). La concentrazione delle particelle interstiziali era maggiore negli strati esterni del filo (almeno 4 atomi ogni 1000 celle unitarie o $1.5 \cdot 10^{13}$ atomi per cm²). Le misure precedenti, che davano densità inferiori per i metalli lavorati a freddo, possono essere spiegate dal fatto che la fessurazione e la formazione di cavità capillari durante la lavorazione a freddo spesso equilibrano l'effetto dell'aumento di densità dovuto all'aumento della concentrazione di atomi interstiziali (blocking dislocation), creato dal processo di scorrimento e deformazione. Lo « strain hardening » sembra dunque esser conseguenza del crescente numero di atomi interstiziali. Quest'ultimi processi sono in accordo con le teorie esposte da SCHMID e BOAS. Dalla diminuzione di densità del filo temperato (in seguito a riscaldamento) si stimò il volume di fessure submicroscopiche per cm³: 10^{-4} cm^3 . Queste possono essere create dallo spostarsi delle dislocazioni e vacanze (formazione di fessure per dislocazione) durante il processo di deformazione. Solo la costante reticolare e le misure di densità dello stesso materiale, danno un quadro corretto delle condizioni interne (in termini di n') di un metallo, od altro materiale cristallino, deformato oppure ricristallizzato.

(*) Traduzione a cura della Redazione.

Die Gamma-Alpha-Reaktion bei Tellur.

F. I. HAVLIČEK

J. Stefan Institut - Ljubljana

(ricevuto il 23 Aprile 1960)

Zusammenfassung. — In mit Tellursäure getränkter Emulsion von Ilford E-1/200 Platten, die mit E_{\max} 33 MeV Bremsstrahlung bestrahlt wurden, wurden Spuren von Alphateilchen ausgemessen. Es zeigten sich hierbei unerwartet hohe Zahlen von Alphateilchen. Ferner wurden auch Winkelabhängigkeiten der Orientierung der Spuren bestimmt und mit Messungen bei anderen Elementen verglichen.

Von einer Ilford E-1/200 Platte wurde die Emulsion in Form zweier Stege einer Breite von ca 2.5 mm entfernt. Auf einem der beiden äußeren Teile der Emulsion wurde etwas Thoriumnitratlösung (P.H. 4) aufgetrocknet und auf dem anderen äußeren Teil 1 cm³ einer Lösung von Tellursäure (P.H. 4), so daß $3.5 \cdot 10^7$ Tellurkerne auf einen cm² kamen. Der mittlere Teil der Platte blieb unpräpariert. Die Platte wurde senkrecht mit 12.3 Rg/cm² Betatron-Gammastrahlen aus einer Entfernung von 360 cm bestrahlt, E_{\max} 33 MeV und entwickelt.

Um die Platte zu eichen, wurden zuerst 60 Spuren von Alphateilchen des mit Thorium präparierten Teils nach ihren horizontalen und vertikalen Koordinaten mikroskopisch (N.A. 1.25; 100×11) ausgemessen und ihre wirklichen Längen c sowie ihre wirklichen Winkeln ϑ in Bezug auf die Plattenebene gerechnet, die in einem c - ϑ Diagramm eingezeichnet wurden.

Nach der Formel

$$c^{*2} = c^2(1 + K^2 \operatorname{tg}^2 \vartheta)/(1 + \operatorname{tg}^2 \vartheta),$$

K ist der Schrumpffaktor der Emulsion und c^* die ursprüngliche Spurenlänge, wurde ein neues Koordinatensystem eingepaßt, nach dem die Stelle des Gaußverteilungsmaximums der Thoriumalphateilchenspuren mit $15 \pm 1.6 (\pm 0.31) \mu\text{m}$ beziehungsweise $3.95 \pm 0.34 (\pm 0.064) \text{ MeV}$ bestimmt wurde.

Die ursprünglichen Winkel θ wurden nicht nach der Formel

$$\operatorname{tg} \vartheta^* = K \operatorname{tg} \vartheta$$

bestimmt, sondern nachträglich empirisch in das Koordinatensystem e^* , ϑ^* eigenpaßt, wobei vorausgesetzt wurde, daß die Spuren ursprünglich beliebig orientiert waren. (Es wurden die wahrscheinlichen Spurenzahlen zwischen den einzelnen Winkeln gerechnet, an den entsprechenden Stellen die Ordinaten eingezeichnet und etwas geglättet.) Diese so gefundenen Winkel θ stellen gegenüber den Winkeln ϑ^* eine Verbesserung dar, da durch sie, eine gewisse Bevorzugung von Winkeln um 45° in der Emulsion — wohl wegen den plastischen Deformationen beim trocknen — nachkorrigiert werden konnte.

Danach wurden abwechselnd in dem mit Tellur und dem unpräparierten Teil der Platte Streifen einer Länge von 1.5 cm und einer Breite von 0.0095 cm auf Spuren von Alphateilchen durchgesehen und diese ausgemessen, sowie schließlich gemäß obiger Eichung deren ursprüngliche Länge und Orientierung bestimmt. Insgesamt wurden 16 und 16 solche Streifen durchgesehen, wobei sich für die präparierten (Tellur) und unpräparierten (Emulsion) Plattenteile, folgende Statistik in Bezug auf die Spurenlänge e^* ergab. (Siehe Tabelle I).

Im Gebiete zwischen 40 und 100 μm zeigt diese Statistik bedeutsame Differenzen. Um die ineinandergreifenden Teile auseinanderzulösen wurden in einem e^* - θ Diagramm die bezüglichen Punkte eingezeichnet und immer dann ein Punkt des Te-Gebiets weggestrichen, wenn in seiner Nähe ein Punkt des Em-Gebiets lag.

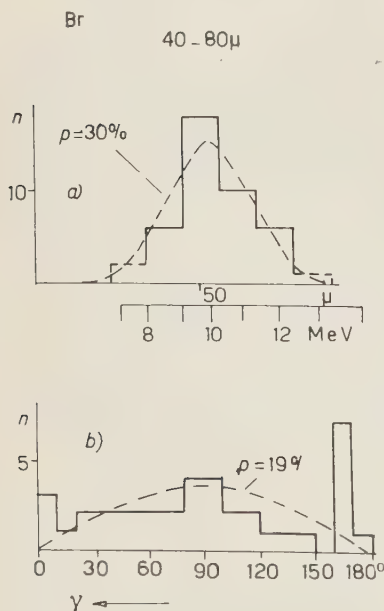


Abb. 1.

Für das Gebiet zwischen 40 und 80 μm wurde aus den dazugehörigen Punkten des Em-Gebiets und den durch sie weggestrichenen Punkten des Te-Gebiets ein Histogramm Abb. 1a. gezeichnet, das sich einer Gauß'schen Verteilung mit einer Wahrscheinlichkeit p von 30% (nach der χ^2 Methode gerechnet) anschließt; das Maximum liegt bei 57 ± 11.5 (± 1.78) μm beziehungsweise bei 10 ± 1.28 (± 0.2) MeV: die erste Toleranz gilt für die Gauß'sche Verteilung, die zweite in der Klammer für den Mittelwert. ERDÖS, SCHERRER und STOLL ⁽¹⁾ haben unter ähnlichen Umständen ein Histogramm erhalten, das sie der Gamma-Alpha Reaktion von $^{79-81}\text{Br}$ zuschreiben. Die Spitze der

⁽¹⁾ P. ERDÖS, P. SCHERRER und P. STOLL: *Helv. Phys. Acta*, **30**, 683 (1957).

TABELLE I.

Spurenlängen $e^*\mu\text{m}$	Spurenzahlen		Differenzen und Toleranzen	
	Em	Te		
0	7	8	1 ± 3.9	
10	32	30	-2 ± 7.9	
20	33	38	5 ± 8.4	
30	18	16	-2 ± 5.6	
40				
50	3	22	19 ± 5	
60	9	16	7 ± 5	
70	5	13	8 ± 4.2	
80	2	10	8 ± 3.5	52 ± 10.2
90	3	7	4 ± 3.2	
	4	10	6 ± 3.7	
100				
110	3	0		
120	5	5		
140	3	2		
160	4	3		
180	2	1		
200	0	1		
220	0	0		
240	3	3		
260	1	3		
280	0	1		
300	2	6		
320	1	1		
340	0	0		
360	0	0		
380	0	1		
400	1	0		
Summen	142	200	58 ± 18.5	

ihrem Histogramm zuzuordnenden Gauß'schen Verteilung liegt bei 9.9 ± 1.7 (± 0.15) MeV. Der Unterschied der Toleranzen 1.28 und 1.7 hängt vielleicht mit der, bei diesen Untersuchungen verwendeten besonderen Platteneichung zusammen. Rechnet man nach der Tabelle von ERDÖS, SCHERRER und STOLL (S. 685) die voraussichtliche Zahl der Alphateilchenspuren, so ergibt sich hier 33 ± 13 , was mit der vorgefundenen Zahl 41 ± 12 gut übereinstimmt. Abb. 1.b gibt ein Histogramm für die dazugehörige Winkelverteilung; die gestrichelte Linie gilt für eine zufällige Winkelverteilung und $p=19\%$ ist die Wahrscheinlichkeit dafür, daß die vorgefundene Winkelverteilung nach dem Histogramm eine zufällige ist.

Nach der gleichen Tabelle von ERDÖS, SCHERRER und STOLL, wären im hier durchgesehenen Gebiet 18 Sterne der Gamma-Alpha Reaktion bei ^{12}C zu erwarten gewesen; vorgefunden wurden 11 ± 3.3 in möglicher Übereinstimmung.

Abb. 2 gibt Histogramme für das Gebiet der statistisch bedeutsamen Differenzen, die Gamma-Alpha Reaktionen beim Tellur zugeschrieben werden sollten. Rechnet man hier aus der Spurenzahl 52, der Zahl der Tellurkerne/cm² und der Intensität der Bestrahlung, die Zahl der Alphaspuren/MolRg aus, dann ergibt sich der ganz unerwartet hohe Wert von $3.2 \pm 0.45 \cdot 10^7$. Charakteristische Spurenlängen und bevorzugte Winkel sind abzulesen. Für die gestrichelten Linien

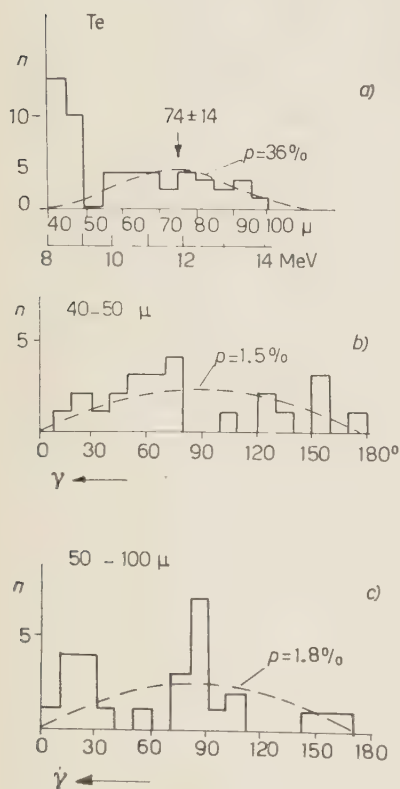


Abb. 2.

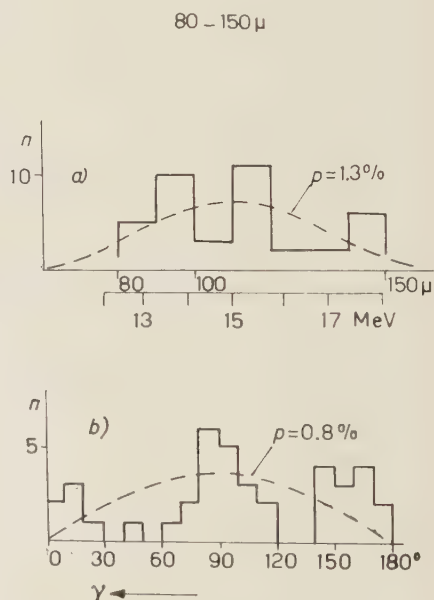


Abb. 3.

und die p -Werte gilt das Gleiche wie beim Brom. Wichtig scheint ferner für die Beurteilung, daß die hier auftretenden Energien der Alphateilchen genügend weit von jeder natürlichen Zerfallsenergie liegen.

In Abb. 3 sind noch die Histogramme für das Gebiet von 80 bis 150 μ gegeben. Das Gebiet über 150 μ zeigt fast nur Winkel um 90°. Vielleicht gehören die beiden Maxima bei 235 und 290 μ also ca 24 und 27 MeV einer Riesenresonanz an ($^{16}\text{O}?$). Das Gebiet von 80 bis 150 μ läßt sich vielleicht dem ^{81}Br zuordnen, da es in gewisser Übereinstimmung mit den Messungen

von TAYLOR und HASLAM⁽²⁾ steht, wenn man hier 5.5 MeV als Energiedifferenz des Alphateilchens gegenüber der Umgebung berücksichtigt. (Siehe auch ERDÖS, SCHERRER und STOLL, S. 682).

Die Unerwartet hohe Teilchenzahl bei der $\text{Te}(\alpha, \gamma)\text{Sn}$ Reaktion läßt vermuten, daß es sich hier vielleicht wie beim Nd⁽³⁾ um eine gewisse Sonderung der Bindung des Alphateilchens gegenüber einem Restkern mit 50 Protonen oder beim Nd von 82 Neutronen handelt. Die Coulomb'sche Barriere, sollte nach den Angaben von IGO⁽⁴⁾ bei ev. nur geringer Auflockerung, genügend schmal für das Austreten von Alphateilchen sein. Ein Anschluß an eine der bestehenden Theorien wie die von COURANT⁽⁵⁾ konnte nicht gefunden werden.

Neben statistisch bedeutsamen Differenzen für die Spurenzahlen der Alphateilchen wurden auch statistisch bedeutsame Differenzen von Spurenzahlen von Deuteronen, jedoch nicht für Protonen gefunden.

Eine gewisse Ähnlichkeit mit Energie und Winkelverteilungen obiger Histogramme besteht mit denen, die für Gamma-Alpha Reaktionen bei ^{12}C gefunden wurden^(6,7).

Es ist beabsichtigt zu versuchen, durch weitere Untersuchungen die hier vorgefundenen hohen Absorptionsquerschnitte beim Tellur zu sichern.

* * *

Das Präparieren der Platten, sowie die Messungen wurden von Fräulein M. MODESTO durchgeführt, die Bestrahlung mit dem Betatron des Instituts von Herrn Dipl. Ing. Z. MILAVEC.

(2) I. G. V. TAYLOR und R. N. H. HASLAM: *Phys. Rev.*, **87**, 1138 (1952).

(3) F. I. HAVLIČEK: *Nuovo Cimento*, **13**, 969 (1959).

(4) G. IGO: *Phys. Rev.*, **115**, 1665 (1959).

(5) E. D. COURANT: *Phys. Rev.*, **82**, 703 (1951).

(6) F. I. HAVLIČEK und B. DOBOVIŠEK: *Phys. Rev.*, **100**, 1355 (1955).

(7) F. I. HAVLIČEK and B. DOBOVIŠEK: *Rep. Inst. J. Stefan*, **2**, 73 (1955).

RIASSUNTO (*)

In emulsioni Ilford E-1/2000 imbevute di acido tellurico e irradiate da bremsstrahlung di $E_{\text{max}} = 33$ MeV si sono misurate le tracce delle particelle alfa. Si riscontrarono quantità inaspettatamente elevate di alfa. Inoltre, si sono determinate anche le dipendenze dell'orientamento delle tracce dagli angoli d'incidenza e si sono confrontate con misure eseguite su altri elementi.

(*) Traduzione a cura della Redazione.

Graphical Analysis of Infrared Divergences (*).

S. OKUBO

Istituto di Fisica Teorica dell'Università - Napoli
Istituto Nazionale di Fisica Nucleare - Sottosezione di Napoli

(ricevuto il 4 Maggio 1960)

Summary. — By the graphical method, it has been proved that all infrared divergences in the quantum electro-dynamics can be summed up into a simple form, and the result is a generalization of the classical Bloch-Nordsieck formula.

1. — Introduction.

It is well known that the infrared divergences in the quantum electro-dynamics are cancelled by soft-photon emissions. This has been proved by several authors ⁽¹⁾ in any orders in the perturbation expansions with respect to the coupling constants, though not completely satisfactorily. However, this simple cancellation is not sufficient practically; since then, the resulting finite cross-section contains still a term proportional to $\log \Delta E$ (where ΔE is the energy-loss), and as the result, it gives a divergent contribution for $\Delta E \rightarrow 0$. SCHWINGER ⁽²⁾ made a conjecture that this defect might be due to the failure of the perturbation calculation and the correct answer would be of the form $\exp [x^2 \log \Delta E]$, which goes to zero for $\Delta E \rightarrow 0$. This conjecture of Schwinger has been subsequently proved by YENNIE and SUURA ⁽³⁾. Recently, we have

(*) The research reported in this document has been sponsored in part by the office chief of Research and Development, U.S. Department of the Army through its European office under contract no. DA-91-591-EUC-1096.

(¹) See e.g. J. M. JAUCH and F. ROHRlich: *Helv. Phys. Acta*, **27**, 613 (1954) and *Theory of Photons and Electrons* (Cambridge Mass., 1955), pp. 390-405.

(²) J. SCHWINGER: *Phys. Rev.*, **76**, 790 (1949).

(³) D. R. YENNIE and H. SUURA: *Phys. Rev.*, **105**, 1378 (1957).

proved ⁽⁴⁾ the same result more rigorously. (Hereafter, we refer it as I). The important point is that all contributions from the infrared divergences can be summed up into a simple form, which is a generalization of the classical Bloch-Nordsieck formula ⁽⁵⁾. These papers ^(3,4) quoted in the above make use of differential equations with respect to the cut-off or coupling constant. As to the result, it is not so clear to see directly what kinds of Feynman diagrams have to be summed up and how the summation becomes so feasible to give such a simple formula. The purpose of this note is to show how the direct summation of Feynman diagrams giving the infrared divergences can be performed and how we get the generalization of the Bloch-Nordsieck formula. This not only is useful for practical calculations, but will also help to a better understanding of the problem. Especially, it would be interesting to compare the technique used here with the previous one ⁽⁴⁾.

2. - Analysis of infrared divergences.

Here, we restrict ourselves to the scattering problem of one electron by the external Coulomb potential with radiative corrections. Extensions to the other cases like the electron-electron scattering treated previously ⁽⁴⁾ are straightforward, though a little more complicated.

First in this section, we consider the scattering without soft-photon emission. Roughly speaking, the infrared divergences are phenomena of the outermost region of the electron-structure, whereas the ultraviolet divergences are phenomena of the innermost.

Typical diagrams giving rise to the infrared divergences are illustrated in Fig. 1, where p and q are the incoming and outgoing

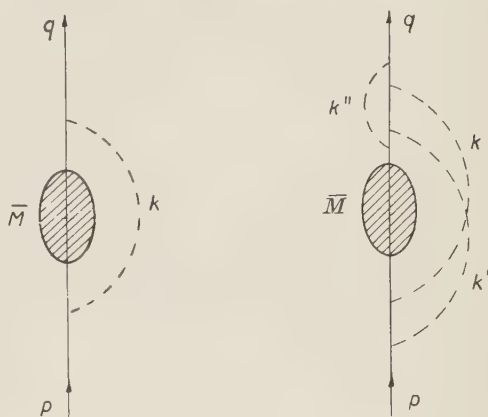


Fig. 1.

four momenta for the electron, respectively, k , k' and k'' are soft-photon lines to cause the divergences, and \bar{M} is the region in which the external Coulomb poten-

⁽⁴⁾ R. E. CAIANIELLO and S. OKUBO: to be published in *Nuovo Cimento* (hereafter, referred to as I).

⁽⁵⁾ F. BLOCH and A. NORDSIECK: *Phys. Rev.*, **52**, 54 (1937); W. PAULI and M. FIERZ: *Nuovo Cimento*, **15**, 16 (1938).

tial or hard photons (real or virtual) interact with the electron so that there will be no contributions for the infrared divergences from this part. It should be noted that we are not necessarily taking into account vacuum polarization corrections

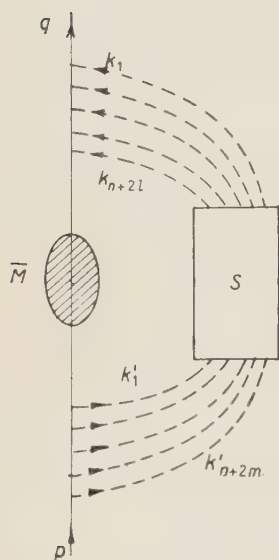


Fig. 2.

for soft photon lines, since they will not give any infrared troubles except for the charge renormalization, and hence they will be included into the region \bar{M} , provided that we use the renormalized charge for the coupling constants anywhere. The most general diagrams in which the infrared divergences can happen are the following ones depicted in Fig. 2, where the meanings of p , q and \bar{M} are the same as in Fig. 1, and the box S simply serves to mix and combine together $2l+n$ soft-photon lines $k_1 \dots k_{n+2l}$ from the outgoing electron line and $2m+n$ lines $k'_1 \dots k'_{n+2m}$ from the incoming electron line to form all possible Feynman diagrams of the type of Fig. 1. Some of the $2l$ momenta out of $k_1 \dots k_{n+2l}$ and some of the $2m$ momenta out of $k'_1 \dots k'_{n+2m}$ have to be coupled directly among themselves, respectively, so as to make the vertex corrections, where as the remaining n -momenta from $k_1 \dots k_{n+2l}$ have to be coupled directly to the other n momenta from $k'_1 \dots k'_{n+2m}$. So, we must have relations like

$$\begin{aligned} k_1 &= k'_1, \dots, k_n = k'_n, & k_{n+1} &= -k_{n+2}, \dots, k_{n+2l-1} = -k_{n+2l}, \\ k'_{n+1} &= -k'_{n+2}, \dots, k'_{n+2m-1} &= -k'_{n+2m}. \end{aligned}$$

Now according to the technique used in I, we decompose the photon Green's function D_F into two parts

$$(1) \quad D_F(x-y) = D_F^{(s)} + D_F^{(h)},$$

where

$$(2a) \quad D_F^{(s)}(x-y) = \frac{-i}{(2\pi)^4} \lim_{\varrho \rightarrow 0} \varrho^2 \int_{|k| < K} d^4 k \frac{1}{k^2 - i\varepsilon} \exp[i\varrho \cdot k(x-y)],$$

$$(2b) \quad D_F^{(h)}(x-y) = \frac{-i}{(2\pi)^4} \lim_{\varrho \rightarrow 0} \left\{ \int_{|k| > K} d^4 k \frac{1}{k^2 - i\varepsilon} \exp[ik(x-y)] + \right. \\ \left. + \int_{|k| < K} d^4 k \frac{1}{k^2 - i\varepsilon} (\exp[ik(x-y)] - \varrho^2 \exp[i\varrho k(x-y)]) \right\}.$$

In eq. (2), K is an arbitrary positive low-photon cut-off and we take it to be sufficiently small for the sake of the next section. The limiting device $q \rightarrow 0$ picks automatically up all the infrared divergences. In the Fig. 2, the region \bar{M} consists essentially of the contributions from $D_F^{(h)}$, the external Coulomb potential and hard real photons if any, whereas the divergent parts due to lines $k_1, k_2, \dots, k_{n+2l}$ and $k'_1 \dots k'_{n+2m}$ are those from the $D_F^{(s)}$ part of D^F . Now, it must be understood here that we take the same q for all D_F functions and bring $q \rightarrow 0$ simultaneously, after the co-ordinate integrations are performed (*). This procedure $q \rightarrow 0$ with the same q for all D_F functions is a particular case of the previous work (4).

Elementary computation easily shows then that the scattering matrix element $M(p, q)$ will take the following form (6)

$$(3) \quad M(p, q) = \sum_{l=0}^{\infty} \sum_{m=0}^{\infty} \sum_{n=0}^{\infty} M_c(p, q) I_{l,m,n}$$

and

$$(4) \quad I_{l,m,n} = \left[\frac{-i\lambda^2}{(2\pi)^4} \right]^{l+m+n} \cdot (p^2)^l \cdot (q^2)^m \cdot (p \cdot q)^n \cdot \\ \cdot \int \dots \int \frac{1}{k_1^{n/2}} \dots \frac{1}{k_{n+l+m}^{n/2}} \sum_S \frac{1}{(qk_1)(qk_1 + qk_2) \dots (qk_1 + qk_2 + \dots + qk_{n+2l})} \cdot \\ \cdot \frac{1}{(pk'_1)(pk'_1 + pk'_2) \dots (pk'_1 + pk'_2 + \dots + pk'_{n+2m})},$$

where the integrals have to be performed with respect to $l+m+n$ independent momenta $k''_1 \dots k''_{l+m+n}$ out of $k_1, \dots, k_{n+2l}, k'_1, \dots, k'_{n+2m}$, restricted in the region $|k| < K$, and the summation over S means to sum up for all possible permutations among $k_1, \dots, k_{n+2l}, k'_1, \dots, k'_{n+2m}$, which are allowed by the Feynman rule. M_c is the contribution from \bar{M} , which is free from the infrared divergence.

Now, note the following identity (7)

$$(5) \quad \sum_{\text{permutation}} \frac{1}{a_1(a_1 + a_2)(a_1 + a_2 + a_3) \dots (a_1 + a_2 + \dots + a_n)} = \frac{1}{a_1} \cdot \frac{1}{a_2} \cdot \frac{1}{a_3} \cdot \dots \cdot \frac{1}{a_n},$$

(*) Note added in proof. - Actually, this assumption to take the same q for all D_F is unnecessary. The final result is independent of a particular limiting process, as can be proved without any changes in the present proof.

(6) For a simple case, see reference (6) of I.

(7) S. N. GUPTA: *Phys. Rev.*, **98**, 1507 (1955); **99**, 1015 (1955).

where we take all possible permutations. Then, the integrand of the right-hand side of eq. (4) will become

$$(6) \quad \frac{1}{k_1'^2} \cdots \frac{1}{k_{n+l+m}^2} \cdot \frac{1}{(qk_1)} \cdots \frac{1}{(qk_{n+2l})} \cdot \frac{1}{(pk_1')} \cdots \frac{1}{(pk_{n+2m})}.$$

However, by this procedure, we are summing up the same Feynman diagrams more than once. This number of redundancy is easily computed to give

$$(7) \quad n! \cdot l! \cdot m! \cdot 2^{(l+m)}.$$

So, we must divide eq. (6) by this factor, and furthermore, remembering that, according to the conservation of momentum, we must have identities like

$$k_1 = k_1', \quad \dots, \quad k_n = k_n'; \quad k_{n+1} = -k_{n+2}, \quad \dots, \quad k_{n+2l-1} = -k_{n+2l}, \\ k_{n+1}' = -k_{n+2}', \quad \dots, \quad k_{n+2m-1}' = -k_{n+2m}'.$$

Thus, finally, eq. (4) will become

$$(8) \quad I_{l,m,n} = \left(-\frac{1}{2} J_{p,p} \right)^l \cdot \left(-\frac{1}{2} J_{q,q} \right)^m \cdot (J_{p,q})^n \cdot \frac{1}{n! m! l!},$$

where

$$(9) \quad J_{p,q} = \frac{-i\lambda^2}{(2\pi)^4} (p \cdot q) \int_{|k| < K} d^4k \frac{1}{k^2 - i\varepsilon} \cdot \frac{1}{(pk)} \cdot \frac{1}{(qk)}.$$

Thus, inserting eqs. (8) and (9) into eq. (3), we have

$$(10) \quad M(p, q) = M_c(p, q) \exp \left[-\frac{1}{2} f \right],$$

$$(11) \quad f \equiv J_{p,p} + J_{q,q} - 2J_{p,q} = \frac{-i\lambda^2}{(2\pi)^4} \int_{|k| < K} d^4k \frac{1}{k^2 - i\varepsilon} \left(\frac{p}{p \cdot k} - \frac{q}{q \cdot k} \right)^2.$$

So, all divergent parts are summed up to give the exponential factor. This agrees with the previous calculations^(3,4). We must note that we are performing a kind of a limiting process for the explicit self-energy diagrams in order to avoid the direct trouble.

3. - Soft-photon emission.

In this section, we consider the soft-photon emissions. At first sight, it appears that there may be interferences between the real and virtual soft photons. However, we will prove shortly that this is not the case. Now, let us pick up a real soft photon emitted with small momentum k and consider the possible interference effects with other small momenta k_1, \dots, k_N , which may be real or virtual (see Fig. 3). If we fix the position of the lines k_1, \dots, k_N but vary the position of the line k in all possible ways, then the infrared divergent parts can be separated out as follows, similarly to the previous section,

$$(12) \quad I_N = \sum_{n=0}^N \left[\prod_{m=0}^n \frac{1}{(qk_1) + \dots + (qk_m)} \right] \cdot \left[\prod_{m=n}^N \frac{1}{(qk_1) + \dots + (qk_m) + (qk)} \right].$$

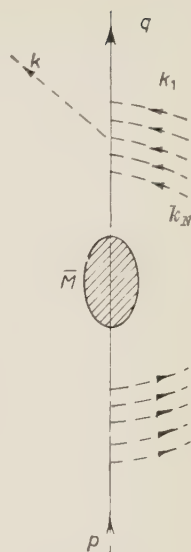


Fig. 2.

Now, we note the following identity which is a certain generalization of eq. (5)

$$(13) \quad \sum_{n=0}^N \left[\prod_{m=0}^n \frac{1}{a_1 + \dots + a_m} \right] \cdot \left[\prod_{m=n}^N \frac{1}{a_1 + \dots + a_m + x} \right] = \frac{1}{x} \cdot \frac{1}{a_1} \cdot \frac{1}{a_1 + a_2} \cdot \dots \cdot \frac{1}{a_1 + \dots + a_N},$$

so that we have

$$(14) \quad I_N = \frac{1}{(qk)} \cdot \frac{1}{(qk_1)} \cdot \frac{1}{(qk_1) + (qk_2)} \cdot \dots \cdot \frac{1}{(qk_1) + (qk_2) + \dots + (qk_N)},$$

which shows that there is no interference between the soft photons k and k_1, k_2, \dots, k_N . Actually, this technique can be also applicable for the preceding section. This independence of soft-photon emissions from each other is essential for the Bloch-Nordsieck formula, as we will see shortly. The necessity of the proof of no-interferences seems to have been overlooked by many investigators except by YENNIE and SUURA⁽³⁾, though their method is not so clear either. Eq. (14) implies that the matrix element for n soft photons emission with momentum $k_1 \dots k_n$ is reduced⁽⁴⁾ to

$$M \left(\begin{matrix} p \\ q \end{matrix} \middle| k_1 \dots k_n \right) = \frac{\lambda}{(2\pi)^{\frac{3n}{2}}} \frac{1}{(2k_1^0)^{\frac{1}{2}}} \left[\frac{(p \cdot \varepsilon_1)}{(p \cdot k_1)} - \frac{(q \cdot \varepsilon_1)}{(q \cdot k_1)} \right] \cdot M \left(\begin{matrix} p \\ q \end{matrix} \middle| k_2, \dots, k_n \right),$$

where ε is the polarization vector. So that, by induction, we have

$$(15) \quad M \left(\begin{matrix} p \\ q \end{matrix} \middle| k_1 \dots k_n \right) = \frac{\lambda^n}{(2\pi)^{\frac{3n}{2}}} \prod_{j=1}^n \frac{1}{(2k_j^0)^{\frac{1}{2}}} \left[\frac{(p \cdot \varepsilon_j)}{(p \cdot k_j)} - \frac{(q \cdot \varepsilon_j)}{(q \cdot k_j)} \right] \cdot M(p, q),$$

which corresponds to eq. (26) of I.

The rest is the same as in I, and we simply sketch the result. When we neglect the energies of soft photons, though incorrectly, then the cross-section for the n soft photons emission is given by the Poisson distribution of Bloch-Nordsieck ⁽⁵⁾

$$(16) \quad \sigma_n = \frac{f^n}{n!} \cdot e^{-f} \cdot \sigma_c,$$

where f is given by eq. (11) and σ_c is finite, so that

$$(17) \quad \sigma_{\text{total}} = \sum_{n=0}^{\infty} \sigma_n = \sigma_c = \text{finite}.$$

More realistically, when we take account of the energies of the soft photons, then instead of eq. (17), we have

$$(18) \quad \sigma_{\text{total}}(\Delta E) = F(\beta) \cdot \exp \left[\beta \log \frac{\Delta E}{K} \right] \cdot \sigma_c,$$

where ΔE is the energy loss of the electron due to the soft photon emissions, and

$$(19) \quad \beta = \frac{\lambda^2}{2(2\pi)^3} \int d\Omega_{\mathbf{k}} \cdot |\mathbf{k}|^2 \cdot \left[\frac{p}{(p \cdot \mathbf{k})} - \frac{q}{(q \cdot \mathbf{k})} \right]^2 \equiv \text{finite}$$

and

$$F(\beta) = 1 - \frac{\pi}{12} \beta^2 + \dots$$

Eq. (18) goes to zero for $\Delta E \rightarrow 0$, which justifies the conjecture by SCHWINGER, stated in the Introduction.

* * *

The author would like to express his gratitude to Professor E. R. CAIANIELLO for his suggestions and encouragements. He is also grateful for Professor M. LÉVY for the kind hospitality at the Ecole Normale Supérieure where a part of this work was done.

RIASSUNTO (*)

Col metodo grafico è stato dimostrato che tutte le divergenze infrarosse nella elettrodinamica quantistica possono essere condensate in una forma semplice, risultandone una generalizzazione della formula classica di Bloch-Nordsieck.

(*) Traduzione a cura della Redazione.

On the Theory of Classical Fluids (*).

L. VERLET

Laboratoire de Physique Théorique et Hautes Energies, Faculté des Sciences - Orsay

(ricevuto il 6 Maggio 1960)

Résumé. — On montre que la sommation d'une large class de diagrammes dans un développement du type « cluster » permet l'établissement d'une équation intégrale pour la fonction de corrélation dans les fluides classiques. Après une approximation, cette équation se réduit à celle de Born, Green et Kirkwood, et elle reproduit plus exactement que celle-ci les coefficients du viriel. On donne les termes correctifs, de plus en plus compliqués, qui permettent de rendre exacte notre équation. On calcule enfin la fonction de corrélation à trois corps, qui, introduite dans l'équation d'Yvon-Born-Green, permet de calculer la fonction de corrélation à deux corps. On confirme ainsi le calcul direct de cette fonction, et on montre que notre équation intégrale inclut des corrections à l'approximation de superposition.

1. — Introduction (**).

The purpose of this paper is to determine the radial distribution function $s(r)$ for classical fluids. Knowing this function, the thermodynamical properties of homogeneous fluids in equilibrium can be deduced. In particular through the use of the virial theorem, the equation of state is obtained

$$(1) \quad \frac{p}{\rho K T} = 1 - \frac{\rho}{6 K T} \int s(r) \frac{\partial V(r)}{\partial r} r \, d\mathbf{r},$$

(*) Supported in part by the United States Air Force through the European Office, Air Research and Development Command.

(**) At the moment when this paper was ready to be sent, Prof. YVON kindly communicated us preprints of a work due to Dr. E. MEERON which is in many points similar to the present paper.

where p is the pressure, ϱ the density ($\varrho = N/V$), K the Boltzmann's constant, T the absolute temperature. We shall limit ourselves to the case where $V(r)$ is a spherically symmetric potential.

The internal energy per particle, E , is given by the sum of the kinetic and potential energies

$$(2) \quad E = \frac{3}{2}KT + \varrho \int s(r)V(r) \mathbf{dr}.$$

The theory of fluctuations enables us to establish the Ornstein-Zernicke relation ⁽¹⁾ which gives the isothermal compressibility through the equation

$$(3) \quad KT \left(\frac{\partial \varrho}{\partial \varrho} \right)_T = 1 + \varrho \int (s(r) - 1) \mathbf{dr}.$$

The calculation of the correlation function presented in this paper is based on partial summations of the cluster expansion ⁽²⁾ of the correlation function, which is expressed as a sum of «cluster integrals» involving the function

$$\xi_0(|\mathbf{r}_i - \mathbf{r}_j|) = \exp [-V(|\mathbf{r}_i - \mathbf{r}_j|)/KT] - 1,$$

which approaches zero when $|\mathbf{r}_i - \mathbf{r}_j|$ tends to infinity.

In Section 2 we build the correlation function by summing the terms made from simple chains of ξ_0 functions (see Fig. 2). Such an expansion has previously been considered ⁽³⁾; we repeat this calculation so as to introduce the necessary notations.

In Section 3 we make an application of the chain expansion scheme to the equation of state of plasmas at high temperature. When the asymptotic form of ξ_0 for large distances is used ⁽⁴⁾, Debye-Hückel laws ⁽⁵⁾ are obtained. It will be shown that a better approximation for ξ_0 can improve the Debye-Hückel laws for finite densities.

In the next paragraph, we introduce a generalized chain expansion in which more and more chains are grafted one over the other (see Fig. 6). A consistent procedure for taking into account more and more complicated terms will be established. The philosophy involved in this approach is the same as Mo-

⁽¹⁾ L. S. ORNSTEIN and F. ZERNICKE: *Amsterdam Proc.*, **17**, 793 (1914); F. ZERNICKE: *Amsterdam Proc.*, **19**, 1520 (1916); L. S. ORNSTEIN and F. ZERNICKE: *Phys. Zeits.*, **19**, 134 (1918); **26**, 761 (1926).

⁽²⁾ H. D. URSELL: *Proc. Camb. Phil. Soc.*, **23**, 685 (1927); J. E. MAYER and M. G. MAYER: *Statistical Mechanics* (New York, 1940); W. G. McMILLAN and J. E. MAYER: *Journ. Chem. Phys.*, **13**, 276 (1945). See also ref. ⁽³⁾ and the excellent review paper of E. SALPETER: *Ann. Phys.*, **5**, 183 (1958).

⁽³⁾ J. E. MAYER and E. W. MONTROLL: *Journ. Chem. Phys.*, **9**, 2 (1941).

⁽⁴⁾ J. E. MAYER: *Journ. Chem. Phys.*, **18**, 1426 (1956).

⁽⁵⁾ P. DEBYE and E. HÜCKEL: *Phys. Zeits.*, **24**, 185 (1923).

rita's⁽⁶⁾, but we include some terms which have been left out by him, so that our results are different. A detailed comparison is made in the Appendix.

This approach will lead us to an integral equation (*) for the correlation function (Section 5). We shall establish the connection between the elements of our theory and some general relations holding for fluids, such as the Ornstein-Zernicke⁽¹⁾ and the Yvon⁽⁷⁾ relations.

We then discuss the virial expansion obtained from the integral equation of Section 5 and the generation of the terms of the cluster series which are obtained when this equation is solved by iteration, with the zero-density correlation function as a start.

In Section 7, we show that the equation obtained when the Yvon-Born-Green set of integro-differential equations⁽⁸⁾ is closed by the superposition approximation⁽⁹⁾ can be reached by approximating our integral equation. We show, in Section 8, how the correction terms to the integral equation can be obtained. These correction terms involve more and more complicated integrals, but it is hoped that the simplest of these terms can be computed. It will be seen that the effect of the correction terms can be obtained, in principle, from the experimental determination of the correlation function.

In the last paragraph, we calculate the three-body correlation function: it will be expressed as a sum of terms involving the two-body correlation function. We show that, putting this three-body correlation function in the Yvon-Born-Green equation, we obtain the two-body correlation function derived in the present paper.

2. - The chain approximation.

The two-body correlation function in classical mechanics is given by the expression

$$(4) \quad s(1, 2) = \frac{V^2 \int \prod_{i < j} \exp \left[-\frac{V(i, j)}{KT} \right] d\mathbf{3} \dots d\mathbf{N}}{\int \prod_{i < j} \exp \left[-\frac{V(i, j)}{KT} \right] d\mathbf{1} \dots d\mathbf{N}},$$

where we use the notation $i, j = |\mathbf{r}_i - \mathbf{r}_j|$.

⁽⁶⁾ T. MORITA: *Progr. Theor. Phys.*, **20**, 920 (1958). See also E. MEERON: *Phys. Fluids*, **1**, 246 (1958).

^(*) After this paper was written, we realized that this integral equation was contained, with different derivations, in the paper of Meeron quoted in ref. ⁽⁶⁾ and in a paper by J. M. J. VAN LEUWEN, J. GROENVELD and J. DE BOER: *Physica*, **25**, 792 (1959).

⁽⁷⁾ J. YVON: *Suppl. Nuovo Cimento*, **9**, 144 (1958); *Actualités scientifiques et industrielles* (Paris, 1935), no. 203.

⁽⁸⁾ M. BORN and H. S. GREEN: *Proc. Roy. Soc. (London)*, **A 188**, 10 (1946).

⁽⁹⁾ J. G. KIRKWOOD: *Journ. Chem. Phys.*, **3**, 300 (1935).

As we said in the introduction, we define the quantity

$$(5) \quad \xi_0(i, j) = \exp \left[-\frac{V(i, j)}{KT} \right] - 1,$$

which tends to zero outside the range of interaction.

It has been shown ⁽²⁾ that (4) can be written as follows:

$$(6) \quad s(1, 2) = \exp \left[-\frac{V(1, 2)}{KT} \right] \exp \left[\sum_{N=1}^{\infty} \varrho^N \beta_N(1, 2) \right].$$

There $\beta_N(1, 2)$ is the « simple 1, 2 irreducible cluster integral » defined by the following symbolic formula, the meaning of which will appear below:

$$(7) \quad \beta_N(1, 2) = \frac{1}{N!} \int d\mathbf{3} \dots d\mathbf{N} + \mathbf{2} \sum \prod \xi_0(i, j).$$

For convenience we shall diagrammatically represent each $\xi_0(i, j)$ appearing in (7) by a line joining the points i and j . The products of all these ξ_0 must be made. The sum sign indicates that one should sum over all the distinguishable diagrams leading to the same integral which can be formed by joining the $N+2$ points by ξ_0 -lines (the points 1 and 2 must not be linked together).

A diagram is considered as reducible:

- a) if a part of the diagram is disconnected;
- 2) if a part of the diagram is connected with the rest through one point only;
- 3) if a part of the diagram can be separated from the rest by cutting a line joining point 1 and a line joining point 2; (the exponential in (6) reproduced this class of reducible diagrams).

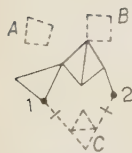


Fig. 1. - Reducible diagram.



Fig. 2. - Chain diagram.

To illustrate these prescriptions we have drawn a reducible diagram in Fig. 1. The A , B , C parts of the diagram violate prescriptions 1, 2, 3 respectively.

In this paragraph we shall consider the simple diagram of $N+2$ points built by joining the points 1 and 2 to the N other points by a simple chain of ξ_0 , which we shall call a « primary chain » as shown in Fig. 2.

There are $N!$ possible ways of forming this diagram and by (7) the corresponding cluster integral is

$$(8) \quad \beta_N^0(1, 2) = \int d\mathbf{3} \dots d\mathbf{N} + \mathbf{2} \xi_0(1, 3) \xi_0(3, 4) \dots \xi_0(N+2, 2).$$

Introducing the Fourier transform of ξ_0

$$(9) \quad \Xi_0(k) = \varrho \int \exp[-i \mathbf{k} \cdot \mathbf{r}] \xi_0(r) d\mathbf{r},$$

one has

$$(10) \quad \varrho^N \beta_N^0(r) = \frac{1}{(2\pi)^3 \varrho} \int \exp[i \mathbf{k} \cdot \mathbf{r}] \Xi_0^{N+1}(k) d\mathbf{k}.$$

Summing over all such diagrams, we introduce the function

$$(11) \quad \gamma_0(r) = \sum_{N=1}^{\infty} \varrho^N \beta_N(r) = \frac{1}{(2\pi)^3 \varrho} \int \exp[i \mathbf{k} \cdot \mathbf{r}] \Gamma_0(k) d\mathbf{k},$$

with

$$(12) \quad \Gamma_0(k) = \frac{\Xi_0^2(k)}{1 - \Xi_0(k)}.$$

Using this approximation in (6), we then have

$$(13) \quad s_0(r) = \exp\left[-\frac{V(r)}{KT}\right] \exp[\gamma_0(r)].$$

3. - An illustrative example: the equation of state of a high temperature plasma.

We shall consider the case of an electron plasma, at high temperature with a uniform background of ions.

We have in this case for the electrons

$$(14) \quad \xi_0(r) = \exp\left[-\frac{\alpha}{r}\right] - 1,$$

where

$$(15) \quad \alpha = \frac{e^2}{KT}.$$

We have plotted in Fig. 3 (curve (1)) $(r/\alpha)\xi_0(r)$.

The calculation of the equation of state with the chain approximation has already been made by another author ⁽⁴⁾ who used for $\exp[-\alpha/r]$ its asymptotic expression for large values of r .

One has in this case

$$(16) \quad \xi_0^{A_2}(r) = -\left[\frac{\alpha}{r}\right]$$

(curve (2) of Fig. 3, represents $(r/\alpha)\xi_0^{As}(r)$) which, with the help of equations (9), (12) and (11) gives

$$(17) \quad \gamma_0^{As}(r) = \frac{\alpha}{r} \left(1 - \exp \left[-\frac{r}{h} \right] \right).$$

There h is the Debye length: $h = (4\pi\alpha\epsilon)^{-\frac{1}{2}}$. This gives for large values of r

$$(18) \quad s^{As}(r) = 1 - \frac{\alpha}{r} \exp \left[-\frac{r}{h} \right],$$

$(r/\alpha)(s_0^{As}(r) - 1)$ has been plotted for $h = 2\alpha$ in Fig. 3 (curve 4).

Using formulas (1) and (2), taking into account the uniform background of positive ions, the Debye-Hückel laws are obtained:

$$(19) \quad \frac{p}{\epsilon K T} = 1 - \frac{1}{3} (\pi\epsilon)^{\frac{1}{2}} \left(\frac{e^2}{K T} \right)^{\frac{3}{2}},$$

$$(20) \quad \frac{E}{K T} = \frac{3}{2} - (\pi\epsilon)^{\frac{1}{2}} \left(\frac{e^2}{K T} \right)^{\frac{3}{2}}.$$

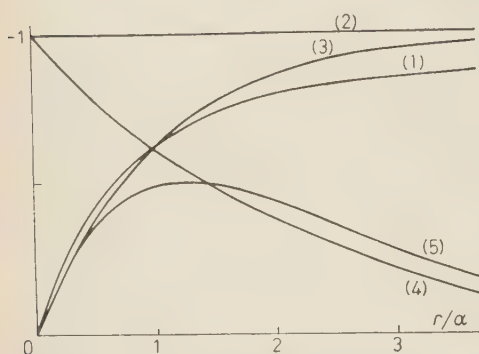


Fig. 3. - Curve (1): $(r/\alpha)\xi_0(r)$. Curve (2): $(r/\alpha)\xi_0^{As}(r)$. Curve (3): $(r/\alpha)\xi_0^{Ap}(r)$. Curve (4): $(r/\alpha)(s^{As}(r) - 1)$ for $\alpha = 2h$. Curve (5): $(r/\alpha)(s(r) - 1)$ for $\alpha = 2h$.

We shall now make an approximation somewhat better than (16), namely:

$$(21) \quad \xi_0^{Ap}(r) = -\frac{\alpha}{r} \left(1 - \exp \left[-\frac{r}{\alpha} \right] \right).$$

$(r/\alpha)\xi_0^{Ap}$ has been plotted in Fig. 3 (curve (3)) and one sees that it is fairly near to the exact curve (curve (1)). Moreover, the validity of approximation (21) does not depend on the density. It has been chosen so as to be able to perform analytically the Fourier transforms (9) and (11). We get in this approximation

$$(22) \quad s(r) = \exp \left[-\frac{\alpha}{r} \left[\exp \left[-\frac{r}{\alpha} \right] + \sqrt{1 - 4h^{-2}} (\exp [-rA_-] - \exp [-rA_+]) \right] \right],$$

where

$$(23) \quad A_{\pm}^2 = \frac{1}{2\alpha^2} (1 \pm \sqrt{1 - 4h^{-2}}).$$

$(r/\alpha)(s(r) - 1)$ has been plotted in Fig. 3 (curve (5)) for $\alpha = 2h$ and can be compared with the asymptotic value obtained above (see Fig. 3, curve (4)). We

express the correction to the Debye-Hückel law in the form

$$(24) \quad \frac{p}{\rho K T} = 1 - \frac{1}{3}(\pi \rho)^{\frac{1}{2}} \left(\frac{e^2}{K T} \right)^{\frac{3}{2}} (1 + \beta),$$

$$(25) \quad \frac{E}{K T} = \frac{3}{2} - (\pi \rho)^{\frac{1}{2}} \left(\frac{e^2}{K T} \right)^{\frac{3}{2}} (1 + \beta).$$

Comparing equations (24)-(25) with the Debye-Hückel laws (19)-(20), we see that β is a measure of the correction for non zero densities introduced by the more exact treatment that we have just made. β is plotted against α/h in Fig. 4 (curve (1)). It shows that the correction to the Debye-Hückel laws is small for values of α smaller than the Debye length.

The same conclusion was reached by ABE⁽¹⁰⁾ who summed the chain-like terms in the cluster series for the pressure and made an expansion in the density. Abe's result for β is plotted in Fig. 4 (curve (2)). It agrees with our result in the low density region.

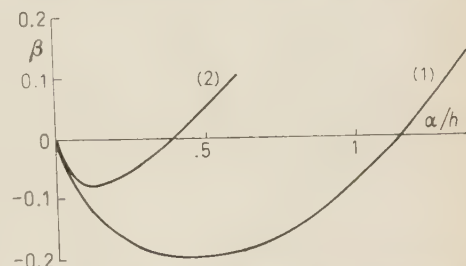


Fig. 4. - The correction factor against α/h as given by the present theory (curve (1)) and by Abe's calculation (curve (2)).

4. - The generalized chain expansion.

We shall now include more terms in the cluster expansion by a natural generalization of the chain diagrams: to a chain diagram built as above, where

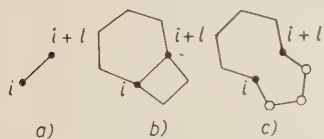


Fig. 5. - Typical elements replacing $\xi_0(i, i+1)$.

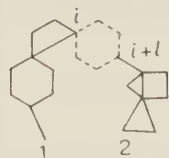


Fig. 6. - A primary chain constructed from ξ_1 .

between points i and $i+1$ there is a $\xi_0(i, i+1)$ (Fig. 5, a), we shall associate the diagrams of type b (Fig. 5, b), where in addition to the ξ_0 term one or more chains start from i to go to $i+1$, and the diagrams of type c (Fig. 5, c), where between i and $i+1$ there is no ξ_0 but at least two chains starting from i and going to $i+1$. We shall call such chains, grafted on the primary chain, secondary chains.

Let us consider a diagram resulting from the operations described above on a primary chain of N points (Fig. 6). We shall sum all the diagrams which

⁽¹⁰⁾ R. ABE: *Progr. Theor. Phys.*, **22**, 213 (1959).

can be formed by considering all the terms of the type a , b and c , situated between i and $i+1$. Let M be the number of points of the initial diagram (including points i and $i+1$). The cluster integral corresponding to the diagram in which points i and $i+1$ are joined by a ξ_0 (diagram of type a) will be of the form

$$(26) \quad \beta_M^a = \int d\mathbf{3} \dots d\mathbf{N} + 2\xi_0(i, i+1) \cdot \\ \cdot F_1(1, 3) \dots F_i(i-1, i) F_{i+1}(i+1, i+2) \dots F_N(N+2, 2),$$

where $F_1 \dots F_N$ are cluster integrals resulting from the integration over the $M-N$ variables belonging to the secondary chains. The factorial in definition (7) disappears when the identity of the M points of the diagram is taken into account.

Let us add between i and $i+1$ l chains of N_1, N_2, \dots, N_l points each, thus forming a b -type diagram between i and $i+1$. We have altogether $M = M + N_1 + \dots + N_l$ points in the resulting diagram. The identity of the M_b points leads to a factor $M_b!$ compensating the $1/M_b!$ coming from (7). It has to be taken into account that the permutation of the l chains leads to identical diagrams, so that the cluster integral in this case is written

$$(27) \quad \hat{\beta}_M^b(N_1 \dots N_l) = \frac{1}{l!} \int d\mathbf{3} \dots d\mathbf{N} + 2\xi_0(i, i+1) \cdot \\ \cdot \beta_{N_1}^0(i, i+1) \beta_{N_2}^0(i, i+1) \dots \beta_{N_l}^0(i, i+1) \cdot \\ \cdot F_1(1, 3) \dots F_i(i-1, i) F_{i+1}(i, i+1) \dots F_N(N+2, 2).$$

The summation of all b -type diagrams included between i and $i+1$ is thus taken into account by adding to the $\xi_0(i, i+1)$ which comes in (26) the contribution

$$(28) \quad (\exp[\gamma_0(i, i+1)] - 1) \xi_0(i, i+1).$$

A similar reasoning yields for the contribution of the c -type diagrams included between i and $i+1$

$$(29) \quad \exp[\gamma_0(i, i+1)] - \gamma_0(i, i+1) - 1.$$

Thus we see that we take into account all the secondary chains grafted on the primary chain between i and $i+1$ if we replace the $\xi_0(i, i+1)$ of the primary chain by $\xi_1(i, i+1)$, where

$$(30) \quad \xi_1(i, i+1) = (\xi_0(i, i+1) + 1) \exp[\gamma_0(i, i+1)] - 1 - \gamma_0(i, i+1).$$

Taking (13) and (5) into account, we have

$$(31) \quad \xi_1(i, i+1) = s_0(i, i+1) - 1 - \gamma_0(i, i+1).$$

This replacement can be on any line of the primary chains. Thus we are led to an improved approximation for the correlation function: $s_1(r)$ is now constructed from ξ_1 chains as $s_0(r)$ was constructed in Section 2 from ξ_0 chains. We can go to the next order of approximation by considering diagrams in which the secondary chains are constructed from ξ_1 instead of ξ_0 (see Fig. 7). In the primary chain each $\xi_0(r)$ is then replaced by

$$(30') \quad \xi_2(r) = \xi_0(r) + \xi_0(r)(\exp [\gamma_1(r)] - 1) + \exp [\gamma_1(r)] - 1 - \gamma_1(r);$$

$\gamma_1(r)$ represents here the sum of the chain constructed from ξ_1 .

Proceeding to higher and higher degrees of complexity, we are thus led to the following system of equations, which define the iteration procedure from which the correlation function is obtained, valid for all $n \geq 0$:

$$(31') \quad \xi_n(r) = s_{n-1}(r) - 1 - \gamma_{n-1}(r),$$

$$(9') \quad \Xi_n(k) = \varrho \int \exp [-i \mathbf{k} \cdot \mathbf{r}] \xi(r) d\mathbf{r},$$

$$(12') \quad \Gamma_n(k) = \Xi_n^2(k)/(1 - \Xi_n(k)),$$

$$(11') \quad \gamma_n(r) = \frac{1}{(2\pi)^3 \varrho} \int \exp i \mathbf{k} \cdot \mathbf{r} \Gamma_n(k) d\mathbf{k},$$

$$(13') \quad s_n(r) = \exp \left[-\frac{V(r)}{KT} \right] \exp [\gamma_n(r)].$$

As we mentioned in the introduction, MORITA has considered a development similar to ours, but some terms included here are missing in Morita's expansion (*).

A detailed comparison is made in the Appendix.

(*) *Note added in proof.* - In an article which appeared recently (*Progr. Theor. Phys.*, **23**, 829 (1960)) MORITA has added to his preceding expansion the missing terms. He thus obtains the eqs. (37-38) of the present paper: moreover, the same author has given the expression of the correction terms to the integral equation as in the preprint of Dr. MEERON and as in the present paper (*Progr. Theor. Phys.*, **23**, 385 (1960)).

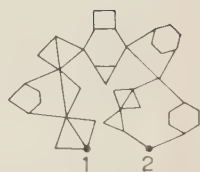


Fig. 7. - A primary chain constructed from ξ_2 .

5. — The integral equation for the generalized chain expansion.

Let us assume that the iteration process converges: in the limit of n going to infinity (31') becomes

$$(32) \quad \xi(r) = g(r) - \gamma(r),$$

where we have put

$$(33) \quad g(r) = s(r) - 1.$$

We note that $g(r)$ approaches zero when r tends to infinity. Taking the Fourier transform of (32), one has

$$(34) \quad G(k) = \varrho \int \exp[-i \mathbf{k} \cdot \mathbf{r}] g(r) d\mathbf{r} = \Xi(k) + I(k),$$

which by (12') becomes

$$(35) \quad G(k) = \Xi(k)/(1 - \Xi(k)),$$

This equation, with (12') and (11') leads to

$$(36) \quad \gamma(1, 2) = \varrho \int d\mathbf{3} g(1, 3) \xi(2, 3).$$

Thus the correlation function is defined through the two coupled equations

$$(37) \quad s(r) = \exp \left[-\frac{V(r)}{KT} \right] \exp [\gamma(r)],$$

$$(38) \quad \gamma(r) = \varrho \int d\mathbf{r}' (s(|\mathbf{r} - \mathbf{r}'|) - 1) (s(r') - 1 - \gamma(r')).$$

This last equation can be put in the following form, convenient for a numerical calculation,

$$(39) \quad \gamma(r) = \frac{2\pi\varrho}{r} \int_0^\infty r' dr' (s(r') - 1 - \gamma(r')) (\Phi(r + r') - \Phi(|r - r'|)),$$

where

$$(40) \quad \Phi(r) = \int_0^r (s(r') - 1) r' dr'.$$

The set of equations (37)-(38) is equivalent to one non-linear integral equation for $\gamma(r)$ or $s(r)$. $\gamma(r)$ is certainly a function more regular than is $s(r)$, and it will be better practically to solve for $\gamma(r)$. The elimination of $\gamma(r)$ will however be useful in the following and we shall perform it now.

From (35) one has

$$(41) \quad \Xi(k) = G(k)/(1 + G(k)) .$$

Thus we have, using (36) and (37),

$$(42) \quad s(1, 2) = g(1, 2) - 1 = \\ - \exp \left[- \frac{V(r)}{KT} - \varrho \int g(1, 3) g(3, 2) d\mathbf{3} - \varrho^2 \int g(1, 3) g(3, 4) g(4, 2) d\mathbf{3} d\mathbf{4} + \right. \\ \left. + \dots + \varrho^N (-1)^{N+1} \int g(1, 3) g(3, 4) \dots g(N+2, 2) d\mathbf{3} \dots d\mathbf{N+2} + \dots \right] .$$

Equation (35) can be written in co-ordinate space

$$(43) \quad g(r) = \xi(r) + \varrho \int g(|\mathbf{r} - \mathbf{r}'|) \xi(r') d\mathbf{r}' .$$

We see that this relation is identical with a quite general relation holding for fluids which has been derived by ORNSTEIN and ZERNICKE⁽¹¹⁾. The present theory enables us, using (32), to calculate $\xi(r)$ which is interpreted in ref. (11) as the direct interaction between two particles.

This function is also of interest in the calculation of the quantity $(\partial p / \partial \varrho)_T$ which goes to zero at the critical point. It is obtained from relation (3)

$$(44) \quad \frac{1}{KT} \left(\frac{\partial p}{\partial \varrho} \right)_T = \frac{1}{1 + \varrho \int g(r) d\mathbf{r}} = 1/(1 + G(0))$$

and, using (34),

$$(45) \quad \frac{1}{KT} \left(\frac{\partial p}{\partial \varrho} \right)_T = 1 - \Xi(0) = 1 - \varrho \int \xi(r) d\mathbf{r} .$$

YVON has derived⁽¹⁷⁾ a relation similar to (45), and the function $\xi(r)$ is apart from a trivial multiplicative constant identical with his function $H_{12}(r)$. YVON has shown, by considering the first terms of the cluster expansion of $\xi(r)$ that its range is of the order of the range ε of the potential, even in the neighborhood of the critical point. We can show more generally that this is indeed the case:

(11) See ref. (1) and L. GOLDSTEIN: *Phys. Rev.*, **84**, 466 (1951).

outside the range of the potential, one has

$$V(r) \approx 0 \quad \text{for } r \geq \varepsilon.$$

We know from experiment ⁽¹²⁾ that even at the critical point $s(r)$ is not very different from one, so that we can suppose that in this case $\gamma(r)$, although of long range, is appreciably smaller than one. We have

$$(46) \quad s(r) \approx 1 + \gamma(r) + 0(\gamma^2) \quad \text{for } r \geq \varepsilon,$$

and, from (9),

$$(47) \quad \xi(r) \approx 0(\gamma^2) \quad \text{for } r \geq \varepsilon.$$

So that, for $r \geq \varepsilon$, $\xi(r)$ is an order of magnitude smaller than $g(r)$. At the critical point, one has

$$\left(\frac{\partial p}{\partial \rho} \right)_T = 0,$$

so that

$$\Xi(0) = 1.$$

If, for example, we choose $\Xi(k)$ of the form

$$(48) \quad \Xi(k) = \mu^2 / (\mu^2 + k^2) \quad (\text{for small } k),$$

which gives for $\xi(r)$

$$(49) \quad \xi(r) = \frac{\mu^2}{2\pi^2 \rho} \frac{\exp[-\mu r]}{r},$$

with $\mu = 1/\varepsilon$ then we have

$$(50) \quad g(r) = \frac{1}{(2\pi)^3 \rho} \int \frac{\Xi(k)}{1 - \Xi(k)} \exp[i \mathbf{k} \cdot \mathbf{r}] d\mathbf{r} d\mathbf{k} = \frac{\mu^2}{2\pi^2 \rho r} \quad \text{for } r \geq \varepsilon.$$

This function is the long range function expected at the critical point ⁽¹¹⁾.

6. — Relation with the virial coefficients.

We shall see now how the virial coefficients are reproduced by the integral equation (37)-(38).

We use first the iteration procedure of Section 3. When only primary chains

⁽¹²⁾ A. EISENSTEIN and N. S. GINGRICH: *Phys. Rev.*, **62**, 261 (1942).

are considered, we get the first three virial coefficients and pieces of all the others. In particular there is a contribution to the fourth virial coefficients, represented by the two diagrams (a) of Fig. 8. The first of these diagrams comes from the single chain of two points, the second term is the reducible diagram which appears in the expansion of the exponential in eq. (6), the corresponding irreducible diagram being a chain with one point.

When secondary chains are considered, there comes a new contribution to all the virial


coefficients of an order higher than the third. The contribution to the fourth virial coefficients is represented by diagrams (b) of Fig. 8. The next order of complication of the chains will modify the virial coefficients starting from the fifth one. It is clear that the diagram (c) of Fig. 8, which is also a contribution to the fourth virial coefficient, will not appear. It is quite evident that an integral equation of the type (37)-(38), involving only 3 points, is unable to generate terms like the one of diagram (c).

We now examine the diagrams which are generated when the integral equation (37)-(38) is solved by iteration, starting from the zero-density correlation function

$$\exp \left[- \frac{V(r)}{KT} \right].$$

From (25), we have, as a first approximation,

$$(51) \quad \gamma_1(1, 2) = \varrho \int \xi_0(1, 3) \xi_0(2, 3) d\mathbf{3},$$

which is symbolized by the diagram: .

Equation (24) gives s_1 , which we can write schematically as

$$s_1(1, 2) = \bullet \cdots \bullet + \text{diagram of two points connected by a line} + \frac{1}{2!} \text{diagram of two points connected by a line with a loop} + \frac{1}{3!} \text{diagram of two points connected by a line with a triangle} + \cdots$$

We see that the first three virial coefficients are obtained as well as one term of the fourth virial coefficient.

In the next order, we have, using (25) again,

$$\gamma_2(1, 2) = \text{diagram of two points connected by a line} + \text{diagram of two points connected by a line with a loop} + \text{diagram of two points connected by a line with a triangle} + \text{diagram of two points connected by a line with a square} + \frac{1}{2!} \text{diagram of two points connected by a line with a loop and a triangle} + \frac{1}{2!} \text{diagram of two points connected by a line with a triangle and a loop} + \cdots$$

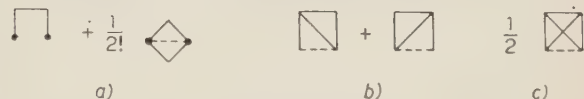


Fig. 8. - Diagrams contributing to the fourth virial coefficients. Here the dotted lines represent $\xi_0 + 1$, the solid line, ξ_0 .

We now have all the contributions to the fourth virial coefficient except, naturally, the term represented by diagram (c) of Fig. 8. We note that with this iteration procedure the chain of n points appears only at the n -th iteration. Thus the terms of the cluster series are summed in an order quite different from that in Section 4. Of course, the same diagrams are ultimately obtained.

7. — Connection with the Born-Green-Kirkwood equation.

We shall show now that the integral equation (37)-(38) contains the equation obtained when the system of integro-differential equations due to Yvon, Born and Green ⁽⁸⁾ is closed by the superposition approximation ⁽⁹⁾.

Let us first briefly rederive the Yvon-Born-Green equations: taking the gradient of (4) with respect of co-ordinate \mathbf{r}_1 , we get the following exact equation:

$$(52) \quad \nabla_1 s(1, 2) = X(1, 2) s(1, 2) + \varrho \int X(1, 3) s(1, 2, 3) d\mathbf{3},$$

where we have put

$$(53) \quad X(1, 2) = -\nabla_1 V(1, 2)/KT.$$

The 3-particle correlation function is defined by

$$(54) \quad s(1, 2, 3) = V^3 \frac{\int \prod_{i < j} \exp \left[-\frac{V(i, j)}{KT} \right] d\mathbf{4} \dots d\mathbf{N}}{\int \prod_{i < j} \exp \left[-\frac{V(i, j)}{KT} \right] d\mathbf{1} \dots d\mathbf{N}}.$$

We shall now use the superposition approximation

$$(55) \quad s(1, 2, 3) = s(1, 2) s(1, 3) s(2, 3).$$

This permits us to express (52) as an integro-differential equation for the correlation function.

To make the comparison with the integral equation (37)-(38), we shall make a trivial modification of eq. (52); for this we use the relation

$$(56) \quad \int s(1, 2) X(1, 2) d\mathbf{2} = 0,$$

which is obtained by noting that, for a homogeneous fluid we have

$$(57) \quad \frac{\nabla_1 \int \prod_{i < j} \exp \left[-\frac{V(i, j)}{KT} \right] d\mathbf{2} \dots dN}{\int \prod_{i < j} \exp \left[-\frac{V(i, j)}{KT} \right] d\mathbf{1} \dots dN} = 0.$$

This leads to the equation

$$(58) \quad \nabla_1 s(1, 2) = X(1, 2) s(1, 2) + \varrho s(1, 2) \int X(1, 3) s(1, 3) [s(2, 3) - 1] d\mathbf{3}.$$

This equation has been extensively applied to the theory of liquid state, in particular by KIRKWOOD and his collaborators⁽¹³⁾. For the sake of brevity we shall call this equation the BGK equation. We shall derive this equation as an approximation of the integral equation (37)–(38) obtained from the generalized chain approach. For this, we take the gradient of (37) with respect to co-ordinate 1

$$(59) \quad \nabla_1 s(1, 2) = X(1, 2) s(1, 2) - \nabla_1 \gamma(1, 2) s(1, 2).$$

Taking the gradient of (38), we obtain

$$(60) \quad \nabla_1 \gamma(1, 2) = \varrho \int (\nabla_1 s(1, 3) - \nabla_1 \gamma(1, 3)) (s(2, 3) - 1) d\mathbf{3}.$$

Combining this equation with the preceeding one, we obtain

$$(61) \quad \begin{aligned} \nabla_1 s(1, 2) = & X(1, 2) s(1, 2) + \varrho s(1, 2) \int X(1, 3) s(1, 3) (s(2, 3) - 1) d\mathbf{3} + \\ & + \varrho s(1, 2) \int (s(1, 3) - 1) (s(2, 3) - 1) \nabla_1 \gamma(1, 3) d\mathbf{3}. \end{aligned}$$

This equation is identical with the BGK equation (58) except for the last term which vanishes only if we replace in it the correlation function by its value for large distances.

The relation between the BGK equation and the integral equation (37)–(38) can be seen in another way: we can, from the BGK equation (58), using defi-

⁽¹³⁾ J. G. KIRKWOOD, V. A. LEWINSON and B. J. ALDER: *Journ. Chem. Phys.*, **20**, 929 (1952).

dition (33), calculate the quantity

$$(62) \quad X(1, 3) s(1, 3) = \nabla_1 g(1, 3) + \varrho s(1, 3) \int X(1, 4) s(1, 4) g(4, 3) d\mathbf{4}.$$

Substituting in (58), we get a term ϱ^2 in which the quantity $X(1, 4) s(1, 4)$ appears. Substituting (62) again and again so as to get rid of this type of term, we obtain,

$$(63) \quad \begin{aligned} \nabla_1 s(1, 2) = s(1, 2) \nabla_1 \left(-\frac{V(1, 2)}{KT} + \varrho \int g(1, 3) g(2, 3) d\mathbf{3} - \right. \\ \left. - \varrho^2 \int g(1, 3) g(3, 4) g(4, 2) d\mathbf{3} d\mathbf{4} + \varrho^3 \int g(1, 3) g(3, 4) g(4, 5) g(5, 2) d\mathbf{3} d\mathbf{4} d\mathbf{5} - \dots \right) - \\ - \varrho^2 s(1, 2) \int \nabla_1 g(1, 3) g(1, 4) g(3, 4) g(4, 2) d\mathbf{3} d\mathbf{4} + \\ + \varrho^3 s(1, 2) \int \nabla_1 g(1, 3) g(1, 4) g(3, 4) g(4, 5) g(5, 2) d\mathbf{3} d\mathbf{4} d\mathbf{5}. \end{aligned}$$

Using (41) and (42), this equation can be put in the compact form

$$(64) \quad \begin{aligned} \nabla_1 s(1, 2) = s(1, 2) \nabla_1 \left(-\frac{V(1, 2)}{KT} + \gamma(1, 2) \right) - \\ - \varrho^2 s(1, 2) \int \nabla_1 g(1, 3) g(1, 4) g(3, 4) \xi(4, 2) d\mathbf{3} d\mathbf{4}. \end{aligned}$$

If we take into account the first term only, we get, after integration, a correlation function identical with ours (eq. (37)). By replacing in the second term the ξ and the g 's by ξ_0 's, we see that it cannot be interpreted as a term of the cluster expansion. Apart from the term of type c (Fig. 8), which cannot be obtained from an integral equation involving only three points, the fourth virial coefficient is correctly obtained from the first term of (54). The second term must be considered as a spurious term due to the superposition approximation. In fact, we shall see in Section 9, that a more correct three-body correlation function brings in counter terms which automatically cancel the spurious terms of equations (64) and (65).

8. — The correction terms.

We now want to include in our approximation scheme the more complicated terms which have been left out of the generalized chain expansion of Section 3. We shall first sum all the combinations of terms whose prototype

is diagram *c* of Fig. 8 with the terms already considered, forming diagrams of the type shown in Fig. 9.

For this purpose we shall consider the iteration scheme defined by the following equations:

$$(65) \quad \gamma_n^{(1)} = \varrho \int \xi_n(1, 3) \xi_n(3, 2) d\mathbf{3} + \varrho^2 \int \xi_n(1, 3) \xi_n(3, 4) \xi_n(4, 2) d\mathbf{3} d\mathbf{4} + \\ + \varrho^3 \int \xi_n(1, 3) \xi_n(3, 4) \xi_n(4, 5) \xi_n(5, 2) d\mathbf{3} d\mathbf{4} d\mathbf{5} + \dots = \\ = -\xi_n(1, 2) + \lambda_n(1, 2) = \varrho \int \xi_n(1, 3) \lambda_n(3, 2) d\mathbf{3},$$

$$(66) \quad \gamma_n^{(2)} = \frac{\varrho^2}{2} \int \lambda_{n-1}(1, 3) \lambda_{n-1}(1, 4) \lambda_{n-1}(2, 3) \lambda_{n-1}(2, 4) \lambda_{n-1}(3, 4) d\mathbf{3} d\mathbf{4},$$

$$(67) \quad \xi_n(r) = s_{n-1}(r) - 1 - \gamma_{n-1}^{(1)}(r),$$

$$(68) \quad s_n(r) = \exp \left[-\frac{V(r)}{KT} \right] \exp [\gamma_n^{(1)}(r) + \gamma_n^{(2)}(r)].$$

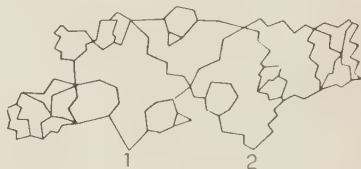


Fig. 9. — A typical diagram obtained from the first correction term to the integral eqs. (37)-(38). The solid lines represent ξ_0 's.

We start with

$$(69) \quad \gamma_{-1}^{(1)}(r) = 0, \quad s_{-1}(r) = \xi_0(r), \quad \lambda_{-1}(r) = \xi_0(r).$$

After the first iteration we obtain for $\gamma_0^{(1)}(r)$ the same result as in Section 3: $\gamma_0^{(1)}(r)$ is the sum of chains of ξ_0 . $\gamma_0^{(2)}$ is represented by diagram *c* of Fig. 8. We notice that at this stage all the four first virial coefficients have been obtained except for the terms represented by diagram *b* of Fig. 8.

We then proceed as in Section 3 to build ξ_1 , which we represent graphically as

$$(70) \quad \xi_1 = \text{diagram 1} + \text{diagram 2} + \frac{1}{2!} \text{diagram 3} + \frac{1}{2!} \text{diagram 4} + \dots \\ + \frac{1}{2!} \text{diagram 5} + \frac{1}{2!} \frac{1}{2!} \text{diagram 6} + \frac{1}{2!} \text{diagram 7} + \frac{1}{2!} \frac{1}{2!} \text{diagram 8} + \dots \\ - \text{diagram 9}$$

The last term corresponds to $-\gamma_n^{(1)}(r)$ in formula (67). It has to be subtracted as was the case in Section 3, so that the chain diagrams are not counted twice. It is clear that a similar term has not to be subtracted for $\gamma_n^{(2)}(r)$.

$\gamma_1^{(1)}(r)$ is the sum of the chains constructed from ξ_1 . $\gamma_1^{(2)}(r)$ is given symbolically by the equation (71):

$$(71) \quad \gamma_n^{(2)}(r) = \frac{1}{2} \text{ [diagram] },$$

where the wiggly lines of the diagrams represent the sum of ξ_0 chains as given by $\lambda_0(r)$ of eq. (65).

Going to the next approximation, ξ_2 will have the same general shape as ξ_1 of eq. (70), but the chains will be now constructed from ξ_1 , and the side of the crossed diagrams will now be made from chains constructed from ξ_0 , as given by $\lambda_0(r)$ of eq. (65).

After an infinite number of iterations have been made, we obtain, comparing (67) and (65),

$$(72) \quad \lambda(r) = s(r) - 1 = g(r).$$

The correlation function is now defined by the set of equations

$$(73) \quad s(r) = g(r) + 1 = \exp \left[-\frac{V(r)}{KT} \right] \exp [\gamma^{(1)}(r) + \gamma^{(2)}(r)],$$

$$(74) \quad \gamma^{(1)}(1, 2) = \varrho \int (g(1, 3) - \gamma^{(1)}(1, 3)) g(3, 2) d\mathbf{3},$$

$$(75) \quad \gamma^{(2)}(1, 2) = \frac{\varrho^2}{2} \int g(1, 3) g(1, 4) g(2, 3) g(2, 4) g(3, 4) d\mathbf{3} d\mathbf{4}.$$

There is some arbitrariness about the way to introduce the correction terms. For instance we might have written instead of eq. (66)

$$(66') \quad \gamma_n^{(2)} = \frac{\varrho^2}{2} \int \lambda_{n-2}(1, 2) \lambda_{n-2}(1, 4) \lambda_{n-2}(2, 4) \lambda_{n-2}(2, 3) \lambda_{n-2}(3, 4) d\mathbf{3} d\mathbf{4},$$

with in addition of conditions (69) the prescription

$$\gamma_{n-2}(r) = 0.$$

We start the iteration procedure as above. We have after the first iteration the same result as in Section 3. After the second iteration we have for ξ_2 the same type of diagram as those given by (70) except that the chains in it are now constructed from ξ_1 . Taking again the example of the fourth virial coef-

ficients, we see that the first iteration gives the diagram (a) of Fig. 8, when the second iteration gives also diagrams (b) and (c). Ultimately, however, the same diagrams are summed and the same limiting equations are obtained.

The next correction terms forming $\gamma^{(3)}(r)$ will be defined as those which cannot be reduced to terms included in $\gamma^{(2)}(r)$ or in $\gamma^{(1)}(r)$, but which can be so reduced by cutting a link somewhere in the representative diagram.

We write graphically the formula for $\gamma^{(3)}(r)$. The lines in the diagrams, after an infinite number of iterations have been made, represent g -functions. These terms generalize the term given by $\gamma^{(2)}(r)$ in equation (75). We separate the contribution of 5-point and 6-point diagrams, which are of order q^3 and q^4 respectively:

$$(76) \quad \left\{ \begin{array}{l} \gamma_{(5)}^{(3)}(r) = \text{diagram 1} + \text{diagram 2} \\ \gamma_{(6)}^{(3)}(r) = \frac{1}{2} \text{diagram 3} + \text{diagram 4} + \frac{1}{2} \text{diagram 5} \end{array} \right.$$

The 5-point diagrams of a higher degree of complication will also be useful in the next paragraph. They are

$$(77) \quad \left\{ \begin{array}{l} \gamma_{(5)}^{(4)}(r) = \text{diagram 1} + \frac{1}{2} \text{diagram 2} \\ \gamma_{(5)}^{(5)}(r) = \frac{1}{6} \text{diagram 3} \end{array} \right.$$

The integrals corresponding to $\gamma^{(3)}$, $\gamma^{(4)}$... are obviously very difficult to calculate. It may be hoped, however, that, given the great number of links they involve, they are small.

We shall put

$$(78) \quad \gamma^o(r) = \gamma^{(1)}(r) ;$$

$\gamma^o(r)$ represents now the sum of the chains constructed from completely re-normalized ξ 's.

The sum of the rest of the contribution to $\gamma(r)$ will be given by

$$(79) \quad \gamma^R(r) = \sum_{i=2}^{\infty} \gamma^{(i)}(r) .$$

The correlation function is now given by

$$(80) \quad s(r) = \exp \left[-\frac{V(r)}{KT} \right] \exp [\gamma^o(r) + \gamma^R(r)] .$$

We easily see that the Ornstein-Zernicke relation (43) is still valid in the present case, with $\xi(r)$ defined by the equation

$$(67') \quad \xi(r) = g(r) - \gamma^c(r).$$

The Yvon relation (34) is also maintained, but the demonstration of the smallness of $\xi(r)$ outside the range of the potential now requires that $\gamma^R(r)$ should be for large distances an order of magnitude smaller than $\gamma^c(r)$, which is probably true, so that the essential of the demonstration of Section 5 remains.

Finally, we note that, supposing $V(r)$ and $s(r)$ known, it is possible to deduce $\gamma^c(r) + \gamma^R(r)$, at least outside the repulsive region of the potential. On the other hand, equation (74) can be written after a Fourier transformation

$$(74') \quad I^c(k) = \frac{G^2(k)}{1 + G(k)},$$

$\gamma^c(r)$ can therefore be obtained equally well from the knowledge of the correlation function. If the experimental determination of this functions were precise enough, it should be possible to measure the effects of the correction terms introduced in this paragraph.

9. - The three-body correlation function.

In this paragraph we shall give the first corrections to the superposition approximation ⁽¹⁴⁾. We shall show that, when the corrected 3-body correlation function is introduced in the Yvon-Born-Green equation (52) the correlation function calculated in the preceding paragraph is obtained and the spurious terms of the BGK equation disappear.

The cluster expansion for the three-body correlation function is given in the paper of SALPETER quoted in ref. (1). The three-body correlation function is defined as

$$(81) \quad s(1, 2, 3) = s(1, 2) s(2, 3) s(3, 2) \exp \left[\sum_{N=1}^{\infty} \varrho^N \beta_N(1, 2, 3) \right].$$

The $\beta_N(1, 2, 3)$ are the exact generalization of the two-body irreducible cluster integrals: an irreducible diagram is defined by the same prescription as in Section 2, except for the last prescription which now reads: 3') a diagram is

⁽¹⁴⁾ Various authors have investigated this problem by considering the first few terms of the expansion of (81): YVON: private communication; R. ABE: *Progr. Theor. Phys.*, **21**, 421 (1959).

reducible if a part of it can be separated from the rest by cutting lines joining points 1, 2 and 3. The $\beta_N(1, 2, 3)$ are given by a formula similar to formula (7) of Section 2.

The first term of the cluster expansion leads to the superposition approximation (we note that in (81) the exact two-body correlation function appears).

The first correction term will be represented by the diagram shown in Fig. 10. In this diagram the dotted lines represent s functions. In the usual cluster expansion the solid lines of the diagram of Fig. 10 would represent ξ_0 functions. It is clear that by the considerations of the preceding paragraph these lines should be now replaced by g functions. Once this replacement has been made, a large class of terms of (81)

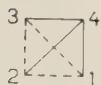


Fig. 10. - The first correction to the superposition approximation. The dotted and solid lines represent s and g functions respectively.

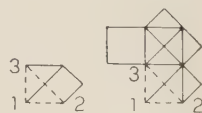


Fig. 11. - Typical diagrams included in the first correction to the superposition as described by Fig. 10. Here the solid lines represent ξ_0 functions.

is summed. For instance diagrams such as the diagrams shown in Fig. 11 are included, when equations (79)-(80) are used to define g .

The term $N = 2$ in the exponent of (81) will give rise to the irreducible diagrams shown in Fig. 12, which are the prototype of the ϱ^2 correction to the superposition approximation.

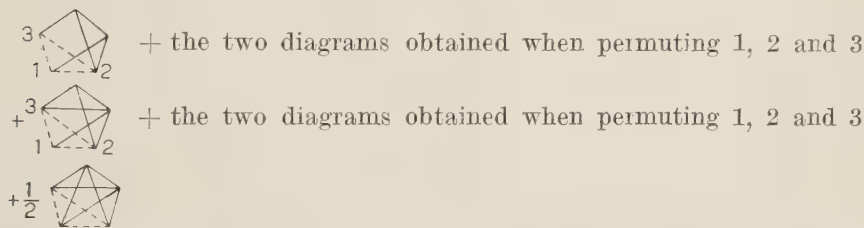


Fig. 12. - The second correction to the superposition approximation. The dotted and solid lines represent s and g functions respectively.

There again the dotted lines represent s functions, the solid lines, g functions when the summation of terms considered in the preceding paragraph has been made.

We shall show now that the introduction of the corrected three-body correlation function in the Yvon-Born-Green equation (52) leads to equations (79)-(80) for the two-body correlation function.

We first consider a three-body correlation function including the first correction to the superposition approximation, which is, writing the expression

represented by the diagram of Fig. 10,

$$(82) \quad s^1(1, 2, 3) = s(1, 2) s(1, 3) s(2, 3) \left(1 + \varrho \int g(1, 4) g(2, 4) g(3, 4) d\mathbf{4} \right).$$

We introduce this function in the Yvon-Born-Green equation (52). This replacement taking (56) into account, yields

$$(83) \quad \nabla_1 s(1, 2) = X(1, 2) s(1, 2) + \varrho s(1, 2) \int X(1, 3) s(1, 3) g(2, 3) d\mathbf{3} + \\ + \varrho^2 s(1, 2) \int X(1, 3) s(1, 3) s(2, 3) g(1, 4) g(2, 4) g(3, 4) d\mathbf{3} d\mathbf{4}.$$

Eliminating the terms containing the potential, as was done in Section 6, and neglecting the terms of an order in ϱ higher than the second, we obtain the equation

$$(84) \quad \nabla_1 s(1, 2) = X(1, 2) s(1, 2) + \varrho s(1, 2) \nabla_1 \int g(1, 3) g(2, 3) d\mathbf{3} - \\ - \varrho^2 s(1, 2) \nabla_1 \int g(1, 3) g(3, 4) g(4, 2) d\mathbf{3} d\mathbf{4} - \\ - \varrho^2 s(1, 2) \int \nabla_1 g(1, 3) g(1, 4) g(3, 4) g(4, 2) d\mathbf{3} d\mathbf{4} + \\ + \varrho^2 s(1, 2) \int \nabla_1 g(1, 3) g(1, 4) g(3, 4) g(4, 2) d\mathbf{3} d\mathbf{4} + \\ + \frac{\varrho^2}{2} s(1, 2) \nabla_1 \int g(1, 3) g(1, 4) g(2, 3) g(2, 4) g(3, 4) d\mathbf{3} d\mathbf{4}.$$

The second and third terms are the beginning of the expansion of $\varrho s(1, 2) \nabla_1 \gamma^c(1, 2)$ as can be seen by a comparison with equations (63)-(64). The fourth term is the first spurious term appearing in the BGK equation (see eq. (63)). It is cancelled by the fifth term. The last term is equal to $\varrho s(1, 2) \nabla_1 \gamma^{(2)}(1, 2)$.

Equation (84) is thus equivalent to the equations (79)-(80) up to the order ϱ^2 .

Using the next correction to the superposition approximation which is represented diagrammatically in Fig. 12, we have pushed the calculation up to the order ϱ^3 . We do not give the details of the calculation as it is too long to be reproduced and quite straightforward. We only quote the results:

- 1) $\gamma^c(1, 2)$ is obtained up to the order ϱ^3 .
- 2) All spurious terms are eliminated up to the order ϱ^3 .

- 3) All the ϱ^3 contributions to $\gamma^R(1, 2)$, given by equations (76)-(77) are obtained with the right coefficients.

We have still to show that the introduction of the corrected three-body correlation function (82) in the Born and Green equation leading to equation (83), added to the requirement that the resulting integrodifferential equation be a three-point equation, leads to the equation (37)-(38). In other words, we shall perform the elimination of the spurious terms of the BGK equation at all orders in ϱ . To do this, we replace in (83), $s(2, 4)$ by its asymptotic value which is unity. Thus we get

$$(85) \quad \nabla_1 s(1, 2) = X(1, 2) s(1, 2) + \varrho s(1, 2) \int F(1, 3) g(3, 2) d\mathbf{3},$$

where

$$(86) \quad F(1, 3) = X(1, 3) s(1, 3) + \varrho \int X(1, 4) s(1, 4) g(4, 3) g(1, 3) d\mathbf{4}.$$

In this last equation, we eliminate the first term with the help of equation (83). This leads to the equation

$$(87) \quad \begin{aligned} F(1, 3) = & \nabla_1 g(1, 3) - \varrho(1 + g(1, 3)) \int X(1, 4) s(1, 4) g(4, 3) d\mathbf{4} - \\ & - \varrho^2 s(1, 3) \int X(1, 5) s(1, 5) g(1, 4) g(5, 4) g(4, 3) d\mathbf{5} d\mathbf{4} + \\ & + \varrho g(1, 3) \int X(1, 4) s(1, 4) g(4, 3) d\mathbf{4}. \end{aligned}$$

We see that in this equation the fourth term is cancelled by the second part of the second term. We shall replace in the third term $s(1, \mathbf{3})$ by its asymptotic value so as to obtain a three-point integral equation.

We then obtain for $F(1, 3)$ the integral equation

$$(88) \quad F(1, 3) = \nabla_1 g(1, 3) - \varrho \int F(1, 4) g(4, 3) d\mathbf{4}.$$

This equation combined with equation (86) leads to equation (61) which is equivalent to the integral equation (37)-(38). The elimination of all the spurious terms of the BGK equation has therefore been achieved and a value of $\gamma^e(r)$ correct to all orders in ϱ is obtained. We conclude that equation (37)-(38) includes the main part of the corrected three-body correlation function (82) and enables us to go one step beyond the superposition approximation used in the BGK equation. Moreover, we have seen that the precision can still be improved by the use of a more correct three-body correlation function which leads to the correction terms described in Section 8.

10. — Conclusion.

In this paper we have established an integral for the three-body correlation function in classical fluids. This equation contains a main equation which is very simple and correction terms. The solution of the main equation appears at first rather easy, but it should be noted that it is a highly non-linear equation. In fact, we have tried to solve it iteratively, both by using the iteration procedure described in Section 3 and by a simple iterative process starting from the zero-density correlation function as in Section 6. In the low density, convergence is attained and both methods lead to the same result; but the two approaches fail to converge in the high density region. It will then be necessary to use a non-iterative method to solve this equation. This computation is presently in progress as well as the calculation of the first corrections to the integral equation.

* * *

We wish to acknowledge some interesting discussions with Prof. J. YVON Dr. P. DE GENNES and Dr. D. E. MCCUMBER.

APPENDIX

Morita's expansion for the two-body correlation function.

MORITA ⁽⁶⁾ has determined the 2-body correlation function with the help of an iteration scheme resembling ours: the correlation function is defined by eq. (9'), (11'), (12'), (13'), but the equation (31') is replaced in his work by the equation

$$(A.1) \quad \xi_n^M(r) = (\xi_{n-1}^M(r) + 1) \exp [\gamma_{n-1}^M(r) - \gamma_{n-2}^M(r)] - 1 - (\gamma_{n-1}^M(r) - \gamma_{n-2}^M(r)),$$

where the superscript refers to the quantities calculated by MORITA.

A direct comparison with the equation (31') may be made if we eliminate $\xi_{n-1}^M(r)$ by a repeated application of (A.1). We thus obtain

$$(A.2) \quad \xi_n^M(r) = \{(\xi_0(r) + 1) \exp [\gamma_{n-1}^M(r)] - 1 - \gamma_{n-1}^M(r)\} - \sum_{i=2}^{i=n} \gamma_{n-i}^M(r) \exp [(\gamma_{n-1}^M(r) - \gamma_{n+1-i}^M(r))] (\exp [\gamma_{n+1-i}^M(r) - \gamma_{n-i}^M(r)] - 1).$$

The term between brackets is identical with $\xi_2(r)$ of (31'). From this term is subtracted a sum of terms which does not vanish when n tends to infinity, so that (A.2) is fundamentally different from (31').

We can illustrate this difference by calculating $\xi_2^M(r)$ ($\xi_1^M(r)$ is identical with $\xi_1(r)$)

$$(A.3) \quad \xi_2^M(r) = \xi_2(r) - \gamma_0(r)(\exp[\gamma_1(r) - \gamma_0(r)] - 1).$$

We see that from $\xi_2(r)$ are subtracted terms such as represented in Fig. 13, in which there is one chain constructed from ξ_0 's and the chains constructed from ξ_1 's, which are not identical with the primary chains. There does not seem to be any reason why such terms should be excluded from the expansion scheme.

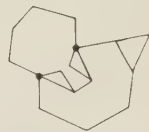


Fig. 13. - A typical term subtracted from $\xi_2(r)$ in Morita's expansion scheme.

RIASSUNTO (*)

Si mostra che la somma di una larga classe di diagrammi in uno sviluppo del tipo « cluster » permette di scrivere una equazione integrale per la funzione di correlazione nei fluidi classici. Con una approssimazione, questa equazione si riduce a quella di Born, Green e Kirkwood e riproduce più esattamente di quella i coefficienti del viriale. Si danno i termini correttivi, sempre più complicati, che permettono di rendere esatta la nostra equazione. Si calcola infine la funzione di correlazione a tre corpi, che, introdotta nell'equazione di Yvon-Born-Green, permette di calcolare la funzione di correlazione a due corpi. Si conferma così il calcolo diretto di questa funzione, e si mostra che la nostra equazione integrale include delle correzioni all'approssimazione di sovrapposizione.

(*) Traduzione a cura della Redazione.

Double Maximum Angular Distributions in High Energy Nuclear Collisions.

J. GIERULA and M. MIĘSOWICZ

Cosmic Ray Department, Institute of Nuclear Research - Kraków
General Physics Department, School of Mining and Metallurgy - Kraków

P. ZIELIŃSKI

Cosmic Ray Department, Institute of Nuclear Research - Warszawa
Physics Department, University of Warszawa - Warszawa

(ricevuto il 12 Maggio 1960)

Summary. — A detailed statistical analysis of the shape of the angular distribution of secondary particles generated in 65 nuclear collisions for primary energies higher than 10^{12} eV has been presented. The double maximum shape of the distribution (in coordinate $\log \tg \theta$) is a general feature of the events with high degree of anisotropy of secondaries in CM system. It has been found that the shape of the angular distribution is in agreement with the predictions of the two-centre model of multiple meson production both for nucleon-nucleon and nucleon-heavy nucleus collision. A new parameter D , which is a measure of the deviation from the normal shape of the distribution towards the two centre distribution and also a coordinate convenient for visualizing this deviation, have been introduced.

1. — Introduction.

In recent years measurements of angular distributions of secondary particles of cosmic ray jets in nuclear emulsion have been carried out in our laboratory in collaboration with the Prague group.

It has been found ⁽¹⁾ that angular distributions of particles produced by

⁽¹⁾ P. CIOK, T. COGHEN, J. GIERULA, R. HOŁYŃSKI, A. JURAK, M. MIĘSOWICZ, T. SANIEWSKA, O. STANISZ and J. PERNER: *Nuovo Cimento*, **8**, 166 (1958).

very high energy nucleons ($E_L > 10^{12}$ eV) show a characteristic shape: in coordinates dN/dx vs. $x = \log_{10} \tan \theta$ (θ are the angles of the secondary particles with the primary direction) the distributions have two symmetrical maxima. On the contrary, the hydrodynamical model predicted normal (Gaussian) distributions both for nucleon-nucleon and nucleon-nucleus collisions.

This has been later confirmed on a more extended experimental material from the literature and from different laboratories ⁽²⁾. The first observations of the bimodal (two-maxima) structure of angular distributions concerned high energy jets with small number of black and gray tracks ($N_h \leq 5$). Then this effect has been found also in the interactions with heavy nuclei ($N_h > 8$) ⁽³⁾.

In order to explain the observed shape of the angular distribution we introduced as a working hypothesis the two-centre model. This model differs in one point from the isobar model ⁽⁴⁾. It has been assumed that the emitting centres are moving in the CM system with smaller velocity than the nucleons after the collision (in general $\bar{\gamma}$ is much smaller than γ_c) ⁽¹⁾. In this way a consistency of the shape of the observed angular distributions and low values of inelasticity could be obtained. Similar models were also proposed by COCCONI ⁽⁵⁾ and NIU ⁽⁶⁾.

Recently the bimodal angular distribution has been discussed by some authors. On one hand some theoretical conceptions have been suggested in connection with this type of distribution ⁽⁷⁾, on the other hand the statistical significance of this effect has been the subject of discussion ⁽⁸⁾. Since the introduction of the two centre model was mainly based on the existence of bimodal distributions and no detailed statistical analysis was published till now, we present here the results of our analysis based on total available material ^(*).

⁽²⁾ P. CIOK, T. COGHEN, J. GIERULA, R. HOLYŃSKI, A. JURAK, M. MIĘSOWICZ, T. SANIEWSKA and J. PERNER: *Nuovo Cimento*, **10**, 741 (1958).

⁽³⁾ J. BARTKE, P. CIOK, J. GIERULA, R. HOLYŃSKI, M. MIĘSOWICZ and T. SANIEWSKA: *Nuovo Cimento*, **15**, 18 (1960).

⁽⁴⁾ G. T. ZACEPIN: *Report at a Seminar in P. N. Lebedev Physical Institute of the USSR Academy of Sciences* (1950); E. L. FEINBERG and D. S. CERNAVSKIJ: *Dokl. Akad. Nauk SSSR*, **81**, 795 (1951); S. TAKAGI: *Progr. Theor. Phys.*, **7**, 123 (1952); H. J. BHABHA: *Proc. Roy. Soc. A* **219**, 293 (1953); W. L. KRAUSHAAR and L. J. MARKS: *Phys. Rev.*, **93**, 326 (1954); D. S. CERNAVSKIJ: *Suppl. Nuovo Cimento*, **8**, 775 (1958).

⁽⁵⁾ G. COCCONI: *Phys. Rev.*, **111**, 1699 (1958).

⁽⁶⁾ K. NIU: *Nuovo Cimento*, **10**, 994 (1958).

⁽⁷⁾ *Proc. of the Moscow Cosmic Ray Conference*, vol. **1** (1960).

⁽⁸⁾ *Informal Meeting during the Cosmic Ray Conference* (Moscow, 1959).

^(*) A summary of the results has been reported in a letter to the Editor of *Acta Phys. Pol.* (**19**, 119 (1960)).

TABLE I. — *List of jets produced by singly charged or neutral particles with energy higher than 10^{12} eV (γ_c higher than 23).*

No.	Designation of the event	Type	γ_c	σ	D	Ref.	Remarks
Jets with $N_h \leq 5$ and $n_s < 20$							
1	63M1	1+10p	236	0.20	0	(⁹)	—
2	29a M1	0+6p	108	0.25	— 0.33	(⁹)	—
3	57P	5+11p	23	0.38	0.09	(¹²)	—
4	3M2	0+9p	29	0.39	0.11	(¹⁰)	—
5	159AA	2+14n	78	0.47	— 0.14	(¹)	—
6	212W	2+10p	30	0.46	— 0.40	(¹⁵)	—
7	P9Br	0+18p	40	> 0.47	< 0	(⁴)	included in the analysis of D -values only
8	30K	3+18p	30	0.55	— 0.22	(⁷)	—
9	3N1Br	0+11n	59	0.56	— 0.09	(⁴)	—
10	231AA	5+18p	37	> 0.56	< -0.22	(¹)	included in the analysis of D -values only
11	18P	5+11p	40	0.57	0.27	(¹²)	—
12	49P	3+11n	28	0.59	0.09	(¹²)	—
13	155K	0+18p	39	0.58	0	(⁷)	—
14	19AA	2+16p	52	0.60	0	(¹)	—
15	59P	5+16p	29	0.61	0	(¹²)	—
16	2L	3+14p	79	0.61	0	(⁸)	—
17	128P	3+7p	27	0.62	0.14	(¹²)	—
18	P9N2Br	4+10n	24	0.63	0	(⁴)	—
19	26P	5+9p	150	0.64	0.33	(¹²)	—
20	27P	0+17p	46	0.67	— 0.06	(¹²)	—
21	155W	0+13p	64	0.66	0.23	(¹⁵)	—
22	4B	0+16p	30	0.70	0.13	(²)	—
23	1B	0+15p	36	0.72	0.07	(²)	—
24	31K	0+16p	34	0.81	0	(⁷)	—
25	P16Br	1+11p	112	0.81	0.09	(⁴)	—
26	P10Br	0+16p	33	0.84	0.25	(⁴)	—
27	70t	0+14n	30	1.00	0	(¹¹)	—
28	P24S4Br	1+6p	49	1.12	0	(⁴)	—
29	P24Br	0+11p	1118	> 1.00	< -0.27	(⁴)	included in the analysis of D -values only
30	« S » Ch	2+15p	202	1.15	0.33	(⁵)	—
31	P20S4Br	5+7p	32	1.27	0.43	(⁴)	—
32	P20Br	0+4p	147	2.17	1.00	(⁴)	—
Jets with $N_h \leq 5$ and $n_s > 20$							
33	7M2	3+43p	37	0.43	0.07	(¹⁰)	—
34	18K	1+21p	35	0.57	0.05	(⁷)	—
35	P5Br	0+32p	67	0.57	0.37	(⁴)	—
36	3B	3+24n	37	0.58	0	(²)	—
37	Ro	3+35p	99	0.63	0.14	(¹³)	—
38	25M1	5+31p	44	0.63	0.03	(⁹)	—
39	To	3+39p	51	0.63	0.03	(⁴)	—
40	10t	0+36p	45	0.70	0	(¹¹)	—
41	30M1	4+96p	27	0.72	0	(⁹)	—
42	P28Br	5+23p	76	> 0.73	< 0.22	(⁴)	included in the analysis of D -values only

TABLE I (continued).

No.	Designation of the event	Type	γ_c	σ	D	Ref.	Remarks
43	31M1	5+48p	23	0.85	0.08	(⁹)	—
44	P2Br	0+22p	68	> 0.95	< 0.27	(⁴)	included in the analysis of D -values only
45	2M2	5+27p	33	0.96	—0.11	(¹⁰)	—
Jets with $5 < N_h \leq 8$							
46	P20N1Br	8+33n	111	0.4	0.09	(⁴)	—
47	180AA	7+15n	27	0.55	—0.07	(¹)	—
48	5M2	6+27p	36	0.60	0.26	(¹⁰)	—
49	P25Br	7+25p	205	> 0.67	< —0.04	(⁴)	included in the analysis of D -values only
50	52M1	6+23p	45	0.86	0.22	(⁹)	—
51	Ch	6+16p	577	1.11	—0.12	(⁶)	—
52	Minnesota	8+75p	300	> 1.27	< 0.09	(⁴)	included in the analysis of D -values only
Jets with $N_h > 8$							
53	23L	9+14p	101	0.44	0.14	(⁸)	—
54	4L	11+46n	50	0.46	—0.04	(⁸)	—
55	19L	9+27n	38	0.52	0.04	(⁸)	—
56	10M2	9+10p	134	0.66	0	(⁹)	—
57	9M2	14+16p	72	0.70	—0.20	(¹⁰)	—
58	30B	16+21n	36	0.71	—0.05	(²)	—
59	15L	13+7p	43	0.86	0.14	(⁸)	—
60	216AA	35+59p	23	0.90	0.12	(¹)	—
61	1M2	13+34n	29	0.94	0.15	(¹⁰)	—
62	P4Br	16+57p	26	0.96	0.23	(⁴)	—
63	Be	20+56p	28	1.03	0.32	(³)	—
64	168K	17+41p	58	1.09	0.41	(⁷)	—
65	171K	23+47p	83	1.25	0.53	(⁷)	—

(¹) Private communication from the Institute of Nuclear Physics of the Academy of Science of the Kazakh SSR - Alma Ata.

(²) Private communication from the Institute for Nuclear Physics of the German Academy of Sciences - Berlin-Zeuthen.

(³) F. D. HÄNNI, C. LANG, E. LOHRMANN, M. TEUCHER and H. WINZELER: *Nuovo Cimento*, **4**, 1473 (1956) - Bern.

(⁴) Private communication from the H. H. Wills Laboratory - Bristol.

(⁵) M. SCHEIN, R. G. GLASSER and D. M. HASKIN: *Nuovo Cimento*, **2**, 647 (1955) - Chicago.

(⁶) M. W. TEUCHER, E. LOHRMANN, D. M. HASKIN and M. SCHEIN: *Phys. Rev. Lett.*, **2**, 313 (1959) - Chicago.

(⁷) Jets measured in the Cosmic Ray Department of the Institute of Nuclear Research-Kraków.

(⁸) Private communication from the Radium Institute USSR Academy of Science - Leningrad

(⁹) Private communication from the P. N. Lebedev Institute of Physics of the USSR Academy of Science - Moscow.

(¹⁰) Private communication from the Atomic Energy Institute of the Academy of Sciences of the USSR - Moscow.

(¹¹) J. G. McEWEN: *Phys. Rev.*, **115**, 1712 (1959) - Ottawa.

(¹²) Private communication from the Institute for Physics the of Czechoslovak Academy of Sciences - Praha.

(¹³) M. KOSHIBA and M. F. KAPLON: *Phys. Rev.*, **97**, 193 (1955) - Rochester.

(¹⁴) A. DEBENEDETTI, C. M. GARELLI, L. TALLONE and M. VIGONE: *Nuovo Cimento*, **4**, 1142 (1956) - Torino.

(¹⁵) Jets measured in the Cosmic Ray Department of the Institute of Nuclear Research - Warszawa.

2. - Experimental material.

The analysis has been performed on all available events with an energy $E_L > 10^{12}$ eV, taken from our laboratory, from published papers and from private communications. In the present analysis we have not investigated jets generated by the α -particles and heavier primaries.

The collection contains 65 jets produced by singly charged or neutral primaries which are presented in Table I.

For each event we know the angles θ_i of the secondary particles with respect to the primary or with respect to the axis determined by the centre of gravity of tracks in the case of the neutral primary.

The primary energy is determined by the formula of Castagnoli *et al.* $\log_{10} \gamma_c = -\langle \log_{10} \text{tg } \theta_i \rangle$ which gives the Lorentz factor γ_c of the primary particle in CM system in the case of nucleon-nucleon collision.

In this case the primary energy $E_L = 10^{12}$ eV corresponds to $\gamma_c = 23$. The events are divided in Table I into three groups according to N_h : The group $N_h \leq 5$ is then divided into two parts according to the number of shower tracks: $n_s < 20$ and $n_s \geq 20$. We classify also the events according to their degree of anisotropy in the CM system determined by the dispersion of the angular distribution

$$\sigma = \sqrt{\frac{\sum_i^{n_s} (\log_{10} \text{tg } \theta_i - \langle \log_{10} \text{tg } \theta_i \rangle)^2}{n_s - 1}},$$

and according to a parameter D which characterizes the deviation of the angular distribution from the normal shape (see Section 3).

In a given group the events are listed in the order of increasing anisotropy parameter σ .

3. - Method of the analysis.

The aim of this analysis is to give a statistical proof that the experimental angular distribution is different from the normal one, which was predicted in particular by the hydrodynamical model, and that it is in better agreement with two-centre model.

The hydrodynamical model predicts a shape of the differential angular distribution dN/dx vs. x which is well approximated by the normal one. In this model the dispersion of the distribution increases with increasing energy,

the normal (Gaussian) shape remaining unchanged. This should be a common feature both of nucleon-nucleon and nucleon-nucleus collisions.

The two-centre model does not give predictions concerning energy dependence of the distribution but connects the degree of anisotropy—the dispersion σ —with the shape of the distribution. The angular distribution is namely a superposition of two isotropic distributions with $\sigma = 0.39$. In this model a greater dispersion of the whole distribution corresponds to a greater shift of the two maxima of the corresponding isotropic distributions. For high anisotropy this leads to the bimodal shape of the distribution.

Starting from this, a very convenient measure of the deviation of the distribution predicted by the two centre model from the normal shape can be

introduced. If we divide the angular distribution into the inner and outer parts by the values $x_{1,2} = \pm 0.674 \sigma$, then the expected numbers of inner (N_i) and outer (N_e) tracks are equal in the case of the normal distribution. For the two-centre distribution the outer part contains more tracks than the inner one (Fig. 1). As a measure of the deviation of the observed distribution from the normal shape we take

$$D = \frac{N_e - N_i}{N_e + N_i} = \frac{N_o - N_i}{n_s}.$$

The expected value of D is positive for the two-centre model distribution and is equal to zero for the normal one. The values of D for individual jets are listed in Table I, column 6.

4. — Results of the quantitative analysis.

4.1. Analysis of composite angular distributions. — In order to obtain a quantitative measure for the described deviation we investigated at first the angular distribution in the full collection of jets taken as a composite jet. For this analysis we had to reject 7 events for which only the upper limit of the dispersion could be evaluated (because of smallness of some angles which could not be measured). These cases however have been taken into account in the further analysis (Section 4.2).

The feature of the distributions to be analyzed is the shape irrespectively of the values of the parameter σ .

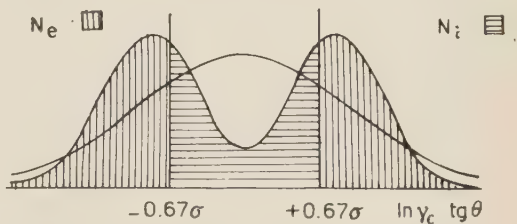


Fig. 1. — Illustration of the definition of D .

Therefore we have standardized the shapes of the distributions by dividing all x_i values by σ . If the investigated standardized distributions are normal the total distribution should be also normal. Fig. 2a shows the histogram

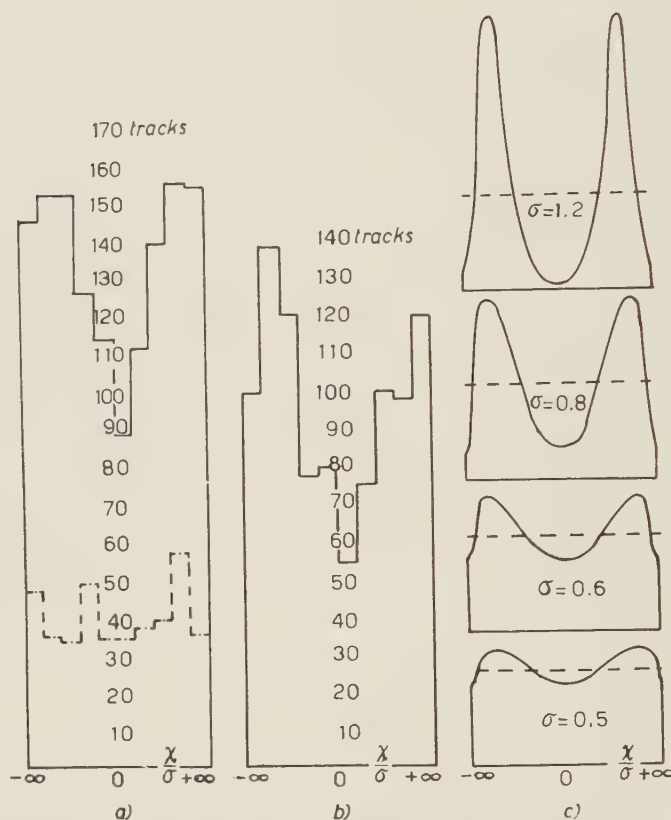


Fig. 2. - Histograms of the composite differential angular distributions for the complete collection of jets: a) continuous line: the complete collection; dashed line: jets with $\sigma < 0.6$; b) jets with $\sigma > 0.6$; c) the angular distributions resulting from the two-centre model for different σ -values; dashed lines: gaussian distributions.

obtained in this way. The values of x/σ are grouped in 10 intervals of equal numbers of tracks expected from the normal distribution. Using this grouping we have the advantage of obtaining a straight line for the differential normal distribution and any deviation from the normal shape is visualized. For the comparison some distributions resulting from the two-centre model, for different σ values, are given in Fig. 2c. We see that the observed distributions deviate from the normal shape in the direction indicated by the two-centre model. As a quantitative measure of the deviation the significance level resulting from the χ^2 test has been used. Thus we see that the devia-

tion from the normal shape for the whole material corresponds to more than 3 standard deviations.

During the Moscow Cosmic Ray Conference and Kiev High Energy Physics Conference the question has been discussed what fraction of high energy events shows the bimodal angular distribution. It has been given for example 20% for this fraction ^(8,9). According to our opinion the question of the relative frequency of double-maximum angular distributions can be answered in a more definite way with the help of the two-centre model. From the point of view of this model we expect the double-maximum distribution only in events of sufficiently high anisotropy. As seen in Fig. 3 the bimodal distribution appears for anisotropy parameters higher than ~ 0.6 . We can analyse such an expected effect on two ways: 1) summarizing the individual angular distributions for events with small and high anisotropy independently, or 2) ascribing to each jet a measure of bimodality of the distribution such as the D -value

introduced in the preceding chapter and comparing the distribution of these values on one hand with the corresponding distributions expected from the two-centre model and on the other hand with the distribution of D resulting from the normal shape of the angular distribution. The latter method will

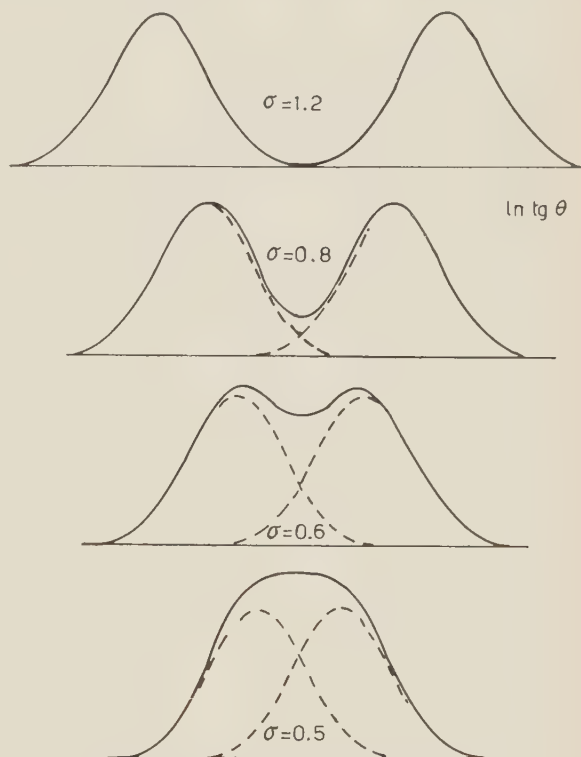


Fig. 3. - The shapes of the differential angular distributions predicted by the two-centre model for several values of the anisotropy parameter σ . Dashed lines correspond to the partial isotropic distributions (emission from individual centres).

⁽⁹⁾ C. F. POWELL: *Report at the IX International Conference on High Energy Physics* (Kiev, 1959).

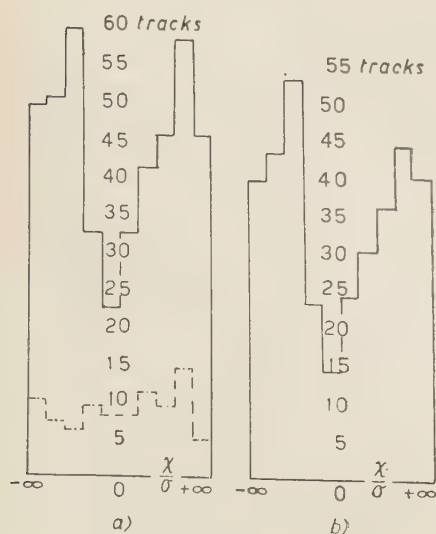
be discussed in Section 4'2. In the following items we present results obtained by superposing the angular distributions for particular groups of jets.

a) Selection according to anisotropy. — We have divided the whole collection of events presented in Fig. 2a into two parts: events with $\sigma < 0.6$ (21 jets; Fig. 2a dashed line) and events with $\sigma > 0.6$ (37 jets; Fig. 2b). The application of χ^2 -test to these distributions shows in the case of higher anisotropy the deviation from the normal distribution on the probability level of more than 3 standard deviations. As seen from the Fig. 2b the shape shows two distinct maxima. The histogram for jets with smaller anisotropy shows a much smaller deviation from the normal distribution. Both facts can be expected from the two-centre model.

However, dividing the whole sample into two parts we ought to consider the possibility of introducing for the part with higher anisotropy a preference of statistical fluctuations towards the bimodal shape. With the help of a sampling experiment we have established that in our conditions such an effect is negligible. Only for the subgroup of events with $N_h \leq 5$, $n_s < 20$, $\sigma > 0.6$ we must take this effect into account (see item c).

Now a question arises: Is the double-maximum distribution the feature of nucleon-nucleon or nucleon-nucleus collisions?

b) Collisions with heavy nuclei. — Let us now consider the group of jets with a great number of heavy prongs *i.e.* $N_h > 8$. This group clearly consists of collisions with heavy nuclei of photographic emulsion *i.e.* Ag and Br. In a previous paper of our group ⁽³⁾ we have found that the double-maximum structure of the angular distribution occurs often in these collisions. The



histograms for this group are shown in Fig. 4a and in Fig. 4b. The division in subgroups with $\sigma < 0.6$ (Fig. 4a dashed line) and $\sigma > 0.6$ (Fig. 4b) leads again to the conclusion that the effect of the double-maximum structure is observed only for higher anisotropy.

An application of the χ^2 test to the group with $\sigma > 0.6$ gives the probability of deviation from the normal

Fig. 4. — Histograms of the composite differential angular distributions for collisions with heavy nuclei: a) continuous line: all jets with $N_h > 8$; dashed line: jets with $\sigma < 0.6$; b) jets with $\sigma > 0.6$.

distribution on the level of more than three standard deviation. For the group with $\sigma < 0.6$ we do not observe any significant deviation from normal distribution.

Then we can say that the double-maximum structure of angular distribution is statistically significant for the strongly anisotropic collisions of nucleons with heavy nuclei.

c) Events with a small number of heavy prongs ($N_h \leq 5$). — In contrast to the preceding group, which consists only of collisions with heavy nuclei, the group of jets with small number of evaporation tracks is not homogeneous. It consists certainly of collisions with nuclei and with (free or quasi-free) nucleons as well. We can however select a subgroup of jets which contains a higher fraction of nucleon-nucleon collisions. This is done using an additional criterion taking into account the number of relativistic tracks n_s .

This selection is based on the following observations.

If we compare the numbers n_s for both groups: $N_h \leq 5$ and $N_h > 8$, we see a correlation between N_h and n_s values.

In the group with $N_h \leq 5$, the average $n_s = 19.6$ and in the group with $N_h > 8$ the average $n_s = 33.3$. But we observe this tendency of increasing multiplicity with increasing N_h also inside both groups taken separately. If we take therefore for further analysis only events with multiplicity, say, $n_s < 20$ we get from the group with $N_h \leq 5$ a part which would be probably enriched in nucleon-nucleon collisions. We call this group the « nucleon-nucleon » collisions. Fig. 5a shows the histogram for the group $N_h \leq 5$. The dashed line corresponds to cases with $\sigma < 0.6$. Fig. 5b corresponds to cases with $\sigma > 0.6$, the dashed line shows the cases with $n_s > 20$. Fig. 5c corresponds to cases $N_h \leq 5$, $n_s < 20$ and $\sigma > 0.6$.

We cannot compare the experimental histogram for jets belonging to this last group with a straight line predicted for the normal distribution. Firstly we should have in mind the already mentioned effect of possible preferential selection of fluctuations.

Secondly we know that the composite histogram is a good estimate of the hypothetic angular distribution only for sufficiently high multiplicities of particular events. Thus we have compared the experimental histogram for « nucleon-nucleon » collisions (Fig. 5c) with another histogram of artificial jets obtained from the sampling experiment (dotted line). This histogram corresponds to the composition of random samples chosen from a normal population. These samples (four samples for each experimental event) imitated jets with respect to the multiplicity and $\sigma > 0.6$ condition. The deviation towards the bimodal shape is clearly seen from the figure. The application of the χ^2 -test for comparing these two histograms gives a deviation on the probability level $P > 85\%$. This value was obtained by applying

for the χ^2 a formula for comparing two experimental distributions (both fluctuating) (A. HALD: *Statistical Theory with Engineering Applications* (1952), Chapter XXIII, § 4).

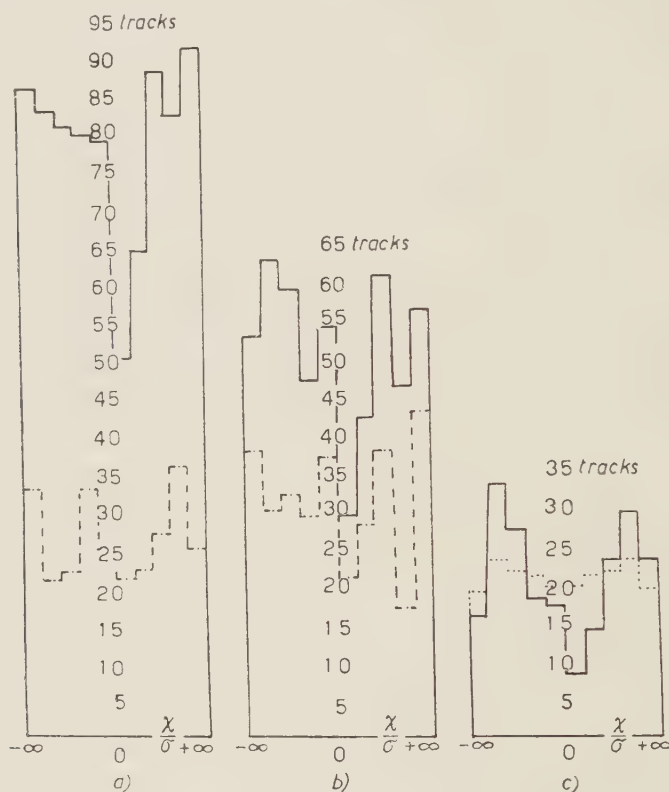


Fig. 5. - Histograms of the composite differential angular distribution for jets with $N_h \leq 5$: a) continuous line: all jets; dashed line: those with $\sigma < 0.6$; b) continuous line: jets with $\sigma > 0.6$; dashed line: those with $n_s > 20$; c) continuous line: jets with $\sigma > 0.6$ and $n_s < 20$ called nucleon-nucleon collisions, dotted line: normalized histogram for corresponding «artificial jets» from the sampling experiment.

Of course this formula gives for the χ^2 smaller values than that used for comparing an experimental histogram with a theoretical one. The observed deviation is a systematic feature of all events of this group as will be seen from the analysis of D .

4.2. *The analysis of fluctuations using the quantity D .* - Now we apply the quantity D (being the measure of deviation from the normality for a given event; for the definition see Section 3) to the analysis of statistical fluctuations of the angular distributions.

The values of D are listed in Table I, column 6. In the Fig. 6 we have given the values D for all 65 jets in function of the anisotropy parameter σ . The full line on this figure represents the dependence expected by the two-centre model. The line $D = 0$ corresponds to the normal shape of the distribution.

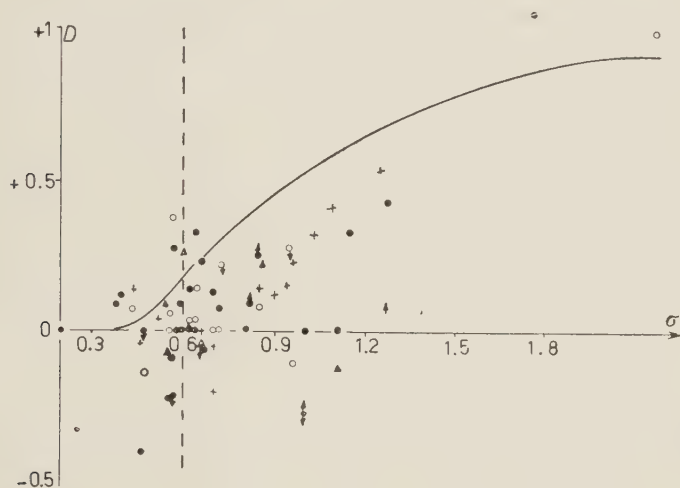


Fig. 6. - The distribution of D -values for all investigated jets as a function of the anisotropy parameter σ . Full dots: events with $N_h \leq 5$ and $n_s < 20$ (N - N collisions); open dots: events with $N_h \leq 5$ and $n_s > 20$; crosses: events with $N_h > 8$ (N -heavy nucleus collisions); triangles: events with $5 < N_h \leq 8$. Arrows: see text. The continuous curve gives the relation predicted by the two-centre model.

The deviation of the experimental points towards positive D values is clearly seen (36 events with $D > 0$, 14 with $D = 0$ and 15 with $D < 0$). This asymmetry is more pronounced for events with $\sigma > 0.6$ (26 events with $D > 0$, 9 with $D = 0$ and 7 with $D < 0$).

The observed values of D are subject to large fluctuations, especially for small n_s . We have made an analysis of fluctuations only for the group with $N_h \leq 5$ and $n_s < 20$ (events regarded as nucleon-nucleon collisions, full dots on Fig. 6). As mentioned above we might expect some excess of events with positive D -values even for jets having a normal distribution if we select events with σ higher than the average value of σ for the whole group. For investigating the magnitude of this possible effect we calculated the D -values for «artificial jets» from our sampling experiment already mentioned. Fig. 7 shows the distribution of D -values for «artificial jets» as a function of σ . The points are symmetrically distributed with respect to the $D = 0$ line both for small and high σ values. (For high values of σ there are 23 events with

$D > 0$, 9 with $D = 0$ and 28 with $D < 0$. For small σ values there are 21 events with $D > 0$, 8 with $D = 0$ and 21 with $D < 0$). On the other hand for experimental jets the corresponding numbers for events with $\sigma > 0.6$ are

10, 6 and 2, and for events with $\sigma < 0.6$ these numbers are 4, 3 and 5 respectively.

For quantitative evaluation of the observed deviation for the group considered as nucleon-nucleon collisions with $\sigma > 0.6$ we compared the distributions of D -values for experimental and «artificial» jets

These distributions deviate one from another on the level of two standard deviations (*).

We want to stress that the asymmetrical distribution of experimental points (full dots in Fig. 6) with respect to the line resulting from the two-centre

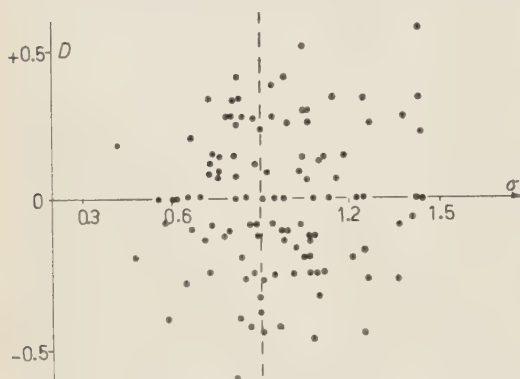


Fig. 7. — The distribution of the D -values for «artificial jets» which imitate the «nucleon-nucleon» collisions (full dots from Fig. 6). The dashed line corresponds to $\sigma = 0.6$ in Fig. 6.

tre model cannot be considered as a departure from the predictions of the model. This could follow from the fact that the curve has been calculated on the assumption of symmetry in the number of particles emitted from each centre. If, however, in reality the emission is not symmetric because of fluctuations, the value $\log \gamma_i = 1/n_s \sum \log \cotg \theta_i$ is shifted towards the grouping of the larger number of tracks what obviously diminishes the value of D . In the events in which the angular distribution can be measured also for π^0 -mesons by means of cascades it has been observed that the asymmetry for charged particles disappeared if we included π^0 -mesons. Thus it seems to be reasonable, in the cases in which both cones are well separated, to replace the usual for-

(*) Let us mention a detail in the calculation of the D -value. Only for high multiplicities we could expect that the interval $(-0.67\sigma, +0.67\sigma)$ covers 50% of tracks. For small multiplicities the following correction was used: instead of the value 0.67 we took a value resulting from Student's distribution for the given multiplicity. For instance, for $n_s = 6$ we obtain the interval $(-0.73\sigma, +0.73\sigma)$ (H. CRAMER: *Mathematical Methods of Statistics*, 1945, Table IV).

The values of D obtained in this way are smaller than without this correction. However for higher multiplicities the difference is negligible. The values given in Table I and in Figs. 6, 7 and 8 are corrected in this manner. We confirmed the approximate validity of the correction for our sample size by means of sampling «jets».

mula for $\log \gamma_c$ by the arithmetic mean of $\log \gamma$ values calculated for the narrow and diffuse cones separately ^(10,11,2).

However such a procedure is not allowed in the present analysis as it could cause a preference of double maximum distributions. Therefore it was not used here but the events with the mentioned shape of the angular distribution having an exceptional high γ_c values are designated in Fig. 6 by an arrow upwards. For similar reasons we have rejected from the histograms of composite angular distributions (Fig. 2, 4 and 5) those events in which a considerable fraction of particles were emitted with angles so small that they could not be measured.

In these cases, only the lower limit of the dispersion σ , and thus the upper limit of D is known. The acceptance of this upper value of D instead of the unknown real value would also lead to a tendency. Nevertheless the points corresponding to these events have been plotted in Fig. 6 but they are designated by an arrow downwards.

5. - Some considerations concerning angular distributions in different group of jets.

In Table II we summarize the data concerning the level of statistical significance of the deviation of the angular distributions of secondary particles from the normal (Gaussian) shape. The data were obtained by applying methods of statistical analysis on the one hand to composite angular distributions (the results of this are given in the fifth column of Table II) and on the other to the distributions of D -values. Both manners lead to the same conclusion: in each group of jets we observe the deviation in the shape of the angular distribution in the direction predicted by the two-centre model. The only exception is the group characterized by $N_h \leq 5$, $\sigma > 0.6$ and $n_s > 20$. The application of the χ^2 -test to the composite distribution of this group gives a rather high deviation from the normal shape (\sim two standard deviations) but from the mean value of D we obtain for this group no significant deviation from $D = 0$. This follows from the fact that in many particular events of this group the angular distribution deviates from the normal shape and the differences of shape between these events are much higher than in other groups. This is clearly seen from the comparison of Fig. 8 and Fig. 5b. The excess of positive D -values is seen in Fig. 8 (open dots) but the shape of

⁽¹⁰⁾ P. CIOK, M. DANYSZ, J. GIERULA, A. JURAK, M. MIESOWICZ, J. PERNEGR, J. VRANA and W. WOLTER: *Nuovo Cimento*, **6**, 1409 (1957).

⁽¹¹⁾ B. EDWARDS, J. LOSTY, D. H. PERKINS, K. PINKAU and J. REYNOLDS: *Phil. Mag.*, **3**, 237 (1958).

TABLE II.

Characteristic of the group	Fig.	No. of jets	No. of tracks	Level of significance of the deviations from the normal distribution	Remarks
All events	2a	58	1332	more than 3 standard dev.	
Events with $\sigma < 0.6$	2a dashed line	21	400	~ 1.5 stand. dev.	
Events with $\sigma > 0.6$	2b	37	932	more than 3 stand. dev.	
$N_h > 8$	4:	13	433	~ 3 stand. dev.	
$N_h > 8, \sigma < 0.6$	4a dashed line	3	87		Nucleon-heavy nucleus collisions
$N_h > 8, \sigma > 0.6$	4b	10	346	more than 3 stand. dev.	
$N_h \leq 5$	5a	40	785	~ 2 stand. dev.	
$N_h \leq 5, \sigma < 0.6$	5a dashed line	16	265	~ 1 stand. dev.	
$N_h \leq 5, \sigma > 0.6$	5b	34	520	~ 2 stand. dev.	
$N_h \leq 5, \sigma > 0.6$ $n_s > 20$	5b dashed line	7	312	~ 2 stand. dev.	But not in the direction predicted by the two-centre model
$N_h \leq 5, \sigma > 0.6$ $n_s < 20$	5c	17	208	~ 2 stand. dev. (from D distribution)	« Nucleon-nucleon » collisions
Secondary jets	9	5	56		

the histogram for this group (Fig. 5b, dashed line) does not show two distinct maxima. This is the illustration of the fact that the procedure of superposing the particular distributions is not applicable to the group of events with different shapes of the angular distribution. It seems that the group under discussion is a mixture of events belonging to some different physical processes

such as collisions of nucleons with light nuclei, peripheral collisions with heavy nuclei and perhaps central nucleon-nucleon collisions. The existence of an admixture of collisions of this last type in this group could be supported by an observation of the Bristol group⁽¹¹⁾ that in jets with $n_s > 22$ the percentage of heavier particles (X-particles) seems to be larger than in jets with $n_s < 22$. Of course this conclusion would be based on the assumption that the X-particles were generated in central collisions.

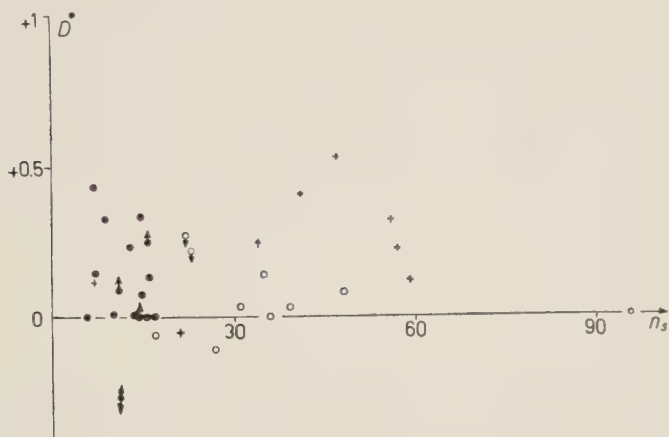


Fig. 8. - The distribution of D -values for events with $\sigma > 0.6$ as a function of the multiplicity n_s . Full dots: events with $N_h \leq 5$ and $n_s < 20$ (« nucleon-nucleon » collisions); crosses: events with $N_h > 8$ (nucleon-heavy nucleus collisions); open dots: events with $N_h \leq 5$ and $n_s > 20$. Events with $5 < N_h < 8$ not shown.

On the contrary other groups of jets discussed in this paper include probably much more unique type of collisions. The group with $N_h > 8$ corresponds certainly to collisions with heavy nuclei *i.e.* Ag or Br. The group with $N_h \leq 5$, $n_s < 20$ can be regarded as rather abundant in nucleon-nucleon collisions according to arguments given in Section 4.1c. In consequence in both of these groups the bimodal angular distribution for events with high anisotropy can be seen not only by means of the D -distribution but also more directly in the shape of the composite distribution. The similarity of the composite angular distributions in these two groups is very expressive, and suggests the relationship in the physical processes. On the other hand the comparison of the distribution of D -values corresponding to high anisotropic collisions with heavy nuclei with those corresponding to high anisotropic collisions characterized by $N_h \leq 5$ and $n_s > 20$, shows a marked difference (Fig. 8). In spite of similar multiplicities the D values for collisions with heavy nuclei are significantly higher than those for the other group of events. This may

be an additional argument for supposing that the collection of events with $N_h \leq 5$ and $n_s > 20$ contains and admixture of collisions other than nucleon-nucleus collisions and nucleon-nucleon collisions with small multiplicity.

Besides the groups specified in Table I a small group of secondary jets could be separately analyzed.

In our collection of jets there are 5 cases of secondary interactions generated by charged particles, probably π -mesons (Table I event 30K, 26P, 31K, P24S4 Br and P20S4 Br). In all these cases we observe the two maxima in the angular distributions (Fig. 9). As the number of cases is small, it is difficult to establish the probability level of this observation.

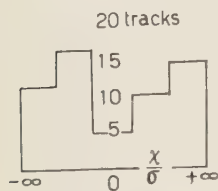


Fig. 9. - The histogram of the composite differential angular distribution for collisions of secondary particles possibly pions.

6. - Conclusions.

From the analysis performed, follows that the experimental effect of the bimodal (double maximum) angular distributions of secondary particles generated in nuclear collisions of energy higher than 10^{12} eV, observed earlier in our laboratories for « nucleon-nucleon » collisions ⁽¹⁾, can be regarded as well established on a more extended experimental material.

The two-centre model served in this analysis as a useful working hypothesis predicting that the occurrence of bimodal angular distributions becomes a general feature for cases of high anisotropy (anisotropy parameter $\sigma > 0.6$). Further analysis has shown new results which do not follow directly from the model, such as the existence of double maximum angular distributions in collisions with heavy nuclei accompanied by large excitation of the target nucleus ($N_h > 8$) ⁽³⁾.

However independently of any model the double maximum shape of the angular distribution of secondary particles is, in our opinion, a well established new feature of strongly anisotropic high energy nuclear collisions.

* * *

It is a pleasant duty to thank all laboratories named in the references to the Table I which have kindly exchanged their original measurement data with our laboratories and thereby rendered possible this analysis. Special thanks are due to Professor M. DANYSZ who initiated the action of the exchange of the experimental data.

RIASSUNTO (*)

Viene presentata una dettagliata analisi statistica della distribuzione angolare delle particelle secondarie generate in 65 collisioni nucleari con energie di primari maggiori di 10^{12} eV. La forma a doppio massimo della distribuzione (in coordinate $\log \tan \theta$), è una caratteristica generale degli eventi ad alto grado di anisotropia dei secondari nel sistema del CM. Si è riscontrato che la forma della distribuzione angolare è in accordo con le predizioni del modello a due centri per la multipla-produzione di mesoni sia per collisioni nucleone-nucleone sia per collisioni nucleone-nucleo pesante. Si sono introdotti un nuovo parametro D , che è una misura della deviazione dalla forma normale verso la distribuzione a due centri, ed altresì una coordinata adatta a visualizzare questa deviazione.

(*) *Traduzione a cura della Redazione.*

Preliminary Report on Cosmic Ray Intensity during Magnetic Storms in July 1959 (*).

J. G. ROEDERER, O. R. SANTOCHI, J. C. ANDERSON,
J. M. CARDOSO and J. R. MANZANO

Comisión Nacional de Energía Atómica - Buenos Aires

(ricevuto il 18 Maggio 1960)

Summary. — The cosmic ray intensity variation during three magnetic storms of July 1959 is analyzed. Data from neutron monitors at Mina Aguilar (4000 m o.s.l. at 12° S geomagnetic latitude), Buenos Aires (0 m o.s.l., 23° S) and Ellsworth (0 m o.s.l., 67° S) were used. A method is described which gives detailed information on the variation of the primary cosmic ray spectrum during magnetic storms. This method is applied to the present case, giving the following results: the shape of the primary variation spectrum responsible for the three July storms was approximately the same as that of the May 1959 storm. During the recovery of the second storm, an injection of considerable intensity of low energy particles was found. The time dependence of this extra flux is determined. During the slow recovery after the last storm, the primary variation spectrum changes its shape in a similar way as in the May storm recovery. The correlation of these effects with geomagnetic activity is shown.

1. — Introduction.

The analysis of two or more superposed cosmic ray storms is of considerable interest. The question arises of whether or not there is a linear superposition of effects, that is, to what extent do mechanisms, causing superposed cosmic ray storms, interfere mutually. The answer to this question would give valuable information on the hydromagnetic properties of the cosmic ray modulating solar plasma beams (¹).

There are many alternative ways to explain the superposition of cosmic ray storms, depending on the model chosen for the explanation of the single

(*) Paper presented to the Antarctic Symposium, Buenos Aires, November 1959.

(¹) W. R. PIGGOTT and C. W. ALLEN: *VIII Rapport de la Commission pour l'étude des relations entre les phénomènes solaires et terrestres* (1957), p. 77.

storm modulation mechanism ^(2,6). If we take, for instance, Dorman's theory ⁽⁵⁾, we may explain qualitatively the occurrence of two successive magnetic storms with overlapping cosmic ray effects, as the action of two solar plasma beams being emitted from two points of active regions which are ejecting particles into a common region of solid angle. These beams impinge on the earth, causing magnetic disturbances and cosmic ray modulation. In the region of plasma superposition, there may be a linear addition of cosmic ray effects or not according to the degree of mutual interaction between frozen magnetic fields and currents of both streams. A linear addition would be attained in the limit of none interaction; deep changes in the modulating effect would occur in the case of strong interaction (if for instance one beam «sweeps away» the other, or if instability is achieved, causing turbulence in the fringe region). In the first case, almost no change in the *shape* of the primary spectrum should be expected; merely the «amplitude» of the variation spectrum should change. In the second case, however, considerable changes in the primary spectrum might be produced.

It is interesting to note that the interaction of superposed plasma beams is expected to be stronger, the more the translational velocities of the two streams differ (*i.e.*, the greater is their relative velocity ^(*)). If we take the lag between the flare and the sudden commencement of the magnetic storm as a measure of the mean velocity of particles in the stream, we conclude that our July streams are of successively increasing velocity: $1.1 \cdot 10^8$ cm/s; $1.5 \cdot 10^8$ and $2.2 \cdot 10^8$ cm/s.

If on the other hand, we consider theories in which turbulent fields intervene ^(4,6), linear superposition of effects in two or more overlapping cosmic ray storms may preferably occur. Finally, theories in which the cosmic ray modulation is not merely localized inside the perturbing region, but extends out into the hydromagnetically «quiet» space ⁽²⁾, may again give only linear addition of effects.

2. — The primary variation spectrum during cosmic ray storms.

Different forms have been suggested for the primary variation spectrum of a cosmic ray storm ⁽⁵⁾. We will use Dorman's notation, writing $\delta D/D$ for the relative (%) variation spectrum. $D(E)$ is the reference differential primary

(2) E. A. BRUNBERG and A. DATNER: *Tellus*, **6**, 254 (1954).

(3) Y. SEKIDO and M. WADA: *Rep. Ions. Res. Japan*, **9**, 174 (1955).

(4) P. MORRISON: *Phys. Rev.*, **101**, 1397 (1956).

(5) L. I. DORMAN: *Izv. Ak. Nauk SSSR, Ser. Fiz.*, **20**, 24 (1956) and *Cosmic Ray Variations* (English Translation).

(6) E. N. PARKER: *Phys. Rev.*, **110**, 1445 (1958).

(*) The shorter would be the time available for the magnetic lines of force of one beam to diffuse into the other.

spectrum taken from a quiet prestorm period. We shall assume for $\delta D/D$ the form

$$(1) \quad \frac{\delta D}{D} = \begin{cases} \delta k(t) \cdot E^{-\gamma} & \text{for } \varepsilon_\lambda < \varepsilon < \varepsilon_0 \\ 0 & \text{for } \varepsilon > \varepsilon_0. \end{cases}$$

In the most general case, the three parameters δk , γ and ε_0 are time dependent. (ε_λ is the geomagnetic cut-off which we suppose to be constant). Now, as the exponent γ is mainly fixed by the modulation mechanism as a whole, we expect it to be fairly constant, unless the type of the mechanism is changed. The same applies to the upper cut-off ε_0 , although a certain time dependence might be expected even during the action of one and the same modulation mechanism. For some theories, $\varepsilon_0 = \infty$.

We shall make the assumption that, for a given type of modulation mechanism, γ and ε_0 are constant in time; the main contribution of cosmic ray intensity time dependence is given by $\delta k(t)$ (depending on the earth's position in the beam, magnetic and electric field intensities, stream density, etc.). We shall call δk the «amplitude» of the variation spectrum. With the form of variation spectrum (1), the superposition of two effects obeying to the same modulation mechanism, would be given by the linear superposition of the amplitudes. If, instead, two *distinct* modulation mechanisms are superposed, we would have

$$(2) \quad \frac{\delta D}{D} = \delta k_1(t) \cdot E^{-\gamma_1} + \delta k_2(t) \cdot E^{-\gamma_2},$$

with two cut-offs ε_{01} and ε_{02} for the first and the second terms, respectively. Finally, a sudden change of the mechanism at the time t_0 would be expressed by a spectrum like (2), with the condition

$$(3) \quad \begin{cases} \delta k_1(t) = \text{constant} & \text{for } t > t_0, \\ \delta k_2(t) = 0 & \text{for } t < t_0. \end{cases}$$

Let us now take the relative intensity variation recorded by a monitor at a given latitude (cut-off ε_λ)

$$\delta I = \frac{\delta N}{N} = \int_{\varepsilon_\lambda}^{\varepsilon_0} \frac{\delta D}{D} W_{\varepsilon_\lambda}(E) \cdot dE,$$

W_{ε_λ} is the coupling function for the given monitor at the given place. With

a variation spectrum of the form (1), we have

$$(4) \quad \delta I = \delta k(t) \int_{\varepsilon_\lambda}^{\varepsilon_0} E^{-\gamma} W_{\varepsilon_\lambda}(E) \cdot dE = \Gamma \cdot \delta k(t);$$

Γ is a coefficient which depends on the monitor, its location and the two parameters γ and ε_0 .

If we now consider two monitors «a» and «b», located at different latitudes, we can define a two dimensional vector $\delta \mathbf{I}$ of components $\delta I_a = \Gamma_a \cdot \delta k(t)$ and $\delta I_b = \Gamma_b \cdot \delta k(t)$. Eq. (4) shows that the direction of this vector is *constant in time* for a variation spectrum of type (1). Notice that the vector $\delta \mathbf{I}$, at a given instant t , is the sum of successive vectors $\Delta \mathbf{I} = \delta \mathbf{I}(t + \Delta t) - \delta \mathbf{I}(t)$ which represent the variation during a recording interval Δt (for instance, hourly or bihourly). The direction of these difference vectors should be constant, too. From the statistical point of view, all this means that δI_a and δI_b should be correlated linearly (*), the coefficient of regression being

$$(5) \quad \alpha_{ab} = \frac{\Gamma_a}{\Gamma_b} = \frac{\int_{\varepsilon_{\lambda_a}}^{\varepsilon_0} E^{-\gamma} \cdot W_a \cdot dE}{\int_{\varepsilon_{\lambda_b}}^{\varepsilon_0} E^{-\gamma} \cdot W_b \cdot dE}.$$

Any deviation from this linear correlation should be due to a change in the modulation mechanism.

We have calculated α_{ab} for the pairs of neutron monitors Ellsworth-Mina Aguilar and Buenos Aires-Mina Aguilar. We used the coupling functions given by DORMAN, (7) normalized to our geomagnetic cut-offs. These coupling functions are shown in Fig. 1. The resulting α values are given in Fig. 2 as a function of the upper

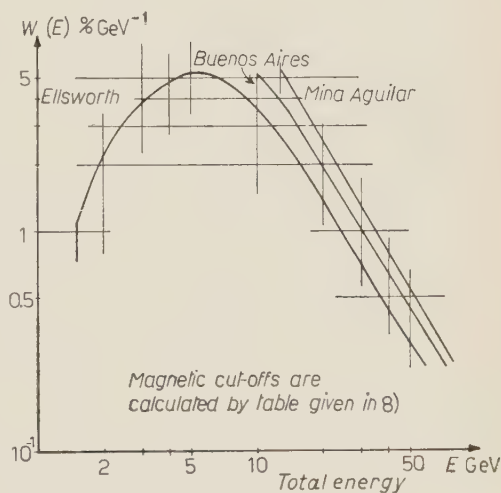


Fig. 1. — Coupling functions for neutron monitors at Mina Aguilar, Buenos Aires and Ellsworth, calculated using curves given in (8).

(*) This is of course also true for two monitors of different coupling function operating at the same place.

(7) L. I. DORMAN: *Cosmic Ray Variation* (English Translation), p. 117.

(8) J. J. QUENBY and W. R. WEBBER: *Phil. Mag.*, **4**, 90 (1959).

cut-off, and for some plausible γ values. Using at least two pairs of stations of significantly different coupling functions, one may be able to determine γ and ε_0 .

So far we have discussed the case of a single spectrum (1). Suppose now that a different, additional modulation mechanism starts its action at $t = t_0$.

This means that after that instant, an additional term $\delta k_2(t) \cdot E^{-\gamma_2}$ appears in the variation spectrum. Therefore, after t_0 , our two dimensional vector $\delta \mathbf{I}$ becomes the sum of two independent vectors

$$(6) \quad \delta \mathbf{I} = \delta \mathbf{I}_1 + \delta \mathbf{I}_2$$

of components

$$(6') \quad \begin{cases} \delta \mathbf{I}_1 \equiv (\delta k_1(t) \Gamma_{a_1}; \delta k_1(t) \Gamma_{b_1}), \\ \delta \mathbf{I}_2 \equiv (\delta k_2(t) \Gamma_{a_2}; \delta k_2(t) \Gamma_{b_2}), \end{cases}$$

where

$$\Gamma_{a,b_2} = \int_{\varepsilon_{\lambda a,b}}^{\varepsilon_{02}} E^{-\gamma_2} \cdot W'_{a,b} \cdot dE.$$

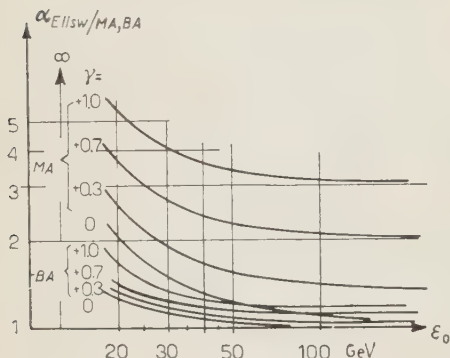


Fig. 2. - Ratio $\alpha_{ab} = \Gamma_a / \Gamma_b$ (eq. (5)) for the pairs of stations Ellsworth-Mina Aguilar and Buenos Aires-Mina Aguilar, as a function of the upper cut-off ε_0 , and for different γ values.

The important fact is that the direction of both vectors is *constant in time*. The linear correlation between δI_a and δI_b would be disturbed after t_0 , and the difference vectors $\Delta \mathbf{I}$ would no longer be parallel after that time (Fig. 3).

If we know *a priori* the *direction* of both vectors $\delta \mathbf{I}_1$ and $\delta \mathbf{I}_2$, we can easily determine the time dependence of both vectors independently given by $\delta k_1(t)$ and $\delta k_2(t)$. If, however, we only know the *direction* of *one* of them, say $\delta \mathbf{I}_1$, we are still able to determine the time dependence of the other (but not that of the first): if $\alpha_1 = \Gamma_{a_1} / \Gamma_{b_1}$ is the slope of $\delta \mathbf{I}_1$, we have, according to (6) and (6'),

$$(7) \quad \delta I_a - \alpha_1 \delta I_b = \delta k_2(t) [\Gamma_{a_2} - \alpha_1 \Gamma_{b_2}].$$

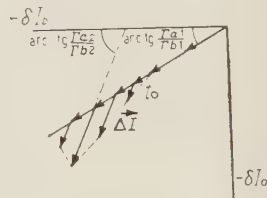


Fig. 3.

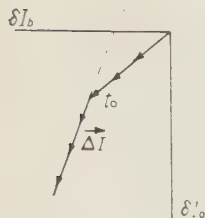


Fig. 4.

As the first member is obtained from experimental data, we can determine the amplitude $\delta k_2(t)$ up to a constant factor $\Gamma_{a_2} - \alpha_1 \Gamma_{b_2}$. Again, if we have records from at least three stations, Γ_{a_2} , Γ_{b_2} and therefore γ_2 , ε_{02} , as well as $\delta k_2(t)$ may be determined. In particular, if $\varepsilon_{\lambda a} < \varepsilon_{02} < \varepsilon_{\lambda b}$,

we have $I_{b_2} = 0$ and the difference $\delta I_a - \alpha_1 \delta I_b$ gives just δI_{a_2} , the contribution of process 2 to the intensity at station «a».

Finally, if rather than a superposition, there is a sudden change in the modulation mechanism at $t = t_0$, we deduce from (3) (3'), (6) and (6') that the difference vectors $\Delta \mathbf{I}$ merely change their direction remaining again parallel to each other after $t = t_0$ Fig. 4.

3. - Experimental results.

The scope of this preliminary report is to give a qualitative analysis of the main behaviour of cosmic ray intensity during July 1959, recorded by three neutron monitors, located at Mina Aguilar, Buenos Aires and Ellsworth, Antarctica (*). Unfortunately, data from our Ushuaia monitor (0 m o.s.l., at

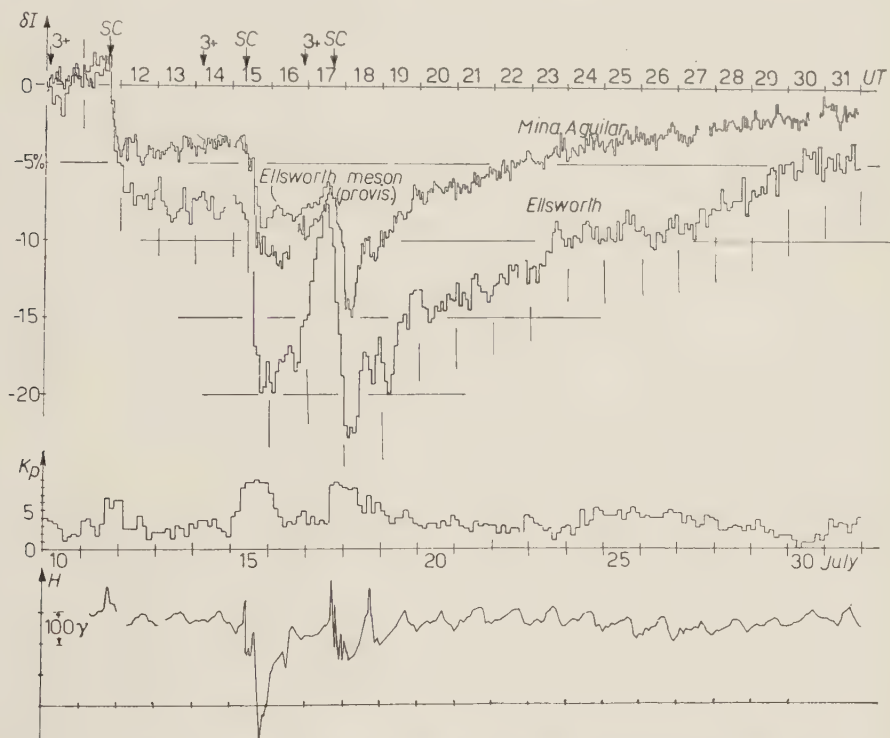


Fig. 5. - Percentage nucleon intensity variations recorded at Mina Aguilar (4000 m, 12° S geom. lat.) and Ellsworth (sea level, 67° S). Meson cubical elescope data of the latter station (corrected for pressure only) are shown for comparison in the interval July 14-17th. K_p values, and the horizontal component of the magnetic field recorded at Pilar (Argentina), are represented at the bottom.

(*) The Ellsworth monitors are operated in collaboration with the Instituto Antártico Argentino and the University of California.

43° S geomagnetic latitude) had to be rejected due to unreliable performance during that month.

Fig. 5 shows the hourly and bihourly percentage intensity at Mina Aguilar and Ellsworth, respectively, referred to an average level during the quietest days preceding the first storm (July 6-9). Buenos Aires percentage intensity is not represented; it is remarkably coincident within 1% with the Mina Aguilar curve during the whole period. K_p indices and the horizontal component of geomagnetic field recorded at Pilar Observatory (*) are shown at the bottom. Many interesting features are revealed at first sight, one of the most remarkable being the strong increase recorded at Ellsworth some hours before the third storm set on (July 17-th). For the same time interval, strong increases of low

energy particle intensity at high altitude have been reported (°). It is worth to try to get as much information as possible on the changes in shape and intensity of the primary cosmic ray spectrum.

We applied the method described in the preceding chapter to the pairs of stations Mina Aguilar-Ellsworth and Mina Aguilar-Buenos Aires. In Fig. 6, δI_{MA} is plotted *vs.* δI_{ELLS} for the period July 10 to 16 (0400 UT); bihourly ΔI vectors are indicated. The total δI vector is obtained joining each angular point with the origin. The mean slope during this period is

$$\alpha_{ELLS-MA} = 1.80 \pm 0.10.$$

Fig. 6. — δI vectors (eqs. (4)-(6')) of the pair of stations Ellsworth and Mina Aguilar, for the first and second storm (10th-17th July). The broken line is a best fit with $\alpha = 1.80$.

spectrum during these days. Buenos Aires and Mina Aguilar monitors have coupling functions (Fig. 1) too close to each other; indeed, the experimental α value for this pair of stations comes out

$$\alpha_{BA-MA} = 0.95 \pm 0.10$$

for the whole July period. Nevertheless, we can at least derive certain limits

(*) 31° 40' S - 63° 53' W geographic coordinates.

(°) H. GHIEMMETTI: private communication on Iowa Conference.

for γ and ε_0 from our experimental α values (Fig. 2). We obtain

$$0 < \gamma < 0.60 ,$$

with the corresponding limits for ε_0 :

$$\text{for } \gamma = 0, \quad \varepsilon_0 = 23 \text{ GeV} ; \quad \text{for } \gamma = 0.6, \quad \varepsilon_0 = \infty .$$

The value $\alpha_{\text{ELLS-MA}} = 1.8$ is slightly higher than that found for the same pair of stations during the May 1959 storm ($1.65 \pm .10$). For the first stage of that storm⁽¹⁰⁾ we find using data from Mina Aguilar, Buenos Aires, Ushuaia, Ellsworth, and Mt. Wellington:

$$\gamma = 0.48 \pm 0.06, \quad \varepsilon_0 \simeq \infty .$$

Taking into account limits of error, we may tentatively state that during the first stage of the July storms (11th-16th), the primary variation spectrum has a γ value comprised between 0.4 and 0.6.

Fig. 7 gives the behaviour of the ΔI vectors during the recovery after the second storm, till the big decrease of the third storm. A clean departure from the «normal» behaviour⁽¹¹⁾ (indicated by the $\alpha = 1.80$ line) suggests the superposition of a different type of primary variation spectrum, which represents an injection of low energy particles (*). Unfortunately, again due to our lack of information from intermediate latitudes (Ushuaia), we are not able to tell about the shape of the additional particles' spectrum. However, we can determine its time dependence according to (7). In Fig. 8 we have represented the «reduced» Mina Aguilar percentage intensity $\alpha_1 \delta I_{\text{MA}}$ ($\alpha_1 = 1.80$), together with the Ellsworth intensity. The difference $\delta I_{\text{ELLS}} - \alpha_1 \delta I_{\text{MA}} = \delta k_2(t)(\Gamma_{\text{ELLS}} - \alpha_1 \Gamma_{\text{MA}})$ is plotted below. If $\Gamma_{\text{MA}} = 0$ (i.e., the additional flux has a cut-off $\varepsilon_{02} < 13 \text{ GeV}$,

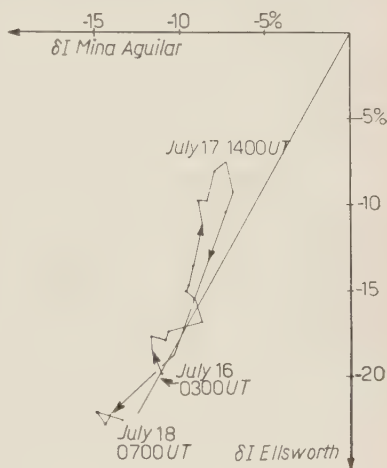


Fig. 7. - δI vectors for the 17th of July, showing the additional flux of low energy particles (see for instance eqs. (6) and (6') and Fig. 3). The $\alpha = 1.80$ lines is drawn for reference.

⁽¹⁰⁾ J. R. MANZANO, J. G. ROEDERER and O. R. SANTOCHI: *Nuovo Cimento*, **18**, 136 (1960).

⁽¹¹⁾ H. CARMICHAEL and J. F. STELJES: *Phys. Rev. Lett.*, **3**, 392 (1959).

(*) One may think, as an alternative, of an extremely fast recuperation of the low energy flux. However, any conventional mechanism could hardly explain a collapse of the modulating process for low energies, while it is still acting on high energy particles.

or $\gamma_2 \geq 1$ (*)), this difference gives directly $\delta I_{2\text{FLIS}}$, the contribution of the additional flux, in % of Ellsworth reference intensity. In this case, $\alpha_1 \delta I_{MA} =$

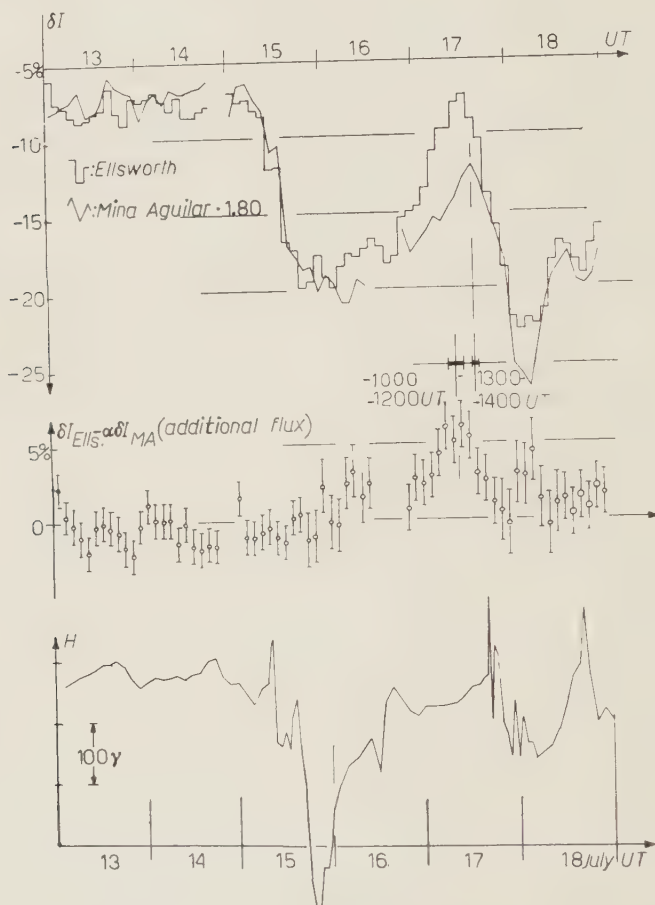


Fig. 8. - Top: Ellsworth percentage intensity and the « reduced » Mina Aguilar intensity (eq. (7)). Center: additional flux (in % at Ellsworth), with statistical errors. Bottom: horizontal component at Pilar.

$= \delta I_{1\text{FLIS}}$, the contribution at Ellsworth of the Forbush decrease modulation mechanism. Note the time difference between the maximum of the additional flux and the onset of the third storm. For the sake of comparison, we again plotted the horizontal field intensity.

(*) The steep increase found at high altitudes supports this hypothesis. Furthermore, a brief preliminary inspection of cubic telescope data from Ellsworth, which do not reveal any additional increase (see Fig. 3), suggests that ε_0 had to be less than $(8 \div 10)$ GeV (the cut off of meson coupling function).

In Fig. 9, the ΔI vectors from 24 hour moving average intensity values are shown for the recovery period after the third storm. We took 24 hour moving average in order to eliminate the considerable daily variation in this period. Taking into account the discussion of Sect. 2, we realize that during the recovery period, the shape of the primary variation spectrum was changing with respect to that of the previous decreasing period. The general behaviour of the curve in Fig. 9 may be interpreted as a much slower recovery of low energy particles than that of the higher energy region. In other words, the primary variation spectrum decreased its γ (or increased its upper limit ε_0 , or both) during the recovery period. It is interesting to note that this general behaviour is much the same as that of the May storm recovery⁽¹⁰⁾. Finally, as to the «fine structure» of the curve in Fig. 9, notice the peculiarity of the days 24, 25 and 26, during which the intensity at Ellsworth stood still while Mina Aguilar (and Buenos Aires) were steadily recovering. Around these days, the horizontal magnetic field intensity decreased, while the K_p index and the amplitude of daily variation increased. The daily variation is shown in Fig. 10, as it was estimated from the difference of 12 and 24 hours moving averages⁽¹²⁾.

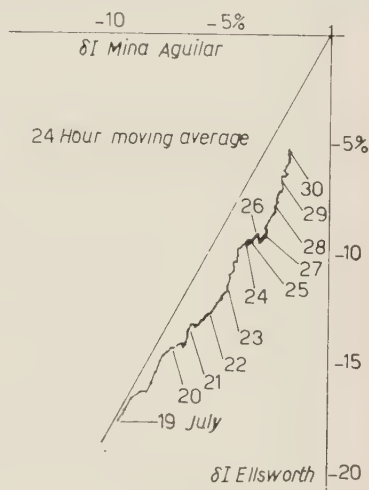


Fig. 9. - δI vectors of Ellsworth and Mina Aguilar, using 24 h moving averages. The gradual departure from the $\alpha=1.80$ line after the 19th of July shows a gradual change in the shape of the primary variation spectrum, indicating that low energy particles recover slower than high energy ones.

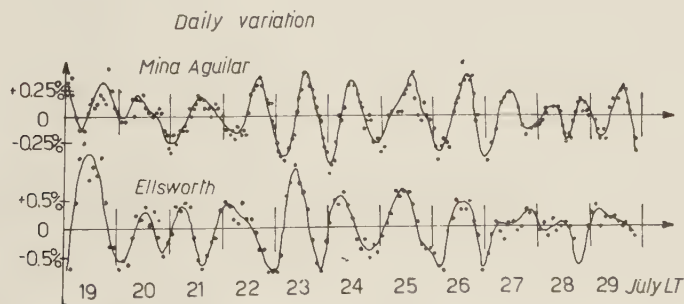


Fig. 10. - Daily variation at Mina Aguilar and Ellsworth, calculated from 24 h and 12 h moving averages⁽¹²⁾.

⁽¹²⁾ J. F. STELJES: *Nuovo Cimento*, **4**, 857 (1959).

15 minutes interval data have not yet been analyzed; a more careful quantitative analysis using meson telescope data (cubical at Ellsworth and Buenos Aires, narrow directional at Buenos Aires) is in progress.

4. - Conclusions.

From the preceding results we deduce that there was no appreciable change in the primary variation spectrum for the three successive Forbush decreases. This may be interpreted as an indication of a linear superposition of cosmic ray modulation effects during the July 1959 disturbances. On July 17th, an injection of low energy particles, probably with a steep energy spectrum occurred. At the final stage, low energy particles recovered slower than high energy particles.

* * *

We thank H. GHIEMMETTI (The Enrico Fermi Institute for Nuclear Studies) for many helpful suggestions and valuable information.

RIASSUNTO (*)

Si analizza la variazione dell'intensità dei raggi cosmici durante le tre tempeste magnetiche del Luglio 1959. Si sono utilizzati i dati dei rivelatori di neutroni di Mina Aguilar (4000 m s.l.m., 67° S di latitudine geomagnetica), Buenos Aires (0 m s.l.m., 23° S) ed Ellsworth (0 m s.l.m., 67° S). Si descrive un metodo che fornisce dettagliate informazioni sulla variazione dello spettro dei raggi cosmici primari durante le tempeste magnetiche. Questo metodo viene applicato al caso presente, ottenendo i seguenti risultati: la forma dello spettro di variazione dei primari, cui è dovuta la tempesta del Luglio, era quasi uguale a quella della tempesta del Maggio 1959. Durante la ripresa dopo la seconda tempesta si è riscontrata una iniezione di intensità considerevole di particelle di bassa energia. Si determina la dipendenza dal tempo di questo flusso aggiuntivo. Durante la lenta ripresa dopo l'ultima tempesta, lo spettro di variazione dei primari cambia la sua forma in maniera simile alla ripresa dopo la tempesta di maggio. Si mostra la correlazione fra questi effetti e l'attività geomagnetica.

(*) Traduzione a cura della Redazione.

Analysis of Cosmic Ray Intensity Time-Dependence Recorded at Mina Aguilar during July 1959.

J. G. ROEDERER, O. R. SANTOCHI, J. C. ANDERSON,
J. M. CARDOSO and J. R. MANZANO

Comisión Nacional de Energía Atómica - Buenos Aires

(ricevuto il 18 Maggio 1960)

Summary. — Intensity variations of nucleonic component at Mina Aguilar (4000 m o.s.l., 12° S geomagnetic latitude) are analyzed as a function of time, for the July 1959 storms. It is suggested that the intensity behaviour is due to a linear addition of three independent Forbush decreases of different amplitudes and relaxation times, but of approximately the same form of primary variation spectrum at high energies. The slow recovery after the third storm is mainly determined by the relaxation time of the second storm.

In a previous report ⁽¹⁾, we pointed out the importance of obtaining information upon the degree of linearity of superposition of cosmic ray effects during the overlapping July 1959 Forbush decreases. We stated in the above-mentioned paper, that a linear superposition of modulation effects in two or more successive storms would in general lead to a variation spectrum of functional form constant in time, being the amplitude of decrease the only time-dependent quantity.

As it can be deduced from the results given in the previous paper ⁽²⁾, no change in the variation spectrum takes place until the recovery after the second storm. This strongly suggests that the modulation mechanism responsible for

⁽¹⁾ J. G. ROEDERER, O. R. SANTOCHI, J. C. ANDERSON, J. M. CARDOSO and J. R. MANZANO: *Nuovo Cimento*, **18**, 120 (1960).

⁽²⁾ Loc. cit. ⁽¹⁾, Fig. 6.

the second storm did not interfere the first one, both acting independently. With respect to the third storm, apart of the additional low energy particle flux detected at Ellsworth on July 17th, we conclude from Fig. 9 of the former report that at least until the 19th of July, the variation spectrum did not change appreciably. We therefore suppose all three Forbush decreases to be linearly superposed.

In this paper we will show a further evidence for linear, independent superposition, at least for energies above the Mina Aguilar geomagnetic cut-off (12.7 GeV). To show this, we consider again the simplified form for the primary variation spectrum (¹)

$$\frac{\delta D}{D} = \delta k(t) E^{-\gamma}.$$

We called the function $\delta k(t)$ the amplitude of the variation spectrum. If no interference between modulation mechanisms of the three storms occurs, γ will be independent of time, and we will have

$$\frac{\delta D}{D} = [\delta k_1(t) + \delta k_2(t) + \delta k_3(t)] E^{-\gamma},$$

and for the percentage intensity variations

$$\delta I = \delta I_1 + \delta I_2 + \delta I_3 = I[\delta k_1(t) + \delta k_2(t) + \delta k_3(t)] \quad (*)$$

where $\delta k_i(t)$ are three independent amplitudes, one function for each storm ($\delta k_i(t) = 0$ for $t < \text{time of storm commencement}$). If we take data from Mina Aguilar, which are less sensitive to low energy flux modulations, and plot δI in logarithmic co-ordinates, Fig. 1, we come to the following conclusions:

- i) the recovery to prestorm level after the third storm is exponential (³);
- ii) this exponential form is not achieved immediately after the third storm, but only two days later, *i.e.* after the 20th;
- iii) the extrapolation of this exponential form to earlier days, points accurately to the minimum after the second storm (**);

(*) For the definition of the constant I , see formula (4) of (¹).

(**) This is also true for Ellsworth neutron monitor data, although at this station the intensity fluctuations around the exponential form are much more pronounced. With respect to Buenos Aires records, it has been already mentioned in (¹) that percentage variations fit within normal fluctuations with those recorded at Mina Aguilar.

(³) P. MORRISON: *Phys. Rev.*, **101**, 1397 (1956).

iv) the recovery after the first storm may also be fitted by an exponential form.

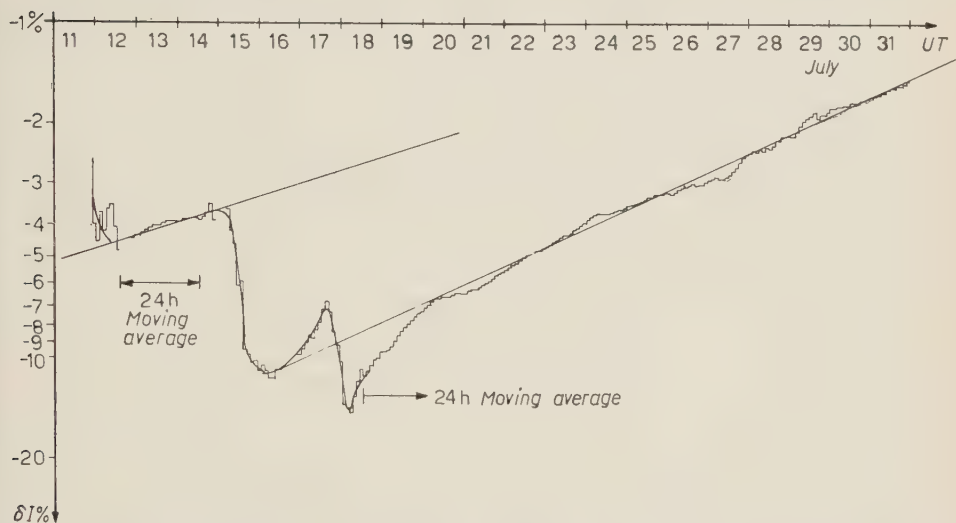


Fig. 1. - Logarithmic plot of percentage variation of nucleon component at Mina Aguilar. The exponential type of recovery is shown. 24 h moving averages are used, except for days in which intensity varies strongly; bihourly data are plotted for these intervals.

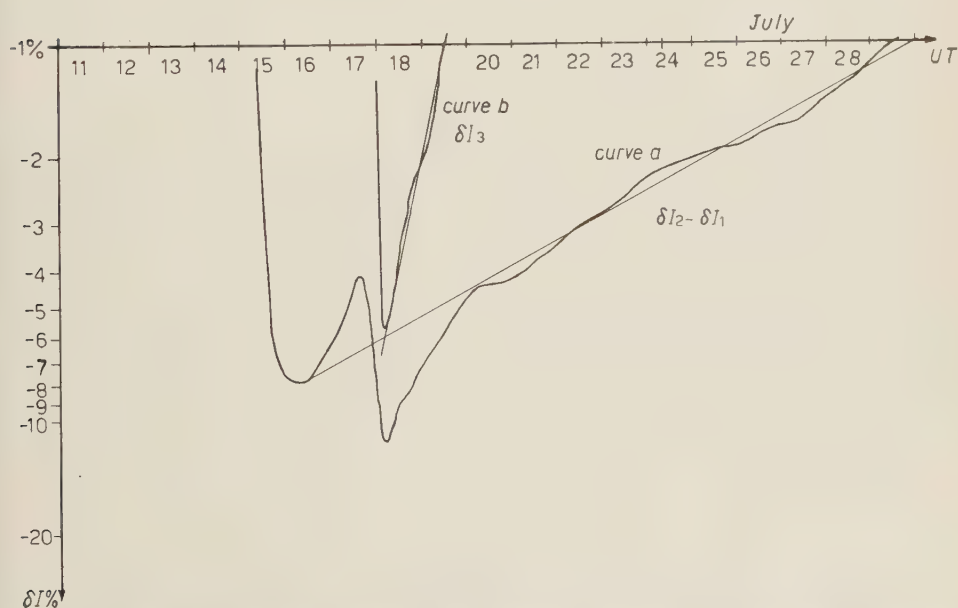


Fig. 2. - Curve *a*: difference between the intensity variation of Fig. 1 and the exponential contribution δI_1 of the first storm recovery. Curve *b*: difference between curve *a* and the exponential contribution δI_2 of the second storm recovery.

With these results, we proceeded as follows: we supposed $\delta k_1(t)$ and therefore dI_1 to be exponential, of the form (see Fig. 1)

$$\delta I_1 \sim \exp \left[-\frac{t}{274} \right] \quad (t \text{ in hours}).$$

If we subtract δI_1 from δI , we obtain a curve sketched in Fig. 2-a. If we now suppose that the main exponential behaviour after the 20th of July belongs to the *second* storm (*), rather than the third one, we have

$$\delta I_2 \sim \exp \left[-\frac{t}{162} \right].$$

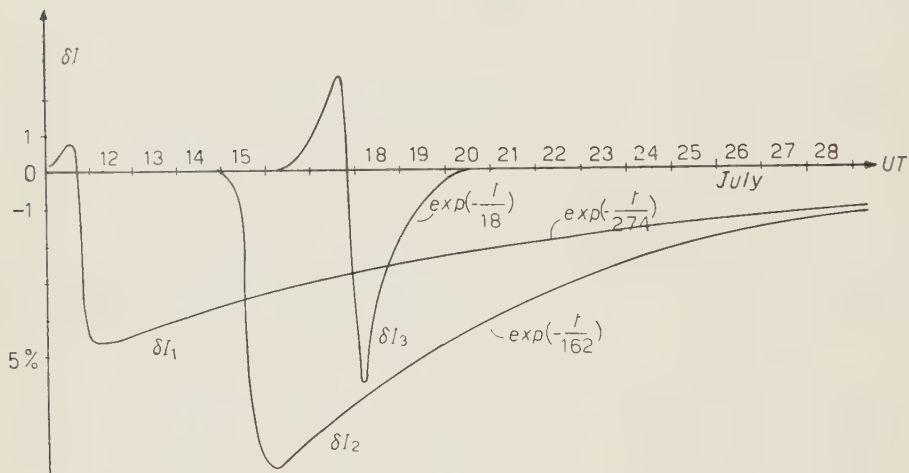


Fig. 3. - Representation of the three independent cosmic ray storms of exponential recovery each, into which the July 1959 intensity variation at Mina Aguilar can be resolved. Total intensity variation (Fig. 1) is given as a linear superposition of these curves.

Subtracting this function from curve *a*), Fig. 2, we are led to δI_3 . The negative part of δI_3 represents the decrease and recovery of the third independent storm; it is shown in Fig. 2 curve *b*). Notice the fact that this very fast recovery again comes out to be of exponential form

$$\delta I_3 \sim \exp \left[-\frac{t}{18} \right].$$

In summary, if we make the assumptions, that undisturbed cosmic ray storm recoveries are essentially of exponential type for high energies (≥ 10 GeV),

(*) This of course means that the recovery in Fig. 1 should not be strictly exponential.

and that cosmic ray effects superpose linearly, we can resolve the July 1959 cosmic ray intensity variations into three single, independently acting Forbush decreases of exponential recovery. These independent cosmic ray storms are shown in Fig. 3. Their sum fits the Mina Aguilar intensity variation curve within normal fluctuations. Characteristic parameters are shown in Table I.

TABLE I.

Storm commencement	Maximum amplitude	Relaxation time for recovery	Prestorm increase
July 11, 16.23 UT	-4.6%	(274 ± 6) h	+0.7%
July 15, 08.02 UT	-8.0%	(162 ± 6) h	none
July 17, 16.38 UT	-5.7%	(18 ± 3) h	+2.5%

* * *

We are deeply indebted to «Compañía Minera Aguilar S.A.» for the efficient co-operation and support given to the High Altitude Cosmic Ray Station Mina Aguilar.

RIASSUNTO (*)

Si analizzano in funzione del tempo le variazioni di intensità della componente nucleonica a Mina Aguilar (4000 m s.l.m., 12° S latitude geomagnetica), per le tempeste del Luglio 1959. Si suggerisce che il comportamento della intensità sia dovuto alla composizione lineare di tre indipendenti decrementi di Forbush di ampiezze e tempi di rilassamento diversi, ma aventi approssimativamente la stessa forma dello spettro di variazione della componente primaria. La lenta ripresa dopo la terza tempesta è dovuta principalmente al tempo di rilassamento della seconda tempesta.

(*) Traduzione a cura della Redazione.

Cosmic Ray Intensity Variations during the Magnetic Storm in May 1959.

J. R. MANZANO, J. G. ROEDERER and O. R. SANTOCHI

Comisión Nacional de Energía Atómica - Buenos Aires

(ricevuto il 18 Maggio 1960)

Summary. — Cosmic ray intensity during the May 1959 magnetic storm is analysed, using neutron monitor and cubic telescope data from Mina Aguilar, Buenos Aires, Ushuaia and Ellsworth (Antarctica). The primary variation spectrum is estimated according to a method outlined in a recent paper ⁽¹⁾. The intensity behaviour during recovery is analysed in detail. Following results are obtained. The primary variation spectrum, acting until the 18th of May, has an approximate form given by $\delta D/D = -\delta k(t) \cdot E^{-0.5}$, valid up to very high energies. Around the 18th, this spectrum changes its shape at low energies (< 2 GeV), in a similar way as it occurred during the July 1959 storm recovery. This change may be interpreted as an additional removal of low energy particles, which lasted at least until the end of the month. On May 14, intensity variation is quite peculiar, in spite of being this a quiet day from the solar and geomagnetic point of view. A world-wide decrease occurs, with a superposed, 10 h lasting increase, which is particularly high at Ellsworth (9% in the neutron monitor, 2% for the cubical telescope). It is shown that Ellsworth was located in a 04 impact zone for a simultaneous solar event. On the 24th, a world-wide, small Forbush decrease occurred, associated with a magnetic storm and a decrease in the horizontal component of the magnetic field. This Forbush decrease, which shows a strong longitude dependence, corresponds to a primary variation spectrum which has the same shape as that responsible for the general recovery acting at the time, *i.e.*, after the low energy change on the 18th.

⁽¹⁾ J. G. ROEDERER, O. R. SANTOCHI, J. C. ANDERSON, J. M. CARDOSO and J. R. MANZANO: *Nuovo Cimento*, **18**, 120 (1960).

1. — Introduction.

The May 1959 Forbush decrease ⁽²⁾ was associated with a sudden magnetic storm commencement which started at 2318 UT on May 11. This storm is presumably linked with the strongest solar flare so far reported in this cycle, which occurred on May 10, at 2102 UT ⁽³⁾, lasting for several hours. A strong increase of low energy proton flux at 10 g/cm² atmospheric depth, was reported for the 12th of May ⁽⁴⁾. During the recovery of cosmic ray intensity solar and geomagnetic activity was still high. Particularly on the days 11, 13 and 17, the solar BT 48 region was extremely active. Geomagnetic activity was high on days 15 and 24.

In the present paper, cosmic ray modulation effects during this period will be analysed, and their connection to solar and geomagnetic activity will be discussed.

Records from following stations were used in this analysis: neutron monitor Mina Aguilar (4000 m o.s.l., 12° S geomagnetic latitude), neutron monitor and cubical telescope Buenos Aires (sea level, 23° S), neutron monitor Ushuaia (sea level, 43° S) and neutron monitor and cubical telescope Ellsworth ^(*) (sea level, 67° S). Cubical telescope data were corrected for pressure only. For this reason, they will be considered for qualitative arguments only. Hourly, or bihourly percentage variations are shown in Fig. 1. The reference level is given by the mean intensity during quiet days preceding the increase in geomagnetic activity on the 4th of May. Buenos Aires neutron monitor data are not shown; percentage variations coincide within minor fluctuations with those at Mina Aguilar. K_p values and the horizontal component of the earth's magnetic field recorded at Pilar (Argentina), are shown below.

A first inspection of Fig. 1 suggests to divide the whole period into seven subintervals:

1) May 11, 23 UT – May 13, ~ 22 UT: big Forbush decrease associated with a SC magnetic storm, which lasted 24 hours. Gradual intensity recovery. Strong solar activity on 11 and 13th.

2) May 13, 22 UT – May 14, 18 UT: sudden decrease of several percent, followed by an increase, detected at all stations, which lasted about 10 hours,

⁽²⁾ F. BACHELET, P. BALATA, A. M. CONFORTO, N. IUCCI and G. MARINI: *Nuovo Cimento*, **13**, 1055 (1959).

⁽³⁾ Preliminary reports, *High Altitude Observatory* (Boulder, Colo.).

⁽⁴⁾ E. P. NEY, J. R. WINCKLER and P. S. FREIER: *Phys. Rev. Lett.*, **3**, 183 (1959).

^(*) Operated in collaboration with the University of California and the Instituto Antártico Argentino.

and which is very strong for the Ellsworth nucleon intensity. Intensity falls back to a minimum, which by the way is the absolute minimum for the whole May disturbance. No important flare was reported for this day; geomagnetic activity was at lowest level compared to preceding and following days.

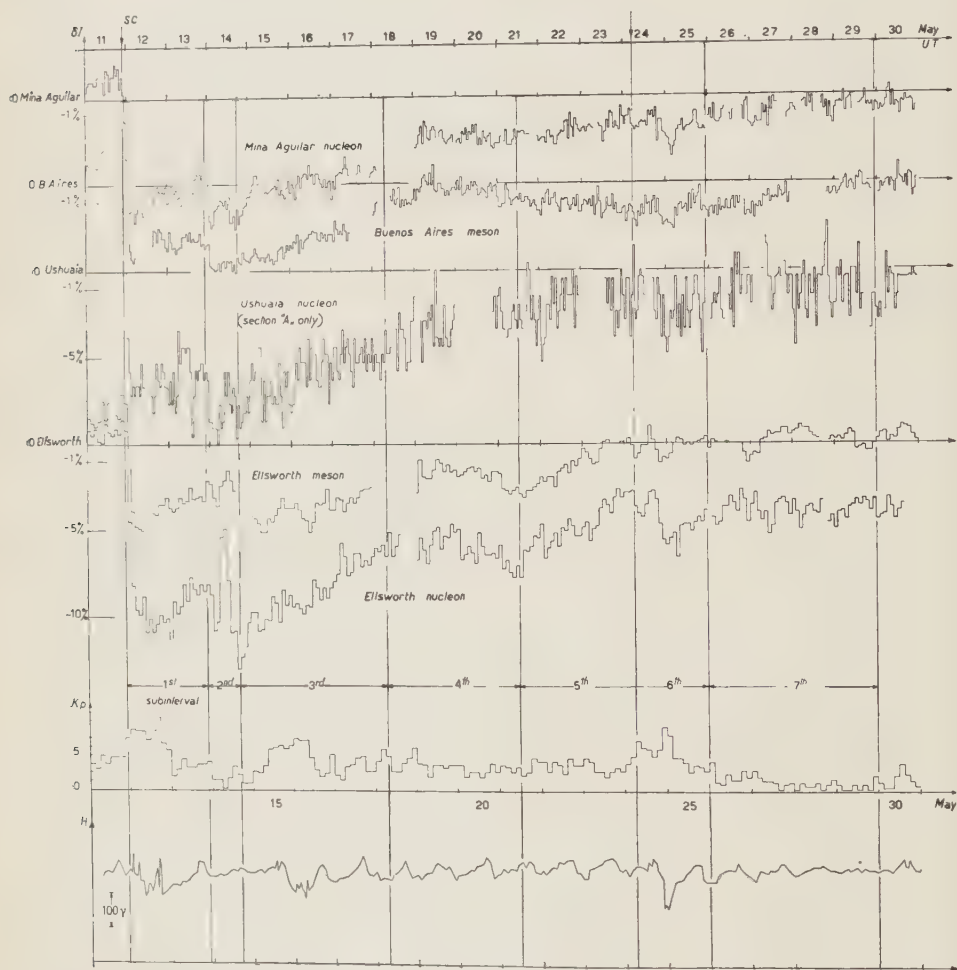


Fig. 1. - Percentage variations of intensity for different detectors. K_p indices and horizontal component of geomagnetic field intensity are shown below. The division of the whole period into seven subintervals according to cosmic ray behaviour is indicated. For further details, see text.

3) May 14, 18 UT - May 18: almost undisturbed recovery at all stations. The magnetic storm on the 15th apparently had no influence on cosmic radiation.

4) May 18 – May 21, ~ 12 UT: general leveling off and/or decrease of intensity. No peculiar geomagnetic events, except constant high activity. Solar activity was high on the 17th, decreasing gradually afterwards.

5) May 21, ~ 12 UT – May 24, 06 UT: undisturbed recovery, except at Buenos Aires N.M. and C.T. No appreciable change in geomagnetic activity; solar activity steadily decreasing.

6) May 24, 06 UT – May 25, 24 UT: small Forbush decrease associated with a magnetic storm of sudden commencement starting 05.40 UT, and a pronounced decrease in horizontal component. Notice the «fine structure» reproduced by all detectors, of two well separated decreases, or maybe one decrease with superposed increase at ~ 1800 UT on the 24th.

7) May 26 – May 30: recovery at low latitudes, and leveling off at high latitudes. Geomagnetic activity decreasing fast. After the 30th geomagnetic activity increases again.

It is a remarkable feature of some of these well defined subintervals of characteristic cosmic ray behaviour, that it is difficult to establish a plausible causal relationship with large solar and terrestrial phenomena so far reported.

2. – The primary variation spectrum.

The first task will be to determine the approximate form of the primary variation spectrum, and to establish whether it changed from interval to interval. We applied the method given in ⁽¹⁾, in order to estimate the parameters of the variation spectrum, expressed in the approximate form

$$\frac{\delta D}{D} = \begin{cases} \delta k(t) \cdot E^{-\gamma} & \text{for } E < \varepsilon_0, \\ 0 & \text{for } E > \varepsilon_0. \end{cases}$$

Bihourly ΔI vectors (⁽¹⁾, Section 2) for the pair of neutron monitors Ellsworth and Mina Aguilar

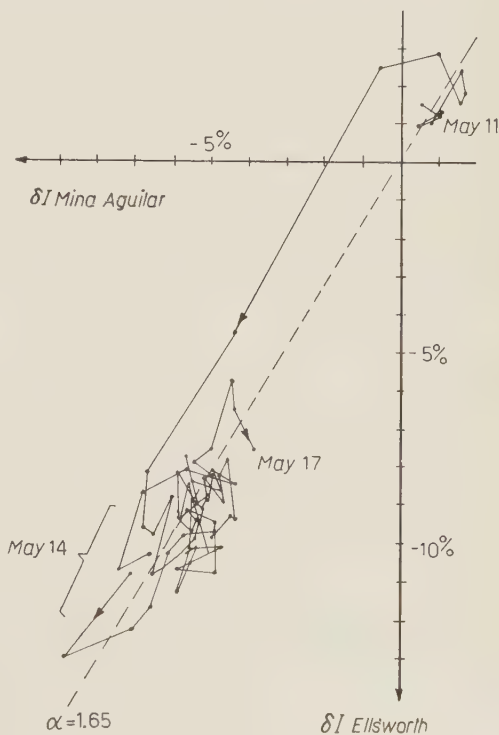


Fig. 2. – Percentage intensity variation diagram for Ellsworth and Mina Aguilar neutron monitors, for the 1st and 3rd subinterval. The increase occurring during the 2nd sub-interval is excluded. The best fit line is shown.

worth-Mina Aguilar and Ushuaia-Mina Aguilar are shown in Fig. 2 and Fig. 3, respectively. From the prestorm increase until the 17th, 24 UT, the best fit is obtained for

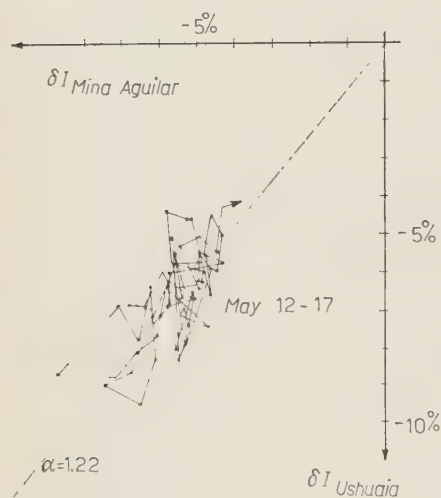


Fig. 3. — Item Fig. 2, for Ushuaia vs. Mina Aguilar. Data of the 11th of May are not available for Ushuaia.

$$\alpha_{\text{ELLS-MA}} = 1.65 \pm 0.10 ,$$

$$\alpha_{\text{USH-MA}} = 1.22 \pm 0.12 .$$

In Fig. 2, we omitted the interval 05 UT to 15 UT of the 14th, during which the steep increase at Ellsworth occurred. Notice that both decreases, that of the 11th and that of the 14th, do not show any appreciable difference in α . This suggests that the primary variation spectrum did not change during the additional decrease in the second subinterval. In other words, both modulation mechanisms were of the same type, having linearly superposed effects on cosmic ray intensity ⁽⁵⁾.

In order to have a further intermediate point in the southern hemisphere, we used data from Mt. Wellington (*), which has a geomagnetic cut-off of 2 GeV total energy, according to ⁽⁶⁾. We obtain

$$\alpha_{\text{MTWELL-MA}} = 1.52 \pm 0.09 .$$

Using the theoretical curves given in ⁽¹⁾, completed with those for Ushuaia and Mt. Wellington, we get a best fit for a spectrum of the form

$$\gamma = 0.48 \pm 0.05 ; \quad \varepsilon_0 \simeq \infty .$$

In Fig. 4, theoretical curves for α are represented as a function of γ , assuming $\varepsilon_0 = \infty$. The experimental α values with their errors are marked on the curves.

⁽⁵⁾ J. G. ROEDERER, O. R. SANTOCHI, J. C. ANDERSON, J. M. CARDOSO and J. R. MANZANO: *Nuovo Cimento*, **18**, 131 (1960).

^(*) We thank the Cosmic Ray Group of the University of Tasmania for sending their data.

⁽⁶⁾ J. J. QUENBY and W. R. WEBBER: *Phil. Mag.*, **4**, 90 (1959).

In order to eliminate the intense daily variation, we smoothed the percentage variations taking 24 hour moving averages after the 15th, 00 UT. We excluded from this procedure the whole 6-th subinterval, in which the

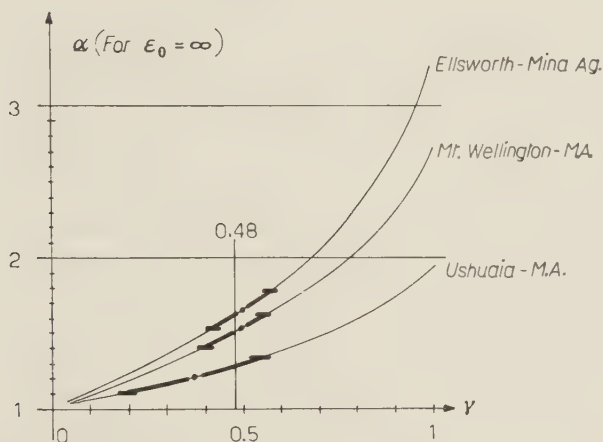
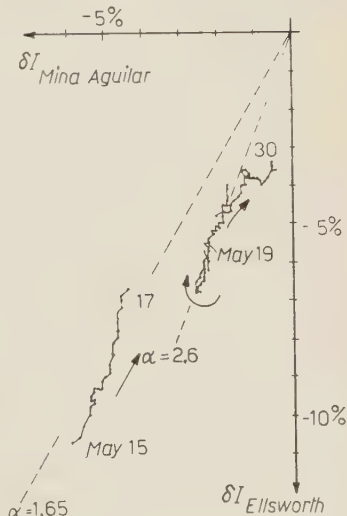


Fig. 4. - Theoretical curves for the coefficient α , corresponding to a variation spectrum of type $\delta k(t)E^{-\gamma}$ extending to highest energies ($\epsilon_0 = \infty$). Experimental values are indicated.

small Forbush decrease took place. Fig. 5 shows the δI correlation diagram for Ellsworth-Mina Aguilar using average intensity. A clear departure from the initial $\alpha = 1.65$ line is seen after the 18th of May, i.e., after the 3-rd subinterval. According to the discussion given in Section 2 of ⁽¹⁾, we conclude that a change in the primary variation spectrum occurred around the 18th, and lasted for the rest of the period. Fig. 6 shows the corresponding diagram for the pair of stations Ushuaia-Mina Aguilar. No appreciable change is seen after the 18th. In order to assure that this change was not a local effect, extending to high energies at Ellsworth, we correlated the intensity variation of both detectors, N.M. and C.T., at Ellsworth. The

Fig. 5. - Percentage variation diagram for smoothed intensity, for the pair of neutron monitors Ellsworth - Mina Aguilar, corresponding to the days after the second subinterval. Data from Mina Aguilar for the 18th of May are not available. The change in the slope occurring after the 3-rd subinterval is indicated (see text).



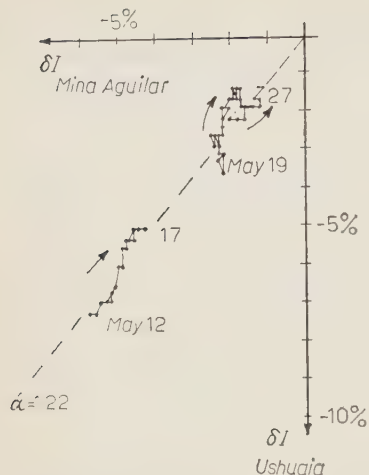
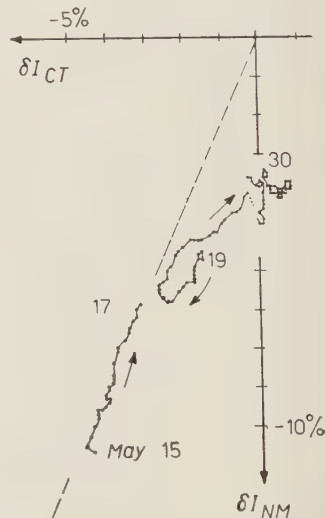


Fig. 6. - Item Fig. 5, for the pair Ushuaia - Mina Aguilar. No appreciable change after the 18th is revealed.

Finally, coming back to Fig. 2, we realize that all ΔI vectors corresponding to the sudden decrease on the 11th, lie well above the $\alpha = 1.65$ line. This effect, which is also found for the first July storm (see Fig. 6 of ⁽¹⁾), is due to a shift in time of cosmic ray storm commencement between Ellsworth and Mina Aguilar. An analysis of this longitude effect ⁽⁷⁾ shows that Ellsworth is (54 ± 6) minutes late with respect to Mina Aguilar in the May storm commencement. Mt. Wellington turns out to be $3^h 45^m \pm 10^m$ late.

Fig. 7. - Item Fig. 5, for the neutron monitor *vs.* cubical telescope at Ellsworth. CT data for the 18th are not available. Again, a departure from the original line is clearly shown for the days following the 3-rd subinterval.



⁽⁷⁾ J. G. ROEDERER, J. R. MANZANO and O. R. SANTOCHI: preprint C.N.E.A., in press.

3. - The increase on May 14.

Fig. 8 shows half-hourly data recorded at our different stations on the 14th of May. Percentage values are referred to the mean intensity at that day. The increase at Ellsworth is many times greater than at the other stations (including Mt. Wellington and others). It is of about 9% for N.M. and 2% for C.T. It starts at (0600 ± 0015) UT, both for N.M. and C.T. Intensity decays gradually until 1800 UT, when it reaches again a minimum (absolute minimum of the May storm). C.T. data are not available after 1600 UT. Violent fluctuations occur during the intensity decay in the nucleonic component; careful checks of equipment operation definitely rule out the possibility of attributing these fluctuations to equipment unstability.

Increases at Mina Aguilar and Ushuaia are of much smaller amplitude; the intensity rise is more gradual, except at Mina Aguilar, where a rather sudden jump is seen at 0330 UT. This is confirmed by 15 minute data. In principle, it would be hard to rule out entirely a contribution of daily variation, which is quite high during neighbouring days, the maximum occurring just around 1000 UT. However, a brief inspection of data from stations differing substantially in longitude from ours, still shows the existence of an increase occurring at nearly the same UT interval.

The magnitude of these increases, referred to a level represented by the extrapolation of the intensity curve of the 3-rd interval into the second sub-interval (Fig. 1), is given by the following rough figures: Mina Aguilar 1.4%; Ushuaia 2.5%; Mt. Wellington 3.2%; Ellsworth 5.6% (mean over 5 hours). These values correspond to neutron monitors only. Excluding Ellsworth, and taking Mina Aguilar as reference, we obtain from Fig. 4 a variation spectrum of $\gamma \simeq 0.9$. This value is similar to the exponent of the primary variation spec-

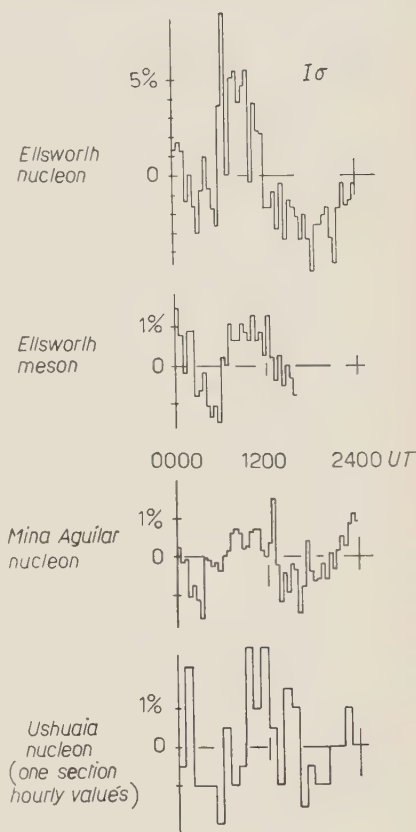


Fig. 8. - 30 min data for the 14th of May, showing the sudden increase with subsequent decay at Ellsworth, and the minor increases at Mina Aguilar and Ushuaia.

trum of the daily variation ⁽⁸⁾. The strong increase at Ellsworth might be interpreted as an additional enhancement of the primary low energy flux.

The most striking feature of these increases, particularly that detected at Ellsworth, is that there was no simultaneous solar event to which it might have been associated. No flare was reported ^(*), and geomagnetic activity was remarkably low at this day, compared to preceding and following days ^(**). If we nevertheless suppose that this additional flux at Ellsworth was of solar origin, and compute impact zones for a solar event which took place at about 0600 UT ⁽⁹⁾, we get the picture of Fig. 9. Some cosmic ray stations located in or near impact zones are shown.

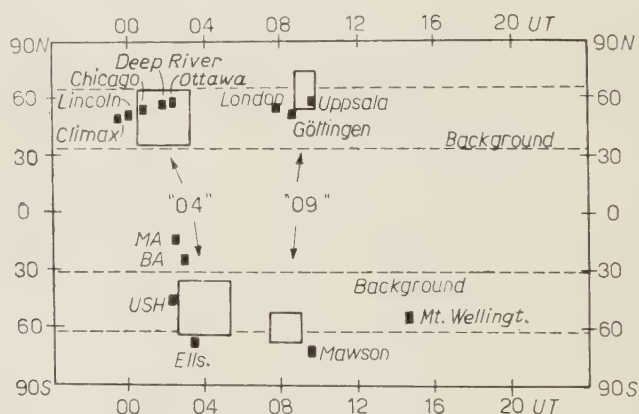


Fig. 9. - Impact zones for a solar event occurring at 0600 UT on May 14.

With respect to Ellsworth, we note that this station lies near the southern edge of the impact zone (drawn for a rigidity of 1 GV). These impact zones, however, are calculated using the centered dipole model, for which the geomagnetic cut-off at Ellsworth would be of about 0.4 GV only. Taking into account higher order corrections, as given in ⁽⁶⁾, the real situation must be different from that sketched in Fig. 9. The impact zones will be distorted by this multipole correction. In the particular case of the « 04 » impact zone in the southern hemisphere, it will be displaced several degrees southwards. There is therefore a great chance for Ellsworth of having been situated in the true impact zone during the increase on May 14. We look forward to analyse 15 minute data from other stations lying in or near the impact zones shown in Fig. 9.

⁽⁸⁾ L. I. DORMAN: *Cosmic Ray Variations*, Translation, Technical Documents Liaison Office, Wright-Patterson Air Force Base, Ohio.

^(*) Note added in proof. - In the meantime, a couple of flares of importance 1 and one of importance 2 were reported to us.

^(**) This, however, may be of some significance.

⁽⁹⁾ J. W. FIBOR: *Phys. Rev.*, **94**, 1017 (1954).

4. - The magnetic storm of May 24.

Cosmic ray intensity behaviour during the 6-th subinterval (Fig. 1) is of greatest interest. In our stations Mina Aguilar, Buenos Aires and Ellsworth (Ushuaia cannot be taken into account in view of the high statistical fluctuations), a first, very small decrease occurs almost simultaneously with the magnetic storm commencement. Then, intensity rises again for some hours, falling back to a minimum towards midnight. This second decrease is much more pronounced than the first one, and coincides more or less with the decrease in the horizontal component. Considering the reduced amount of data from foreign stations available to us at present time, it is not clear to us whether this splitting up into two decreases is of world-wide character or not.

If we consider the second, bigger decrease as the « true » Forbush decrease, it shows an extremely strong longitude dependence: Ellsworth is about two hours in advance with respect to Mina Aguilar; Rome⁽²⁾ leads 5 hours and Mt. Wellington as much as 12 hours.

This shift in time has to be taken into account in our ΔI vector diagrams. The result is shown in Fig. 10, for the pair of stations Ellsworth and Mina Aguilar; the latter having been delayed two hours with respect to the former. The slope is given by

$$\alpha_{\text{ELLS-MA}} = 2.3 \pm 0.2,$$

which is more or less coincident with the (2.6 ± 0.2) slope corresponding to the general variation at that time (see Fig. 5). α values for other stations are

$$\alpha_{\text{USH-MA}} = 1.3 \pm 0.2,$$

$$\alpha_{\text{MT WELL-MA}} = 1.5 \pm 0.2.$$

These results, together with those of Sect. 2, tell us that the primary variation spectrum acting after the 18th, did not change its form appreciably during the storm of May 24; it merely modulated its amplitude. We insist on the fact that it is not the original variation spectrum, responsible for the first stage of the big storm, which is left untouched by the May 24 storm. Rather, it is the modified spectrum, acting after the 18th, to which a similar variation spectrum is superposed on the 24th. In other words, the relative depression of low energy flux, present after the 18th (Sect. 2) is not removed nor changed during the storm in the 6-th subinterval. The cosmic ray modu-

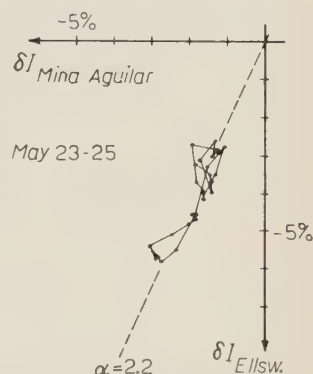


Fig. 10. - Percentage intensity variation diagram for the small Forbush decrease occurring on May 24, for neutron monitors at Ellsworth and Mina Aguilar.

lation mechanism for this storm must be the same, although independently acting, as that responsible for the general recovery during its final stage. This result, if confirmed to be of world-wide character, may be used as a check of different theories for modulation mechanisms which cause cosmic ray Forbush decreases.

Finally, as an alternative, we may advance the hypothesis that what we see during the 6-th interval, is a Forbush decrease starting more or less in coincidence with the sudden commencement of the magnetic storm (0540 UT), and to which an extra flux of primary particles is superposed. This extra flux causes an intensity increase, which lasts $(8 \div 10)$ hours and which is strongly longitude-dependent. Once this flux vanishes, intensity falls back to the corresponding Forbush decrease level.

* * *

We thank II. GHIELMETTI (E.F.I.N.S., Chicago) for valuable informations and Mrs. A. MANZANO and Miss L. LANFRANCO for collaboration in the calculations.

RIASSUNTO (*)

Si analizza l'intensità dei raggi cosmici durante la tempesta magnetica del Maggio 1959, usando i dati dei rivelatori di neutroni e dei telescopi cubici di Mina Aguilar, Buenos Aires, Ushuaia et Ellsworth (Antarctica). Lo spettro di variazione dei primari è stimato secondo un metodo delineato in uno scritto recente ⁽¹⁾. Si analizza dettagliatamente il comportamento dell'intensità durante la ripresa. Si ottengono i seguenti risultati. Lo spettro di variazione di primari, che agisce sino al 18 Maggio, ha una forma approssimata data da $\delta D/D = \delta k(t) \cdot E^{-0.5}$ valida sino ad altissime energie. Verso il 18 questo spettro cambia forma a basse energie (< 3.5 GeV), in modo simile a quanto accadde durante la ripresa dopo la tempesta del luglio 1959. Questo cambiamento può essere interpretato come una rimozione addizionale delle particelle di bassa energia, che si protrasse almeno sino alla fine del mese. Il 14 Maggio la variazione di intensità è spiccatamente peculiare, malgrado che questa fosse una giornata tranquilla dal punto di vista solare e geomagnetico. Si ha un decremento su scala mondiale, con un incremento sovrapposto, durato 10 ore, che è particolarmente alto ad Ellsworth (9% nel rivelatore di neutroni, 2% nel telescopio cubico). Si mostra che Ellsworth era collocato nella zona d'urto 04 per un evento solare simultaneo. Il 24 si ebbe un piccolo decremento Forbush su scala mondiale, associato ad una tempesta magnetica ed un decremento nella componente orizzontale del campo magnetico. Questo decremento di Forbush, che è spiccatamente dipendente dalla latitudine, corrisponde ad uno spettro di variazione dei primari che ha la stessa forma di quello cui è dovuta la ripresa generale in azione al momento, cioè, dopo il cambiamento nelle basse energie del 18.

(*) Traduzione a cura della Redazione.

The Mass of the Λ^0 Hyperon (*).

J. LODGE (**)

Goucher College - Towson, Md.

F. ANDERSON (**), E. B. BRUCKER (**), A. PEVSNER and R. STRAND

The Johns Hopkins University - Baltimore, Md.

(ricevuto il 21 Maggio 1960)

Summary. — The mass of the Λ^0 -hyperon has been measured using nuclear emulsions: $M_{\Lambda} = (1115.55 \pm 0.15) \text{ MeV}$.

1. — Introduction.

The Q -value of the Λ^0 -hyperon decay

$$(1) \quad \Lambda^0 \rightarrow p + \pi^- + Q$$

has been measured in experiments with nuclear emulsions and cloud chambers exposed to cosmic radiation (¹⁻³). Separated negative K-meson beams are now

(*) This work is supported in part by the Office of Scientific Research, A.R.D.C. of the United States Air Force.

(**) Supported in part by the National Science Foundation.

(**) On leave of absence from University College, Dublin.

(**) Now at Duke University, Durham, N.C.

(1) E. R. COHEN, K. M. CROUSE and J. W. M. DUMOND: *Fundamental Constants of Physics* (New York, 1957).

(2) C. D'ANDLAU, R. ARMENTEROS, A. ASTIER, H. C. DESTAEBLER, B. P. GREGORY, L. LEPRINCE-RINGUET, F. MULLER, C. PEYROU and J. H. TINLOT: *Nuovo Cimento*, **6**, 1135 (1957).

(3) M. W. FRIEDLANDER, D. KEEFE, M. G. K. MENON and M. MERLIN: *Phil. Mag.*, **45**, 533 (1954).

available at the large accelerator laboratories. With the large flux of Λ^0 -hyperons from nuclear interactions of these negative K -mesons, it becomes possible to obtain a large sample of decays in nuclear emulsions in which both secondary particles are brought to rest. From range-energy relations precise information on the energy release or Q -value in the reaction (1) can be obtained. The Barkas group has made a nuclear emulsion study of the Λ^0 - Q -value at the Bevatron, using K^- -meson interactions as a source of the hyperons (4). Since there was a wide dispersion in the Q -values obtained in the previous studies, another determination of the Q -value was undertaken in this laboratory.

For the decay (1) the mass of the Λ^0 -hyperon, m_Λ , can be determined by measurements of the energies and momenta of the secondary particles. The appropriate equation is

$$(2) \quad m_\Lambda^2 = m_p^2 + m_\pi^2 + 2U_p U_\pi - 2p_p p_\pi \cos \theta,$$

where U_p , U_π , p_p , p_π , m_p , m_π are the total energies, the momenta, and the masses of the proton and the pion respectively, and θ is the opening angle between the directions of emission of these secondary particles. The pion and proton masses used in the work are $m_\pi = (139.63 \pm 0.006)$ MeV and $m_p = (938.21 \pm .01)$ MeV (1). The Q -value is given by

$$(3) \quad Q = m_\Lambda - m_p - m_\pi.$$

In emulsions the primary measurements are the range of the secondary particles, the projection of the angle between the secondary particle tracks on the plane of the emulsion pellicle and the dip angles of the secondary tracks with respect to the plane of the emulsion pellicle at the point of decay of the Λ^0 . The relationship between range and energy in nuclear emulsion has recently been reviewed by BARKAS (5), and we have used the standard emulsion relationship derived in this work to obtain particle energies from measured ranges by correcting for the density of our emulsion. The procedure used for measuring the emulsion density and the range and angles of the secondary particles will be described below.

2. - Experimental Arrangement.

A stack of Ilford G-5 nuclear emulsion consisting of 125 pellicles, 400 μ m thick, and 4 in. \times 6 in. in area was irradiated in the separated K^- beam of BARKAS and HECKMAN (6) at the Berkeley Bevatron. The beam entered the

(4) W. H. BARKAS: *Padua-Venice Conference* (1957).

(5) W. H. BARKAS: *Nuovo Cimento*, **8**, 201 (1958).

(6) H. H. HECKMAN: *Description and Characteristics of Separated K-beam*, University of California, Bevatron Report 323.

stack perpendicular to the 4 in. \times 6 in. surface and was restricted to an area 2 in. \times 6 in. Since vertical tracks do not impede the scanning of pellicles as much as horizontal tracks, this method of exposure allowed a larger flux than is usual to enter the stack. The total exposure comprised $2 \cdot 10^{14}$ protons on the bevatron target which gave a flux of several hundred K^- -meson tracks per square centimeter.†

3. — Calibration.

There were significant variations in the shrinkage of the pellicles in the stack. During the time span of the experiment these variations were given by a standard deviation of $\pm 2\%$. There was one extreme variation of 8%. At a given time the variation in shrinkage from pellicle to pellicle is given by a standard deviation of $\pm 3\%$. The maximum variation was 13%. The thickness of each pellicle was measured before processing at three locations with a dial gauge accurate to one micron. The standard deviation in the shrinkage at one of these locations as predicted from measurements at the other locations is $\pm 0.25\%$ with an extreme variation of 2%.

The density of the emulsion was determined by two methods. Every seventh pellicle was immersed in carbon tetrachloride and its density was determined from Archimedes' principle. The average density of the emulsion from eighteen determinations was $(3.8347 \pm 0.0084) \text{ g/cm}^3$. This result was consistent with the value determined from the ranges of fourteen protons from sigma plus hyperon decay at rest in the emulsion stack.

The consistency of the density measurements with the dial gauge thickness measurements was checked by measuring the areas of the processed pellicles. The area, the dial gauge thickness, and the weight in air determine the density of the pellicle. The average density from these data agrees with the above value. Conversely, the thickness of a pellicle is determined by its area and density. The thicknesses determined in this way differ from the average dial gauge value by no more than one micron for any pellicle. These internal consistencies give us confidence in our density and thickness measurements.

4. — Scanning and measurements.

The stack was area-scanned in the region where the negative K -mesons came to rest. Despite the intense exposure, the fact that the background tracks entered perpendicular to the emulsion plane made it possible to find

sixty two-prong events where both tracks could be traced to rest in the emulsion and identified as a stopping negative pion and a stopping proton. This paper reports the results of measurements on thirty of these events, of which twenty-five are identified as resulting from the decay of Λ^0 -hyperons.

The ranges of the pions and the protons were measured by several observers using a Koristka R-4 microscope and a Brower scattering microscope. The ranges were divided into straight segments, and the three rectangular components of each segment were measured. These data, together with the known shrinkage, were used to determine the true length of the segment. Errors in the measurement of range due to small angle scattering were minimized by using segments no greater than several hundred microns in length.

The track lengths in individual pellicles were measured at least twice by different observers. These measurements were required to agree to within one micron or to one-half of one percent of the track length in the pellicle whichever was larger. The X -motion screw of the Koristka R 4 microscope was calibrated with a ruled optical diffraction grating.

The projected angles were measured with a Leitz goniometer and a $100\times$ objective. Several independent measurements were made for each projected angle as well as for each dip angle. To measure the dip angle, each track was aligned with the X -motion screw of the Koristka R-4 microscope and was divided into ten cells, each approximately $10\text{ }\mu\text{m}$ long. The vertical co-ordinate and lateral co-ordinate of each cell-end were measured. These co-ordinates were plotted. If these points did not show a vertical scatter, a line was constructed through them. This result and the shrinkage of the pellicle at that time determine the dip angle of the track.

In addition, macroscopic distortion of the emulsion can change the angles of tracks. The distortion coefficient ⁽⁷⁾ was measured at each vertex. Corrections for distortion were negligible except for one case where the projected angle was changed by two degrees.

5. - Results.

A list of the measured ranges, the opening angles, the calculated Λ^0 -masses and their associated statistical errors for the thirty selected events is given in Table I. The statistical error is deduced from the measurement errors on the primary quantities and the errors due to range straggling. A histogram of the Λ^0 -mass values obtained for all thirty events is given in Fig. 1. It should

(7) J. V. MAJOR: *Br. Journ. Appl. Phys.*, **3**, 309 (1952).

TABLE I.

Event number	Measured proton range - μm uncorr.	Measured pion range - μm uncorr.	Opening angle degrees		m_Λ MeV	
A-9	1 559	13 048	$141^\circ 00' \pm 0.6^\circ$		1115.87 ± 0.59	
-234	3 507	19 827	99 51	.7	6.10	.67
-245	582	15 123	153 45	.6	5.71	.60
-435	5 739	11 776	116 41	1.6	5.30	.79
-485	2 241	12 977	132 26	.4	5.98	.58
-486	2 037	10 469	152° 47'	1.3	5.28	.57
-498	6 926	7 676	134 5	.4	5.11	.52
E-1	5 432	8 773	135 45	.4	5.79	.54
-2	1 205	27 769	83 31	.8	4.97	.70
-54	1 262	14 516	136 25	2.1	5.98	.70
-160	555	16 188	141° 52'	.5	5.47	.61
-319	4133	14 836	111 32	.8	5.68	.64
-436	601	14 954	157 19	1.4	5.96	.60
-453	161	17 908	167 15	1.6	5.13	.61
-552	2 291	10 142	146 31	.3	4.55	.56
-591	912	14 983	140° 46'	1.8	5.86	1.06
-656	3 534	8 953	145 52	.8	5.14	.71
M-115	212	36 291	59 33	.6	5.74	.79
-135	534	16.863	133 54	2.5	4.87	1.37
S-227	1 772	19 450	107 40	.5	5.98	.78
-336	371	20 360	122° 34'	.7	5.69	.73
-594	1 810	11 456	155 19	.5	6.31	.61
-643	116	32 897	63 1	.8	4.50	.78
A ₁ S-4	131	23 220	124 23	1.8	6.39	.98
M ₁ S-208	4 719	7 367	156 29	1.7	5.66	.87
E-224	5 937	30 100	114° 37'	1.0	1135.77	.97
-426	955	10 915	130 8	1.2	1109.08	.83
M-114	219	8 806	134 57	1.1	1102.64	.46
S-73	451	31 930	168 25	1.1	1132.97	.88
S-151	13 959	31 093	167 45	1.0	1164.01	1.23

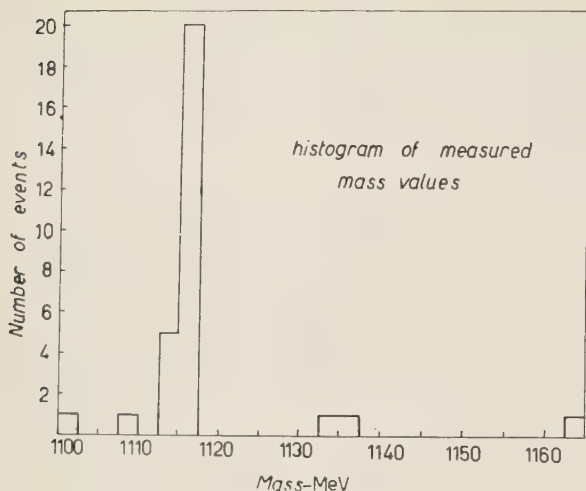


Fig. 1.

be noted that twenty-five of the events are closely grouped together, and the remaining five events are widely dispersed. An ideogram for the Q -value of these twenty-five events is given in Fig. 2.

The weighted mean Q -value for the twenty-five events is

$$Q = (37.71 \pm 0.14) \text{ MeV}.$$

This implies a value for the mass of the Λ^0 -hyperon

$$M_{\Lambda} = (1115.55 \pm 0.15) \text{ MeV}.$$

The quoted error includes now both the statistical errors listed in Table I, which were used to weight the individual Q -values, and a systematic error. The systematic error is derived from uncertainties in the calibration of the emulsion, uncertainties in the masses of the pion and the proton, and the uncertainty in the range energy relation ⁽⁵⁾. The systematic error was calculated for each event. An average systematic error of 0.06 MeV in the Q -value and 0.08 MeV in the mass is combined with the statistical error on the mean of 0.12 MeV to give the final error. It should be noted that the internal standard deviation corresponding to the spread of events in our histogram yields a statistical error of .10 MeV on the mean.

This result is consistent with the recent results of emulsion experiments

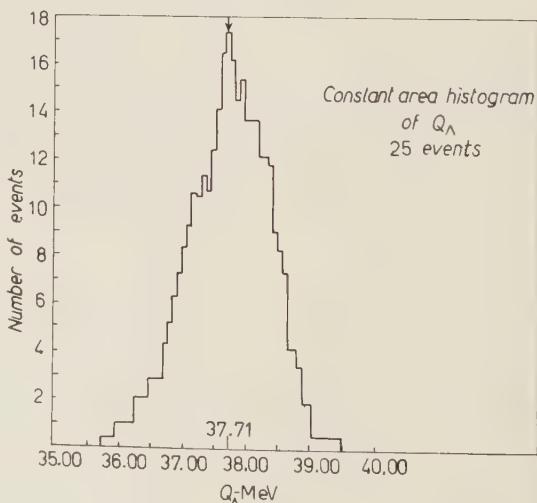


Fig. 2.

using K^- -beams at the Bevatron ^(8,9). The Q -values quoted by these groups are $Q = (37.58 \pm .18)$ MeV ⁽⁸⁾ and $Q = (37.55 \pm .13)$ MeV ⁽⁹⁾ respectively.

* * *

We wish to thank Dr. E. J. LOFGREN and the Bevatron staff for their assistance in making the exposure possible, and Dr. H. H. HECKMAN for his aid in using the K^- -beam. We would also like to thank the scanning group at The Johns Hopkins University, and Miss HELENE PERRY and Mrs. DORIS ELLIS deserve special mention for their help with measurements and calculations.

⁽⁸⁾ J. BOGDANOWICZ, M. DANYSZ, A. FILIPOWSKI, G. MARQUIT, E. SKRZYPCZAK, A. WROBLEWSKI and J. ZAKRZEWSKI: *Nuovo Cimento*, **11**, 727 (1959).

⁽⁹⁾ C. J. MASON, W. H. BARKAS, J. N. DYER, H. H. HECKMAN, N. A. NICKOLS and F. M. M. SMITH: *Bull. Am. Phys. Soc.*, Ser. II, **5**, 224 (1960).

RIASSUNTO (*)

Si è misurata, usando emulsioni nucleari, la massa dell'iperone Λ^0 :

$$M_{\Lambda} = (1115.55 \pm 0.15) \text{ MeV}.$$

(*) Traduzione a cura della Redazione.

$\pi^0 - \pi^-$ Mass Difference as Determined from Double Dalitz Pairs (*).

N. P. SAMIOS (**)

Columbia University - New York, N.Y.

(ricevuto il 6 Giugno 1960)

Summary. — The π^- , π^0 mass difference was determined by measuring the momenta of the two internally converted electron positron pairs from π^0 -decay. A total of 119 events gave a value $m_{\pi^-} - m_{\pi^0} = (4.69 \pm 0.07)$ MeV.

1. — Introduction.

A measurement of the π^0 momentum in the reaction,

$$(A) \quad \pi^- + p \rightarrow n + \pi^0,$$

where π^- mesons are captured at rest, allows a determination of the π^- , π^0 mass difference. Previous values were obtained by either a measurement of the γ -ray energy spectrum from π^0 -decay ^(1,2), the correlation angle of the two γ -rays from the π^0 -decay ^(3,4), or the neutron time of flight ^(5,7). These

(*) Work performed under contract with the United States Atomic Energy Commission.

(**) Now at Brookhaven National Laboratory, Upton, Long Island, New York.

(1) W. K. H. PANOFSKY, R. L. AAMODT and J. HADLEY: *Phys. Rev.*, **81**, 565 (1951).

(2) J. KUEHNER, A. W. MERRISON and S. TORNABENE: *Proc. Phys. Soc. (London)*, to be published.

(3) W. CHINOWSKY and J. STEINBERGER: *Phys. Rev.*, **93**, 586 (1954).

(4) J. M. CASSELS, D. P. JONES, P. G. MURPHY and P. L. O'NEIL: *Proc. Phys. Soc. (London)*, **74**, 92 (1959).

(5) M. GETTNER, L. HOLLOWAY, D. KRAUS, K. LANDÉ, E. LEBOY and W. SELOVE: *Phys. Rev. Lett.*, **2**, 471 (1959).

(6) P. HILLMAN, W. C. MIDDLEKOPP, T. KAMOGATA and E. ZAVATTINI: *Nuovo Cimento*, **14**, 887 (1959).

(7) R. P. HADDOCK, A. ABASHIAN, K. M. CROWE and J. B. CZIRR: *Phys. Rev. Lett.*, **3**, 478 (1959).

results are shown in Table I. This is a report of a determination of the π^0 momentum, and thereby the mass difference, by measuring the momentum of

TABLE I. - *List of previous measurements of π^- , π^0 mass difference.*

Experimenter	Mass difference
PANOFSKY <i>et al.</i>	5.42 ± 1.02
CHINOWSKY and STEINBERGER . .	4.50 ± 0.31
CASELS <i>et al.</i>	4.55 ± 0.07
MERRISON <i>et al.</i>	$4.55^{+0.20}_{-0.15}$
SELOVE <i>et al.</i>	4.91 ± 0.26
HILLMAN <i>et al.</i>	4.60 ± 0.04
CROWE <i>et al.</i>	4.60 ± 0.01
SAMIOS	4.69 ± 0.07

the two internally converted electron-positron pairs (*i.e.* Dalitz pairs) from the π^0 -decay.

2. - Experimental details.

π^- -mesons from the Nevis Cyclotron were slowed down by polyethylene absorber and made to stop in a hydrogen bubble chamber, 12 in. in diameter and 6 in. in depth, placed in a 5.5 kG magnetic field. A total of 725 000 pictures were taken with $\sim 15 \pi^-$ stoppings per picture. The expected branching ratio R_{π^0} where

$$R_{\pi^0} = \frac{\pi^0 \rightarrow e^+ + e^- + e^+ + e^-}{\pi^0 \rightarrow 2\gamma}$$

is 1/30 000, as calculated by KROLL and WADA ⁽⁸⁾. On this basis, the number of events expected is of the order

$$N \approx \frac{7.25 \cdot 10^5 \cdot 15}{3 \cdot 10^4} \cdot \frac{1.62}{2.62} = 218$$

(assuming a Panofsky ratio of 1.62) ⁽⁹⁾. 205 events, where both pairs converted, were actually observed. Of these, 119 had all four tracks clearly de-

⁽⁸⁾ N. KROLL and W. WADA: *Phys. Rev.*, **98**, 1355 (1955).
⁽⁹⁾ N. P. SAMIOS: *Phys. Rev. Lett.*, **4**, 470 (1960).

finer and of sufficient length for adequate measurement. One of these events is shown in Fig. 1.

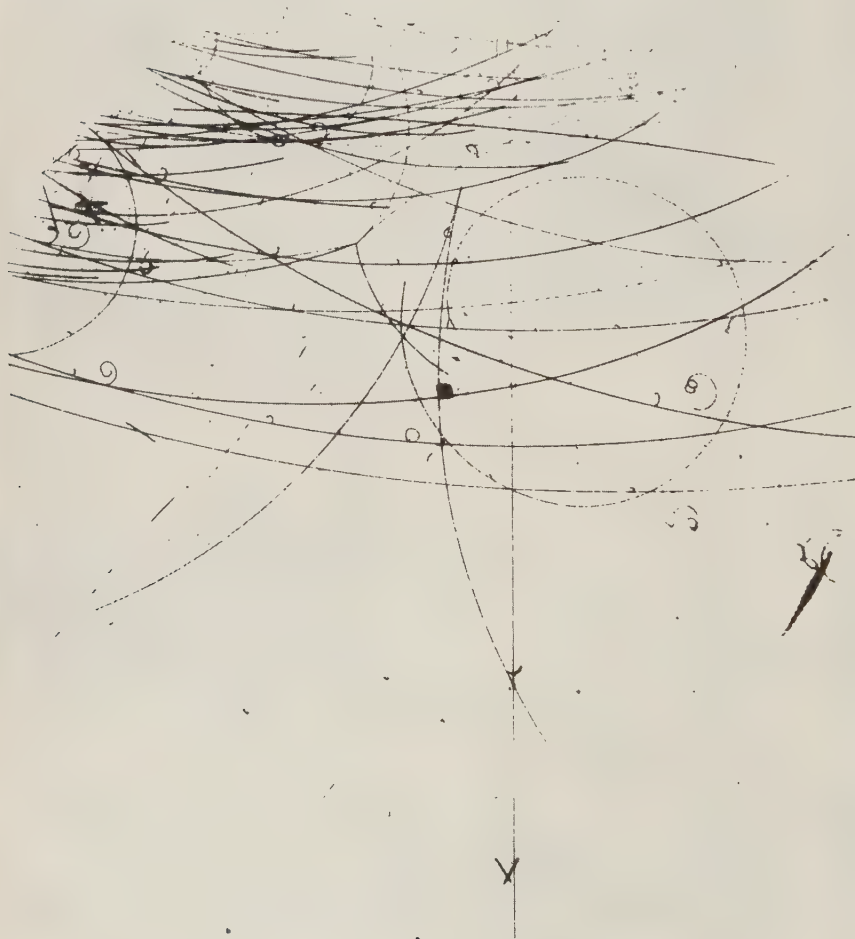


Fig. 1. - Picture of a π^0 which decays into two internally converted electron positron pairs.

3. - Measurements.

Each of the 119 events was measured a minimum of five times on a digitized measuring table. The momentum and direction cosines of each track

was then calculated. The momentum was corrected for ionization loss, 0.219 MeV/c/cm and radiation loss (0.000815 p) MeV/c/cm. The ionization loss was determined by measuring electrons which spiraled many times and then stopped in the chamber. This was done for electrons where $p \leq 26$ MeV/c, and has been shown by Dr. AGNES LECOURTOIS that this loss is constant to 2% for $p > 10$ MeV/c. The radiation correction was calculated using a radiation length of 72.5 g/cm². The magnetic field was measured by a proton resonance and flip coil and fitted by an expression constrained by Maxwell's equations. The change in field from center to the edge of the chamber was of the order of 4% and its variation throughout the run was $\pm 2\%$. A multiple scattering error was also calculated for each track, given by

$$\frac{\Delta P}{P} = \frac{0.29}{\beta \cos \alpha \sqrt{l}},$$

where: α = dip angle,

l = length of track in cm,

$\beta = v/c = 1.0$.

A net momentum error composed of a measurement error, as determined by the multiple independent measurements, and the multiple scattering error as indicated above was calculated by taking these two errors in quadrature. Errors for the direction cosines were also determined from the repeated measurements of each event.

4. - Analysis.

From energy considerations in reaction (A), one can deduce the following:

$$m_{\pi^-} - m_{\pi^0} = (m_n - m_p) + T_{\pi^0} + T_n,$$

where: T_n = neutron kinetic energy,

T_{π^0} = π^0 kinetic energy,

m 's are the respective masses.

Since the π^0 and neutron are non-relativistic, the kinetic energies can be written as follows (dropping terms less than 0.001 MeV):

$$T_{\pi^0} = \frac{P_{\pi^0}^2}{2m_{\pi^0}} - \frac{P_{\pi^0}^4}{8m_{\pi^0}^3}, \quad T_n = \frac{P_n^2}{2m_n}$$

and errors

$$\Delta T_n = \frac{\Delta(P_n^2)}{2m_n}, \quad \Delta T_{\pi^0} = \frac{\Delta(P_{\pi^0}^2)}{2m_{\pi^0}},$$

with $P_{\pi^0} = P_n$ since the reaction occurs at rest.

In calculating $P_{\pi^0}^2$, the sum of the electron-positron energies was normalized to 137.9 MeV, each track weighted by its momentum error, in order to eliminate the effect of magnetic field drift. This corresponds to the value expected for the π^0 energy using a π^0 mass deduced from the result of CASSELS *et al.* ⁽⁴⁾, $m_{\pi^-} - m_{\pi^0} = 4.55$ MeV. The value for $P_{\pi^0}^2$ for any event was insensitive to this normalization value, changing by $\sim 0.2\%$ for a 1 MeV change in this constant. From the measured quantities, one can calculate $P_{\pi^0}^2$ as a function of 12 independent variables; these being the scalar momentum and two direction cosines for each track (one of the direction cosines being eliminated since the sum of their squares must be equal to 1). Therefore:

$$P_{\pi^0}^2 = f(P_i, \hat{r}_i) \quad i = 1, 2, 3, 4$$

$$\hat{r}_{ix}^2 + \hat{r}_{iy}^2 + \hat{r}_{iz}^2 = 1$$

the error on $P_{\pi^0}^2$ being

$$\Delta(P_{\pi^0}^2) = \sqrt{\sum_i \left(\frac{\partial f}{\partial x_i} \right)^2 (\delta x_i)^2}, \quad x_i = i\text{-th independent variable.}$$

The main contribution to the error came from the uncertainty in the scalar momentum of the tracks, the average uncertainty in P^2 being of the order of 30% per event. The number of events expected to occur in flight in the total sample of 205 events can be calculated from the cross-section for low energy charge exchange scattering. At these low energies $\sigma(\pi^- + p \rightarrow \pi^0 + n)$ is of the order of 5 mb ⁽¹⁰⁾, which would yield one event in flight in the total exposure. Two have been observed. The contamination from events in flight is therefore negligible. Furthermore, the binding energy of the lowest state of the π^- proton system is of the order of 3 keV which can be neglected with respect to the measurement accuracy of this experiment.

5. - Results.

Each of the 119 events was normalized in the prescribed manner, and the square of the π^0 momentum and its error computed on an IBM 650. Each

⁽¹⁰⁾ H. A. BETHE, F. DE HOFFMANN and S. S. SCHWEBER: *Mesons and Fields* (Evanston, Ill., 1955).

of the events was then weighted by $1/(\% \text{ error})^2$ in order to obtain the best value, $P_{\pi^0}^2 = (809.380 \pm 18.454) (\text{MeV}/c)^2$. Fig. 2 is a plot of the distribution

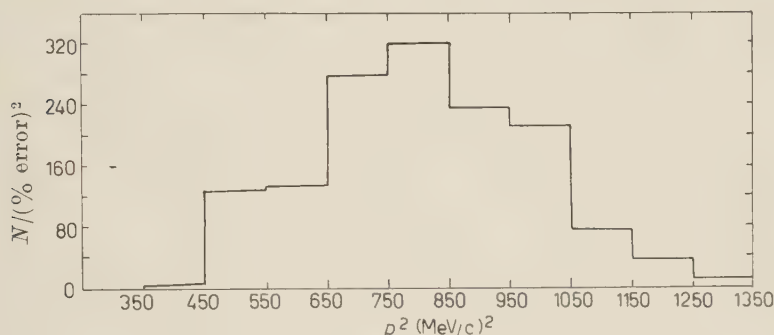


Fig. 2. - Plot of P^2 versus $N/(\% \text{ error})^2$ for the 119 events.

of these events with their proper weighting as a function of p^2 . This yields a mass difference

$$m_{\pi^-} - m_{\pi^0} = (4.69 \pm 0.07) \text{ MeV} .$$

in agreement with all the previous measurements.

* * *

I wish to thank the Columbia Bubble Chamber Group for aid in taking the pictures and for some useful discussions; Mr. DON BURD for programming the IBM 650; and the crew of scanners IRENE GARDER, DINA GOURSKY, JOHN IMPEDUGLIA, HANK MARGOSIAN, ALEX RYTOW, GAILI KANELETZ, ALEXIS WOSKRY, DON McCURE, and DAVE MAUK for their painstaking work in finding these events. Finally, I wish to acknowledge the help of Dr. ALBERT PRODELL who collaborated on the early phases of this work.

RIASSUNTO (*)

La differenza di massa π^- , π^0 è stata determinata misurando gli impulsi di due coppie elettrone positrone convertite internamente da decadimento π^0 . Un totale di 119 eventi diede un valore $m_{\pi^-} - m_{\pi^0} = (4.69 \pm 0.07) \text{ MeV}$.

(*) Traduzione a cura della Redazione.

Photoproduction of Pions on Kaons.

J. DUFOUR

Faculté des Sciences - Bordeaux ()*

M. GOURDIN

*Faculté des Sciences - Orsay (**) and Faculté des Sciences - Bordeaux*

J. TROTIN

Faculté des Sciences - Bordeaux

(ricevuto il 7 Giugno 1960)

Resumé. — On se propose, dans cet article, de traiter, par la technique de Mandelstam, la photoproduction des mésons π sur les mésons K, nécessaire à l'étude de la photoproduction des mésons K sur les nucléons. En se restreignant aux états intermédiaires de plus basses masses et en ne retenant que la transition dipolaire magnétique, on obtient pour les deux amplitudes dues à la partie isovectorielle du courant électromagnétique deux équations intégrales couplées de Mushkelishvili-Omnès et pour l'amplitude due à la partie isoscalaire une équation du même type. Celles-ci se réduisent à des équations intégrales de Fredholm. La connaissance des solutions approchées pour la photoproduction des mésons π sur les mésons π et des déphasages P de la diffusion méson π -méson K permettra de les résoudre numériquement. Ces derniers calculs seront donnés ultérieurement.

(*) Postal address: Service de Physique Théorique, Chemin Brunet, Talence, Gironde

(**) Postal address: Laboratoire de Physique Théorique et Hautes Energies, B.P. 12 Orsay, Seine et Oise.

1. - Introduction.

1'1. - In order to study the photoproduction of K-mesons on nucleons, we have to consider the following graph:

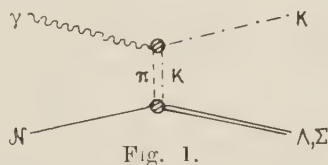


Fig. 1.

Application of the unitarity condition for the S -matrix leads us to consider two transition amplitudes:

- a) Photoproduction of π mesons on K-mesons $\gamma + K \rightarrow \pi + K$.
- b) Production of an hyperon anti-nucleon pair, simply related to the associated production amplitude of strange particles ⁽¹⁾.

The object of this paper is to study the first amplitude by using the Mandelstam technique of integral representation for the reaction amplitude ⁽²⁾.

1'2. - We assume the same parity for K^+ and K^0 or for K^- and \bar{K}^0 ⁽³⁾. The K-mesons are an isospin doublet as the nucleons. Consequently, the vertex $\pi K K$ is forbidden by parity conservation and there exist no Born terms in this problem.

We only consider three graphs, in the approximation of the lowest mass intermediate states.

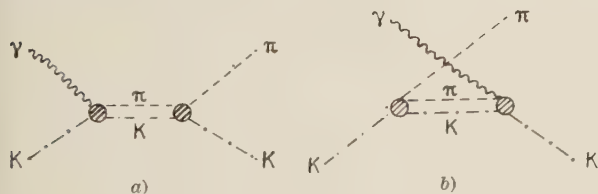


Fig. 2. - Photoproduction graphs.

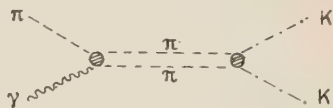


Fig. 3. - $K\bar{K}$ pair production graph.

1'3. - The problem of photoproduction of π -mesons on K-mesons is also interesting in the sense in which it possesses the isospin characteristics of the corresponding problem on nucleons. Except the Born contributions, we have

⁽¹⁾ M. GOURDIN and M. RIMPAULT: *Production associée de particules étranges* (Bordeaux, 1959, PTB-2).

⁽²⁾ S. MANDELSTAM: *Phys. Rev.*, **112**, 1344 (1958).

⁽³⁾ A. PAIS: *Phys. Rev.*, **112**, 624 (1958).

the same graphs to consider. The electromagnetic current has the two isoscalar and isovector aspects.

Because of parity conservation we have only magnetic multipoles. For the graph 2-*a* and its crossed 2-*b*, the unitarity condition has the well known form: for an isospin eigenstate I , the phase of the multipole transition amplitude J is the phase of the π -K scattering amplitude corresponding to the same I and the same J ⁽⁴⁾. The determination of the π -K scattering amplitude is in progress ⁽⁵⁾ and numerical solutions will be shortly given.

The graph 3 is entirely known from magnetic multipole amplitude for photoproduction of pions on pions ⁽⁶⁾ and from the $K\bar{K}$ pair production by two π -mesons ⁽⁵⁾. In this diagram the isoscalar part of the electromagnetic current only occurs and only one amplitude is affected by this graph.

We then obtain, in the photoproduction channel, Mushkelishvili-Onnès integral equations, coupled by isospin, which we can reduce, after introduction of a left hand cut, to Fredholm type integral equations as in the simpler case of photoproduction of pions on pions ⁽⁶⁾. The knowledge of the π -K phase shifts permits, in principle to solve numerically these equations.

1.4. — In the two appendices, we have computed the left hand cuts in the complex plane of the variable W^2 —the square of the total energy in the center of mass system for the photoproduction channel—due to:

- a) The crossed photoproduction graph 2-*b*,
- b) The $K\bar{K}$ pair production graph 3.

These cuts can be complex and this is a general feature when more than two different masses are involved in the problem. In particular this circumstance does not appear in all scattering problems.

2. — Invariance properties.

2.1. — Let us call the ingoing four momenta for the photon k , for the π -meson q and for the K-mesons p_1 and p_2 .

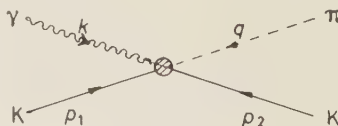


Fig. 4.

⁽⁴⁾ M. GELL-MANN and K. M. WATSON: *Annual Review of Nuclear Science*, 4 (1954).

⁽⁵⁾ M. GOURDIN, Y. NOHROT and PH. SALIN: *Diffusion meson π -meson K* (Bordeaux, 1959, PTB-1), and *Pion-Kaon scattering* (to be published).

⁽⁶⁾ M. GOURDIN and A. MARTIN: *Nuovo Cimento*, 16, 78 (1960).

⁽⁷⁾ G. CHEW, F. LOW, M. GOLDBERGER and Y. NAMBU: *Phys. Rev.*, 106, 345 (1957).

We define three scalar quantities

$$s_1 = -(k + p_1)^2, \quad s_2 = -(k + p_2)^2, \quad t = -(p_1 + p_2)^2,$$

with, on the mass shell, the relation

$$s_1 + s_2 + t = \mu^2 + 2\kappa^2,$$

where μ is the π -meson mass and κ the K-mesons mass.

We consider three channels:

Channel I photoproduction of π -meson $(k) + (p_1) \rightarrow (-q) + (-p_2)$

Channel II photoproduction of π -meson $(k) + (p_2) \rightarrow (-q) + (-p_1)$

Channel III $K\bar{K}$ pair production $(k) + (q) \rightarrow (-p_1) + (-p_2)$.

The general S -matrix element is written in the form

$$(1) \quad S_{fi} = \delta_{fi} + i(2\pi)^4 \delta_4(k + q + p_1 + p_2) \frac{1}{(2\pi)^6} \frac{1}{4(p_1^0 p_2^0 k^0 q^0)^{\frac{1}{2}}} T_{fi}.$$

2.2. - The problem of the isospin dependence of T is the same as for the photoproduction of π -mesons on nucleons. We can define three invariant quantities (7)

$$\mathcal{F}_\alpha^{(0)} = \delta_{3\alpha}, \quad \mathcal{F}_\alpha^{(1)} = \frac{1}{2} [\tau_\alpha, \tau_3], \quad \mathcal{F}_\alpha^{(2)} = \tau_\alpha$$

for the photoproduction of a π -meson in the isospin state α . The invariants $\mathcal{F}_\alpha^{(0)}$ and $\mathcal{F}_\alpha^{(1)}$ correspond to the isovector part of the electromagnetic current and $\mathcal{F}_\alpha^{(2)}$ to the isoscalar part. We can put

$$T_\alpha = \sum_{s=0}^{s=2} \mathcal{F}_\alpha^{(s)} M^{(s)}.$$

The three functions $M^{(s)}$ are now independent of the isospin.

In the channels I and II the total isospin can be $\frac{1}{2}$ and $\frac{3}{2}$. It is well known that the isoscalar part $M^{(2)}$ contains only $I = \frac{1}{2}$ and for the isovector part the eigenstates for the isospin are

$$(2) \quad M^{(\frac{1}{2})} = M^{(0)} + 2M^{(1)}, \quad M^{(\frac{3}{2})} = M^{(0)} - M^{(1)}.$$

In the channel III, the total isospin is $I = 0$ and $I = 1$. It is easy to see that $M^{(0)}$ is a pure state $I = 0$ state, $M^{(1)}$ a pure $I = 1$ state and $M^{(2)}$ a pure $I = 1$ state.

2.3. - From Lorentz and gauge invariance, if we retain only a first order electromagnetic interaction, we can write $M^{(s)}$ in the following form

$$(3) \quad M^{(s)} = \frac{1}{2i} \varepsilon_{\lambda\mu\nu\rho} e_\lambda q^\mu p_1^\nu p_2^\rho U^{(s)}(s_1 s_2 t),$$

where e_λ is the polarization vector for the photon and the $U^{(s)}$ three scalar functions of s_1 , s_2 and t .

2.4. - We then can cross the two K-meson lines and this is equivalent to the transformation: $s_1 \leftrightarrow s_2$, $t \leftrightarrow t$ with hermitic conjugation of operators. It follows immediately for the scalar functions simple symmetry properties

$$(4) \quad \begin{cases} U^{(0)}(s_2, s_1, t) = U^{(0)}(s_1, s_2, t), \\ U^{(1)}(s_2, s_1, t) = -U^{(1)}(s_1, s_2, t), \\ U^{(2)}(s_2, s_1, t) = U^{(2)}(s_1, s_2, t). \end{cases}$$

2.5. *Channel I.* - In the center of mass system, the four momenta are defined as follows

$$k = (\mathbf{k}, k), \quad q = (-\mathbf{q}, -\omega_q), \quad p_1 = (-\mathbf{k}, e_k), \quad e_2 = (\mathbf{q}, -e_q),$$

with

$$\omega_q = \sqrt{\mathbf{q}^2 + \mu^2}, \quad e_q = \sqrt{\mathbf{q}^2 + \kappa^2}.$$

Let us call θ the angle between \mathbf{k} and \mathbf{q} , the scalar invariants will be

$$(5) \quad \begin{cases} s_1 = (k + e_k)^2 = (\omega_q + e_q)^2 = W^2, \\ s_2 = (k - e_q)^2 - (\mathbf{k} + \mathbf{q})^2 = \kappa^2 - 2ke_q - 2kq \cos \theta, \\ t = (e_k - e_q)^2 - (\mathbf{k} - \mathbf{q})^2 = 2\kappa^2 - 2e_k e_q + 2kq \cos \theta. \end{cases}$$

With the gauge $e_4 = 0$ and $\mathbf{e} \cdot \mathbf{k} = 0$, the $M^{(s)}$ amplitudes, that we call $C^{(s)}(\mathbf{e}; W, \cos \theta)$, can be written

$$(6) \quad C^{(s)}(\mathbf{e}; W, \cos \theta) = \frac{W}{2} (\mathbf{e}, \mathbf{k}, \mathbf{q}) V^{(s)}(W, \cos \theta).$$

Because of parity conservation, only magnetic multipole radiations occur. We can expand the $V^{(s)}$ amplitudes in multipoles by (*)

$$(7) \quad C^{(s)}(\mathbf{e}; W, \cos \theta) = \frac{kqW}{2} \sum_J C_J^{(s)}(W) i \mathbf{e} \cdot \mathbf{l}_k P_J(\cos \theta_{qk}),$$

(*) R. STORA: private communication.

where \mathbf{l}_k is the incident angular momentum operator defined by $\mathbf{l}_k = (1/i)\mathbf{k} \times \nabla_k$; if this gradient acts on $P_J(\cos \theta_{kq})$ one obtains

$$(8) \quad C^{(s)}(\mathbf{e}; W, \cos \theta) = \frac{W}{2} (\mathbf{e}, \mathbf{k}, \mathbf{q}) \sum_j C_j^{(s)}(W) P'_j(\cos \theta_{kq}) .$$

In order to calculate the reciprocal relation one uses the following relation for the photon polarization

$$\sum_{\epsilon} (\mathbf{e} \cdot \mathbf{l}_k)^2 = J(J+1)$$

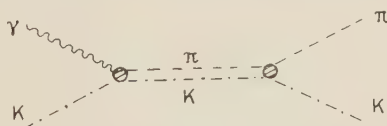
and one deduces the amplitude $C_j^{(s)}(W)$:

$$(9) \quad C_j^{(s)}(W) = \frac{2J+1}{4\pi} \frac{1}{J(J+1)} \frac{2}{kqW} \sum_{\epsilon} \int d\Omega_q P_J(\cos \theta_{kq}) (-i\mathbf{e} \cdot \mathbf{l}_k) C^{(s)}(\mathbf{e}; W, \cos \theta) .$$

This expression can be easily transformed with equation (6); after summation over the polarizations, the multipole amplitude is given by

$$(10) \quad C_j^{(s)}(W) = \frac{2J+1}{2J(J+1)} \int_{-1}^{+1} (1-x^2) P'_j(x) V^{(s)}(W, x) dx .$$

The unitarity condition, for the S -matrix has a simple expression if we retain only, as intermediate states, the $\pi+K$ states. Under this assumption, the multipole of order J , in the isospin state I ($I=\frac{1}{2}, \frac{3}{2}$) has the same phase, $\bar{\delta}_J^{(I)}$ as the corresponding π - K scattering amplitude (Fig. 2).



If $C_j^{(\frac{1}{2})}$ and $C_j^{(\frac{3}{2})}$ are related to $C_j^{(0)}$ and $C_j^{(1)}$ by the relation (2), we have

$$(11) \quad \begin{cases} \text{Im } C_j^{(\frac{1}{2})}(W) = C_j^{(\frac{1}{2})}(W) \exp [-i\bar{\delta}_j^{(\frac{1}{2})}] \sin \bar{\delta}_j^{(\frac{1}{2})} , \\ \text{Im } C_j^{(\frac{3}{2})}(W) = C_j^{(\frac{3}{2})}(W) \exp [-i\bar{\delta}_j^{(\frac{3}{2})}] \sin \bar{\delta}_j^{(\frac{3}{2})} , \\ \text{Im } C_j^{(2)}(W) = C_j^{(2)}(W) \exp [-i\bar{\delta}_j^{(2)}] \sin \bar{\delta}_j^{(2)} . \end{cases}$$

2.6. Channel III. — If \mathbf{K} and \mathbf{p} are the relative momenta in the center of mass system

$$k = (\mathbf{K}, K), \quad q = (-\mathbf{K}, \omega_K), \quad p_1 = (-\mathbf{p}, -e_p), \quad p_2 = (\mathbf{p}, -e_p),$$

we have for the scalar invariants the expressions

$$(12) \quad \begin{cases} s_1 = \kappa^2 - 2K e_p - 2K p \cos \Phi, \\ s_2 = \kappa^2 - 2K e_p + 2K p \cos \Phi, \\ t = 4(p^2 + \kappa^2) = (K + \omega_K)^2, \end{cases}$$

where Φ is the angle between \mathbf{K} and \mathbf{p} .

We choose the gauge $e_4 = 0$, $\mathbf{e} \cdot \mathbf{K} = 0$ and we call the $M^{(s)}$ amplitudes $D^{(s)}(\mathbf{e}; t, \cos \Phi)$. From equation (3) we have

$$(13) \quad D^{(s)}(\mathbf{e}; t, \cos \Phi) = e_\nu(\mathbf{e}, \mathbf{K}, \mathbf{p}) S^{(s)}(t, \cos \Phi).$$

With the same technique used in channel I, we expand $D^{(s)}(\mathbf{e}; t, \cos \Phi)$ in magnetic multipole amplitudes

$$(14) \quad D^{(s)}(\mathbf{e}; t, \cos \Phi) = K p e_\nu \sum_J D_J^{(s)}(t) i \mathbf{e} \cdot \mathbf{l}_K P_J(\cos \Phi_{Kp}).$$

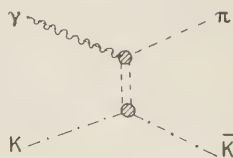
By inversion, the function $D_J^{(s)}(t)$ is given by

$$(15) \quad D_J^{(s)}(t) = \frac{2J+1}{2J(J+1)} \int_{-1}^{+1} (1-y^2) P_J'(y) S^{(s)}(t, y) dy.$$

We study now the unitarity condition. Let us first consider intermediate states containing only pions. Because of parity conservation, we must have an even number of pions and consequently, such intermediate states proceed from the isoscalar part of the electromagnetic current and affect only the $D^{(2)}$ amplitude. For the other two, the intermediate state of lower mass is a KK state and we neglect this.

It is easy to see that the imaginary part of the multipole J is proportional to the partial amplitude $F_J^{(1)}(t)$ corresponding to the $K\bar{K}$ pair production from two pions⁽⁵⁾ and to the multipole of order J , $B_J(t)$, describing the photo-production of pions on pions^(6,8). We obtain (Fig. 3)

$$(16) \quad \text{Im } D_J^{(2)}(t) = \frac{1}{16\pi} \frac{q^2}{p e_p} B_J(t) F_J^{(1)*}(t).$$



(8) M. GOURDIN: *Lectures given in Corsica Summer School (1960)*.

From the unitarity condition, the phase of $B_J(t)$ and $F_J^{(1)*}(t)$ is the pion-pion phase shift $\delta_J^{(1)}(t)$. The function $\text{Im } D_J^{(2)}(t)$ is real as expected.

3. — Mandelstam representation.

3'1. — In the following, we restrict ourselves to magnetic dipole contribution only.

We assume, for the three scalar functions $U^{(0)}$, $U^{(1)}$, $U^{(2)}$, a Mandelstam representation ⁽²⁾. Because of the pseudoscalar character of the π -meson, the three pion vertex is forbidden and the Cini-Fubini method of reduction to unidimensional spectral representation can be applied ⁽⁹⁾. We can write

$$(17) \quad U^{(s)}(s_1, s_2, t) = f^{(s)}(s_1, Z_1) + (-1)^s f^{(s)}(s_2, Z_2) + g^{(s)}(t, Y),$$

where we take for Z_1 , Z_2 , Y the cosine of the reaction angle in the center of mass system respectively for the channels I, II and III. We can expand the functions $f^{(s)}$ and $g^{(s)}$ in Legendre polynomials of Z and Y . For magnetic dipoles we only retain the first term of such a development

$$(18) \quad U^{(s)}(s_1, s_2, t) = \frac{1}{\pi} \int_{(\mu+\kappa)^2}^{\infty} \sigma^{(s)}(x) dx \left[\frac{1}{x - s_1 - i\varepsilon} + (-1)^s \frac{1}{x - s_2 - i\varepsilon} \right] + \frac{1}{\pi} \int_{(2\mu)^2}^{\infty} \frac{\tau^{(s)}(t') dt'}{t' - t - i\varepsilon},$$

3'2. — In order to determine the weight functions $\tau^{(s)}(t)$ we apply the unitarity condition in the channel III. From results given in the previous section, we have

$$\tau^{(s)}(t) = \text{Im } D_1^{(s)}(t).$$

It follows that

$$\tau^{(0)}(t) = \tau^{(1)}(t) = 0$$

and

$$(19) \quad \tau^{(2)}(t) = \frac{1}{16\pi} \frac{q^2}{p e_p} B_1(t) F_1^{(1)*}(t),$$

with $t = 4(q^2 + \mu^2) = 4(p^2 + \kappa^2)$.

We have already determined the function $B_1(t)$ ⁽⁶⁾ ⁽⁸⁾,

$$B_1(t) = \frac{e\mathcal{A}}{\mu^3} \exp [\varrho_1^{(1)}(t) + i\delta_1^{(1)}(t)] \Phi(t)$$

⁽⁹⁾ M. CINI and S. FUBINI: *Ann. of Phys.*, **3**, 352 (1960).

and an approximate solution for $F_1^{(1)}(t)$ ⁽⁵⁾,

$$F_1^{(1)}(t) = \lambda \exp [\varrho_1(t) + i \delta_1^{(1)}(t)] .$$

This gives for $\tau^{(2)}(t)$ the form

$$\tau^{(2)}(t) \simeq \frac{1}{16\pi} \frac{t - 4\mu^2}{4p e_p} \left(\frac{eA}{\mu^3} \lambda \right) \exp [2\varrho_1^{(1)}(t)] \Phi(t) .$$

To describe the contributions from the graph represented in Fig. 3 to the photoproduction of pions on kaons, we introduce the real function

$$(20) \quad b(t) = \frac{1}{16\pi} \int_{(2\mu)^2}^{\infty} \frac{(t' - 4\mu^2) B_1(t) F_1^{1*}(t')}{4p' e_{p'} (t' - t)} dt' ,$$

where t is a function of W and $\cos \theta$ as given in equation (5).

3.3. Amplitudes due to the isovector part of the electromagnetic current. — We extract, in channel I, the dipole amplitude $C_1^{(1)}(W)$ following equation (10):

$$(21) \quad C_1^{(1)}(W) = \frac{1}{\pi} \int_{(\kappa + \mu)^2}^{\infty} \frac{\sigma^{(1)}(W'^2) dW'^2}{W'^2 - W^2 - i\varepsilon} + \frac{3}{4\pi} \int_{-1}^{+1} \sin^2 \theta d \cos \theta \left[\int_{(\kappa + \mu)^2}^{\infty} \frac{\bar{\sigma}^{(1)}(s') ds'}{s' - s_2} \right] .$$

The weight functions $\sigma^{(1)}(s)$ and $\bar{\sigma}^{(1)}(s)$ are known by unitarity condition (10):

$$(22) \quad \sigma^{(1)}(W^2) = \text{Im } C_1^{(1)}(W) = C_1^{(1)}(W) \exp [-i \bar{\delta}_1^{(1)}(W)] \sin \bar{\delta}_1^{(1)}(W) ,$$

where $\bar{\delta}_1^{(1)}(W)$ is the $J=1$, $I=\frac{1}{2}$, $\frac{3}{2}$ pion-kaon phase shift. By crossing, we have ⁽⁵⁾

$$(23) \quad \begin{cases} \bar{\sigma}^{\frac{1}{2}}(s) = \frac{4}{3} \sigma^{\frac{3}{2}}(s) - \frac{1}{3} \sigma^{\frac{1}{2}}(s) \\ \bar{\sigma}^{\frac{3}{2}}(s) = \frac{1}{3} \sigma^{\frac{3}{2}}(s) + \frac{2}{3} \sigma^{\frac{1}{2}}(s) . \end{cases}$$

For the second integral of equations (21) we can define a left hand cut (see Appendix I). We put

$$(24) \quad \frac{3}{4\pi} \int_{-1}^{+1} \sin^2 \theta d \cos \theta \frac{1}{s' - s_2} = \frac{1}{\pi} \int_{L_1(s')} \frac{E(s', z)}{W^2 - z} dz ,$$

where the function $E(s', z)$ —essentially the Jacobian of the change of variable—and the cut $L_1(s')$ are defined in Appendix I.

With equations (22), (23) and the left hand cut (24) we obtain for $C_1^{(\frac{1}{2})}(W)$ and $C_1^{(\frac{3}{2})}(W)$ a system of coupled Mushkelishvili-Onnès integral equations:

$$(25) \quad C_1^{(I)}(W) = \frac{1}{\pi} \int_{(\kappa+\mu)^2}^{\infty} \frac{C_1^{(I)}(W') \exp[-i\bar{\delta}_1^{(I)}(W')] \sin \bar{\delta}_1^{(I)}(W')}{W'^2 - W^2 - i\epsilon} dW'^2 + \\ + \frac{1}{\pi} \int_{(\kappa+\mu)^2}^{\infty} \bar{\sigma}^{(I)}(s') ds' \int_{L_1(s')} \frac{E(s', z)}{W^2 - z} dz.$$

The general solution of (25) is well known

$$(26) \quad C_1^{(I)}(W) = \exp[\bar{\varrho}_1^{(I)}(W) + i\bar{\delta}_1^{(I)}(W)] \left[\Phi_1^{(I)}[W^2 - (\kappa + \mu)^2] + \right. \\ \left. + \sum_{I'=\frac{1}{2}, \frac{3}{2}} \lambda_{(I')}^{(I)} \int_{(\kappa+\mu)^2}^{\infty} N^{(I')}(W^2, W'^2) \exp[i\bar{\delta}_1^{(I')}(W')] \sin \bar{\delta}_1^{(I')}(W') C_1^{(I')}(W') dW'^2 \right].$$

The kernel $N^{(I)}(W^2, W'^2)$ is an integral defined on the left hand cut,

$$(27) \quad N^{(I)}(W^2, W'^2) = \frac{1}{\pi} \int_{L_1(W'^2)} \frac{E(W'^2, z) \exp[-\bar{\varrho}_1^{(I)}(z)]}{W^2 - z} dz,$$

and $\Phi_1^{(I)}[W^2 - (\kappa + \mu)^2]$ corresponds to the solutions of the associated homogeneous integral equations and consequently depends of the asymptotic behaviour of the π -K phase shifts $\bar{\delta}_{(1)}^{(I)}(W)$ ⁽¹⁰⁾.

The coefficients $\lambda_{(I')}^{(I)}$ are given by crossing properties and equations (2):

$$\lambda_{(\frac{1}{2})}^{(\frac{1}{2})} = -\frac{1}{3}, \quad \lambda_{(\frac{3}{2})}^{(\frac{1}{2})} = \frac{4}{3}, \quad \lambda_{(\frac{3}{2})}^{(\frac{3}{2})} = \frac{2}{3}, \quad \lambda_{(\frac{1}{2})}^{(\frac{3}{2})} = \frac{1}{3}.$$

With the trivial change of function

$$(28) \quad C_1^{(I)}(W) = \exp[\varrho_1^{(I)}(W) + i\delta_1^{(I)}(W)] \Psi_1^{(I)}(W),$$

we clearly exhibit the Fredholm form of the integral equation (26) and finally obtain, for the real function $\Psi_1^{(I)}(W)$, ($I = \frac{1}{2}, \frac{3}{2}$),

$$(29) \quad \Psi_1^{(I)}(W) = \Phi_1^{(I)}[W^2 - (\kappa + \mu)^2] + \\ + \sum_{I'=\frac{1}{2}, \frac{3}{2}} \lambda_{(I')}^{(I)} \int_{(\kappa+\mu)^2}^{\infty} N^{(I')}(W^2, W'^2) \exp[\bar{\varrho}_1^{(I')}(W')] \sin \bar{\delta}_1^{(I')}(W') \Psi_1^{(I')}(W') dW'.$$

⁽¹⁰⁾ M. GOURDIN and A. MARTIN: *Nuovo Cimento*, **10**, 699 (1958).

From the knowledge of the $\bar{\delta}_1^{(D)}(W)$ phase shift one can numerically solve this system of two coupled integral equations. Numerical results will be given later.

3.4. *Amplitude due to the isoscalar part of the electromagnetic current.* — We evidently use for this case the same method as in the previous section. The new fact is the two pions intermediate state contribution $b(t)$. In order to extract its P wave part, we introduce a second left hand cut $L_2(x)$ (see Appendix II). We put

$$(30) \quad \frac{3}{4\pi} \int_{-1}^{+1} \sin^2 \theta \, d \cos \theta \frac{1}{t' - t} = \frac{1}{\pi} \int_{L_2(t')} \frac{E(t', z)}{W^2 - z} dz$$

and obtain for the Mushkelishvili-Omnès integral equation,

$$(31) \quad C_1^{(2)}(W) = \frac{1}{\pi} \int_{(\kappa + \mu)^2}^{\infty} \frac{\sigma^{(2)}(s') \, ds'}{s' - s_1 - i\varepsilon} + \frac{3}{4\pi} \int_{-1}^{+1} \sin^2 \theta \, d \cos \theta \left[\int_{(\kappa + \mu)^2}^{\infty} \frac{\sigma^{(2)}(s') \, ds'}{s' - s_2} + \int_{(2\mu)^2}^{\infty} \frac{\tau^{(2)}(t') \, dt'}{t' - t} \right],$$

the following solution, after application of the unitarity condition (11):

$$(32) \quad C_1^{(2)}(W) = \exp [\bar{\varrho}_1^{(\frac{1}{2})}(W) + i\bar{\delta}_1^{(\frac{1}{2})}(W)] \Psi_1^{(2)}(W),$$

where the real function $\Psi_1^{(2)}(W)$ is solution of a Fredholm equation,

$$(33) \quad \Psi_1^{(2)}(W) = \Phi_1^{(\frac{1}{2})}[W^2 - (\kappa + \mu)^2] + M(W) + \int_{(\kappa + \mu)^2}^{\infty} N^{(\frac{1}{2})}(W^2, W'^2) \exp [\bar{\varrho}_1^{(\frac{1}{2})}(W')] \sin \bar{\delta}_1^{(\frac{1}{2})}(W') \Psi_1^{(2)}(W') \, dW'^2,$$

where $M(W)$ is a known function corresponding to contributions from channel III:

$$(34) \quad M(W) = \frac{1}{\pi} \int_{(2\mu)^2}^{\infty} \tau^{(2)}(t') \, dt' \int_{L_2(t')} \frac{E(t', z)}{W^2 - z} \exp [-\bar{\varrho}_1^{(\frac{1}{2})}(z)] \, dz.$$

4. — Conclusion.

The magnetic dipole amplitudes $C_1^{(\frac{1}{2})}(W)$, $C_1^{(\frac{3}{2})}(W)$ and $C_1^{(2)}(W)$ satisfy Fredholm integral equations (29) and (33). There is no difficulty, in principle, to solve such equations, by the determinant method or more rapidly by numerical computations. But it is necessary to know the $\pi K \rightarrow \pi K$ and the $\pi\pi \rightarrow K\bar{K}$ amplitudes in the states $J=1$ or equivalently the π -K phase shifts.

This later problem, which is also an intermediate step in the calculation of the associated production of strange particles, is difficult because, as in the present one, there are no Born terms. In the other hand, its resolution depends of the π - π phase shifts and we have not yet in this question experimental data but only theoretical speculations.

APPENDIX I

We consider the integral

$$K(s, x) = \frac{3}{4} \int_{-1}^{+1} \sin^2 \theta \frac{1}{x - s_2} d \cos \theta,$$

where

$$\begin{cases} s_2 = \kappa^2 - 2ke_q - 2kq \cos \theta, \\ s = (k + e_k)^2 = (\omega_q + e_q)^2. \end{cases}$$

Because of the even character of the integral $K(s, x)$ we can transform it into

$$K(s, x) = \frac{3}{2} \int_0^1 \sin^2 \theta \frac{(x - \kappa^2) + 2ke_q}{(x - \kappa^2 + 2ke_q)^2 - 4k^2 q^2 \cos^2 \theta} d \cos \theta$$

and the integrand is now a rational quantity in the variable s . We finally obtain the form

$$K(s, x) = \frac{3}{2} \int_0^1 (1 - u^2) \cdot \frac{2s[2s(x - \kappa^2) + (s - \kappa^2)(s + \kappa^2 - \mu^2)]}{[2s(x - \kappa^2) + (s - \kappa^2)(s + \kappa^2 - \mu^2)]^2 - (s - \kappa^2)^2[s - (\kappa + \mu)^2][s - (\kappa - \mu)^2]} u^2 du.$$

We use the auxiliary notation

$$\begin{aligned} N(s, x) &= 2s(x - \kappa^2) + (s - \kappa^2)(s + \kappa^2 - \mu^2), \\ D(s, x; u^2) &= N^2(s, x) - u^2(s - \kappa^2)^2[s - (\kappa + \mu)^2][s - (\kappa - \mu)^2], \end{aligned}$$

and we are interested to the roots in s of the fourth order polynomial $D(s, x; u^2)$.

A.1. - For $u^2 = 0$, $D(s, x; 0)$ reduces to $N^2(s, x)$ and the roots are of order two. Let us call $\alpha_1(x)$ and $\alpha_2(x)$ these two roots. It is easy to prove, with the

explicit form of $N(s, x)$ that:

- they are of opposite sign,
- they are two decreasing functions of x .

It is important to note that $\alpha_2[(\kappa + \mu)^2] > (\kappa - \mu)^2$ and to define a value of x for which

$$\alpha_2(x_1) = (\kappa - \mu)^2, \quad x_1 = \frac{\kappa(\kappa^2 + \kappa\mu - \mu^2)}{\kappa - \mu}.$$

We never can have, with an appropriate choice of values for κ and μ , $x_1 = (\kappa + \mu)^2$ and this situation is general in a three mass problem.

A-2. — For $u^2 = 1$, one root of D becomes $-\infty$ and another 0. We can put

$$D(s, x; 1) \equiv sP(s, x),$$

where $P(s, x)$ is a second order polynomial with roots $d_1(x)$ and $d_2(x)$. The situation for the position of α_1 , α_2 , d_1 , d_2 , is given in the following table.

TABLE I. — Roots of $N(s, x)$ and $P(s, x)$.

x	$(\kappa + \mu)^2$	x_1	x_2	$+\infty$
α_1	α_1^M	$\searrow \alpha_1(x_1)$	$\searrow \alpha_1(x_2)$	$\searrow -\infty$
α_2	α_2^M	$\searrow (\kappa - \mu)^2$	$\searrow \alpha_1(x_2)$	$\searrow 0$
d_1	d	$\searrow d_1(x_1)$	$\searrow 0$	$\searrow -\infty$
d_2	d	$\nearrow (\kappa - \mu)^2$	$\searrow d_2(x_2)$	$\searrow 0$

The values d and x_2 are given by

$$d = \frac{\kappa(\kappa^2 - \kappa\mu - \mu^2)}{\kappa + \mu}, \quad x_2 = \frac{\kappa^2(2\kappa^2 - \mu^2)}{\kappa^2 - \mu^2},$$

the other quantities introduced in the table are without precise interest.

We now can discuss the roots of $D(s, x; u^2)$ in the various regions.

With the form given for $D(s, x; u^2)$ and the Table I we immediately verify the following relations:

$$\left\{ \begin{array}{ll} D(\alpha_1, x; u^2) \leq 0 & (\kappa + \mu^2) < x, \\ D(\alpha_2, x; u^2) \leq 0 & x_1 < x, \\ D(\alpha_2, x; u^2) \geq 0 & (\kappa + \mu)^2 < x < x_1, \\ D(0, x; u^2) \geq 0 & (\kappa + \mu^2) < x. \end{array} \right.$$

Region I $x > x_2$: we have four real roots for $D(s, x; u^2)$:

$$-\infty < s_1 < \alpha_1(x) < s_2 < d_1(x) < 0 < s_3 < \alpha_2(x) < s_4 < d_2(x) .$$

Region II $x_2 > x > x_1$: four real roots:

$$-\infty < s_1 < \alpha_1(x) < s_2 < 0 < d_1(x) < s_3 < \alpha_2(x) < s_4 < d_2(x) .$$

Region III $x_1 > x > (\kappa + \mu)^2$: the situation becomes more complicated.

First, we always have two negative roots:

$$-\infty < s_1 < \alpha_1(x) < s_2 < 0 .$$

For the two other, the reality depends of the values of u^2 and the situation is the following:

u^2	1	$u_0^2(x)$	0
s_3	$d_1(x)$	$\nearrow d_3(x)$	$\alpha_2(x)$
s_4	$d_2(x)$	$\searrow d_3(x)$	$\alpha_2(x)$

for $0 < u^2 < u_0^2(x)$ s_3 and s_4 are imaginary conjugate of each other.

We now return to the expression of $K(s, x)$. We take as new variables, instead of u , the roots s_j of $D(s, x; u^2) = 0$. With the general form

$$u^2(z) = \frac{A(z)}{B(z)} = \frac{z^4 + az^3 + bz^2 + cz + d}{z^4 + ez^3 + fz^2 + gz + d}$$

and the roots $A(s) - u^2 B(s) = (1 - u^2)(s - s_1)(s - s_2)(s - s_3)(s - s_4)$ we put $s_j = z$ and use symmetrical functions in order to express the three other roots in terms of z . We finally obtain

$$\frac{du}{(1 - u^2)(z - s_k)(z - s_l)(z - s_m)} = \frac{u(z)}{2} \frac{dz}{A(z)} .$$

If we replace $A(z)$ by $N^2(z, x)$, we obtain

$$\frac{N(z, x) du}{(1 - u^2)(z - s_k)(z - s_l)(z - s_m)} = \frac{1}{2} \frac{u(z)}{N(z)} dz ,$$

$u(z)$ is a positive quantity, in the range $0 - 1$

$$u(z) = \left[\frac{N^2(z, x)}{(z - \kappa^2)^2 [z - (\kappa + \mu)^2] [z - (\kappa - \mu)^2]} \right]^{\frac{1}{2}} .$$

We now discuss the preceding expressions for the three regions and the four roots, putting

$$N(s_j, x) = \omega_j |N(s_j, x)|,$$

where ω_j describes the phase of the function $N(s_j, x)$. In all cases (s_j real or complex), $u^2(z)$ is a real positive quantity, and the integrand has the expression

$$\frac{u(z)}{N(z, x)} = \frac{\omega_j}{|z - \kappa^2| |z - (\kappa + \mu)^2|^{\frac{1}{2}} |z - (\kappa - \mu)^2|^{\frac{1}{2}}}.$$

Regions I and II. The four roots are real and localized in the following manner:

$$s_1 < \alpha_1 < s_2 < 0 < s_3 < \alpha_3 < s_4 < (\kappa - \mu)^2.$$

We easily deduce

$$\omega_1 = \omega_4 = +1, \quad \omega_2 = \omega_3 = -1.$$

Region III. For the two negative roots, we have the same situation

$$\omega_1 = 1, \quad \omega_2 = -1.$$

For s_3 and s_4 we divide the range of integration for u in two parts:

a) $u_0(x) \leq u \leq 1$. s_3 and s_4 are real and less than α_2 . The values for ω_j are $\omega_3 = \omega_4 = -1$.

b) $0 \leq u \leq u_0(x)$. s_3 and s_4 are complex conjugate and we arbitrarily choose the roots s_3 and s_4 , ω_j is then the phase of $N(z, x)$ for one root, the symmetry of the final result in s_3 and s_4 guarantees its reality.

We are now able to write the function $K(W^2, x)$ with a left hand cut

$$K(W^2, x) = \int_{L_1(x)} \frac{E(x, z)}{W^2 - z} dz,$$

with the following notations for $E(x, z)$ and $L_1(x)$:

$$E(x, z) = \frac{3}{2} \frac{z[1 - u^2(z)]}{|z - K^2| |z - (\kappa + \mu)^2|^{\frac{1}{2}} |z - (\kappa - \mu)^2|^{\frac{1}{2}}},$$

$$L_1(x) = L^{(+)}(x) + L^{(-)}(x),$$

where $L^{(-)}(x)$ corresponds to negative roots s_1 and s_2 :

$$L^{(-)}(x) = \begin{cases} \text{real cut from } -\infty \text{ to } d_1(x) & \text{for } x > x_2 \\ \text{real cut from } -\infty \text{ to } 0 & \text{for } x_2 > x > (\kappa + \mu)^2 \end{cases}$$

and $L^{(\pm)}(x)$, corresponding to roots s_3 and s_4 , differs in three regions:

$$L^{(\pm)}(x) = \begin{cases} \text{real cut from } 0 & \text{to } \bar{d}_2(x) & \text{for } x > x_2 \\ \text{real cut from } \bar{d}_1(x) & \text{to } \bar{d}_2(x) & \text{for } x_2 \geq x \geq x_1 \\ \text{complex cut} & & \text{for } x_1 \geq x > (\kappa + \mu)^2. \end{cases}$$

In the complex plane of z , this later cut is given by

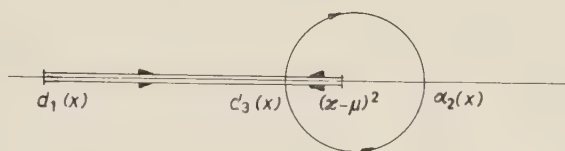


Fig. 5.

APPENDIX II

We now have to consider the same type of integral as in the Appendix I

$$K'(s, x) = \frac{3}{4\pi} \int_{-1}^{+1} \sin^2 \theta \frac{1}{x - t} d \cos \theta,$$

where

$$\begin{cases} t = 2\kappa^2 - 2e_k e_q + 2kq \cos \theta, \\ s = (k + e_k)^2 = (\omega_q + e_q)^2 = W^2. \end{cases}$$

By symmetry considerations one can obtain the form

$$K'(s, x) = \frac{3}{2\pi} \int_0^1 (1 - u^2) \frac{2s N'(s, x)}{D'(s, x, u^2)} du,$$

with the following notations:

$$N'(s, x) = 2s(x - 2\kappa^2) + (s + \kappa^2)(s + \kappa^2 - \mu^2),$$

$$D'(s, x; u^2) = N'^2(s, x) - u^2(s - \kappa^2)^2[s - (\kappa + \mu)^2][s - (\kappa - \mu)^2].$$

If we study the roots of $D'(s, x; u^2) = 0$ in s when x goes from $4\mu^2$ to

$+\infty$ and u^2 from 0 to 1, there appear three regions:

<i>Region I</i>	$x > 4\kappa^2$	4 real negative roots,
<i>Region II</i>	$4\kappa^2 > x > x_1 = \kappa^2 + \frac{\mu^2}{2} + \kappa\sqrt{\kappa^2 - \mu^2}$	2 real negative roots, 2 complex conjugate roots,
<i>Region III</i>	$x_1 > x > 4\mu^2$	4 imaginary roots.

We then can define a left hand cut which can be complex and we write $K'(s, x)$ in the form

$$K'(W^2, x) = \frac{1}{\pi} \int_{L_2(x)} \frac{E(x, z)}{W^2 - z} dz,$$

where $E(x, z)$ has the same definition as in the first Appendix, with, for $u^2(z)$, the new expression

$$u^2(z) \equiv \frac{N'^2(z, x)}{[z - \kappa^2]^2 [z - (\kappa + \mu)^2] [z - (\kappa - \mu)^2]}.$$

Let us call $\alpha_1(x)$ and $\alpha_2(x)$ the roots of $N'(s, x) = 0$, $d_1(x)$, $d_2(x)$ and zero the roots of $D'(s, x, 1) = 0$. The ways of integration $L_2(x)$ in the complex plane of the variable z , depend on the values on x and are defined as follows:

Region I: We have two real cuts from $-\infty$ to $d_1(x)$ and from 0 to $d_2(x)$.

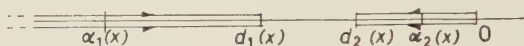


Fig. 6.

Region II: The roots $d_1(x)$ and $d_2(x)$ become complex. If we call $d_3(x)$ the root of order two of D' corresponding to $u^2 - u_0^2(x)$ we obtain a complex cut.

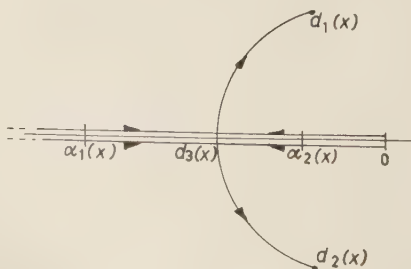


Fig. 7.

Region III: $\alpha_1(x)$ and $\alpha_2(x)$ become also complex conjugate and we obtain the following cut:

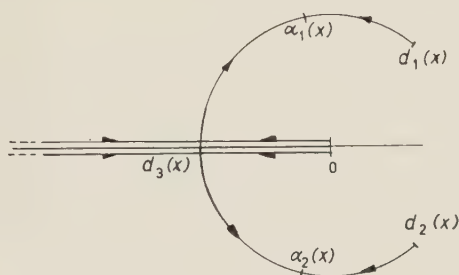


Fig. 8.

The directions indicated on the previous figures correspond to the variation of u^2 from 0 to 1.

RIASSUNTO (*)

In questo scritto ci si propone di trattare, con la tecnica di Mandelstam, la fotoproduzione dei mesoni π sui mesoni K, necessaria allo studio della fotoproduzione di mesoni K sui nucleoni. Limitandosi agli stati intermedi di masse più basse e considerando solo la transizione dipolare magnetica, si ottiene per le due ampiezze dovute alla parte isovettoriale della corrente elettromagnetica due equazioni integrali accoppiate di Mushkelishvili-Omnès e per l'ampiezza dovuta alla parte isoscalare una equazione dello stesso tipo. Queste si riducono a delle equazioni integrali di Fredholm. La conoscenza delle soluzioni approssimate per la fotoproduzione dei mesoni π sui mesoni π e gli sfasamenti P della diffusione mesone π -mesone K permetterà di risolverle numericamente. Questi ultimi calcoli saranno dati successivamente.

(*) Traduzione a cura della Redazione.

Phenomenology of Σ -Nucleon Scattering (*) (**).

M. T. VAUGHN (***)

Department of Physics, Purdue University - Lafayette, Ind.

(ricevuto il 20 Giugno 1960)

Summary. — A discussion is given of some phenomenological aspects of Σ -nucleon scattering. It is noted that with Σ^+ beams likely to be available in the near future, triple scattering experiments are only slightly more difficult than single scattering experiments. A method of determining separately 1S and 3S phase shifts at low energies is noted. A discussion is given of the qualitative features of low-energy Σ -nucleon scattering to be expected if one or the other of the global symmetry models $G_{\pi\Sigma} \approx \pm G_{\pi N}$ is valid, and possibilities of distinguishing between the two cases are examined, utilizing the Mandelstam representation for the scattering amplitude, some consequences of which are derived in the appendix. In particular, the analytic properties of the partial wave amplitudes are deduced; it is found that owing to the unequal masses of Σ and nucleon, the singularities of the partial wave amplitudes do not all lie on the real axis in the complex plane of the energy variable.

1. — Introduction.

It is quite appealing to suppose that there exists a universal pion-baryon interaction of the form

$$(1) \quad L_{int} = G_{NN} \bar{N} \boldsymbol{\tau} N \cdot \boldsymbol{\pi} + G_{\Xi\Xi} \bar{\Xi} \boldsymbol{\tau} \Xi \cdot \boldsymbol{\pi} + G_{\Lambda\Sigma} (\bar{\Sigma} \boldsymbol{\Lambda} \cdot \boldsymbol{\pi} + \text{h. c.}) + i G_{\Sigma\Sigma} \bar{\Sigma} \times \Sigma \cdot \boldsymbol{\pi},$$

with simple relationships between the coupling constants. Gell-Mann for instance, has proposed the relations ⁽¹⁾

$$(2a) \quad G_{NN} = G_{\Lambda\Sigma} = G_{\Sigma\Sigma} = G_{\Xi\Xi} \equiv G_{\pi},$$

(*) Based on part of a Ph. D. thesis submitted to Purdue University.

(**) Supported in part by the U. S. Air Force Office of Scientific Research.

(***) Now at Physics Department, University of Pennsylvania, Philadelphia, Penn.

(1) M. GELL-MANN: *Phys. Rev.*, **106**, 1296 (1957).

whereas the seven-dimensional charge space formalism of Peaslee ⁽²⁾, on the other hand, contains a universal pion-baryon interaction in which the relations

$$(2b) \quad G_{\mathcal{N}\mathcal{N}} = -G_{\Lambda\Sigma} = -G_{\Sigma\Sigma} = G_{\Xi\Xi} \equiv G_{\pi}$$

are satisfied.

The principal evidence to date supporting one or the other of these proposals is the experimental data on Λ -hypernuclear binding energies ⁽³⁾. Several authors have shown ⁽⁴⁾ that the data are not inconsistent with either of the assumptions (2a) or (2b) (the sign of $G_{\Lambda\Sigma}$ per se is not observable), but no reliable quantitative estimate of the magnitude of $G_{\Lambda\Sigma}$ can be made, owing both to the lack of knowledge of the detailed behavior of the hyperon-nucleon potential at small distances, and the uncertainties in relating hypernuclear binding energies to the strength of the two-body potential.

The present note is a discussion of some of the qualitative features of Σ -nucleon scattering which may provide evidence on the sign and rough order of magnitude of $G_{\Sigma\Sigma}$; the possibility of distinguishing between (2a) and (2b) from the behavior of Σ -nucleon scattering in the state of isotopic spin $\frac{3}{2}$ is examined in some detail.

2. - Phenomenology of Σ -nucleon scattering.

In so far as charge independence is valid, the Σ -nucleon scattering matrix can be decomposed into a matrix for isotopic spin $T = \frac{1}{2}$ and a matrix for $T = \frac{3}{2}$; below the threshold for the process

$$(3) \quad \Sigma + \mathcal{N} \rightarrow \Lambda + \mathcal{N} + \pi$$

the $T = \frac{3}{2}$ matrix describes purely elastic scatterings while even for zero kinetic energy Σ , the unelastic process

$$(4) \quad \Sigma + \mathcal{N} \rightarrow \Lambda + \mathcal{N}$$

in the $T = \frac{1}{2}$ channel is energetically allowed. While this latter process is of interest in itself, it makes the analysis of the elastic scattering more compli-

(2) D. C. PEASLEE: *Phys. Rev.*, **117**, 873 (1960).

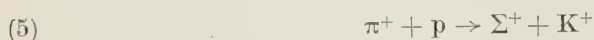
(3) These data have been summarized by R. H. DALITZ: *Proc. of the Kiev Conference on High-Energy Physics* (1959).

(4) D. B. LICHTENBERG and M. ROSS: *Phys. Rev.*, **107**, 1714 (1957); F. FERRARI and L. FONDA: *Nuovo Cimento*, **9**, 842 (1958); R. H. DALITZ and B. W. DOWNS: *Phys. Rev.*, **111**, 967 (1958); and M. T. VAUGHN: *Purdue University Ph. D. thesis* (1960).

cated; consequently, attention will be confined here to the elastic Σ -nucleon scattering in the $T = \frac{3}{2}$ channel.

Since the Pauli principle does not restrict the allowed spin and angular momentum states of the Σ -nucleon system, measurement of the differential scattering cross-section only does not suffice to uniquely determine the scattering phase shifts, even in the low energy limit when only S -waves are important. Consequently, experiments must be performed in which either the incident beam of Σ -particles is polarized and/or a measurement is made of the polarization of the scattered beam of Σ .

Fortunately, such experiments seem just as feasible as the simple scattering experiments in which no measurement is made of the polarization of the Σ (either in the initial state or in the final state). It is known from the work of COOL *et al.* ⁽⁵⁾ that the reaction



with $T_{\pi}^{\text{lab}} = 1.0$ GeV produces a polarized beam of Σ^+ -particles ⁽⁶⁾; furthermore, the observed asymmetry ⁽⁵⁾ in the decay $\Sigma^+ \rightarrow p + \pi^0$ allows an analysis of the state of polarization of a Σ^+ beam.

Then for the elastic Σ^+ -p scattering with a polarized Σ^+ beam, the following quantities can be measured:

a) The differential scattering cross-section

$$(6) \quad I_p(\theta, \varphi) = I_0(\theta) [1 + P(\theta) \mathbf{P} \cdot \mathbf{n}],$$

where \mathbf{P} is the polarization of the incident Σ^+ beam, \mathbf{n} is the unit normal to the scattering plane, $\mathbf{P} \cdot \mathbf{n} = P \cos \varphi$. From this can be determined the differential cross-section $I_0(\theta)$ for scattering of an unpolarized beam and the polarization parameter $P(\theta)$ for Σ^+ -p scattering.

b) The average polarization $\langle \mathbf{P}_f(\theta) \rangle$ of the scattered Σ^+ beam, defined by

$$(7) \quad \langle \mathbf{P}_f(\theta) \rangle = \left\{ \int_0^{2\pi} I_p(\theta, \varphi) \mathbf{P}_f(\theta, \varphi) d\varphi \right\} / \left\{ \int_0^{2\pi} I_p(\theta, \varphi) d\varphi \right\},$$

⁽⁵⁾ R. L. COOL, B. CORK, J. W. CRONIN and W. A. WENZEL: *Phys. Rev.*, **114**, 912 (1959).

⁽⁶⁾ It is of course to be noted, however, that the Σ^+ beam produced by reaction (5) will have laboratory kinetic energies ≥ 200 MeV, so that in order to observe low energy Σ^+ -p scattering, one must use a Σ^+ beam from a reaction such as $K^- + p \rightarrow \Sigma^+ + \pi^-$ (in flight); this may produce a polarized Σ^+ beam at moderate K^- energies.

defines a quantity $Q(\theta)$ by

$$(8) \quad I_0(\theta) \langle \mathbf{P}_f(\theta) \rangle \equiv Q(\theta) \mathbf{P}.$$

Note that a determination of the ratio $Q(\theta)/I_0(\theta)$ requires only a measurement of the ratio of the up-down asymmetry (with respect to the plane of production of the Σ^+) of the decay protons from the Σ^+ scattered at an angle θ to the same up-down asymmetry, for the unscattered Σ^+ beam; no *a priori* knowledge of either the asymmetry parameter α for the Σ^+ decay or the polarization of the incident Σ^+ beam is needed.

c) A further subdivision of the data leads to a determination of the triple scattering parameters $D(\theta)$, $R(\theta)$, $4(\theta)$; this, however, yields no new information at low energies, in which we are primarily interested here ⁽⁷⁾.

The non-relativistic transition amplitude M for Σ -nucleon scattering in the $T = \frac{3}{2}$ channel at a fixed energy can be written as a matrix in the spin space of the two particles; this matrix can be decomposed in a well-known way into a linear combination of invariants constructed from the spins and momenta of the particles ⁽⁸⁾; write

$$(9) \quad M = \sum_{j=1}^5 M_j(\theta) O_j,$$

where θ is the c.m. scattering angle; the O_j are taken to be

$$(10) \quad \begin{cases} O_1 = 1, & O_2 = (\boldsymbol{\sigma}_\Sigma + \boldsymbol{\sigma}_N) \cdot \mathbf{n} / \sqrt{2}, \\ O_3 = \boldsymbol{\sigma}_\Sigma \cdot \mathbf{n} \boldsymbol{\sigma}_N \cdot \mathbf{n}, & O_4 = \boldsymbol{\sigma}_\Sigma \cdot \mathbf{q} \boldsymbol{\sigma}_N \cdot \mathbf{q}, \quad O_5 = \boldsymbol{\sigma}_\Sigma \cdot \mathbf{s} \boldsymbol{\sigma}_N \cdot \mathbf{s}, \end{cases}$$

where $\boldsymbol{\sigma}_\Sigma$, $\boldsymbol{\sigma}_N$ are Σ and nucleon spin operators, \mathbf{q} , \mathbf{s} are unit vectors in the direction of $\mathbf{p}' - \mathbf{p}$ and $\mathbf{p}' + \mathbf{p}$, respectively (\mathbf{p} , \mathbf{p}' are the initial and final momenta of the Σ in the c.m. system), and \mathbf{n} is a unit vector in the direction of $\mathbf{p} \times \mathbf{p}'$. (An additional term of the form $M_6(\theta) O_6$, with $O_6 = (\boldsymbol{\sigma}_\Sigma - \boldsymbol{\sigma}_N) \cdot \mathbf{n} / \sqrt{2}$ may in principle be present here; in the presence of such a term, the polarizations of the scattered Σ and recoil nucleon are not equal, even if the incident Σ beam is unpolarized. However, $M_6(\theta)$ is presumably of order $(m_\Sigma - m_N)/(m_\Sigma + m_N)$ relative to $M_5(\theta)$, and is neglected here; the necessary modifications

⁽⁷⁾ Triple scattering is fully discussed by L. WOLFENSTEIN: *Ann. Rev. Nucl. Sci.*, **6**, 43 (1956).

⁽⁸⁾ This decomposition has been given previously by many authors; see, for example, M. GOLDBERGER, Y. NAMBU and R. OEHME: *Ann. Phys.*, **2**, 226 (1957), which contains references to earlier work.

of the formulas presented here, should this term prove to be not negligible, are quite straightforward.)

The observables of interest are given by ⁽⁹⁾

$$(11) \quad I_0(\theta) = \sum_{j=1}^5 |M_j(\theta)|^2,$$

$$(12) \quad \dot{I}_0(\theta) P(\theta) = \text{Re} [M_1(\theta) + M_3(\theta)] M_2^*(\theta) / \sqrt{2},$$

$$(13) \quad Q(\theta) = |M_1(\theta)|^2 - \frac{1}{2}(1 - \cos \theta) |M_4(\theta)|^2 - \frac{1}{2}(1 + \cos \theta) |M_5(\theta)|^2.$$

Of particular interest is the low-energy limit of eqs. (11)–(13), when only *S*-waves are scattered appreciably; the observables are then given by

$$(14) \quad I_0(\theta) = (3 \sin^2 \delta_t + \sin^2 \delta_s) / 4p^2,$$

$$(15) \quad P(\theta) = 0,$$

$$(16) \quad Q(\theta) = [\sin^2 \delta_t + \cos(\delta_t - \delta_s) \sin \delta_s \sin \delta_t] / 2p^2,$$

where δ_s , δ_t are singlet and triplet *S*-wave phase shifts (more precisely, δ_t is the *z*-eigenphase shift in the even parity $J=1$ channel, which is a mixture of 3S and 3D wave) ⁽¹⁰⁾.

3. – Qualitative features of Σ -nucleon scattering arising from a universal pion-baryon interaction.

If it is assumed that the pion-hyperon coupling strength is of the same order of magnitude as the pion-nucleon coupling strength, and if it is assumed that the *K*-meson exchange contribution to the Σ -nucleon interaction is small ($< 15\%$, say), then several remarks can be made about the qualitative features of the Σ -nucleon interaction in the $T = \frac{3}{2}$ state. One must distinguish between the cases $G_{\Sigma\Sigma} \approx \pm G_{\mathcal{N}\mathcal{N}}$.

If $G_{\Sigma\Sigma} \approx + G_{\mathcal{N}\mathcal{N}}$, then the pion exchange contribution to the $T = \frac{3}{2}$ Σ -nucleon interaction is similar to the $T=1$ nucleon-nucleon interaction. In particular, the interaction in the singlet state will be quite strongly attractive,

⁽⁹⁾ WOLFENSTEIN ⁽⁷⁾ has given a general discussion of the relation of observables to the transition matrix.

⁽¹⁰⁾ The possibility of distinguishing singlet scattering and triplet scattering in the low-energy limit by measurement of $Q(\theta)$ has been noted also by GARDNER and WELTON: *Phys. Rev. Lett.*, **3**, 281 (1959).

perhaps strong enough that a bound 1S_0 state can exist⁽¹¹⁾. In the triplet state, the interaction will be rather weak (corresponding to the triplet odd parity nucleon-nucleon interaction without spin-orbit force)—the central potential contains a small repulsive term from single pion exchange and a small attractive term from two pion exchange, where the tensor force is weaker (by a factor of about three) than the tensor force effective in the deuteron.

Consequently, one can expect to find that the major contribution to the low energy scattering will come from the singlet spin state, and, in the absence of a bound state, there should be a peak in the singlet cross-section corresponding to a virtual level at low positive energy; the triplet scattering is quite likely to be small enough that, in spite of its greater statistical weight, it does not obscure the peak in the singlet cross-section.

In the case $G_{\Sigma\Sigma} \approx -G_{\Lambda\Lambda}$, corresponding to the pion-hyperon interaction of Peaslee's seven-dimensional charge space⁽²⁾, the sign of the contribution to the potential from exchange of an odd number of pions is reversed, while the sign of the even pion exchange contribution is unaltered. In this case, both the one and two pion exchange contributions to the triplet central potential are attractive, though still rather weak. The one-pion exchange tensor force is of opposite sign, this is of little consequence at low energies, however, when only an effective 3S phase shift can be measured. The singlet potential, on the other hand, is rather weaker in the present case, owing to the fact that the large attractive two-pion exchange contribution to the potential is partially cancelled by the now repulsive one-pion exchange potential. This in the singlet state, the scattering should be considerably smaller in the case $G_{\Sigma\Sigma} \approx -G_{\Lambda\Lambda}$; in particular there should be no bound state or low energy virtual state, and the singlet and triplet scattering should be of the same order of magnitude⁽¹²⁾.

Thus, for example, a measurement of the low energy total scattering cross-section and a measurement of the ratio

$$(17) \quad R \equiv \frac{Q}{I_0} = \frac{2a_t^2 + 2a_s a_s}{3a_t^2 + a_s^2}$$

at zero kinetic energy (a_s , a_t are the singlet and triplet scattering lengths;

⁽¹¹⁾ Several authors have discussed the possible existence of such a bound state: see D. LICHTENBERG and M. ROSS: *Phys. Rev.*, **107**, 1714 (1957); F. FERRARI and L. FONDA: *Nuovo Cimento*, **6**, 1027 (1957); M. VAUGHN: *Bull. Am. Phys. Soc.*, **2**, 353 (1957); and G. A. SNOW: *Phys. Rev.*, **110**, 1192 (1958).

⁽¹²⁾ The unknown behavior of the potential at small distances may play a crucial role here — it is quite possible that the net effect of the one and two pion exchange contributions may be to give a small low energy 1S phase shift; on the other hand, it is also possible that the repulsive core in the Σ -nucleon potential is perceptively weaker than the well-known core in the N - N potential.

respectively) should suffice to distinguish between the two possible relative signs.

If in addition, the energy dependence of, say, the 1S_0 phase shift can be measured with sufficient accuracy that a rough determination can be made of the parameters a_s , r_{0s} , P_s of the effective range expansion ⁽¹³⁾

$$(18) \quad p \operatorname{ctg} \delta_s = -\frac{1}{a_s} + \frac{1}{2} p^2 r_{0s} - P_s r_{0s}^2 p^4 + \dots,$$

then the sign of $G_{\Sigma\Sigma} G_{NN}$ can be extracted by a procedure used by CINI, FUBINI and STANGHELLINI in the analysis of nucleon-nucleon scattering ⁽¹⁴⁾, which is motivated by, but not dependent on the complete validity of, Mandelstam's conjecture on the analytic properties of scattering amplitudes ⁽¹⁵⁾, which is specialized to the case of Σ -nucleon scattering in the Appendix.

One attempts to fit the data with a function of the form

$$(19) \quad K(p^2) = p \operatorname{ctg} \delta_s = -\frac{1}{a_s} + \frac{1}{2} p^2 r_{0s}^2 - \frac{P_s r_{0s}^2 p^4}{(1 + D p^2)}.$$

If 1D , 1G , ... phase shifts are negligible at energies in which the last term in eq. (18) is observable, then the analytic properties of the singlet scattering amplitude at $\theta = 90^\circ$ imply

$$(20) \quad \sqrt{2} K(-\tfrac{1}{2} m_\pi^2) = -m_\pi,$$

$$(21) \quad K'(-\tfrac{1}{2} m_\pi^2) = \frac{1}{\gamma} + \frac{1}{m_\pi \sqrt{2}},$$

where γ is proportional to the product $G_{\Sigma\Sigma} G_{NN}$; an explicit expression for γ is given in the Appendix (eq. (A.19)); here it is merely noted that γ is positive if $G_{\Sigma\Sigma} G_{NN}$ is positive, and negative if $G_{\Sigma\Sigma} G_{NN}$ is negative.

The parameters P_s , D are then given by

$$(22) \quad \frac{1}{4} m_\pi^2 r_{0s}^3 P_s = \frac{\left[\frac{1}{a_s} + \frac{1}{4} m_\pi^2 r_{0s} - \frac{m_\pi}{\sqrt{2}} \right]^2}{\frac{1}{a_s} + \frac{m_\pi^2}{2\gamma} - \frac{m_\pi}{2\sqrt{2}}},$$

$$(23) \quad \frac{1}{2} m_\pi^2 D = \frac{\frac{2}{a_s} + \frac{1}{4} m_\pi^2 r_{0s} + \frac{m_\pi^2}{2\gamma} - \frac{3m_\pi}{2\sqrt{2}}}{\frac{1}{a_s} + \frac{m_\pi^2}{2\gamma} - \frac{m_\pi}{2\sqrt{2}}}.$$

⁽¹³⁾ J. M. BLATT and J. D. JACKSON: *Phys. Rev.*, **76**, 18 (1949).

⁽¹⁴⁾ M. CINI, S. FUBINI and G. STANGHELLINI: *Phys. Rev.*, **114**, 1633 (1959).

⁽¹⁵⁾ S. MANDELSTAM: *Phys. Rev.*, **112**, 1344 (1958).

In proton-proton scattering P_s is known to be small and positive ($\sim .03$)^(14,16), and for the $T = \frac{3}{2}$ Σ -nucleon scattering, P_s is also likely to be positive if $G_{\Sigma\Sigma}G_{\mathcal{N}\mathcal{N}} > 0$; on the other hand, if $G_{\Sigma\Sigma}G_{\mathcal{N}\mathcal{N}} < 0$, P_s will certainly be negative, and somewhat larger in magnitude.

A crude estimate of the difference in the 1S_0 phase shift between the two cases can be made with the aid of a simple boundary condition model: it is supposed that the potential for $r < r_0 \sim 1.0f$ is independent of the sign of the pion-hyperon coupling constant, while for $r > r_0$ the potential is given exactly by the one-pion exchange potential; for a given boundary condition on the wave function at $r = r_0$, the WKB approximation can be used to determine the difference between the phase shifts associated with the two choices for the sign of the one-pion exchange potential in the outside region. For $|G_{\Sigma\Sigma}G_{\mathcal{N}\mathcal{N}}| \approx 15$, the difference between the two phase shifts at $T_{\text{lab}}^\Sigma = 40 \text{ MeV}$ is $\approx 11^\circ$ ($r_0 = 1.0f$) or $\approx 17^\circ$ ($r_0 = 0.7f$), while at $T_{\text{lab}}^\Sigma = 100 \text{ MeV}$, the difference is $\approx 8^\circ$ ($r_0 = 1.0f$) or $\approx 12^\circ$ ($r_0 = 0.7f$). Thus it will probably be necessary for the experiments to determine the 1S_0 phase shift at 40 MeV, say, to within $(4 \div 5)^\circ$, in addition to the scattering length and effective range.

An alternative possibility for determining the product $G_{\Sigma\Sigma}G_{\mathcal{N}\mathcal{N}}$ from hyperon-nucleon scattering (Σ^+ -p scattering in particular) is a complete triple scattering experiment at $T_{\text{lab}}^\Sigma \sim (200 \div 300) \text{ MeV}$ (the lower end of this energy range is preferable, since the reaction $\Sigma^+ + p \rightarrow \Lambda + p + \pi^+$ will almost certainly be important near 300 MeV). Such an experiment may well prove more feasible, due to the fact that, as explained in Section 2, triple scattering experiments with a Σ^+ beam are only slightly more difficult than ordinary single scattering experiments, and a Σ^+ beam with lab kinetic energy of $(200 \div 300) \text{ MeV}$ is more readily available than a low energy Σ^+ beam. A straightforward phase shift analysis of such an experiment, along the lines of recent analyses of the 310 MeV p-p scattering data⁽¹⁷⁾ should then yield the sign and magnitude of $G_{\Sigma\Sigma}G_{\mathcal{N}\mathcal{N}}$.

* * *

The author takes pleasure in thanking D. C. PEASLEE for suggesting this problem, and for interesting discussions.

⁽¹⁶⁾ H. P. NOYES and D. Y. WONG: *Phys. Rev. Lett.*, **3**, 191 (1959).

⁽¹⁷⁾ P. CIZFRA, M. MACGREGOR, M. MORAVCSIK and H. STAPP: *Phys. Rev.*, **114**, 880 (1959); M. MACGREGOR, M. MORAVCSIK and H. STAPP: *Phys. Rev.*, **116**, 1248 (1959)

APPENDIX

Application of the Mandelstam representation to Σ -nucleon scattering.

Consider elastic Σ -nucleon scattering; let $p, p'; q, q'$ be the initial and final four-momenta of the nucleon and the Σ , respectively; introduce the usual scalar variables

$$(A.1) \quad s = (p + q)^2, \quad t_1 = (p - p')^2, \quad t_2 = (q - p')^2.$$

These are related on the mass shell by

$$(A.2) \quad s + t_1 + t_2 = 2(m_\Sigma^2 + m_N^2).$$

These variables are related to the barycentric momentum p and scattering angle θ by

$$(A.3) \quad s = (E_p^\Sigma + E_p^N)^2,$$

$$(A.4) \quad t_1 = -2p^2(1 - \cos \theta),$$

$$(A.5) \quad t_2 = (E_p^\Sigma - E_p^N)^2 - 2p^2(1 + \cos \theta).$$

Now p^2 can be expressed in terms of s as

$$(A.6) \quad p^2 = [s^2 - 2s(m_\Sigma^2 + m_N^2) + (m_\Sigma^2 - m_N^2)^2]/4s,$$

so that t_1, t_2 can be expressed in terms of s and $\xi \equiv \cos \theta$ as

$$(A.7) \quad t_1 = -[s^2 - 2s(m_\Sigma^2 + m_N^2) + (m_\Sigma^2 - m_N^2)^2](1 - \xi)/2s,$$

$$(A.8) \quad t_2 = -[s - 2(m_\Sigma^2 + m_N^2)](1 + \xi)/2 + (m_\Sigma^2 - m_N^2)^2(1 - \xi)/2s.$$

Consider now the amplitude $A_T(s, \cos \theta)$ for Σ -nucleon scattering in a state of isotopic spin T . This may be considered as the amplitude for scattering of spinless particles, or as one of the six invariant amplitudes associated with the scattering of two spin $\frac{1}{2}$ particles⁽¹⁸⁾. The conjecture of Mandelstam⁽¹⁾, applied to the present problem, is that the only singularities of the scattering amplitude considered as a function of two complex variables, consist of poles for

$$t_1 = m_\pi^2,$$

$$t_2 = m_K^2,$$

and branch cuts along the lines

$$s_0 \leq s < \infty,$$

$$t_{10} \leq t_1 < \infty,$$

$$t_{20} \leq t_2 < \infty,$$

⁽¹⁸⁾ These are essentially the $G_i(\nu, Q^2)$ of reference⁽⁸⁾, except that there are now six invariants instead of five.

where $t_{10} = 4m_\pi^2$, $t_{20} = (m_K + m_\pi)^2$ and $s_0 = (m_\Lambda + m_N)^2$ for $T = \frac{1}{2}$, $s_0 = (m_\Sigma + m_N)^2$ for $T = \frac{3}{2}$.

Repeated application of Cauchy's theorem then yields for $A_T(s, \cos \theta)$ the integral representation

$$(A.9) \quad A_T(s, \cos \theta) = \frac{\Gamma_\pi}{m_\pi^2 - t_1} + \frac{\Gamma_K}{m_K^2 - t_2} + \int_{s_0}^{\infty} ds' \int_{t_{10}}^{\infty} dt'_1 \frac{A_{13}(s', t_1)}{(s' - s)(t'_1 - t_1)} + \\ + \int_{s_0}^{\infty} ds' \int_{t_{20}}^{\infty} dt'_2 \frac{A_{23}(s', t'_2)}{(s' - s)(t'_2 - t_2)} + \int_{t_{10}}^{\infty} dt'_1 \int_{t_{20}}^{\infty} dt'_2 \frac{A_{12}(t'_1, t'_2)}{(t'_1 - t_1)(t'_2 - t_2)},$$

where the residues Γ_π , Γ_K are proportional to $G_{\Sigma\Sigma}G_{NN}$, and $F_{\Sigma\Sigma NN}^2$, with constants of proportionality depending on the spin and isotopic spin state under consideration; possible subtractions which may be required have been suppressed because they do not alter the analytic properties of the scattering amplitude.

The analytic properties of the scattering amplitude for fixed real ξ ($|\xi| < 1$) considered as a function of the complex variable s are then readily obtained by locating the points where the denominators of (A.9) can vanish. This is most easily done by writing

$$(A.10) \quad t'_1 - t_1 = [s - s_1^+(t'_1)][s - s_1^-(t'_1)]/2s,$$

$$(A.11) \quad t'_2 - t_2 = [s - s_2^+(t'_2)][s - s_2^-(t'_2)]/2s,$$

where

$$(A.12) \quad (1 - \xi)s_1^\pm(t'_1) = (m_\Sigma^2 + m_N^2)(1 - \xi) - t'_1 \pm \\ \pm \{[(m_\Sigma^2 + m_N^2)(1 - \xi) - t'_1]^2 - (m_\Sigma^2 - m_N^2)^2(1 - \xi)^2\}^{\frac{1}{2}},$$

$$(A.13) \quad (1 + \xi)s_2^\pm(t'_2) = (m_\Sigma^2 + m_N^2)(1 + \xi) - t'_2 \pm \\ \pm \{[(m_\Sigma^2 + m_N^2)(1 + \xi) - t'_2]^2 - (m_\Sigma^2 - m_N^2)^2(1 + \xi)^2\}^{\frac{1}{2}}.$$

Then for fixed real ξ , the representation (A.9) can be transformed to

$$(A.14) \quad A_T(s, \xi) = \frac{2\Gamma_\pi s}{[s - s_1^+(m_\pi^2)][s - s_1^-(m_\pi^2)]} + \frac{2\Gamma_K s}{[s - s_2^+(m_K^2)][s - s_2^-(m_K^2)]} + \\ + s \int_{s_0}^{\infty} \frac{ds'}{s' - s} \left\{ \int_{L_1^+} ds_1^+ \frac{A_{13}(s', t'_1)}{s_1^+(s_1^+ - s)} - \int_{L_1^-} ds_1^- \frac{A_{13}(s', t'_1)}{s_1^-(s_1^- - s)} \right\} + \\ + s \int_{s_0}^{\infty} \frac{ds'}{s' - s} \left\{ \int_{L_2^+} ds_2^+ \frac{A_{23}(s', t'_2)}{s_2^+(s_2^+ - s)} - \int_{L_2^-} ds_2^- \frac{A_{23}(s', t'_2)}{s_2^-(s_2^- - s)} \right\} + \\ + s^2 \int_{L_1^+} \frac{ds_1^+}{s_1^+(s_1^+ - s)} \left\{ \int_{L_2^+} ds_2^+ \frac{A_{12}(t'_1, t'_2)}{s_2^+(s_2^+ - s)} - \int_{L_2^-} ds_2^- \frac{A_{12}(t'_1, t'_2)}{s_2^-(s_2^- - s)} \right\} - \\ - s^2 \int_{L_1^-} \frac{ds_1^-}{s_1^-(s_1^- - s)} \left\{ \int_{L_2^+} ds_2^+ \frac{A_{12}(t'_1, t'_2)}{s_2^+(s_2^+ - s)} - \int_{L_2^-} ds_2^- \frac{A_{12}(t'_1, t'_2)}{s_2^-(s_2^- - s)} \right\},$$

where the dependence of s_1^\pm , s_2^\pm and the contours of integration L_1^\pm , L_2^\pm on ξ has not been written out explicitly.

The contours L_1^\pm , L_2^\pm are the curves in the complex planes of the variables s_1^\pm , s_2^\pm defined by

$$(A.15) \quad \begin{cases} L_1^\pm: s_1^\pm = s_1^\pm(t'_1), & 4m_\pi^2 \leq t'_1 < \infty, \\ L_2^\pm: s_2^\pm = s_2^\pm(t'_2), & (m_K + m_\pi)^2 < t'_2 < \infty, \end{cases}$$

with $s_1^\pm(t'_1)$, $s_2^\pm(t'_2)$ given by (A.13).

This representation exhibits explicitly the singularities of $A_T(s, \cos \theta)$ for fixed real $\cos \theta$. The precise location of the singularities depends on $\cos \theta$: in the forward direction, the K-meson pole lies closest to the physical region $s < (m_\Sigma + m_N)^2$, but the next singularity (the branch cut associated with the $K + \pi$ intermediate state) is not much more distant from the threshold of the physical region, and it does not seem possible to derive any practical benefit from the presence of the pole; in the backward direction, the pion pole lies closest to the physical threshold, and the next singularity (the two-pion branch cut) is about four times as far away from the threshold, so that a suitable extrapolation procedure may permit determination of the residue at the pole, provided sufficiently precise experimental data can be obtained.

For $\theta = 90^\circ$, the pion pole is still much the nearest singularity, and extrapolation to the pole can in principle be carried out by the procedure of CINI, FUBINI and STANGHELLINI⁽¹⁴⁾; it is relevant to note that the position of the pole is at

$$(A.16) \quad s = s_1^+(m_\pi^2) = m_\Sigma^2 + m_N^2 - m_\pi^2 + \{[m_\Sigma^2 + m_N^2 - m_\pi^2]^2 - (m_\Sigma^2 - m_N^2)^2\}^{\frac{1}{2}}$$

and the residue at the pole is given by

$$(A.17) \quad \Gamma = \frac{\Gamma_{\pi s_1^+}(m_\pi^2)}{\{[m_\Sigma^2 + m_N^2 - m_\pi^2]^2 - (m_\Sigma^2 - m_N^2)^2\}^{\frac{1}{2}}}.$$

For the $T = \frac{3}{2}$ singlet scattering amplitude, the residue at the pole is given by

$$(A.18) \quad \Gamma = \frac{G_{\Sigma\Sigma} G_{NN}}{4\pi} \left(\frac{m_\pi}{2m_N} \right) \left(\frac{m_\pi}{2m_\Sigma} \right) \cdot \frac{2m_\Sigma m_N}{\{[m_\Sigma^2 + m_N^2 - m_\pi^2]^2 - (m_\Sigma^2 - m_N^2)^2\}^{\frac{1}{2}}} [s_1^+(m_\pi^2)]^{\frac{1}{2}},$$

where the appropriate kinematical factors have been included. It is also to be noted that considered as a function of $\omega = p^2$, the scattering amplitude for $\theta = 90^\circ$ has a pole at $\omega = -\frac{1}{2}m_\pi^2$, the residue γ being given by

$$(A.19) \quad \gamma = \frac{G_{\Sigma\Sigma} G_{NN}}{4\pi} \left(\frac{m_\pi}{2m_N} \right) \left(\frac{m_\pi}{2m_\Sigma} \right) \frac{m_\Sigma m_N}{[s_1^+(m_\pi^2)]^{\frac{1}{2}}}$$

for the $T = \frac{3}{2}$ singlet scattering amplitude $T_{ss}(\omega, 90^\circ)$, which is approxi-

mated by

$$(A.20) \quad T_{ss}(\omega, 90^\circ) = \frac{\exp[i\delta_s] \sin \delta_s}{p},$$

if the 1D , 1G , ... phase shifts are negligible; it is then easy to derive eqs. (20) and (21) by the methods of reference ⁽¹⁴⁾.

The analytic properties of the partial wave amplitudes $A_{TL}(s)$ can also be derived from the representation (A.9) by observing that ⁽¹⁹⁾

$$(A.21) \quad A_{TL}(s) = \frac{1}{2} \int_{-1}^1 A_T(s, \cos \theta) P_L(\cos \theta) d(\cos \theta).$$

Since (A.9) exhibits explicitly the dependence of $A_T(s, \cos \theta)$, this integral may be done by noting that

$$(A.22) \quad \begin{cases} t'_1 - t_1 = D(s)[\Delta_1 - \cos \theta], \\ t'_2 - t_2 = D(s)[\Delta_2 - \cos \theta], \end{cases}$$

where $D(s) = [s^2 - 2s(m_\Sigma^2 + m_N^2) - (m_\Sigma^2 - m_N^2)^2]/2s$, and

$$(A.23) \quad \begin{cases} \Delta_1 = 1 + 2 \frac{st'_1}{s^2 - 2s(m_\Sigma^2 + m_N^2) + (m_\Sigma^2 - m_N^2)^2}, \\ \Delta_2 = 1 + 2 \frac{st'_2 - (m_\Sigma^2 - m_N^2)^2}{s^2 - 2s(m_\Sigma^2 + m_N^2) + (m_\Sigma^2 - m_N^2)^2}, \end{cases}$$

and making use of the well-known integral

$$(A.24) \quad Q_L(\Delta) = \frac{1}{2} \int_{-1}^1 \frac{P_L(\cos \theta)}{\Delta - \cos \theta} d(\cos \theta).$$

The singularities of the partial wave amplitudes $A_{TL}(s)$ in the complex plane are then seen to consist of the three curves C_1 , C_2 , C_3 defined by

$$(A.25) \quad \begin{cases} C_1: & \text{the straight line } s_0 \leq s < \infty, \\ C_2: & \text{the curve } s = s(\Delta_1) \quad (-1 \leq \Delta_1 \leq 1), \\ C_3: & \text{the curve } s = s(\Delta_2) \quad (-1 \leq \Delta_2 \leq 1). \end{cases}$$

⁽¹⁹⁾ The author is indebted to A. KLEIN for suggesting this starting point.

These branch cuts cover the lines L_1 , L_2 , L_3 defined by

$$(A.26) \quad \begin{cases} L_1: & \text{the straight line } s_0 < s < \infty, \\ L_2: & \text{the straight line } -\infty < s \leq s_1, \\ L_3: & \text{the circle } |s| = m_\Sigma^2 - m_N^2, \end{cases}$$

where

$$(A.27) \quad s_1 = m_\Sigma^2 + m_N^2 - \frac{1}{2}m_\pi^2 + \{ (m_\Sigma^2 + m_N^2 - \frac{1}{2}m_\pi^2)^2 - (m_\Sigma^2 - m_N^2)^2 \}^{\frac{1}{2}}.$$

These singularities have also been noted by MACDOWELL for the pion-nucleon partial wave amplitudes (with appropriate modifications in the mass spectrum) ⁽²⁰⁾.

In a practical application to low-energy Σ -nucleon scattering, it is more convenient to consider the amplitude as a function of the variable $\omega = p^2$; if the contributions from K-meson intermediate states are neglected, the singularities of the partial wave amplitudes in the complex ω plane are branch cuts for $-\infty < \omega \leq -\frac{1}{4}m_\pi^2$ and $0 < \omega < \infty$. The procedure of NOYES and WONG ⁽¹⁶⁾ can then be used to obtain an improvement on the effective range formulas by taking the one-pion branch cut into account exactly; the results of reference ⁽¹⁴⁾ and the present note follow if the one-pion branch cut is replaced by a phenomenological pole at $\omega = -\frac{1}{2}m_\pi^2$ ⁽²¹⁾.

⁽²⁰⁾ S. MACDOWELL: *Phys. Rev.*, **116**, 774 (1959).

⁽²¹⁾ H. P. NOYES: private communication. We are indebted to Dr. NOYES for a discussion of this point.

RIASSUNTO (*)

Si presenta una discussione di alcuni aspetti fenomenologici dello scattering dei nucleoni Σ . Si nota che con raggi Σ^+ , che verosimilmente saranno disponibili nel prossimo futuro, esperimenti di scattering triplo sono solo di poco più difficili degli esperimenti di scattering semplice. Si nota un metodo per determinare separatamente gli spostamenti di fase 1S e 3S . Si presenta una discussione delle caratteristiche qualitative dello scattering a bassa energia Σ -nucleone, che si devono avere se l'uno o l'altro dei modelli di simmetria globale $G_{\pi\Sigma} \approx \pm G_{\pi N}$ è valido, e si esamina la possibilità di distinguere fra i due casi, utilizzando la rappresentazione di Mandelstam per l'ampiezza di scattering, alcune conseguenze della quale sono dedotte in appendice. In particolare si deducono le proprietà analitiche delle ampiezze d'onda parziali; si trova che, per la ineguaglianza delle masse del Σ e del nucleone, le singolarità delle ampiezze d'onda parziali non giacciono tutte sull'asse reale nel piano complesso della variabile dell'energia.

(*) Traduzione a cura della Redazione.

LETTERE ALLA REDAZIONE

(La responsabilità scientifica degli scritti inseriti in questa rubrica è completamente lasciata dalla Direzione del periodico ai singoli autori)

Classification of Gravitational Radiation (*).

J. WEBER and D. ZIPOY

University of Maryland - College Park, Md.

(ricevuto il 13 Giugno 1960)

PETROV ⁽¹⁾ proved that by a suitable orientation of the reference tetrad the Riemann tensor may be reduced to one of three canonical forms, in a six dimensional representation. Later PIRANI ⁽²⁾ showed that gravitational radiation is present if the Riemann tensor is of type II or III, but not if it is of type I. It is the purpose of this note to show that all gravitational waves which are locally plane at some given point have a Riemann tensor there which is of canonical form of type II, with both invariants equal to zero.

We introduce a geodesic coordinate system, with pole at the point where the wave is locally plane. Let the x^1 direction be the direction of propagation. The quantities $g_{\mu\nu, \alpha}$ and $g_{\mu\nu, \alpha\beta}$ vanish. With these assumptions, and the use of Einstein's vacuum field equations $R_{\mu\nu} = 0$ it then follows without approximation that in a locally Lorentz frame all components of the Riemann tensor vanish except the following ones

$$(1) \quad \left\{ \begin{array}{lll} R_{1220} = \frac{1}{2} g_{22,10} \\ R_{1020} = -\frac{1}{2} g_{22,00} & R_{1230} = \frac{1}{2} g_{23,10} & R_{1212} = -\frac{1}{2} g_{22,11} \\ R_{2030} = -\frac{1}{2} g_{23,00} & R_{1320} = \frac{1}{2} g_{23,10} & R_{1213} = -\frac{1}{2} g_{23,11} \\ R_{3030} = -\frac{1}{2} g_{33,00} & R_{1330} = \frac{1}{2} g_{33,10} & R_{1313} = -\frac{1}{2} g_{33,11} \end{array} \right.$$

and

$$(2) \quad g_{22,00} + g_{33,00} = 0.$$

(*) Supported by the National Science Foundation.

(1) A. Z. PETROV: *Sci. Not. Kazan State Univ.*, **114**, 55 (1954).

(2) F. A. E. PIRANI: *Phys. Rev.*, **105**, 1089 (1957).

In the six dimensional description the Riemann tensor therefore assumes the form

$$(3) \quad R_{AB} = \begin{vmatrix} 0 & 0 & 0 & 0 & 0 & 0 \\ 0 & -\frac{1}{2}g_{33,11} & \frac{1}{2}g_{23,11} & 0 & -\frac{1}{2}g_{23,10} & -\frac{1}{2}g_{33,10} \\ 0 & \frac{1}{2}g_{23,11} & -\frac{1}{2}g_{22,11} & 0 & \frac{1}{2}g_{22,10} & \frac{1}{2}g_{23,10} \\ 0 & 0 & 0 & 0 & 0 & 0 \\ 0 & -\frac{1}{2}g_{23,10} & \frac{1}{2}g_{22,10} & 0 & -\frac{1}{2}g_{22,00} & -\frac{1}{2}g_{23,00} \\ 0 & -\frac{1}{2}g_{33,10} & \frac{1}{2}g_{23,10} & 0 & -\frac{1}{2}g_{23,00} & -\frac{1}{2}g_{33,00} \end{vmatrix}$$

The terms involving g_{23} may be made to vanish by rotation of axes in the 2, 3 plane. Making use of (2) and noting that $g_{\mu\nu,11} = -g_{\mu\nu,10} = g_{\mu\nu,00}$ then enables (3) to be written

$$(4) \quad R_{AB} = \begin{vmatrix} 0 & 0 & 0 & 0 & 0 & 0 \\ 0 & -\frac{1}{2}g_{33,11} & 0 & 0 & 0 & \frac{1}{2}g_{33,11} \\ 0 & 0 & \frac{1}{2}g_{33,11} & 0 & \frac{1}{2}g_{33,11} & 0 \\ 0 & 0 & 0 & 0 & 0 & 0 \\ 0 & 0 & \frac{1}{2}g_{33,11} & 0 & \frac{1}{2}g_{33,11} & 0 \\ 0 & \frac{1}{2}g_{33,11} & 0 & 0 & 0 & -\frac{1}{2}g_{33,11} \end{vmatrix}$$

Comparing (4) with Petrov's canonical forms⁽²⁾ shows that (4) is of type II with $\alpha = \beta = 0$, $\sigma = g_{33,11}$. We may conclude that (4) is valid asymptotically for the gravitational radiation from all physical systems which are not cosmologically large.

We emphasize that these relations follow without approximation, from the assumption that the waves are locally plane. This argument shows that any type III solutions always must become vanishingly small compared with the type II part whenever the wave approaches planeness in some given region.

For weak radiation fields, with second derivatives of $g_{\mu\nu}$ going to zero as $1/r$, TRAUTMAN concluded that the Riemann tensor is also Petrov type II. Our result is somewhat different from that of Trautman since the requirement of local planeness does not necessarily imply weak fields in the $1/r$ zone.

(2) A. TRAUTMAN: *Bull. Acad. Sci. Polon.*, **6**, 407 (1958).

$\pi\pi$ Interaction in Peripheral πN Collisions.

D. I. BLOHINČEV

Joint Institute for Nuclear Research - Moscow

(ricevuto il 18 Luglio 1960)

New experimental data on inelastic πN interaction (the momentum of primary pions being about 7 GeV/c⁽¹⁾) make it possible to apply the nucleon model described earlier in (2) for a more fundamental estimation of $\pi\pi$ interaction.

As the latest calculations show (3), the contribution of $\pi\pi$ interaction to elastic $\pi\pi$ scattering at the pion energy of (5÷6) GeV/c is not great. Therefore, the accuracy of determining $\pi\pi$ interaction from elastic πN scattering is extremely low.

Further, it should be noted, that since π -mesons are pseudoscalar, the nuclear charge of nucleons g is equal to the nuclear charge of antinucleons \bar{g} (in case of scalar interaction they would be opposite). Therefore, in the pion dissociation $\pi \rightleftharpoons N + \bar{N}$ the nuclear monopole (but not a dipole) is formed, and the interaction between this virtual pair and a π -meson must be quite comparable with πN or $\pi\bar{N}$ interactions. In view of this, an estimate of the cross section

for $\pi\pi$ interaction made by us beforehand (2) gives only the lower limit.

The contribution of $\pi\pi$ interaction to inelastic πN scattering accompanied by meson production turns out to be not small (cfr. (3)). Therefore, this scattering may be more successfully used for the determination of $\pi\pi$ interaction.

The density of charged π -mesons in the single-pion region $r > \hbar/mc$ (r is the distance from the nucleon centre, m is the pion mass) in the nucleon model described in (2) may be approximated by the formula

$$(1) \quad n(r) = \frac{0.15}{4\pi} \left(\frac{mc}{\hbar} \right)^3 \sqrt{\frac{6}{2\xi + 4}} \frac{\exp[-2(\xi - 1)]}{\xi^2},$$

where $\xi = r/(\hbar/mc)$. The absorption coefficient of pions, the collision parameter being $b > \hbar/mc$, will be equal to

$$k(r) = \frac{3}{2} (r) \sigma_{\pi\pi},$$

where $\sigma_{\pi\pi}$ is the cross section for pion-pion interaction, the factor $\frac{3}{2}$ takes into account neutral mesons.

The partial cross section for the pion

(1) V. A. BELYAKOV, WANG SHU-FENG *et al.*: *JINR* (Dubna, in print).

(2) D. I. BLOKHINTSEV, B. M. BARBASEV and V. S. BARASENKOV: *Nuovo Cimento*, **10**, 602 (1959).

(3) WANG ZHUNG: *JINR* (Dubna, in print.)

interaction with a nucleon may be written as $2\pi b \, db \, \zeta(b)$, where $\zeta(b)$ is the pion absorption coefficient along the path corresponding to the collision parameter b . As $k(r)$ is small in the peripheral region (in the «atmosphere») of a nucleon

$$(2) \quad \zeta(b) = \int k(r) \, dS,$$

where S is integrated over the pion path corresponding to the collision parameter b . The total cross section for the peripheral collision ($b > \hbar/mc$) is equal to

$$\sigma_p = 2\pi \int_{\hbar/mc}^{\infty} b \, db \, \zeta(b).$$

A numerical calculation of this integral under different assumptions on the cross section $\sigma_{\pi\pi}$ yielded the following data:

$\sigma_{\pi\pi}$	10 mb	25 mb	50 mb
σ_p	0.14 mb	0.35 mb	0.70 mb

On the other hand, from the data of (1) the cross sections for the processes $\pi^- + p \rightarrow p' + \pi' + \pi'' + \dots$ when the momentum transfer ($p_1 < mc$) and the kinetic energy transfer ($\Delta T < mc^2$) are small, is

$$\sigma_{\pi^- + p \rightarrow p' + \pi' + \pi'' + \dots} = (1.3 \pm 0.5) \text{ mb}.$$

However, it is impossible to distinguish experimentally the processes with an even number of pions $\pi' + \pi'' + \dots$ from those with an odd number. According to the average multiplicity of neutral mesons $r_0 = 1$ one can draw the conclusion that the cross section for the peripheral processes ($p_1 < mc$, $\Delta T < mc^2$) for the production of an even number of pions will be

$$\sigma_{\pi^- + p \rightarrow p' + \pi' + \pi'' + (\text{ret})} = (0.7 \pm 0.7) \text{ mb}.$$

The statistical error is found to be large ($\sim 100\%$). This cross section may be identified with the cross section σ_p we

calculated for the peripheral processes taking place when the collision parameter is greater than $b > \hbar/mc$.

Comparing the experimental cross section with the table for σ_p , we see that the mean value of $\sigma_{\pi\pi}$ is 50 mb (with a statistical error $\pm 100\%$).

Note that under the same conditions the total cross section $\sigma_{\pi N}$ is equal to 26 mb. Therefore, the peripheral processes, with the collision parameter $b > \hbar/mc$, are only a small part of all the processes. This result, by the way, is quite obvious, if one looks at the curve showing the distribution of a pion charge in a nucleon as calculated in (2).

The same result points out that the central regions of a nucleon $r < \hbar/mc$ are very opaque. Indeed, it is easy to see from the data on the total cross section $\sigma_{\pi N}$ and from the data for σ_p that the mean absorption coefficient \mathcal{E} for the collision parameters $b < \hbar/mc$ is equal to 0.4. On the other hand, in the region $r \simeq 0.3(\hbar/mc)$ (the region of the maximum of the pion cloud density) this coefficient is close to 1, i.e., the total absorption.

This result is in agreement with the idea about an opaque kernel of a nucleon as is obtained from the optical model (cf. (2,4)).

The position of the maximum of the pion density is also in agreement with the mean transverse momentum P_{\perp} transferred to the nucleon. It is P_{\perp} which is equal to 370 MeV/c, while the corresponding dimension is

$$b = 0.4 \cdot 10^{-13} \text{ cm} = 0.3 \frac{\hbar}{mc}.$$

Thus, one must consider that for the processes of pion-nucleon interaction the region of the pion cloud spreading from $0.3(\hbar/mc)$ to \hbar/mc is important.

(*) D. I. BLOHINČEV, V. S. BARAŠENKOV and V. G. GRISIN: *Nuovo Cimento*, **9**, 249 (1958).

(*) The author expresses his gratitude to R. M. LEBEDEV, V. PETRŽILKA and K. D. TOLSTOV *et al.* (1) for presenting the data and discussions.

(Σ^0, Λ^0) **Relative Parity and the Dalitz Decay of the Σ^0 Hyperon (*)**.

J. SUCHER and G. A. SNOW

Department of Physics, University of Maryland - College Park

(ricevuto il 5 Agosto 1960)

The determination of the relative parity, \mathcal{P} , of the Σ^0 and Λ^0 hyperon is of considerable interest. FEINBERG⁽¹⁾ has shown that the branching ratio of the Dalitz decay, $\Sigma^0 \rightarrow \Lambda^0 + e^+ + e^-$, to the ordinary decay, $\Sigma^0 \rightarrow \Lambda^0 + \gamma$, depends on the value of \mathcal{P} , being 1/184 for even ($\mathcal{P} = +1$) and 1/165 for odd ($\mathcal{P} = -1$) relative parity. It is the purpose of this note to point out that if a reaction can be found in which polarized Σ^0 hyperons are produced, then the angular correlation between the spin of the Λ^0 and the plane of the electron-positron pair in the Σ^0 Dalitz decay is very sensitive to the value of \mathcal{P} . The spin direction of the Λ^0 may be determined from the asymmetry⁽²⁾ in the angular distribution of the decay pion from $\Lambda^0 \rightarrow p + \pi^-$.

The effective interaction responsible for the ordinary Σ^0 decay is taken to be⁽³⁾ $H' = g \bar{\psi}_{\Lambda^0} \sigma_{\mu\nu} \psi_{\Sigma^0} F^{\mu\nu}$ for $\mathcal{P} = +1$, and $H' = g' \bar{\psi}_{\Lambda^0} \gamma_5 \sigma_{\mu\nu} \psi_{\Sigma^0} F^{\mu\nu}$ for $\mathcal{P} = -1$. Consider a Σ^0 in its rest frame with its spin in the direction of the unit vector \mathbf{n} . The square of the matrix element for the decay $\Sigma^0 \rightarrow \Lambda^0 + e^+ + e^-$, summed over the electron spins, with the Λ^0 spin in the direction \mathbf{n}' , has the form

$$I = (1/k^2)^2 (F + \mathbf{G} \cdot \mathbf{n}'),$$

up to a constant factor. Here k is the sum of the electron and positron four-momenta: $k = p_+ + p_- = (E_+ + E_-, \mathbf{p}_+ + \mathbf{p}_-) = (k_0, \mathbf{k})$, with $k^2 = k_0^2 - \mathbf{k}^2$. The scalar F and the vector \mathbf{G} are given, in the case of even relative parity, by⁽⁴⁾

$$(1+) \quad \left\{ \begin{aligned} F_e &= \frac{1}{2} k^2 (\mathbf{k}^2 + q_0^2) + 2m^2 \mathbf{k}^2, \\ G_e &= \left[\frac{1}{2} k^2 (-\mathbf{k}^2 + q_0^2) + 2m^2 \mathbf{k}^2 \right] \mathbf{n} + \left[k^2 (q_0^2 - 4m^2) \mathbf{n} \cdot \hat{\mathbf{k}} - k^2 q^2 \hat{\mathbf{k}} \cdot \hat{\mathbf{q}} \mathbf{n} \cdot \hat{\mathbf{q}} \right] \hat{\mathbf{k}} + \\ &\quad + \left[-k^2 q^2 \hat{\mathbf{k}} \cdot \hat{\mathbf{q}} \mathbf{n} \cdot \hat{\mathbf{k}} + k^2 q^2 \mathbf{n} \cdot \hat{\mathbf{q}} \right] \hat{\mathbf{q}}, \end{aligned} \right.$$

(*) Supported in part by the United States Air Force and by the United States Atomic Energy Commission.

(1) G. FEINBERG: *Phys. Rev.*, **109**, 1019 (1958). See also G. FELDMAN and T. FULTON: *Nucl. Phys.*, **8**, 106 (1958).

(2) Summary by D. A. GLASER: *Proc. of Ninth Conference on High Energy Nuclear Physics* (Kiev, 1959), unpublished.

(3) We make the same assumptions as in ref.⁽¹⁾ regarding structure dependent effects.

(4) In eqs. (1±) terms proportional to the Λ^0 velocity have been dropped, since $|\mathbf{k}/M_\Lambda| < .07$.

where $q = p_+ - p_- = (E_+ - E_-, \mathbf{p}_+ - \mathbf{p}_-) = (q_0, \mathbf{q})$, $\hat{\mathbf{k}} = \mathbf{k}/|\mathbf{k}|$, $\hat{\mathbf{q}} = \mathbf{q}/|\mathbf{q}|$, and m is the electron mass. In the case of odd relative parity one finds

$$(1) \quad \begin{cases} F_0 = \frac{1}{2} k^2 (k_0^2 + k^2 + q_0^2) + 2m^2 k_0^2, \\ \mathbf{G}_0 = \left[\frac{1}{2} k^2 (k^2 + q_0^2) + 2m^2 k_0^2 \right] \mathbf{n} - [k^2 (q_0^2 + k^2) \mathbf{n} \cdot \hat{\mathbf{k}} + k^2 q^2 \hat{\mathbf{k}} \cdot \hat{\mathbf{q}} \mathbf{n} \cdot \hat{\mathbf{q}}] \hat{\mathbf{k}} - \\ \quad - [-k^2 q^2 \hat{\mathbf{k}} \cdot \hat{\mathbf{q}} \mathbf{n} \cdot \hat{\mathbf{k}} + k_0^2 q^2 \mathbf{n} \cdot \hat{\mathbf{q}}] \hat{\mathbf{q}}. \end{cases}$$

The polarization \mathbf{P} of the Λ^0 is given by $\mathbf{P} = \mathbf{G}/F$. If the Σ^0 is polarized only partially, the symbol \mathbf{n} in eqs. (1 \pm) must be interpreted as the polarization of the Σ^0 , as we shall do henceforth.

The nature of the above results is greatly clarified by a consideration of the special case of equal electron-positron energies: $E_+ = E_- = E$. Then one finds, on neglecting m/E ($\approx .013$ for Σ^0 decay) relative to unity, and for $3(m/E) \leq \sin(\theta/2) \leq 1/3$, where θ is the angle between \mathbf{p}_+ and \mathbf{p}_- ,

$$(2+) \quad \mathbf{P}_e \approx \mathbf{n} + 2(\mathbf{n} \cdot \hat{\mathbf{q}}) \hat{\mathbf{q}},$$

$$(2-) \quad \mathbf{P}_o \approx \mathbf{n} + 2(\mathbf{n} \cdot \hat{\mathbf{k}} \cdot \hat{\mathbf{q}}) \hat{\mathbf{k}} \cdot \hat{\mathbf{q}}.$$

In eq. (2 $-$), the identity $(\mathbf{n} \cdot \hat{\mathbf{k}} \times \hat{\mathbf{q}}) \hat{\mathbf{k}} \times \hat{\mathbf{q}} = \mathbf{n} - (\mathbf{n} \cdot \hat{\mathbf{k}}) \hat{\mathbf{k}} - (\mathbf{n} \cdot \hat{\mathbf{q}}) \hat{\mathbf{q}}$ has been used. These equations may be compared with the corresponding ones for photon emission studied by GATTO⁽⁵⁾, in which case

$$(3+) \quad \mathbf{P}_e = -\mathbf{n} + 2(\mathbf{n} \cdot \hat{\mathbf{k}} \times \mathbf{e})(\hat{\mathbf{k}} \times \mathbf{e}),$$

$$(3-) \quad \mathbf{P}_o = -\mathbf{n} + 2(\mathbf{n} \cdot \mathbf{e}) \mathbf{e},$$

where \mathbf{e} denotes the polarization vector of the photon and $\hat{\mathbf{k}}$ is its direction of motion, with $\mathbf{e} \cdot \hat{\mathbf{k}} = 0$. Since $\mathbf{q} \cdot \mathbf{k} = E_+^2 - E_-^2$, we have $\hat{\mathbf{q}} \cdot \hat{\mathbf{k}} = 0$ when $E_+ = E_-$, so that the vector $\hat{\mathbf{q}}$ is quite analogous to the photon polarization, in our special case. The fact that the formulas for $\mathcal{P} = +1$ and $\mathcal{P} = -1$ are switched in going from the photon to the pair is related to the pseudo-scalar nature of an electron-positron pair.

It can be seen from eqs. (2 \pm) that in the region where these equations are valid there will be a substantial difference between \mathbf{P}_e and \mathbf{P}_o as long as $|\mathbf{n} \cdot \hat{\mathbf{k}}| \ll 1$. In particular, if the pair is produced in a plane perpendicular to \mathbf{n} , we get simply

$$(4) \quad \mathbf{P}_e \approx -\mathbf{n}, \quad \mathbf{P}_o \approx +\mathbf{n}.$$

Thus, in this case, there is a maximum difference between \mathbf{P}_e and \mathbf{P}_o , if the Σ^0 is polarized. Only the sense of the up-down asymmetry of the Λ^0 decay pion relative to the plane of the Σ^0 Dalitz decay need then be determined, provided the direction of the polarization of the Σ^0 is known. This direction can, however, be inferred from the pion asymmetry in the ordinary Σ^0 decay, since, on averaging over \mathbf{e} and $\hat{\mathbf{k}}$ in eqs. (3 \pm), the polarization of the Λ^0 is given by $\mathbf{P} = -\frac{1}{3} \mathbf{n}$ for either case of relative parity.⁽⁵⁾

(5) R. GATTO: *Phys. Rev.*, **109**, 610 (1958).

In the more general case, where $E_+ \neq E_-$, $\theta \geq 5^\circ$, but still $k^2/k_0^2 \approx 1$, one finds $F_e \approx F_o$. These less stringent conditions on \mathbf{p}_+ and \mathbf{p}_- are expected to be satisfied for the bulk of the events $\Sigma^0 \rightarrow \Lambda^0 + e^+ + e^-$. From eqs. (1 \pm) it follows that, if also $|\mathbf{n} \cdot \hat{\mathbf{k}}| \ll 1$, then $\mathbf{G}_e \approx -\mathbf{G}_o$, so that still $\mathbf{P}_e \approx -\mathbf{P}_o$. Further inspection of eqs. (1 \pm) indicates that \mathbf{P}_e and \mathbf{P}_o will in general differ substantially even if the restriction $|\mathbf{n} \cdot \hat{\mathbf{k}}| \ll 1$ is removed.

In conclusion, since the branching ratio for the Dalitz decay of the Σ^0 is quite small, the determination of the (Σ^0, Λ^0) relative parity via these decays is clearly difficult. However, if a two-body Σ^0 production reaction can be found in which the Σ^0 is appreciably polarized, then the analysis of ~ 100 Dalitz decay events should provide an unambiguous determination of \mathcal{P} . Except for the Σ^0 polarization requirement, which could of course be a serious drawback, the analysis described above would be a more reliable way of establishing the relative parity than the determination of the absolute branching ratio ⁽¹⁾. Finally, it is clear from eqs. (3 \pm) that measurement of the polarization direction of the photon in ordinary Σ^0 decay (from a polarized Σ^0) could also determinate the (Σ^0, Λ^0) relative parity ⁽⁵⁾.

* * *

One of us (G.A.S.) would like to thank A. ROSENFELD and W. WADA for useful discussions.

The Influence of a Possible Pion-Pion Interaction on the Photoproduction of Charged Pions.

B. DE TOLLIS, E. FERRARI and H. MUNCZEK (*)

Istituto di Fisica dell'Università - Roma

Istituto Nazionale di Fisica Nucleare - Sezione di Roma

(ricevuto il 16 Agosto 1960)

As is well known, the experimental evidence for photoproduction of charged pions is not in very good agreement with the prediction of the theory. The formulae derived on the basis of the dispersion relation approach by CHEW, GOLDBERGER, Low and NAMBU (1), and subsequently slightly modified and calculated numerically by ROBINSON (2) give the right order of magnitude of the cross section for positive pions, at 90° in the c.m.s., but not the correct behaviour as a function of energy. The disagreement is stronger at energies near the resonance (300 MeV); at low energies, recent experimental results (3) seem to show a better agreement with the theory. The most serious discrepancy between theory and experiment is given however by the π^-/π^+ ratio at 90° , which is slowly but steadily decreasing with the energy while the theory predicts a nearly constant value.

In this paper we will show that the theoretical predictions on the π^-/π^+ ratio at 90° can be brought in better agreement with experiment by taking into account the presence of a possible pion-pion interaction, which has been already investigated by several authors (4). This interaction is supposed to take place in a resonant $T=1$, $J=1$ state. Starting from the Mandelstam representation, CINI and FUBINI

(*) On leave of absence from Facultad de Ciencias Exactas and Comision Nacional de la Energia Atomica, Buenos Aires, Argentina, with a grant from « Universidad Nacional de Buenos Aires ».

(1) G. F. CHEW, M. L. GOLDBERGER, F. E. Low and Y. NAMBU: *Phys. Rev.*, **106**, 1345 (1957).

(2) C. ROBINSON: *Tables of Cross-Sections for π^+ -Production from Hydrogen, according to the theory of CHEW, GOLDBERGER, Low and NAMBU*; University of Illinois report (May 22, 1959). Hereafter the results contained in this paper will be referred to as CGLNR.

(3) See for example G. BERNARDINI: *Kiev Conference Report on Pion Photoproduction and Compton Effect on Nucleon*, unpublished (1959), in particular Fig. 14, whose data are reported in our Fig. 3.

(4) The influence of the pion-pion interaction on pion-nucleon scattering has been investigated by W. R. FRAZER and J. R. FULCO: *Phys. Rev. Lett.*, **2**, 365 (1959); *Phys. Rev.*, **117**, 1603, 1609 (1960); J. BOWCOCK, N. N. COTTINGHAM and D. LURIE: *Nuovo Cimento*, **16**, 918 (1960). The last paper contains further reference on the subject.

have shown ⁽⁵⁾ that an approximate one-dimensional representation can be written for the scattering matrix at sufficiently low energies in which the lowest angular momentum contributions are taken into account for all the three reactions described by the same invariant amplitude. Pion-pion interaction leads in this approximate representation to a branch-cut in the momentum transfer variable of photoproduction from $4\mu^2$ to ∞ . If the interaction is strong enough as to lead to a sharp resonance the cut can be replaced by a pole at the value of the resonance energy of the channel nucleon-antinucleon giving one photon and one pion. In such a case the effect of the $J=1$, $T=1$ pion-pion resonance is simply to add to the expression of the scattering amplitude of CLGNR a contribution of the form of the lowest order perturbation term with an intermediate « particle » of spin 1 and isotopic spin 1. This property has been fully discussed in ⁽⁴⁾, ⁽⁵⁾ and we take it here as demonstrated ⁽⁶⁾. We therefore calculate here the contribution of the graph shown in Fig. 1.

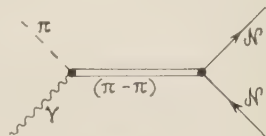


Fig. 1.

The form of the corresponding matrix element is fixed by invariance and parity requirements, and by the spin properties of the intermediate « particle ».

We write the contribution S'_β (β is the isotopic spin index) to the total S -matrix element as:

$$(1) \quad S'_\beta = i(2\pi)^4 \delta_4(p_1 + k - p_2 - q) \frac{1}{\sqrt{4k_0 \omega E_1 E_2}} \bar{u}(p_2) \mathcal{M} u(p_1) \tau_\beta,$$

with

$$(2) \quad \mathcal{M} = \frac{8\pi A}{(p_2 - p_1)^2 + (4\mu)^2} \left[i\gamma_\mu - \frac{\mu'_n - \mu_p}{2M} \frac{\gamma_\mu \gamma_\nu - \gamma_\nu \gamma_\mu}{2} (p_2 - p_1)_\nu \right] \varepsilon_{\mu\nu\lambda\varrho} k_\nu e_\lambda q_\varrho,$$

where k , q , p_1 , p_2 are the 4-momenta of the photon, pion, initial and final nucleon respectively; k_0 , ω , E_1 , E_2 the corresponding energies; e is the polarization vector of the photon; μ'_p and μ_n are the anomalous magnetic moments of proton and neutron, M =nucleon mass, μ =pion mass. The « mass » of the resonant state is assumed to be $\sim 4\mu$. The value $(\mu'_p - \mu_n)/2M$ for the ratio between the « electric » and « magnetic » interaction is suggested from comparison with the corresponding electromagnetic vertex (see ref. ⁽⁴⁾ for an analogous treatment). The constant A is proportional to the « strength » of the photon-three pion interaction. The contribution (2), written in terms of the invariants M_A , M_B , M_C , M_D defined in ⁽¹⁾ reads

$$(3) \quad \mathcal{M} = \frac{8\pi A}{(p_2 - p_1)^2 + (4\mu)^2} \left[M_D - \frac{\mu'_p - \mu_n}{2M} \{ M_A(2q \cdot k + \mu^2) - M_B \} \right].$$

In order to carry out the calculation, one has simply to sum the coefficients of the invariants appearing in (3) to the corresponding four amplitudes $A^{(0)}$, $B^{(0)}$, $C^{(0)}$, $D^{(0)}$ defined in ref. ⁽¹⁾. Since \mathcal{M} does not depend explicitly on the phase-shifts, it has to be multiplied also by a recoil factor $(1 + \omega/M)^{-1}$. We want to take into account also another effect which can influence the expression of the total matrix element. As it has already been pointed out in ^(4,5), the high energy region should

⁽⁵⁾ M. CINI and S. FUBINI: *Ann. Phys.*, **3**, 352 (1960).

⁽⁶⁾ This has been confirmed by the work of M. GOURDIN, D. LURIE and A. MARTIN: *Effect of a Pion-Pion Scattering Resonance on Low Energy Meson Photoproduction*, to be published in *Nuovo Cimento*.

contribute approximately an additive constant to those invariant amplitudes which are even in the variable ν , that is $A^{(0)}$, $B^{(0)}$, $C^{(-)}$ and $D^{(0)}$. Neglecting such constants amounts to assuming specific properties of the integrands at high energies. We shall then replace the invariant coefficient $A^{(0)}$ with $A^{(0)} + 8\pi a$ throughout and do the same for $B^{(0)}$, $C^{(-)}$ and $D^{(0)}$; we shall consider the four constants a , b , c , d , as well as the strength Λ , as adjustable parameters, trying however to fit the data with the least number of them. One finds that at 90° the influence of b and d can be safely neglected, and the other constants can be taken as real ⁽⁷⁾.

Some of the invariant amplitudes of the CGLNR formula contain the s -wave and the small p -wave phase shifts of the pion-nucleon scattering. In ref. ⁽²⁾ a linear dependence on the momentum for the s -phase shifts, and an effective range formula for the p -phase shifts have been assumed. We preferred to use for the s - and small p -phase shift the experimental results directly ⁽⁸⁾. In spite of the very large errors which affect some of the data used, one finds values which are remarkably different from the ones used in ref. ⁽²⁾, especially at higher energies. A better approximation than the effective range formula for the small p -phase shifts could be obtained by putting all of them equal to zero.

After carrying out the calculations, one finds:

1) The introduction of the pion-pion interaction Λ gives the required decreasing behaviour of the ratio. The decrease is more rapid near 300 MeV, as an effect of the resonant 33-phase shift, which shows also in the original CGLNR curve (curve A in Fig. 2). The introduction of the constant Λ alone gives a decrease

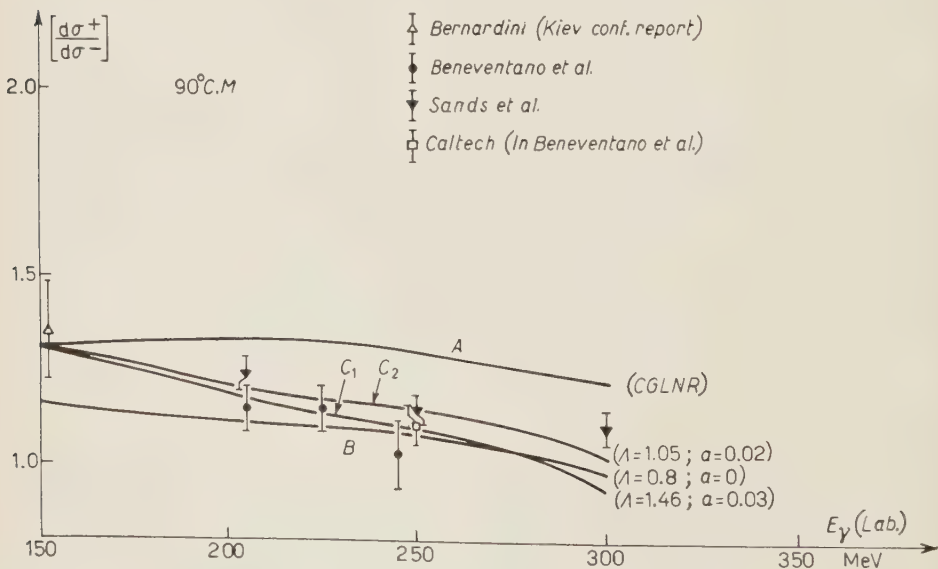


Fig. 2.

⁽⁷⁾ Another parameter which should be considered is the s -wave contribution $N^{(-)}$, defined in ref. ⁽¹⁾. Usually this constant is put equal to zero: a rough evaluation however is possible, and gives for $\omega^2 N^{(-)}$ a nearly constant value, about 0.06. When the constant c is considered, any variation of $\omega^2 N^{(-)}$ can be practically absorbed into a corresponding variation of c , so that the preceding estimate can be taken as reliable.

⁽⁸⁾ We thank Dr. C. PELLEGRINI for his help in the collection of these data.

too slow to fit all the experimental points well (curve *B* in Fig. 2). A better result is obtained by taking a small negative value for *a*. Curves *C*₁ and *C*₂ refer to two of the possible choices of *A* and *a*. The first one fits the experimental data of BENEVENTANO *et al.* ⁽⁹⁾ (obtained with the emulsion technique up to 250 MeV). The second one considers also the experimental data of SANDS *et al.* ⁽¹⁰⁾ (obtained with counters). The ratio is rather insensitive to *c* and *N*⁽⁻⁾, and to the variations within the errors of the small *p*-phase shifts: on the other hand, if *A*=0 no choice of the other constants gives the correct result.

2) As far the π^+ -distribution at 90° is concerned (we consider the coefficient a_0^+ defined in ref. ⁽⁹⁾ and ⁽³⁾) we see that the behaviour of this curve is substantially unaltered by the new constants introduced: only the magnitude is affected, and with a convenient choice for the constant *c* it can be normalized at any value: in particular one can reproduce the original CGLNR curve up to 300 MeV. A modification of this behaviour can be obtained by altering the values of the parameter *f*²

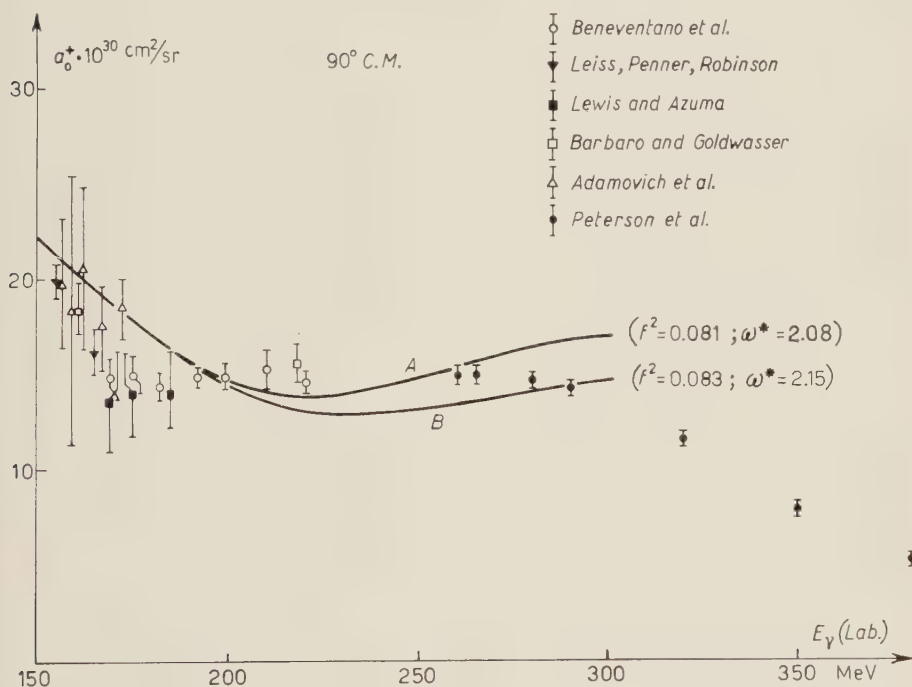


Fig. 3.

and ω^* of the resonant 33-phase shift: curves *A* and *B* in Fig. 3 are calculated for the values $f^2=0.081$, $\omega^*=2.08$ (as in ref. ⁽²⁾) and $f^2=0.083$, $\omega^*=2.15$ (as in ref. ⁽³⁾). The variation of these parameters does not influence the π^-/π^+ ratio.

⁽⁹⁾ M. BENEVENTANO, G. BERNARDINI, G. STOPPINI and L. TAU: *Nuovo Cimento*, **10**, 1109 (1958).

⁽¹⁰⁾ M. SANDS, J. G. TEASDALE and R. L. WALKER: *Phys. Rev.*, **95**, 592 (1954). The same data are reported again in G. NEUGEBAUER, W. O. WALES and R. L. WALKER: *Phys. Rev. Lett.*, **2**, 429 (1959).

No one of these choices, however, is fully satisfactory in the whole range of energy considered (up to $(300 \div 350)$ MeV): on the other hand, one can think that the situation is not made worse with respect to the one without the corrections considered in this paper. More detailed work on the same subject at other angles and on critical examination of the role of the constants introduced will be done later.

* * *

We thank Prof. M. CINI for constant advice and helpful suggestions. We thank also Proff. M. BENEVENTANO, L. ODIAN and G. STOPPINI for clarifying discussions on the experimental aspect of the problem.

On a Contradiction between Experimental Results on Nucleon Form Factors and Certain Symmetries of Strong Interactions.

PH. MEYER (*) and J. PRENTKI

CERN - Geneva

(ricevuto il 27 Agosto 1960)

A number of consequences of the symmetries of strong interactions on the electromagnetic properties of hyperons have been deduced previously ^(1,5). The main object of this note is to point out that in some of the symmetrical theories of strong interactions that have been proposed, the contribution of the pion intermediate states to the isoscalar electromagnetic form factors of nucleons and hyperons vanishes at all orders in the strong interactions. This is a consequence of a known theorem ^(2,6) proved under symmetry assumptions which will be specified later on.

Let us write the hamiltonian of strong and electromagnetic interactions as

$$(1) \quad H_{\text{strong}} = g_1 \bar{N} \boldsymbol{\tau} N \boldsymbol{\pi} + g_4 \bar{\Xi} \boldsymbol{\tau} \Xi \boldsymbol{\pi} + g_2 \bar{\Lambda} \boldsymbol{\Sigma} \boldsymbol{\pi} + g_3 \bar{\Sigma} \boldsymbol{T} \Sigma \boldsymbol{\pi} + g_5 \bar{\Lambda} K + \\ + g_6 \bar{N} \boldsymbol{\tau} \Sigma K + g_7 \bar{\Xi} \Lambda K + g_8 \bar{\Xi} \boldsymbol{\tau} \Sigma K + \text{h.c.},$$

$$(2) \quad H_{\text{em}} = j_\mu A_\mu + J A_\mu^2 = ie[\frac{1}{2} \bar{N} \gamma_\mu (1 + \tau_3) N + \frac{1}{2} \bar{\Xi} \gamma_\mu (\tau_3 - 1) \Xi + \\ + \bar{\Sigma} \gamma_\mu T_3 \Sigma + \frac{1}{2} \bar{K} (1 + \tau_3) \partial_\mu K - \frac{1}{2} (\partial_\mu K) (1 + \tau_3) K + \pi T_3 \partial_\mu \pi] A_\mu + \\ + e^2 [\frac{1}{2} \bar{K} (1 + \tau_3) K + \pi T_3^2 \pi] A_\mu^2,$$

N , Ξ , K denote the isotopic spinors of the corresponding fields, $\boldsymbol{\Sigma}$ and $\boldsymbol{\pi}$ are isotopic vectors, $\bar{K} \equiv i\tau_2 K$, T_3 is the third component of the isotopic spin-one matrix. In (1) the appropriate γ_5 have been omitted and (2) is to be understood as properly symmetrized.

We shall assume that the strong interactions have the N - Ξ symmetry. In

(*) On leave from Université de Bordeaux and Faculté des Sciences, Orsay.

(1) D. C. PEASLEE: *Nuovo Cimento*, **6**, 1 (1957).

(2) M. GELL-MANN: *Annual International Conference on High Energy Physics at CERN* (1958), edited by B. FERRETTI (CERN, Geneva, 1958).

(3) G. FEINBERG and R. E. BEHREND: *Phys. Rev.*, **115**, 745 (1959).

(4) K. TANAKA: preprint.

(5) G. FEINBERG: preprint.

(6) R. PUGH: *Phys. Rev.*, **109**, 989 (1958).

this scheme, specially considered by SALAM and POLKINGHORNE (⁷), N and Ξ fields are coupled in a symmetrical way to π 's and K 's, and the $N - \Xi$ mass difference is neglected:

$$(3) \quad g_1 = g_4, \quad g_5 = \pm g_7, \quad g_6 = \pm g_8, \quad m_N = m_\Xi.$$

The theorem of interest whose consequences shall be studied can be stated as follows: if the strong interactions have the $N - \Xi$ symmetry the transition amplitude between states containing only pions, photons, and K -mesons vanishes at all orders of the strong and electromagnetic interactions for a process in which the sum of the total number of initial and final pions involved is odd.

For completeness we shall sketch the proof. Let us define the transformation $U = GV$ where $G = C \exp[i\pi T_2]$ is the product of a charge conjugation and a rotation of π around the 2nd axis in isotopic spin space and where V is the transformation,

$$(4) \quad V: \begin{cases} N \rightarrow \Xi, & K \rightarrow \bar{K}, \\ \Xi \rightarrow -N, & \bar{K} \rightarrow -K. \end{cases}$$

The combined transformation U is then given by

$$(5) \quad U: \begin{cases} N \rightarrow G\Xi, & \Sigma \rightarrow G\Sigma, & \pi \rightarrow G\pi = -\pi, \\ \Xi \rightarrow -GN, & A \rightarrow GA, & K \rightarrow G\bar{K} = -K, \\ & & A_\mu \rightarrow A_\mu. \end{cases}$$

It can be easily seen that H_{strong} is separately invariant under G (from assumed charge independence) and under V (from relations (3) between the coupling constants). On the other hand H_{em} is invariant only under the combined transformation U , the isotopic scalar part of j_μ and the isotopic vector part of J both changing sign under G and under V . We therefore conclude that the complete hamiltonian is invariant under the transformation U if $N - \Xi$ symmetry is assumed (*). The theorem stated above then follows immediately from relation (5) (**). It is obvious that if the theorem holds for the $N - \Xi$ symmetry it holds a fortiori for global symmetry in which $g_1 = g_2 = g_3 = g_4$, and K interactions are neglected.

One consequence of the above theorem is that in a theory which has the $N - \Xi$ symmetry or the global symmetry the $\pi^0 \rightarrow 2\gamma$ decay is forbidden (^{3,6}). However the fact that π^0 does decay is not so strong a statement against the usefulness of the proposed symmetries since a break in the symmetry, which we know must exist from the $N - \Xi$ mass difference, will allow the decay. Nevertheless it points to the fact that in π^0 decay each graph which contains a $N - \bar{N}$ loop is partially suppressed by the corresponding $\Xi - \bar{\Xi}$ loop. Therefore it might not be meaningless to calculate π^0 decay in lowest order perturbation taking into account the hyperons (^{8,9}).

(⁷) A. SALAM and J. C. POLKINGHORNE: *Nuovo Cimento*, **2**, 685 (1955).

(*) Note that if we have the minus sign in relations (3) then invariance is obtained if the sign is exchanged in the $N - \Xi$ transformations (4) and (5).

(**) K -mesons can be included in initial and final states because conservation of strangeness requires the total number to be even.

(⁸) T. KINOSHITA: *Phys. Rev.*, **94**, 1384 (1954).

(⁹) J. TIOMNO: *Nuovo Cimento*, **6**, 256 (1957).

One then gets for the π^0 life time

$$(6) \quad \frac{1}{\tau} = \left(\frac{\alpha}{4\pi}\right)^2 \left(\frac{g_1^2}{4\pi\hbar c}\right) \left(\frac{\mu c^2}{\hbar}\right) \left(\frac{\mu}{M_N} - \frac{\mu}{M_{\Xi}} \frac{g_4}{g_1}\right)^2,$$

or

$$(7) \quad \tau = \tau_0 \left[\frac{M_{\Xi}}{M_{\Xi} - M_N(g_4/g_1)} \right]^2,$$

where τ_0 is the perturbation result, neglecting the Ξ . If one takes $g_4 = g_1$, τ is increased over τ_0 by a factor 12. With $g_1^2/4\pi\hbar c = 13$ this gives for the lifetime $\tau \approx 6 \cdot 10^{-16}$ s which, considering the crude approximations, is still compatible with the present experimental upper limit on the π^0 lifetime ⁽¹⁰⁾.

Another consequence of the stated theorem concerns the isotopic scalar electromagnetic form factors of the baryons. If the N - Ξ or global symmetry holds, the vertex formed with one photon line and an odd number of pion lines vanishes. On the other hand it is known from G invariance ⁽¹¹⁾ that the intermediate pion states with an even number of pions contribute to the isovector form factors, and those with an odd number of pions contribute to the isoscalar part. The conclusion is then that the assumed symmetries imply that the pion contribution to the isoscalar form factors of nucleons and hyperons vanish at all orders in the strong interactions. In the language of dispersion theory this means that the first mass states which contribute to the isoscalar form factor are the K - K pairs. If only these high mass states contribute to the dispersion integrals one would then expect the isoscalar form factor to be nearly constant for small values of the square of the 4-dimensional momentum transfer. By definition it implies a small isoscalar contribution to the mean square radius of both the charge and the magnetization density distributions. This is in contradiction with the large value of the mean square radius of the proton charge distribution and the almost zero value of the corresponding neutron charge distribution found experimentally ⁽¹²⁾. Apart from the problem of the mean square radius, the K contribution seems to be unable to account for the isoscalar form factors themselves ⁽¹¹⁾. The situation would be specially difficult in the case of global symmetry where the K couplings are assumed to be small.

We wish to emphasize that N - Ξ symmetry is necessary to draw the above conclusions. If for instance only restricted symmetry is assumed, *i.e.* $g_2 = g_3$, but nothing is said about the equality of N - π and Ξ - π couplings, the vanishing of the pion contribution to the isoscalar form factors does not result any more.

Though one knows that the proposed symmetries can only be approximate it might be hoped that they are still useful concepts when no real K particles are involved in the process considered. The above considerations on the electromagnetic properties of nucleons seem to invalidate such a point of view in the case of N - Ξ and global symmetry, but not in the case of restricted symmetry.

* * *

One of us (P. M.) would like to thank CERN for its kind hospitality.

⁽¹⁰⁾ G. BERNARDINI *et al.*: preprint.

⁽¹¹⁾ P. FEDERBUSH, M. GOLDBERGER and S. B. TREIMAN: *Phys. Rev.*, **112**, 642 (1958).

⁽¹²⁾ R. HOFSTADTER *et al.*: *Rev. Mod. Phys.*, **30**, 482 (1958).

W. ESPE - *Werkstoffkunde der Hochvakuumtechnik*. Vol. I: *Metalle und metallisch leitende Werkstoffe*. Deutscher Verlag der Wissenschaften, Berlin, 1959, pp. 910, 669 figure, DM 145.

Con questo ponderoso volume ha inizio la riedizione del noto e utilissimo testo di Espe e Knoll, pubblicato nel 1936 dallo Springer Verlag, fondamentale opera di consultazione per ogni tecnica che utilizzi l'alto e altissimo vuoto, riedizione che è curata da uno dei suoi autori, professore alla T.H. di Bratislava (Č.S.R.). Esso si rifà completamente all'antico testo, come suddivisione degli argomenti e presentazione, la quale permette un'agevole consultazione malgrado la quantità di notizie riportate. Ma rispetto ad esso le dimensioni sono sestuplicate.

A questo primo volume dovrà far seguito un secondo sui materiali silicei (vetro, quarzo, ceramica, mica, asbesto) e un terzo sui materiali ausiliari da vuoto (sostanze fluorescenti, gomme, grassi, mastici, olii, gas, vapori), inoltre è in progetto uno sulle saldature da vuoto metallo-vetro-ceramica e sui getter.

In questo volume vengono trattati (in 910 pg contro le 157 del vecchio testo), tutti i metalli e le leghe usate nella tecnica dell'alto vuoto. Dopo alcune nozioni metallografiche, vengono trattati i metalli e le leghe ad alto punto di fusione, i metalli nobili, quelli non nobili

e loro leghe e composti, i metalli rari, gli alcalini, alcalino-terrosi, il mercurio, ed il carbonio. Di ognuno vengono forniti dapprima dei dati di natura generale (come i processi di ottenimento, lavorazione, le proprietà chimiche, fisiche, ecc. e le varie ditte produttrici nel caso di leghe speciali, spesso sotto forma di tabelle; poi le varie applicazioni che essi trovano nella tecnica del vuoto. Il tutto è corredato da continue citazioni bibliografiche.

Nell'ultimo capitolo (circa 300 pg.) vengono poi esposti tutti i metodi speciali di preparazione per l'alto vuoto: lavorazione, degassamento, saldature e trattamenti superficiali.

Il libro è aggiornato fino all'Aprile 1957, pur riportando ancora alcuni lavori e risultati importanti posteriori a questa data. Come già detto il volume è ricchissimo di grafici e tabelle, che facilitano la ricerca delle notizie richieste; ricerca che d'altra parte viene guidata dalla fitta e omogenea suddivisione del testo in capitoli, paragrafi, capoversi (anche se all'inizio richiede un poco di attenzione per essere compresa). Il testo si rivolge soprattutto al campo della costruzione delle valvole termoioniche, al quale si fa continuamente riferimento, e per esso si trova la sua piena utilizzazione. Per un laboratorio di fisica può forse in certi punti essere eccessivo, con i suoi riferimenti a tecniche industriali, ma per la ricchezza di notizie contenutevi esso rappresenta senz'altro un'opera

fondamentale di consultazione per la conoscenza dei materiali da adoperare in ogni applicazione della tecnica del vuoto.

F. DUPRÉ

L. HOLZER — *Zahlentheorie*. Teubner, Leipzig, Teil I (1958), pp. VI-202; Teil II (1959), pp. VI-126. Vol. 13 e 14 della Mathematische Naturwissenschaftliche Bibliothek.

Nel primo volume l'autore è riuscito a concentrare in modo veramente assai perspicuo tutta la parte elementare della teoria dei numeri algebrici. Precisamente nel 1° capitolo si danno le proprietà fondamentali delle congruenze, nel 2° si approfondiscono le proprietà di residui quadratici, nel 3° si danno le prime proprietà degli interi algebrici giungendo sino alla ricerca delle unità ed al calcolo del numero delle classi per i corpi quadratici.

Anche se non sappiamo di applicazioni della vera e propria teoria dei numeri algebrici, anche in vista delle sempre crescenti applicazioni dell'algebra (in particolare, algebre e campi finiti), pensiamo che almeno una gran parte del contenuto di questo volume sarebbe bene che entrasse nel bagaglio culturale di chiunque voglia usare con profitto la matematica.

Il secondo volume è invece un po' più specialistico. Nel 1° capitolo partendo dalla ricerca delle unità in un corpo di numeri algebrici si arriva alla teoria di Hilbert per i corpi di Galois; nel 2° capitolo si svolge la parte classica della teoria del corpo di classi. Questa nuova trattazione può essere assai utile anche se — forse per il carattere della collezione — non si fa nessun cenno ai recenti amplissimi sviluppi della teoria.

MICHELE SCE

H. FASSBENDER — *Einführung in die Messtechnik der Kernstrahlung und die Anwendung der Radioisotope*; Georg Thieme Verlag, Stuttgart, 1958, pp. XI-223, figg. 142, tab. 15.

Gli straordinari progressi delle tecniche di misura della radiazione e delle applicazioni degli isotopi radioattivi hanno indotto l'Autore a raccogliere in questo volumetto ciò che può riuscire utile a un pubblico di non specialisti per una visione generale dell'argomento: il medico, il biologo, il tecnico e, sotto certi aspetti, lo studente potranno trovarvi una guida semplice per acquisire i principi fondamentali, un congruo numero di informazioni quantitative, un orientamento sulla letteratura specializzata.

Il libro è diviso in quattro parti. La prima introduce alcune nozioni sulla struttura dell'atomo e del suo nucleo, sulla dinamica delle reazioni nucleari, sui metodi di produzione delle radiazioni. La seconda parte dà un quadro descrittivo delle tecniche di rivelazione delle radiazioni e dei metodi di misura, con riferimenti ad apparecchiature commerciali, le cui caratteristiche sono spesso illustrate. Nella terza parte si passano in rassegna le applicazioni diagnostiche e terapeutiche degli isotopi radioattivi nonché il loro impiego nella chimica e nella tecnica. Chiude il volume una parte dedicata alla dosimetria, agli effetti della radiazione su organi e tessuti viventi, ed alle protezioni, con grafici e tabelle di uso corrente.

Il libro ha un'impostazione essenzialmente pratica: i fondamenti scientifici sono riassunti in modo rapido e dogmatico, e in questo senso non pare che il libro sia utilmente dedicato a chi affronti l'argomento per la prima volta e voglia criticamente assimilarlo. Il lettore vi troverà peraltro una fonte notevole di informazioni utili a chi si serve della radioattività come strumento di lavoro indipendentemente dalle questioni fondamentali ad essa inerenti.

Il volumetto si presenta ben ordinato e generalmente aggiornato ed è indubbiamente consigliabile a chiunque intenda interessarsi alle applicazioni degli isotopi radioattivi.

C. MANDUCHI

H. PFEIFER - *Elektronisches Rauschen*. Teil I, Rauschquellen; B. G. Teubner Verlagsgesellschaft, Leipzig, 1959; pp. VI-302. DM. 25.

Il libro rappresenta una lettura di notevole interesse per quanti si occupano di elettronica e di alte frequenze.

L'opera inizia presentando innanzitutto i metodi di indagine matematica che sono legati al problema in questione ed i principi fisici che stanno a fondamento di esso.

Segue una serie di capitoli nei quali vengono prese in esame le cause di

disturbo per vari componenti elettronici quali: antenne, diodi semiconduttori, transistori, resistenze a strato di carbone e microfoni a carbone e per ognuno di essi l'autore arriva a calcolare il generatore equivalente (di tensione o di corrente) che potrà sostituire la sorgente di rumore.

A parte vengono trattati i tubi ad alto vuoto e per ogni elettrodo di essi viene esposto il calcolo dei segnali equivalenti di disturbo, dopo di che si analizza l'effetto dei singoli disturbi nei campi di applicazione delle basse e delle alte frequenze.

A conclusione della prima parte di quest'opera sta una interpretazione quantitativa dei fenomeni considerati.

In appendice si trovano utili tabelle dalle quali si possono ricavare le grandezze equivalenti già calcolate per vari tubi di maggior impiego nel campo delle alte frequenze.

P. KUSSTATSCHER

PROPRIETÀ LETTERARIA RISERVATA

Direttore responsabile: G. POLVANI

Tipografia Compositori - Bologna

Questo fascicolo è stato licenziato dai torchi il 10 - X - 1960